AD_____

Award Number: W81XWH-10-1-0461

TITLE: Characterization and Targeting of the Aldehyde Dehydrogenase Subpopulation in Ovarian Cancer

PRINCIPAL INVESTIGATOR: Charles N. Landen, Jr., MD, MS

CONTRACTING ORGANIZATION: University of Alabama at Birmingham
Birmingham, AL 35249

REPORT DATE: July 2014

TYPE OF REPORT: Annual

PREPARED FOR: U.S. Army Medical Research and Materiel Command
Fort Detrick, Maryland 21702-5012

REPORT DOCUMENTATION PAGE

Form Approved
OMB No. 0704-0188

1. REPORT DATE July 2014	**2. REPORT TYPE** Annual	**3. DATES COVERED** 1 JUL 2013- 30 JUN 2014

4. TITLE AND SUBTITLE
Characterization and Targeting of the Aldehyde Dehydrogenase Subpopulation in Ovarian Cancer

5a. CONTRACT NUMBER

5b. GRANT NUMBER:W81XWH-10-1-0461

5c. PROGRAM ELEMENT NUMBER

5d. PROJECT NUMBER

6. AUTHOR(S)

Charles N. Landen, Jr., MD, MS

E-Mail: clanden@uab.edu

5e. TASK NUMBER

5f. WORK UNIT NUMBER

7. PERFORMING ORGANIZATION NAME(S) AND ADDRESS(ES)
University of Alabama at Birmingham
Birmingham, AL 35249

8. PERFORMING ORGANIZATION REPORT NUMBER

9. SPONSORING / MONITORING AGENCY NAME(S) AND ADDRESS(ES)
U.S. Army Medical Research and Materiel Command
Fort Detrick, Maryland 21702-5012

10. SPONSOR/MONITOR'S ACRONYM(S)

11. SPONSOR/MONITOR'S REPORT NUMBER(S)

12. DISTRIBUTION / AVAILABILITY STATEMENT
Approved for Public Release; Distribution Unlimited

13. SUPPLEMENTARY NOTES

14. ABSTRACT

Despite a common outstanding response to primary therapy, most ovarian cancer patients will experience recurrence due to what is often microscopic undetectable disease. One possible cause of this is a chemoresistant population of cells with stem cell characteristics. We have examined one potential population in particular, the ALDH-positive population. We have shown that ALDH1A1-positive cells are more tumorigenic than ALDH1A1-negative cells, contribute to poor patient outcomes, and contribute to chemoresistance. These effects can be reversed by downregulating ALDH1A1 expression with nanoparticle-delivered siRNA. Additionally, we have shown that CSCs are clinically significant, in that chemoresistant tumors have increased density of ALDH and CD133 cells. Importantly, they do not seem to explain the entire story, as there are still many CSC-negative cells present at the conclusion of treatment. Specifically, endoglin (CD105) and hedgehog family members (Gli1 and Gli2) appear to play important roles in chemotherapy resistance, and when targeted enhance response to chemotherapy. To further identify other important players, we have further developed the patient-derived xenograft (PDX) model where patient samples are directly implanted into mice, and when formed, treated with chemotherapy. The treated tumors, like patient specimens, are enriched with ALDH1-positive cells. Further characterization of the surviving population is underway, in conjunction with separately-funded protocols.

15. SUBJECT TERMS
Ovarian Cancer, aldehyde dehydrogenase, ALDH1A1, cancer stem cell

16. SECURITY CLASSIFICATION OF:			**17. LIMITATION OF ABSTRACT**	**18. NUMBER OF PAGES**	**19a. NAME OF RESPONSIBLE PERSON**
a. REPORT	**b. ABSTRACT**	**c. THIS PAGE**			USAMRMC
U	U	U	UU	146	**19b. TELEPHONE NUMBER** *(include area code)*

Table of Contents

Characterization and targeting of the ALDH subpopulation in ovarian cancer

Charles N. Landen, Jr., MD, MS
University of Alabama at Birmingham, Birmingham, AL
Ovarian Cancer Academy OC093443 July 2013- June 2014 Annual Report

*****Please note this report is a cumulative report, covering the entire period from start of award to current, as requested in conjunction with a request to transfer grant to a new institution*****

INTRODUCTION:

While most ovarian cancer patients initially respond to chemotherapy, most will ultimately recur and succumb to disease, suggesting that there is a subpopulation of cells within a heterogeneous tumor that has either inherent or acquired resistance to chemotherapy(1). Recently subpopulations of cancer cells in solid tumors have been observed to have properties of stem cells, and therefore designated as "cancer stem cells" (CSC's) or tumor initiating cells (TIC's) (2, 3). The intent of this project is to characterize whether ovarian cells that express aldehyde dehydrogenase (ALDH1A1) have cancer stem cell properties, and if targeting ALDH1A1 would lead to a reversal of the chemoresistant properties. Characteristics of cancer stem cell that will be assessed include tumorigenicity experiments, evidence of multipotentiality, and enhanced resistance to chemotherapeutics. The effects of ALDH1A1 downregulation will be determined both *in vitro* and *in vivo*, using small interfering RNA (siRNA) encapsulated in nanoparticles that allow efficient *in vivo* delivery. If our hypotheses are confirmed, we will have identified a subpopulation of ovarian cancer cells that might survive initial chemotherapy and contribute to resistance, and furthermore may find a clinically feasible novel methodology to target these cells to improve outcomes in this devastating disease. If ALDH1 cells are not explaining the full population of chemoresistant cells, these studies will provide the opportunity to more fully characterize which cells are mediating survival of primary therapy.

BODY:

Task 1: Determine tumorigenicity of ALDH1A1 subpopulations

The goal of task 1 was to determine the tumorigenicity of ALDH1A1 subpopulations. In a prior report, we described results published in Molecular Cancer Therapeutics(4) showing tumorigenicity of ALDH1A1-positive cells compared to ALDH1A1-negative cells from the A2780cp20 cell line. As summarized in Table 1, ALDEFLUOR-positive cells exhibited increased tumorigenic potential, with 100% tumor initiation after injection of 100,000, 25,000, or 5,000 cells, and 1 tumor established after 1,000 cells injected. ALDEFLUOR-negative cells were also able to form tumors, although at a lower rate: two of 5 mice formed tumors after injection of 25,000 or 100,000 cells, and no tumors formed after injection of 5,000 or 1,000 cells.

Table 1. Tumorigenicity of ALDH1A1-positive and ALDH1A1-negative cells.

A2780cp20 cells injected IP	**1 mil**	**250k**	**100k**	**25k**	**5k**	**1k**	**Serial transplantation rate**
ALDEFLUOR-negative	5/5	4/5	2/5	2/5	0/5	0/5	0/5
ALDEFLUOR-positive			5/5	5/5	5/5	1/5	5/5

The TD50, or dose of cells required to permit tumor formation in 50% of animals, was 50-fold lower with ALDEFLUOR-positive cells.

An additional important characteristic is demonstration that cancer stem cells have enhanced potential for differentiation. We also demonstrated that tumors formed after injection of ALDEFLUOR-positive cells contained both positive and negative ALDH1A1 populations. However, no ALDEFLUOR-positive cells were found in the tumors that formed after injection of ALDH1A1-negative cells (Figure 4A,B in attached manuscript). This was confirmed with IHC (Figure 4C,D). A similar differentiation capacity was noted *in vitro* (Figure 4E,F). Of the ALDEFLUOR-positive cells, the population gradually reverted to 75.3%, 54.2%, and 51.4% ALDEFLUOR-positive, respectively for each timepoint. However, the ALDEFLUOR-negative cells could not produce any ALDEFLUOR-positive cells.

An additional element of this task is to determine whether ALDH1A1-positive cells from patient tumors have enhanced tumorigenicity. Initial attempts to examine this led to few tumors forming from either population, either due to toxicity of the processing procedure required to separate cells to single-cell populations, or because of the inherent low rate of tumor formation from primary xenografts. We have adjusted our initial approach to use tumors growing in mice, established after immediate implantation into mice. These cells will have demonstrated xenograft tumorigenicity, and because they can be collected in a more controlled setting, should require less aggressive and more rapid digestion, enhancing viability. Our protocols for establishing primary xenografts have been optimized, described in more detail under task 2, and will be utilized in the next year.

Task 2: Determine if ALDH1-positive cells survive chemotherapy in the tumor microenvironment.

Although ALDH1 and other putative cancer stem cell populations have enhanced tumorigenicity, that does not necessarily mean that they have preferential survival in patient tumors. We utilized a unique cohort of patients in whom we have both primary and recurrent ovarian cancer specimens. We performed IHC on these for ALDH1, CD44, and CD133 to determine whether recurrent tumors, which are generally more chemoresistant, are predominantly composed of these populations. What we discovered was very interesting, and was published in Clinical Cancer Research(5). Many recurrent tumors were indeed composed of a greater number of each of these CSC populations, most significantly in the case of CD133. Interestingly, many tumors actually had less of each population in the recurrent tumor, most notably in the case of ALDH1. But if the patients were stratified by the setting in which their tumors were collected, the difference was even more striking. Tumors collected immediate after receiving primary therapy, the time at which cells surviving would ultimately cause recurrent disease, were higher in both ALDH1 (2-fold) and CD133 (24-fold) cells. CD44 was higher, but not to a statistically significant degree. Tumors collected at first recurrence were very similar to their primary tumor. This is clinically consistent, because many patients will again have a

positive response to chemotherapy when having a first recurrence. It is also consistent with the stem cell hypothesis, since surviving cancer stem cells would be expected to give rise to a heterogeneous tumor resembling the initial tumor.

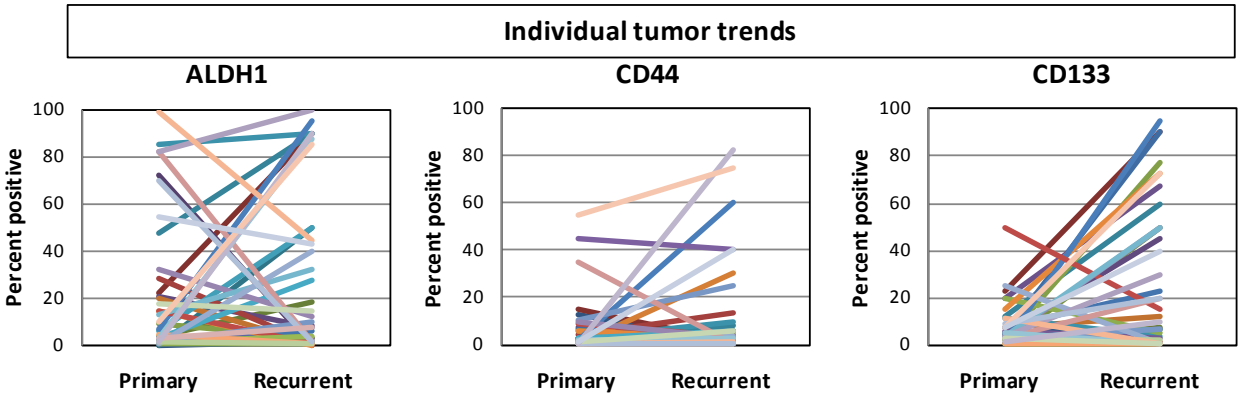

Figure 1. Patient tumors collected in the recurrent setting were more densely positive for CD133 cells compared to tumors collected at primary therapy from the same patient. Each line represents a patient.

To examine whether this is also noted in a setting where chemotherapy administration and tumor collection is more controlled, we have established protocols for development of primary xenografts in SCID mice. We first examined which sites of implantation are optimal for xenograft formation. We have implanted and compared growth in four sites: 1) subcutaneous, 2) subrenal capsule, 3) intraperitoneal, and 4) mammary fat pad. After attempts in 23 patients, these respective sites have yielded take rates (defined as at least one tumor formed that can be re-established and expanded) of 91.3%, 8.0%, 23.5%, and 63.6%, respectively (Figure 2A). To determine if the tumors are only composed of putative tumor initiating cells, we have performed immunohistochemistry for ALDH1A1, CD44, and CD133, and found that there is less than 10% variability between xenograft and patient tumors. They also retain the heterogeneity and histologic classification of patient tumors. Even mixed-histology tumors display both histologic subtypes in the growing holografts. Most importantly, these xenografts retain biologic tumor heterogeneity and respond to combined platinum/taxane therapy similarly to how patients respond from whom these matched tumors were obtained. Once tumors have been established, at least one is collected for banking purposes, but remaining mice are randomized to continued observation or treatment with combination carboplatin and paclitaxel. Mice are treated for 4 weeks (or until complete response), and response recorded based on traditional RESIST criteria. In the first 13 holografts established, patients who ultimately had only a partial response (PR) to primary therapy had a

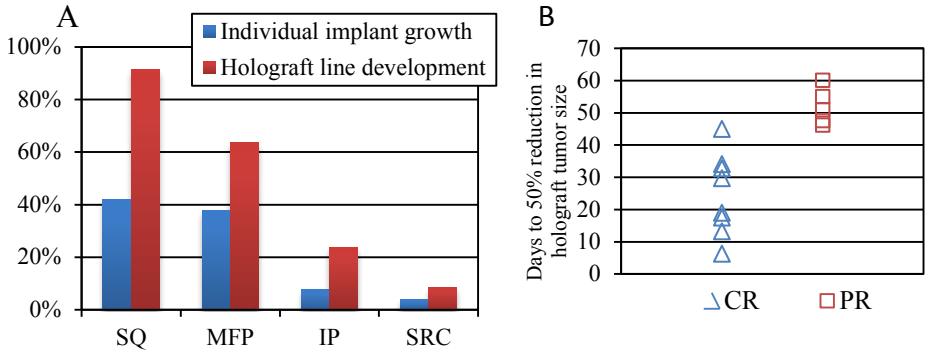

Figure 2. "Holografts" are efficiently established after SQ implantation (A), and response to chemo correlates with patient response (B).

much slower tumor reduction (or no response at all) compared to patients who had a complete response (CR) ($p<0.001$, Figure 2B).

To further characterize the similarity of the PDX tumors to original patient samples, we have also performed a quantitative PCR array for 84 oncogenes that are recognized targets for therapy, on 4 pair of PDX tumors and patient tumors. There was not a significant difference in gene expression in 79 of the cancer drug target genes, with an overall R^2-value of .7441 (Figure 3). 5 genes had a decrease in expression in the PDX sample when compared to the patient specimen. These genes were PDGFRA, PDGFRB, FLT1, KDR and FLT4. All of these genes would be expected to be decreased in the PDX tumor, since they are genes produced by the host, and the primers for qPCR are human-specific. If these genes are removed from the analysis and only tumor cell-specific gene expression is considered, the R^2-value increases to 0.8891. Therefore, while the PDX model may not be ideal for targeting proteins expressed by stromal cells, overall there is consistency in expression of targetable oncogenes, supporting use of the model for drug development.

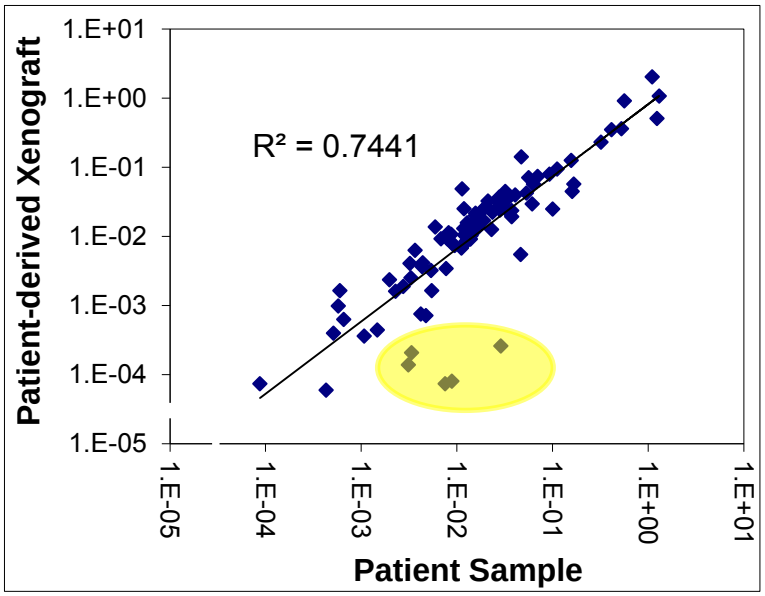

Figure 3. Quantitative PCR array comparing PDX tumors and human samples. Yellow field identifies genes with reduced expression in the PDX tumors, all of which are stromal genes.

With the model validated, we turned our attention to changes in tumors with chemotherapy treatment, in an effort to identify pathways contributing to chemoresistance. In order to determine whether putative cancer stem cells are enriched in treated samples, we previously reported that on average, there was a significant increase in ALDH1 and CD133-positive CSCs comprising treated tumors. CD44 was only increased in two tumors, and not significant overall. These are consistent with findings from patient tumors. However, it is important to note that treated tumors are not composed of ONLY these cells. In order to determine if ALDH1A1 and other putative cancer stem cells make up the majority of the xenograft tumors collected after chemotherapy, we performed IHC for these markers on treated tumors. We found that on average, there was a significant increase in ALDH1 and CD133-positive CSCs comprising treated tumors (Figure 4). CD44 was only increased in two tumors, and not significant overall. These are consistent findings from patient tumors. However, it is important to

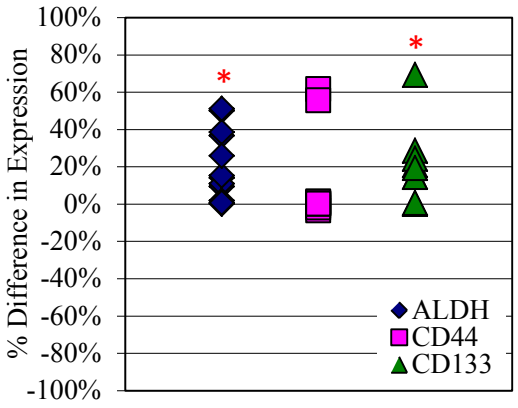

Figure 4. Xenografts with a significant response to carboplatin/paclitaxel therapy are enriched in ALDH and CD133-positive cells (*=$p<0.05$)

note that treated tumors are not composed of ONLY these cells.

Therefore we subjected untreated and treated PDX tumors to RNASeq analysis, and in pairwise fashion examined the genes and pathways changing with chemotherapy treatment, either by enrichment of the surviving population, or induced by chemotherapy exposure. Initially 6 pair of tumors have been sequenced and analyzed (support for sequencing provided in a separate grant, not funded by this grant, but work is related).

Initially, analysis of all 6 tumor pairs together only found 85 genes that were, on average, significantly different when comparing the 6 treated and untreated tumors. However, when subjected to pathway analysis with IPA software, some very interesting trends are apparent (Table 2). Several pathways are indeed significant altered among several tumors. These include EIF2 signaling (the #1 pathway in 4 of the 6 pair), mTOR signaling, antigen presentation, protein ubiquitination, mitochondrial dysfunction, glycolysis, and remodeling of epithelial adherens junctions.

Table 2. Pathways significantly altered in PDX tumors treated with chemotherapy.

Tumor 106	
Ingenuity Canonical Pathways	fold increase
EIF2 Signaling	47.40
Regulation of eIF4 and p70S6K Signaling	15.40
mTOR Signaling	15.20
Antigen Presentation Pathway	9.85
Protein Ubiquitination Pathway	6.44
Mitochondrial Dysfunction	5.20
Remodeling of Epithelial Adherens Junctions	5.11
Atherosclerosis Signaling	4.92
RhoGDI Signaling	3.66
Clathrin-mediated Endocytosis Signaling	3.64

Tumor 108	
Ingenuity Canonical Pathways	fold increase
EIF2 Signaling	7.75
Mitochondrial Dysfunction	6.85
Protein Ubiquitination Pathway	6.12
Glycolysis I	5.69
mTOR Signaling	3.45
Aryl Hydrocarbon Receptor Signaling	2.95
Regulation of eIF4 and p70S6K Signaling	2.69
Superpathway of Serine and Glycine Biosynthesis I	2.69
4-hydroxyproline Degradation I	2.63
Cell Cycle: G1/S Checkpoint Regulation	2.60

Tumor 115	
Ingenuity Canonical Pathways	fold increase
Role of NFAT in Regulation of the Immune Response	3.26
Ephrin A Signaling	3.20
PKCÎ¸ Signaling in T Lymphocytes	2.59
Systemic Lupus Erythematosus Signaling	2.08
Axonal Guidance Signaling	2.08
Pentose Phosphate Pathway (Oxidative Branch)	2.03
G Protein Signaling Mediated by Tubby	2.00
Complement System	2.00
Calcium-induced T Lymphocyte Apoptosis	1.91
Antiproliferative Role of Somatostatin Receptor 2	1.87

Tumor 116	
Ingenuity Canonical Pathways	fold increase
EIF2 Signaling	70.90
mTOR Signaling	24.80
Regulation of eIF4 and p70S6K Signaling	23.90
Mitochondrial Dysfunction	9.90
Antigen Presentation Pathway	5.92
Complement System	4.61
Remodeling of Epithelial Adherens Junctions	4.56
Glutathione Redox Reactions I	4.10
Crosstalk between Dendritic Cells and Natural Killer Cells	3.89
Regulation of Actin-based Motility by Rho	3.69

Tumor 121	
Ingenuity Canonical Pathways	fold increase
EIF2 Signaling	64.90
Regulation of eIF4 and p70S6K Signaling	24.50
mTOR Signaling	21.00
Mitochondrial Dysfunction	7.67
RhoGDI Signaling	5.66
Protein Ubiquitination Pathway	5.62
Epithelial Adherens Junction Signaling	5.36
Remodeling of Epithelial Adherens Junctions	5.16
Glycolysis I	4.51
Antigen Presentation Pathway	4.11

Tumor 136	
Ingenuity Canonical Pathways	fold increase
Atherosclerosis Signaling	13.00
LXR/RXR Activation	12.10
Altered T Cell and B Cell Signaling in Rheumatoid Arthritis	8.83
Hepatic Fibrosis / Hepatic Stellate Cell Activation	8.37
Crosstalk between Dendritic Cells and Natural Killer Cells	7.76
Coagulation System	7.58
Dendritic Cell Maturation	7.45
B Cell Development	7.01
Inhibition of Matrix Metalloproteases	6.99
T Helper Cell Differentiation	6.37

Intriguingly, it was the same 4 tumors in which these pathways were altered, suggesting either a link between them, or duplication of family members leading to their reveal as important. In the other two pair, most of the pathways significantly altered were participants in the immune system. Therefore, not only are several pathways in common among the multiple pair, there appears to be a dichotomy, whereby one family of tumors may respond to chemo with one set of pathways relating to metabolism and controls on translation/transcription/protein turnover, and the other through the immune system. Additional work is required to validate these findings, and identify ways to target the system to enhance chemotherapy response.

Task 3: Target ALDH1 with siRNA *in vivo*

There are no known inhibitors of ALDH1A1 for *in vivo* studies. Therefore, as previously reported, we utilized a method for delivery of siRNA *in vivo* using DOPC nanoparticles. In this study nude mice were injected intraperitoneally with either SKOV3TRip2 or A2780cp20 cells and randomized to four treatment groups to begin 1 week after cell injection: 1) control siRNA in DOPC, delivered IP twice per week; 2) docetaxel 35 mg, delivered IP weekly (for SKOV3TRip2 model) or cisplatin 160 μg, delivered IP weekly (for A2780cp20 model); 3) ALDH1A1-siRNA in DOPC, IP twice per week; or 4) ALDH1A1-siRNA in DOPC plus docetaxel (for SKOV3TRip2) or cisplatin (for A2780cp20). After four weeks of treatment, mice were sacrificed and total tumor weight recorded. Immunohistochemical analysis confirmed reduced ALDH1A1 expression with ALDH1A1-siRNA/DOPC treatment compared to controls but not with chemotherapy alone. In SKOV3TRip2 xenografts (Figure 5F in appended manuscript) there was a non-significant reduction in tumor growth with docetaxel treatment of 37.0% ($p=0.17$) and with ALDH1A1 siRNA treatment of 25.0% ($p=0.38$) compared to control-DOPC. The combination of ALDH1A1 siRNA and docetaxel resulted in significantly reduced growth, by 93.6% compared to control siRNA ($p<0.001$), by 89.8% compared to docetaxel plus control siRNA ($p=0.003$), and by 91.4% compared to ALDH1A1 siRNA ($p=0.002$). In A2780cp20 (Figure 5G in appended manuscript), there was a similar non-significant reduction in tumor weight with cisplatin alone of 43.9% ($p=0.32$) and with ALDH1A1 siRNA treatment of 57.0% ($p=0.19$). These effects may be even less significant than the mean tumor weights suggest, given the presence of two especially large tumors in the control siRNA group. However, again combined therapy showed a sensitization to chemotherapy with ALDH1A1 siRNA, with combination therapy reducing growth by 85.0% compared to control siRNA ($p=0.048$), by 73.4% compared to cisplatin plus control siRNA ($p=0.013$), and by 65.3% compared to ALDH1A1 siRNA alone ($p=0.039$). Given the minimal effects of either single agent and the consistent finding of significant improvement with combined therapy, these data suggest a synergy between ALDH1A1 downregulation and both taxane and platinum chemotherapeutic agents, though formal dose-finding experiments would be required to definitively prove synergy.

Although the methods used here are being pursued in phase I clinical trials, we are continuing to explore whether other nanoparticle systems might improve delivery of siRNA in vivo. We are currently collaborating with a colleague to explore the use of protein cage nanoparticles. These nanoparticles are composed of repeating subunits of peptides, the structure of which can be modified to present ligands for receptor-mediated delivery. If we can enhance delivery to desired cells, such as tumors, doses of siRNA might be increased, and constructs against proteins that would normally be toxic to normal cells might be utilized. Studies in this are

preliminary and ongoing, but we have been able to demonstrate delivery of fluorescent-tagged siRNA to tumor tissues *in vivo*, and siRNA-mediated downregulation of a desired target *in vitro*.

Task 4: Evaluate mechanisms of ALDH1-mediated chemoresistance

We have achieved successful transfection the ALDH1A1-negative A2780ip2 cell line with a construct producing ALDH1A1. The construct was obtained through Addgene (plasmid #11610), produced in the laboratory of Dr. Steven Johnson. However, the ALDH1 protein produced does not appear to be active, as assessed by the Aldefluor assay. Therefore we cannot reasonably expect that biologic effects can be elicited. We are in the process of repeating the transfection, in order to determine the effects of forced overexpression of ALDH1A1 in a null line. In the meantime, microarrays have been completed on ALDH-positive and –negative cells (representative genes presented in Table 3), and confirmation/examination of individual genes is underway. We are also discussing collaboration with a colleague with expertise in metabolism and mitochondrial mechanisms of chemotherapy resistance. Several genes involved in mitochondrial metabolism are overexpressed in the ALDH1-positive cells, using the Illumina microarray data. Confirmation of these genes with qPCR will be performed, as will mitochondrial metabolism experiments that might determine differential regulation of metabolism in ALDH-positive and –negative cells.

Table 3. Differential expression ALDH-positive and –negative AL2780cp20 cells

SYMBOL	ALDHneg mean	ALDHpos mean	Ratio Pos:Neg	T-test
OVEREXPRESSED				
ALDH1A1	2321.55	18392.72	7.92	0.0017
NSUN5C	68.08	193.72	2.85	0.0057
ZNF286A	70.46	145.51	2.07	0.0088
2-Sep	58.28	118.05	2.03	0.0078
PRRG4	103.39	209.32	2.02	0.0021
CD97	71.23	142.09	1.99	0.0007
TWIST2	76.32	149.70	1.96	0.0044
MAT2B	78.75	151.76	1.93	0.0024
AP1M2	72.74	137.81	1.89	0.0089
NDRG2	84.04	159.13	1.89	0.0090
C2CD2	132.93	251.12	1.89	0.0014
CDCA1	85.56	155.65	1.82	0.0052
C7orf28A	74.91	131.89	1.76	0.0026
ZNF714	287.74	486.13	1.69	0.0093
ZNF501	87.71	147.49	1.68	0.0085
TCF20	58.51	96.52	1.65	0.0006
KCNH2	65.48	104.66	1.60	0.0066
RAD51L1	84.59	133.86	1.58	0.0036

REDUCED EXPRESSION				
STRC	135.54	90.32	0.67	0.0019
ZNF3	231.49	153.44	0.66	0.0003
HOXB1	199.72	132.32	0.66	0.0053
ZFP37	219.24	144.25	0.66	0.0005
CHES1	887.74	581.44	0.65	0.0086
DAAM1	625.07	402.09	0.64	0.0088
ZMIZ2	318.61	204.68	0.64	0.0089
DKFZ	99.51	62.03	0.62	0.0097
FBXO2	325.58	202.91	0.62	0.0060
ALDH3A2	636.03	395.36	0.62	0.0089
DAAM1	596.23	368.13	0.62	0.0031
NOV	1011.84	614.10	0.61	0.0073
SFH	203.09	119.64	0.59	0.0067
SCARA3	217.30	127.41	0.59	0.0008
CGAO	102.98	60.02	0.58	0.0097
LIPC	291.32	166.38	0.57	0.0041
PKP4	366.28	208.85	0.57	0.0086
ZNF304	164.21	91.06	0.55	0.0042
AGPAT7	370.26	189.80	0.51	0.0052

In conjunction with this list, as well as genes identified in stem cell pathway analysis of patient primary/recurrent pair, two genes have been further characterized for their contribution to chemotherapy resistance.

First, the endoglin pathway was evaluated. Endoglin expression was intriguing, as it had previously only been known to be expressed in developing endothelial cells. Therefore, Western blot and qPCR were used to evaluate endoglin expression in multiple ovarian cancer lines. Anti-endoglin siRNAs were used to downregulate expression in ES2 and HeyA8MDR. In vitro, the effects of endoglin-knockdown individually and with chemotherapy were evaluated by MTT assay, cell-cycle analysis, alkaline comet assay, and γ-H2AX foci formation. In vivo, mice inoculated with ES2 or HeyA8MDR cell lines were administered chitosan-encapsulated anti-ENG siRNA or control siRNA with and without carboplatin.

As described in the accompanying manuscript, endoglin was indeed highly expressed in at least 4 ovarian cancer cell lines (Figure 5). Inhibition of endoglin expression with siRNA significantly decreased cell viability (by 50%, $p<0.001$, and 84%, $p<0.001$, respectively), increased apoptosis, induced double-stranded DNA damage, and increased cisplatin sensitivity. In an orthotopic mouse model, anti-endoglin treatment decreased tumor weight in both ES2 and HeyA8MDR models when compared to control (41.2% reduction, $p=0.001$; and 35.6% reduction, $p=0.014$; respectively, Figure 6). Endoglin inhibition with carboplatin administration was associated with even greater response when compared to control (61.2% and 57.7% reduction, $p<0.001$ for both).

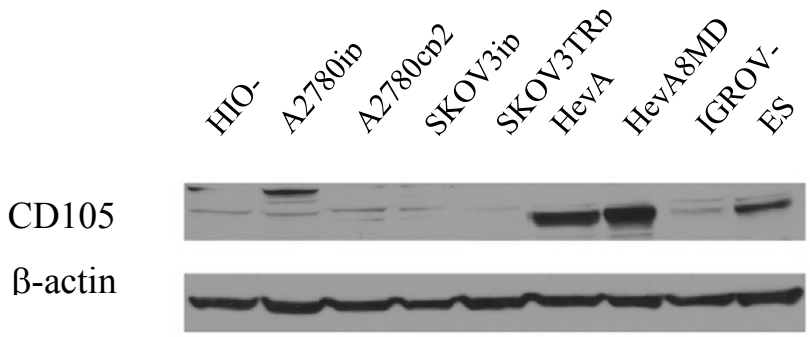

Figure 5. Expression of CD105 (endoglin) in ovarian cancer cell lines.

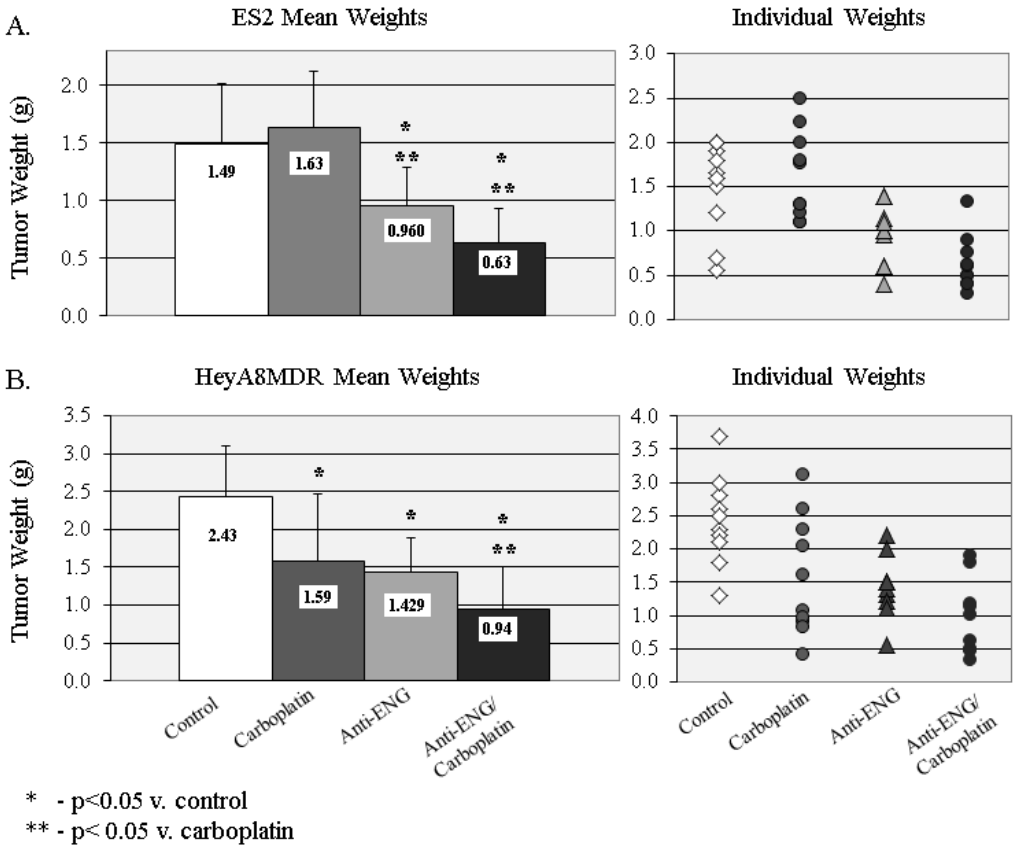

Figure 6. SiRNA-mediated downregulation of CD105 (endoglin) in orthotopic models of ovarian cancer – ES2 (A) and HeyA8MDR (B).

In parallel, the Hedgehog pathway was examined for its potential in chemotherapy resistance. The hedgehog (HH) pathway has been implicated in the formation and maintenance of a variety of malignancies, including ovarian cancer; however, it is unknown whether HH signaling is involved in ovarian cancer chemoresistance. The goal of this investigation was to determine the effects of antagonizing the HH receptor, Smoothened (Smo), on chemotherapy response in ovarian cancer. As reported in the accompanying manuscript, expression of HH pathway

members was assessed in 3 pairs of parental and chemotherapy-resistant ovarian cancer cell lines (A2780ip2/A2780cp20, SKOV3ip1/SKOV3TRip2, HeyA8/HeyA8MDR) using qPCR and Western blot. Cell lines were exposed to increasing concentrations of two different Smo antagonists (cyclopamine, LDE225) alone and in combination with carboplatin or paclitaxel. Selective knockdown of Smo, Gli1 or Gli2 was achieved using siRNA constructs. Cell viability was assessed by MTT assay. A2780cp20 and SKOV3TRip2 orthotopic xenografts were treated with vehicle, LDE225, paclitaxel or combination therapy. Chemoresistant cell lines demonstrated higher expression (>2-fold, $p<0.05$) of HH signaling components compared to their respective parental lines. Smo antagonists sensitized chemotherapy-resistant cell lines to paclitaxel (Figure 7A), but not to carboplatin (data not shown). With treatment, cells had a profound G2 phase arrest (Figure 7B-C). LDE225 treatment also increased sensitivity of ALDH-positive cells to paclitaxel. A2780cp20 and SKOV3TRip2 xenografts treated with combined LDE225 and paclitaxel had significantly less tumor burden than those treated with vehicle or either agent alone. Increased taxane sensitivity appeared to be mediated by a decrease in P-glycoprotein (MDR1) expression. Selective knockdown of Smo, Gli1 or Gli2 all increased taxane sensitivity. Smo antagonists reverse taxane resistance in chemoresistant ovarian cancer models, suggesting combined anti-HH and chemotherapies could provide a useful therapeutic strategy for ovarian cancer

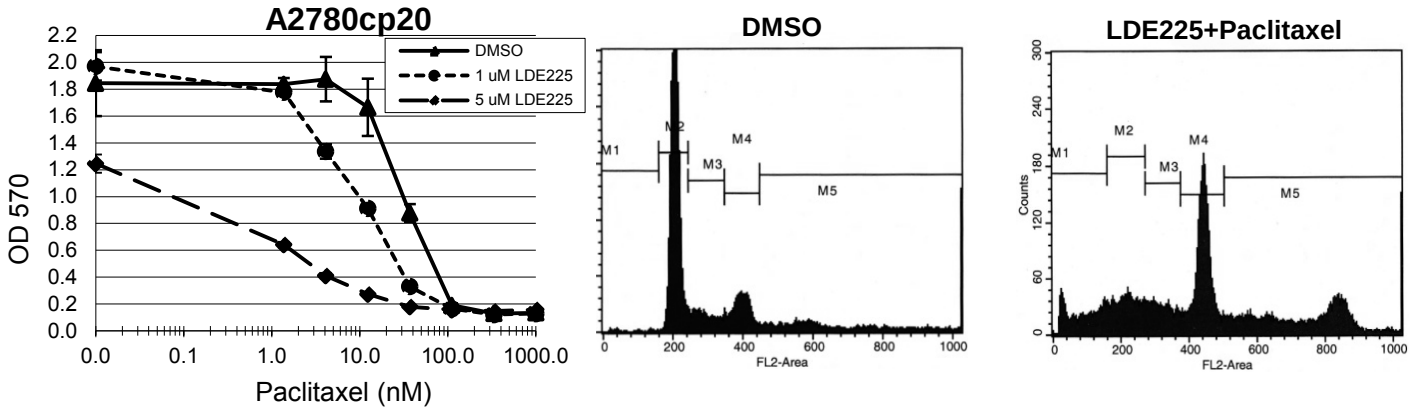

Figure 7. (A) Treatment of the chemoresistant cell line A2780cp20 with LDE225 sensitized cells to paclitaxel, and (B,C) led to a dramatic phase G2 arrest

KEY RESEARCH ACCOMPLISHMENTS:

- ALDH-positive cells from the A2780cp20 and SKOV3TRip2 cell lines have approximately 50-fold increased tumorigenicity compared to ALDH-negative cells.
- Tumors treated with chemotherapy are enriched in the ALDH1 And CD133 CSC population, compared to matched samples collected prior to therapy.
- Tumors collected immediately at the completion of primary therapy are enriched to an even greater degree than tumors collected at first recurrence.
- Efficient establishment of primary xenografts directly from patient tumors is feasible, and mimic patient tumors in histologic make-up, CSC density, and response to chemotherapy.

- Xenograft tumors from mice treated with chemotherapy are similarly enriched in ALDH1 and CD133 CSCs.
- Treatment of tumor-bearing mice with ALDH1A1-targeting siRNA in DOPC sensitized normally-resistant cell lines to cisplatin or paclitaxel.
- ALDH1-positive and –negative cells have differential expression of multiple genes, and mitochondrial metabolism may contribute to the chemoresistant properties of ALDH-positive cells.
- Stem cell pathway genes endoglin and hedgehog mediators Gli1 and Gli2 contribute to chemotherapy resistance, and targeting these genes restores sensitivity to chemotherapy.

REPORTABLE OUTCOMES:

- Publications (since initiation of the award, from a total of 70):

1. **Landen CN**, Goodman B, Katre AA, Steg AD, Nick AM, Stone RL, Miller LD, Mejia PV, Jennings NB, Gershenson DM, Bast RC, Jr., Coleman RL, Berestein G, and Sood AK. Targeting Aldehyde Dehydrogenase Cancer Stem Cells in Ovarian Cancer. *Mol Can Ther* 9(12): 3186-99, 2010. † PMID: 20889728
2. Frederick PJ, Ramirez PT, McQuinn L, Milam MR, Weber DM, Coleman RL, Gershenson DM, **Landen Jr CN**. Preoperative Factors Predicting Survival After Secondary Cytoreduction for Recurrent Ovarian Cancer. Int J Gyn Cancer, 21(5): 831-6, 2011. PMID: 21613957
3. Nick AM, Stone RL, Armaiz-Pena G, Ozpolat B, Tekederli I, Graybill WS, **Landen CN**, Villares G, Vivas-Mejia P, Bottsford-Miller J, Kim HS, Lee JS, Kim SM, Baggerly KA, Ram PT, Deavers MT, Coleman RL, Lopez-Berestein G, Sood AK. Silencing of p130cas in Ovarian Carcinoma: A Novel Mechanism for Tumor Cell Death. *J Natl Cancer Inst*, 103(21): 1596-612, 2011. PMID: 21957230
4. Steg AD, Katre AA, Goodman B, Han HD, Nick AM, Stone RL, Coleman RL, Alvarez RD, Lopez-Berestein G, Sood AK, **Landen CN**. Targeting the Notch Ligand Jagged1 in Both Tumor Cells and Stroma in Ovarian Cancer. *Clin Can Res,* 17(17): 5674-85, 2011. PMID: 21753153
5. Stone RL, Nick AM, McNeish IA, Balkwill F, Han HD, Bottsford-Miller J, Rupaimoole R, Armaiz-Pena GN, Pecot CV, Coward J, Deavers MT, Vasquez HG, Urbauer D, **Landen CN**, Wei H, Gershenson H, Matsuo K, Shahzad MMK, King ER, Tekedereli I, Ozpolat B, Ahn EH, Bond VK, Wang R, Drew AF, Gushiken F, Collins K, DeGeest K, Lutgendorf SK, Chiu W, Lopez-Berestein G, Afshar-Kharghan V, Sood AK. Paraneoplastic Thrombocytosis in Ovarian Cancer. *NEJM,* 366(7): 610-8, 2012. PMIS: 22335738
6. Steg AS, Bevis KS, Katre AA, Ziebarth A, Alvarez RD, Zhang K, Conner M, **Landen CN**. Stem cell pathways contribute to clinical chemoresistance in ovarian cancer. *Clin Can Res,* 18(3):869-81, 2012. PMID: 22142828

7. Ziebarth AJ, **Landen CN** Jr, Alvarez RD. Molecular/genetic therapies in ovarian cancer: future opportunities and challenges. *Clin Obstet Gynecol*, 55(1):156-72, 2012. PMID: 22343235

8. Kim KK, Zsebik GN, Straughn JM, **Landen CN**. Management of Complex Pelvic Masses Using a Multivariate Index Assay: A Decision Analysis. *Gyn Onc*, 126: 364-8, 2012. PMID: 22659191

9. Steg AS, Katre AA, Bevis KS, Ziebarth A, Dobbin ZC, Shah MS, Alvarez RD, **Landen CN**. Smoothened Antagonists Reverse Taxane Resistance in Ovarian Cancer. Mol Cancer Ther, 11(7): 1587-97, 2012. † PMID: 22553355

10. Qin Y, Xu J, Aysola K, Oprea G, Reddy A, Matthews R, Okoli J, Cantor A, Grizzle WE, Partridge EE, Reddy ESP, **Landen CN**, and Rao VN. BRCA1 Proteins Regulate Growth of Ovarian Cancer Cells by Tethering Ubc9. *Am J Can Res*, 2(5): 540-8, 2012. PMID: 22957306

11. Li H, Cai Q, Wu H, Vathipadiekal V, Dobbin ZC, Li T, Hua X, **Landen CN**, Birrer MJ, Sánchez-Beato M, Zhang R. SUZ12 promotes human epithelial ovarian cancer by suppressing apoptosis via silencing HRK. *Mol Can Res*, 10(11): 1462-72, 2012. PMID: 22964433

12. Ziebarth AJ, Nowsheen S, Steg AS, Shah MM, Katre AA, Dobbin ZC, Han HD, Lopez-Berestein G, Sood AK, Conner MG, Yang ES, **Landen CN**. Endoglin (CD105) contributes to platinum resistance and is a target for tumor-specific therapy in epithelial ovarian cancer. *Clin Can Res*, 19(1): 170-82, 2013. PMID: 23147994

13. Chen H, **Landen CN**, Li Y, Alvarez RD, Tollefsbol TO. Epigallocatechin Gallate and Sulforaphane Combination Treatment Induce Apoptosis in Paclitaxel-Resistant Ovarian Cancer Cells through hTERT and Bcl-2 Down-regulation. *Exp Cell Res,* 319(5): 697-706, 2013. PMID: 23333498

14. Chen H, **Landen CN**, Li Y, Alvarez RD, Tollefsbol TO. Enhancement of Cisplatin-mediated Apoptosis in Ovarian Cancer Cells through Potentiating G2/M Arrest and p21 Upregulation by Combinatorial Epigallocatechin Gallate and Sulforaphane. *J Oncol,* 872957, 2013. PMID: 23476648

15. Schultz MJ, Swindall AF, Wright JW, Sztul ES, **Landen CN**, Bellis SL. ST6Gal-I sialyltransferase confers cisplatin resistance in ovarian tumor cells. *J Ovar Res,* 6(1): 25, 2013. PMID: 23578204

16. Dobbin ZA, **Landen CN**. The importance of the PI3K/AKT/mTOR pathway in the progression of ovarian cancer. *Int J Mol Sciences*, 14(4): 8213-27, 2013. PMID: 23591839

17. Erickson BK, Conner MG, **Landen CN Jr**. The Role of the Fallopian Tube in the Origin of Ovarian Cancer. *Am J Obstet Gynecol,* 209 (5): 409-14, 2013. PMID: 23583217

18. **Landen CN** and Lengyl E. Summary of the 2013 American Association for Cancer Research (AACR) Annual Meeting. *Gynecol Oncol,* 130 (1): 6-8, 2013. PMID 23926600

19. Fauci JM, Sabbatino F, Wang Y, Londoño-Joshi AI, Straughn JM Jr, **Landen CN**, Ferrone S, Buchsbaum DJ. Monoclonal antibody-based immunotherapy of ovarian cancer: Targeting ovarian cancer cells with the B7-H3-specific mAb 376.96. *Gynecol Oncol,* 132: 203-210*,* 2013. PMID 24216048
20. Dobbin ZC and **Landen CN.** Isolation and Characterization of Potential Cancer Stem Cells from Solid Human Tumors - Potential Applications. Curr. Protoc. Pharmacol, 63:14.28.1-14.28.19, 2013. PMID 24510756
21. Bradley A, Zheng H, Ziebarth A, Sakati W, Branham-O'Connor M, Blumer JB, Liu Y, Kistner-Griffin E, Rodriguez-Aguayo C, Lopez-Berestein G, Sood AK, **Landen CN** Jr, Eblen ST. EDD enhances cell survival and cisplatin resistance and is a therapeutic target for epithelial ovarian cancer. *Carcinogenesis.* Jan 2014. [Epub ahead of print]. PMID 24379240
22. Shah MS and **Landen CN**. Ovarian Cancer Stem Cells: Are They Real and Why are they Important? *Gynecol Oncol,* 132(2): 483-89, 2014. PMID 24321398
23. Arend RC, Londoño-Joshi AL, Samant RS, Li Y, Conner M, Hidalgo B, Alvarez RD, **Landen CN**, Straughn JM, DJ Buchsbaum. Inhibition of Wnt/ß-catenin pathway by niclosamide: a therapeutic target for ovarian cancer. *Gynecol Oncol, in press.*
24. Shah MM, Dobbin ZC, Nowsheen S, Wieglos M, Katre AA, Alvarez RD, Konstantinopoulos PA, Yang ES, **Landen CN**. An ex-vivo assay of XRT-induced Rad51 foci formation predicts response to PARP-inhibition in ovarian cancer. *Gynecol Oncol, in press*.

- Abstracts presented (since initiation of the award, from a total of 111):

1. **Landen CN**, Goodman B, Han HD, Nick AM, Stone RL, Jennings N, Alvarez R, Coleman R, Lopez-Berestein G, Sood AK. Dual Threat: Targeting the Notch Ligand Jagged1 in Both Tumor and Stroma in Ovarian Cancer. *Proceedings of the 41st Annual Society of Gynecologic Oncologists Meeting*, 2010.
2. Lu C, Chahzad MM, Moreno-Smith M, Lin YG, Jennings NB, Allen JK, Hu W, Stone RL, Matsuo K, **Landen CN**, Coleman RL, Sood AK. Targeting pericytes in ovarian carcinoma. *Proceedings of the American Association of Cancer Research,* 2010*.*
3. Nick AM, Stone RL, Spannuth WA, **Landen CN**, Villares G, Armaiz-Pena G, Carroll AR, Ozpolat B, Tekedereli I, Vivas-Mejia P, Coleman RL, Lopez-Berestein G, Sood AK. Silencing p130cas in ovarian carcinoma induces autophagic cell death. *Proceedings of the American Association of Cancer Research,* 2010*.*
4. Stone RL, Nick AM, Afshar-Kharghan V, Vasquez HG, **Landen CN**, Armaiz-Pena G, Carroll AR, Matsuo K, Shahzad MM, Spannuth WA, Mora EM, King ER, DeGeest K, Lutgendorf S, Sood AK. Mechanisms of paraneoplastic thrombocytosis in ovarian carcinoma. *Proceedings of the American Association of Cancer Research,* 2010*.*
5. **Landen CN**, Goodman B, Nick AM, Stone RL, Miller LD, Mejia PV, Jennings NB, Gershenson DM, Bast RC, Coleman RL, Lopez-Berestein G, and Sood AK. Targeted

therapy against aldehyde dehydrogenase in ovarian cancer. *Proceedings of the American Association of Cancer Research,* 2010.

6. Bevis KS, Steg AD, Katre AA, Ziebarth AA, Zhang K, Conner MG, **Landen CN**. The significance of putative ovarian cancer stem cells to recurrence. *Center for Clinical and Translational Science Annual Scientific Symposium,* 2010. §

7. Ziebarth AA, Steg AD, Bevis KS, Katre AA, Alvarez RA, **Landen CN**. Targeting the Hedgehog pathway reverses taxane resistance in ovarian cancer. *Proceedings of the 42nd Annual Society of Gynecologic Oncologists Meeting*, 2011.

8. Bevis KS, Katre AA, Steg AD, Erickson BK, Frederick PJ, Backes TK, Zhang K, Conner MG, **Landen CN**. Examination of matched primary and recurrent ovarian cancer specimens supports the cancer stem cell hypothesis. *Proceedings of the 42nd Annual Society of Gynecologic Oncologists Meeting*, 2011.

9. Zsebik G, Kim K, Straughn JM, **Landen CN**. Management of Complex Pelvic Masses Using the OVA1 Test: A Decision Analysis. *Proceedings of the 42nd Annual Society of Gynecologic Oncologists Meeting*, 2011.

10. Ziebarth AA, Zheng H, Bradley A, Sakati W, Eier S, Lopez-Berestein G Sood AK, Eblen S, **Landen CN**. The ubiquitin ligase EDD mediates platinum resistance and is a target for therapy in epithelial ovarian cancer. *Proceedings of the 42nd Annual Society of Gynecologic Oncologists Meeting*, 2011.

11. Steg AD, Ziebarth AA, Katre A, **Landen CN Jr**. Targeting hedgehog reverses taxane resistance by Gli-dependent and independent mechanisms in ovarian cancer. *Proceedings of the American Association of Cancer Research,* 2011.

12. Ziebarth A, Steg AD, Katre AA, Zhang K, Nowsheen S, Yang HS, Connor M, Lopez-Berestein G, Sood AK, and **Landen CN**. Targeting Endoglin (CD105) induces apoptosis, improves platinum sensitivity both in vivo and in vitro, and is a potential therapeutic target in epithelial ovarian cancer. *9th International Conference on Ovarian Cancer*, MD Anderson Cancer Center, Houston, TX, 2011. Oral presentation.

13. Ziebarth A, Steg AD, Katre AA, Zhang K, Nowsheen S, Yang SH, Connor MG, Lopez-Berestein G, Sood AK, **Landen CN**. A novel role for the TGF-β co-receptor endoglin (CD105) in platinum resistant epithelial ovarian cancer. *43rd Annual Society of Gynecologic Oncologists Meeting*, 2012.

14. Ziebarth A, Dobbin ZC, Katre AA, Steg AD, Alvarez RD, Conner MG, and **Landen CN**. Primary ovarian cancer murine xenografts maintain tumor heterogeneity and biologically correlate with patient response to primary chemotherapy. *43rd Annual Society of Gynecologic Oncologists Meeting*, 2012.

15. Yang E, Nowsheen S, Cooper T, **Landen CN**, Bonner J. Poly (ADP-Ribose) Polymerase Inhibition Attenuates Radiation-Induced Non-Homologous End-Joining Repair and Augments Cervical Cancer Response to Radiation. *43rd Annual Society of Gynecologic Oncologists Meeting*, 2012.

16. Kim KH, Bevis KS, Walsh-Covarrubias J, Alvarez RD, Straughn JM, **Landen CN**. Optimizing the Research Experience in Gynecologic Oncology Fellowships. *43rd Annual Society of Gynecologic Oncologists Meeting*, 2012.

17. Dobbin ZC, Katre AA, Ziebarth A, Shah MM, Steg AD, Alvarez RD, Conner MG, **Landen** CN. An Optimized Primary Ovarian Cancer Xenograft Model Mimics Patient Tumor Biology and Heterogeneity. *Ovarian Cancer: Prevention, Detection and Treatment of the Disease and its Recurrence*, Pittsburg, PA, 2012. §

18. Zimmerman J, Crittenden F, **Landen CN**, Alvarez RD, Brezovich I, Kuster N, Costa F, Barbault A, Pasche B. Amplitude Modulated Radiofrequency Electromagnetic Fields as a Novel Treatment for Ovarian Cancer. *34th Annual Meeting of the Bioelectromagnetics Society*, Brisbane, Australia, 2012.

19. Dobbin ZC, Katre AA, Ziebarth A, Shah MM, Steg AD, Alvarez RD, Conner MG, **Landen CN**. Use of an optimized primary ovarian cancer xenograft model to mimic patient tumor biology and heterogeneity. *American Society of Clinical Oncology*, 2012.

20. Leath CA, Alvarez RA, **Landen CN**. Determination of Potential Ovarian Cancer Stem Cells in Patients with High Grade Serous Cancer Undergoing Neoadjuvant Chemotherapy. *WRHR Scholars Research Symposium*, Philadelphia, PA, 2012.

21. Walters C, Straughn J, Landen C, Estes J, Huh W, Kim K. Port-Site Metastases after Robotic Surgery for Gynecologic Malignancy. *43rd Annual Society of Gynecologic Oncologists Meeting*, 2013.

22. Shah M, Nowsheen S, Katre A, Dobbin Z, Erickson B, Alvarez R, Konstantinopoulos P, Yang E, Landen C. Towards personalized PARP therapy: XRT-induced Rad51 predicts response to ABT-888 in ovarian cancer. *43rd Annual Society of Gynecologic Oncologists Meeting*, 2013.

23. Ziebarth AJ, Nowsheen S, Steg AD, Shah MM, Katre AA, Dobbin ZC, Sood AK, Conner MG, Yang ES, and **Landen CN**. Endoglin (CD105) is a target for ovarian cancer cell-specific therapy through induction of DNA damage *Proceedings of the American Association of Cancer Research,* 2013.

24. Erickson BK, Steg AD, Dobbin ZC, Katre AA, Alvarez RD, **Landen CN**. Examination of the chemoresistant subpopulation in ovarian cancer identifies DNA repair genes contributing to survival after primary therapy. *Proceedings of the American Association of Cancer Research,* 2013.

25. Erickson BK, Dobbin ZC, Shim E, Alvarez RD, Conner MG, **Landen CN**. Identical TP53 mutations support a common origin for mixed histology epithelial ovarian cancer. *Proceedings of the American Association of Cancer Research,* 2013.

26. Burke MR, Steg AD, Jeong DH, Dobbin ZC, **Landen CN.** GSI-1 synergizes with LDE225 in ovarian cancer cells by inhibiting the proteasome *Proceedings of the American Association of Cancer Research,* 2013.

27. Jackson WP, Katre AA, Dobbin ZC, Steg AD, **Landen CN**. Pathway analysis of chemoresistance in ovarian cancer cell lines. *Proceedings of the American Association of Cancer Research*, 2013.

28. Jimenez H, Zimmerman JW, **Landen CN**, Brezovich I, Chen D, Kuster N, Capstick M, Gong Y, Barbault A, Pasche B. Amplitude-Modulated Radiofrequency Electromagnetic Fields Inhibit Ovarian Cancer cell Growth. Platform presentation. *Bioeletromagnetics Society*, 2013.

29. Dobbin ZC, Katre AA, Shah MM, Erickson BK, Chen H, Alvarez RD, Conner MG, Chen D, **Landen CN**. An Ovarian Patient-Derived Xenograft (PDX) Model to Identify the Chemoresistant population. *AACR Special Conference: Advances in Ovarian Cancer Research: from Concept to Clinic*, 2013

30. Burke M, Steg A, Jeong DH, Dobbin ZC, **Landen CN**. GSI-1 Synergizes with LDE225 In Ovarian Cancer Cells by Inhibiting the Proteasome. *Medical Student Research Day*, 2013.

31. Meredith R, Torgue J, Shen S, Banaga E, Bunch P, **Landen CN**. Phase I Trial of Intraperitoneal Alpha Radioimmunotherapy with ^{212}Pb-TCMC-trastuzumab. *12th International Congress of Targeted Anticancer Therapies*, Washington, DC, March 2014.

32. Walters Haygood CL, Arend RC, Londono-Joshi A, Kurpad C, Katre AA, Conner MG, **Landen Jr. CN**, Straughn JM, Buchsbaum DJ. *Ovarian Cancer Ascites Stem Cell Population Compared oo Primary Tumor. Annual Meeting of the Society of Gynecologic Oncologists*. Tampa, FL. March 2014.

33. Erickson BK, Dobbin ZC, Kinde I, Martin JY, Wang Y, Roden R, Huh WK, Vogelstein B, Diaz LA, **Landen Jr CN**. *Testing the Accuracy of Mutation detection for the Prevention of Ovarian Neoplasia: the TAMPON study. Annual Meeting of the Society of Gynecologic Oncologists*. Tampa, FL. March 2014.

34. Dobbin ZC, Katre AK, Shah MM, Erikson BK, Chen H, Alvarez RD, Conner MG, Chen D, and **Landen CN**. *An ovarian patient-derived xenograft model to identify the chemoresistant population*. 10th Biennial Ovarian Cancer Research Symposium. Seattle, WA. September, 2014.

35. Arend RC, Gangrade A, Walters Haygood CL, Kurpad C, Metge BJ, Samant RS, Li PK, Li Y, Bhasin D, **Landen CN**, Alvarez RD, Straughn JM, Buchsbaum DJ. *Overcoming Platinum Resistance in Ovarian Cancer with Niclosamide*. 10th Biennial Ovarian Cancer Research Symposium. Seattle, WA. September, 2014.

- Grants awarded for which data generated by this work contributed preliminary data:

    - Principle Investigator. *Identifying mediators of chemoresistance in ovarian cancer*. The Norma Livingston Foundation. 50,000, 5/1/2012-4/30/2014.
    - Principle Investigator. *Development of a Personalized Therapy Model in Cervical Cancer*. Pilot Project, SPORE in Cervical Cancer. 9/1/2012 – 8/31/2013. $30,000.
    - Co-Investigator, *Ribosome biogenesis, turnover and function as a therapeutic target for ovarian cancer*, Program Project Grant Pilot Fund, UAB Comprehensive Cancer Center, 8/1/2014 – 7/31/2015, $150,000.
    - Co-Principle Investigator. Predicting response of ovarian cancers to PARP Inhibitors. The ROAR Foundation. 12/14/2012 – 12/13/2014. $100,000.

- Co-Investigator, Using RPS25 to Target the Survival Pathway in Ovarian Cancer, Faculty Development Award, UAB Comprehensive Cancer Center, 3/15/14 – 3/14/15, $40,000.
- Co-Investigator, Glycosylation-dependent mechanisms regulating ovarian tumor cell survival. R01 GM111093, NIH/NIGMS, 4/1/2014 – 3/31/2017, $570,000 total direct.

- Granted with award pending:
  - Co-Investigator, Developing ovarian cancer stem-like cell targeted therapy to prevent disease recurrence. OCRP Pilot Award, 9/1/2014-8/31/2016, $51,532 total direct to Landen lab.

- Funding applied for with decision pending:
  - Co-Investigator, Novel Virotherapy-Based Approaches to Enhance Immunotherapy for Ovarian Cancer. OCRF Program Project Pilot Award.
  - Co-Investigator, Ovarian Cancer Learning Collaborative (OCLC)". OCRF Program Project Pilot Award.
  - Mentor and collaborator, Understanding the role of mitochondria in ovarian cancer chemoresistance. OCRF Liz Tilberis Early Career Award.
  - Co-Investigator, DNA repair enzyme Tyrosyl-DNA Phosphodiesterase I as a novel therapeutic target for ovarian cancer. Department of Defense Pilot Award.
  - Co-Investigator, The DNA repair enzyme tyrosyl-DNA phosphodiesterase I as novel therapeutic target, NIH/NCI R01.
  - Co-Investigator, Targeting mRNA translation to alter the DNA damage response in ovarian cancer, NIH/NCI R21.

CONCLUSIONS:

Our data demonstrate that ALDH1A1-positive cells are more tumorigenic than ALDH1A1-negative cells, contribute to poor patient outcomes, and contribute to chemoresistance. Importantly, these effects can be reversed by downregulating ALDH1A1 expression with nanoparticle-delivered siRNA. Additionally, we have shown that increased tumorigenicity is not only an important ex vivo assessment of CSCs, but that they are clinically significant as well, in that chemoresistant tumors have increased density of ALDH and CD133 cells. This suggests that they represent at least part of the chemoresistant population within a heterogeneous tumor. Importantly, they do not seem to explain the entire story, as there are still many CSC-negative cells present at the conclusion of treatment. Further evaluation of the mechanism stem cell pathways have on chemotherapy resistance have found that endoglin (CD105) and hedgehog mediators Gli1 and Gli2 are strongly associated with resistance. Targeted either of these pathways restored sensitive to paclitaxel or carboplatin *in vitro* and *in vivo*. Although response to

chemotherapy in PDX models is highly variable at the individual gene level, pathway analysis reveals multiple pathways that commonly altered in many tumors. The immune system also appears to mediate a robust response in some tumors. Future work will attempt to delineate which of these pathways is most contributory, and how they may be best targeted to kill the final chemotherapy resistant population in ovarian cancer.

REFERENCES:

1. Bast RC, Jr., Hennessy B, Mills GB. The biology of ovarian cancer: new opportunities for translation. Nat Rev Cancer. 2009 Jun;9(6):415-28. PubMed PMID: 19461667. Pubmed Central PMCID: 2814299.
2. Dalerba P, Cho RW, Clarke MF. Cancer stem cells: models and concepts. Annual review of medicine. 2007;58:267-84. PubMed PMID: 17002552. eng.
3. Rosen JM, Jordan CT. The increasing complexity of the cancer stem cell paradigm. Science. 2009 Jun 26;324(5935):1670-3. PubMed PMID: 19556499. Pubmed Central PMCID: 2873047.
4. Landen CN, Jr., Goodman B, Katre AA, Steg AD, Nick AM, Stone RL, et al. Targeting aldehyde dehydrogenase cancer stem cells in ovarian cancer. Mol Cancer Ther. 2010 Dec;9(12):3186-99. PubMed PMID: 20889728. Pubmed Central PMCID: 3005138.
5. Steg AD, Bevis KS, Katre AA, Ziebarth A, Dobbin ZC, Alvarez RD, et al. Stem cell pathways contribute to clinical chemoresistance in ovarian cancer. Clin Cancer Res. 2012 Feb 1;18(3):869-81. PubMed PMID: 22142828. Pubmed Central PMCID: 3271164.

APPENDICES:

- Appendix 1: Publications
    - **Landen CN**, Goodman B, Katre AA, Steg AD, Nick AM, Stone RL, Miller LD, Mejia PV, Jennings NB, Gershenson DM, Bast RC, Jr., Coleman RL, Berestein G, and Sood AK. Targeting Aldehyde Dehydrogenase Cancer Stem Cells in Ovarian Cancer. *Mol Can Ther* 9(12): 3186-99, 2010. † PMID: 20889728
    - Steg AS, Bevis KS, Katre AA, Ziebarth A, Alvarez RD, Zhang K, Conner M, **Landen CN**. Stem cell pathways contribute to clinical chemoresistance in ovarian cancer. *Clin Can Res*, 18(3):869-81, 2012. PMID: 22142828
    - Steg AD, Katre AA, Goodman B, Han HD, Nick AM, Stone RL, Coleman RL, Alvarez RD, Lopez-Berestein G, Sood AK, **Landen CN**. Targeting the Notch Ligand Jagged1 in Both Tumor Cells and Stroma in Ovarian Cancer. *Clin Can Res*, 17(17): 5674-85, 2011. PMID: 21753153
    - Steg AS, Katre AA, Bevis KS, Ziebarth A, Dobbin ZC, Shah MS, Alvarez RD, **Landen CN**. Smoothened Antagonists Reverse Taxane Resistance in Ovarian Cancer. *Mol Cancer Ther*, 11(7): 1587-97, 2012.
    - Ziebarth AJ, Nowsheen S, Steg AS, Shah MM, Katre AA, Dobbin ZC, Han HD, Lopez-Berestein G, Sood AK, Conner MG, Yang ES, **Landen CN**. Endoglin (CD105) contributes to platinum resistance and is a target for tumor-specific therapy in epithelial ovarian cancer. *Clin Can Res*, 19(1): 170-82, 2013.

- Dobbin ZC and **Landen CN.** Isolation and Characterization of Potential Cancer Stem Cells from Solid Human Tumors - Potential Applications. Curr. Protoc. Pharmacol, 63:14.28.1-14.28.19, 2013. PMID 24510756
- Shah MS and **Landen CN**. Ovarian Cancer Stem Cells: Are They Real and Why are they Important? *Gynecol Oncol,* 132(2): 483-89, 2014. PMID 24321398
- Shah MM, Dobbin ZC, Nowsheen S, Wieglos M, Katre AA, Alvarez RD, Konstantinopoulos PA, Yang ES, **Landen CN**. An ex-vivo assay of XRT-induced Rad51 foci formation predicts response to PARP-inhibition in ovarian cancer. *Gynecol Oncol, in press*.

- Appendix 2: Curriculum Vitae, Charles N. Landen, Jr.

Published OnlineFirst October 1, 2010; DOI:10.1158/1535-7163.MCT-10-0563

Molecular Cancer Therapeutics

Targeting Aldehyde Dehydrogenase Cancer Stem Cells in Ovarian Cancer

Charles N. Landen, Jr, Blake Goodman, Ashwini A. Katre, et al.

Mol Cancer Ther 2010;9:3186-3199. Published OnlineFirst October 1, 2010.

Published OnlineFirst October 1, 2010; DOI:10.1158/1535-7163.MCT-10-0563

Therapeutic Discovery

Molecular Cancer Therapeutics

Targeting Aldehyde Dehydrogenase Cancer Stem Cells in Ovarian Cancer

Charles N. Landen Jr[1], Blake Goodman[2], Ashwini A. Katre[1], Adam D. Steg[1], Alpa M. Nick[2], Rebecca L. Stone[2], Lance D. Miller[3], Pablo Vivas Mejia[4,5], Nicolas B. Jennings[2], David M. Gershenson[2], Robert C. Bast Jr.[4], Robert L. Coleman[2,6], Gabriel Lopez-Berestein[4,6,7], and Anil K. Sood[2,6,7]

Abstract

Aldehyde dehydrogenase-1A1 (ALDH1A1) expression characterizes a subpopulation of cells with tumor-initiating or cancer stem cell properties in several malignancies. Our goal was to characterize the phenotype of ALDH1A1-positive ovarian cancer cells and examine the biological effects of ALDH1A1 gene silencing. In our analysis of multiple ovarian cancer cell lines, we found that ALDH1A1 expression and activity was significantly higher in taxane- and platinum-resistant cell lines. In patient samples, 72.9% of ovarian cancers had ALDH1A1 expression in which the percentage of ALDH1A1-positive cells correlated negatively with progression-free survival (6.05 vs. 13.81 months; $P < 0.035$). Subpopulations of A2780cp20 cells with ALDH1A1 activity were isolated for orthotopic tumor–initiating studies, where tumorigenicity was approximately 50-fold higher with ALDH1A1-positive cells. Interestingly, tumors derived from ALDH1A1-positive cells gave rise to both ALDH1A1-positive and ALDH1A1-negative populations, but ALDH1A1-negative cells could not generate ALDH1A1-positive cells. In an *in vivo* orthotopic mouse model of ovarian cancer, ALDH1A1 silencing using nanoliposomal siRNA sensitized both taxane- and platinum-resistant cell lines to chemotherapy, significantly reducing tumor growth in mice compared with chemotherapy alone (a 74%–90% reduction; $P < 0.015$). These data show that the ALDH1A1 subpopulation is associated with chemoresistance and outcome in ovarian cancer patients, and targeting ALDH1A1 sensitizes resistant cells to chemotherapy. ALDH1A1-positive cells have enhanced, but not absolute, tumorigenicity but do have differentiation capacity lacking in ALDH1A1-negative cells. This enzyme may be important for identification and targeting of chemoresistant cell populations in ovarian cancer. *Mol Cancer Ther; 9(12); 3186–99. ©2010 AACR.*

Introduction

Ovarian cancer was expected to be diagnosed in 21,550 women in 2009 and take the lives of 14,600 women (1). Although ovarian cancer is among the most chemosensitive malignancies at the time of initial treatment (surgery and taxane/platinum-based chemotherapy), most patients will develop tumor recurrence and succumb to chemoresistant disease (2). An understanding of the mechanisms mediating survival of subpopulations of ovarian cancer cells is necessary to significantly improve outcomes in this disease.

In many malignancies, a subpopulation of malignant cells termed cancer stem cells or tumor-initiating cells has been hypothesized to represent the most tumorigenic and treatment-resistant cells within a heterogeneous tumor mass. Defined by their enhanced ability to generate murine xenografts and give rise to heterogeneous tumors that are composed of both tumor-initiating cell and non-tumor-initiating cell populations, these cells may also be more chemoresistant and depend on unique biological processes compared with the majority of tumor cells (3, 4). In ovarian cancer, many of these properties have been identified in populations of CD44/c-kit–positive cells (5), CD133-positive cells (6–8), and Hoechst-excluding cells (the side population; ref. 9).

Among several markers that have been used to identify cancer stem cells, aldehyde dehydrogenase-1A1

Authors' Affiliations: [1]Department of Obstetrics and Gynecology, University of Alabama at Birmingham, Birmingham, Alabama; [2]Department of Gynecologic Oncology, U.T.M.D. Anderson Cancer Center, Houston, Texas; [3]Department of Cancer Biology, Wake Forest University School of Medicine, Winston-Salem, North Carolina; [4]Department of Experimental Therapeutics, U.T.M.D. Anderson Cancer Center, Houston, Texas; [5]The University of Puerto Rico Comprehensive Cancer Center, Rio Piedras, PR; and [6]Center for RNA Interference and Non-Coding RNA; [7]Department of Cancer Biology, U.T.M.D. Anderson Cancer Center, Houston, Texas

Note: Supplementary material for this article is available at Molecular Cancer Therapeutics Online (http://mct.aacrjournals.org/).

Corresponding Author: Charles N. Landen Jr., Department of Obstetrics and Gynecology, The University of Alabama at Birmingham, 1825 University Blvd, 505 Shelby Bldg, Birmingham, AL 35294. Phone: 205-934-0473; Fax: 205-934-0474. E-mail: clanden@uab.edu

doi: 10.1158/1535-7163.MCT-10-0563

Published OnlineFirst October 1, 2010; DOI:10.1158/1535-7163.MCT-10-0563

(ALDH1A1) has been a valid marker among several malignant and nonmalignant tissues (10–20). It holds the attractive distinction of not only being a potential marker of stemness but potentially playing a role in the biology of tumor-initiating cells as well (10). ALDH1A1, 1 of 17 ALDH isoforms, is an intracellular enzyme that oxidizes aldehydes, serving a detoxifying role, and converts retinol to retinoic acid, mediating control on differentiation pathways. The ALDH1A1 population defines normal hematopoietic stem cells, being used to isolate cells for stem cell transplants in patients. Using the ALDEFLUOR assay, a functional flow cytometric assay that identifies cells with active ALDH1A1, tumor-initiating cell-enriched populations have been identified in multiple malignancies (20), including breast (11–14), colon (15, 16), pancreas (17), lung (18), and liver (19). Whether or not the ALDH1A1-active population is enriched for tumor-initiating cells has not been demonstrated for ovarian cancer. More importantly, although ALDH1A1 is implicated in chemoresistance pathways, it is not known whether targeting ALDH1A1 can sensitize resistant cells to chemotherapy and therefore represent a potential target for cancer stem cell–directed therapy. We sought to characterize expression of ALDH1A1 in ovarian cancer cell lines and patient samples, determine whether it contains tumor-initiating cell properties, and examine whether targeting ALDH1A1 sensitizes cells to chemotherapy in both *in vitro* and *in vivo* ovarian cancer models.

Materials and Methods

Cell lines and culture

The ovarian cancer cell lines SKOV3ip1, SKOV3-TRip2, HeyA8, HeyA8MDR, A2780ip2, A2780cp20, IGROV-AF1, and IGROV-cp20 (21, 22) were maintained in RPMI-1640 medium supplemented with 15% fetal bovine serum (Hyclone). SKOV3TRip2 [taxane-resistant, a kind gift of Dr. Michael Seiden (23)] and HeyA8MDR were maintained with the addition of 150 nmol/L of paclitaxel. The HIO-180 SV40-immortalized, nontumorigenic cell line derived from normal ovarian surface epithelium was a kind gift of Dr. Andrew Godwin. All cell lines were routinely screened for *Mycoplasma* species (GenProbe detection kit) with experiments done at 70% to 80% confluent cultures. Purity of cell lines was confirmed with STR genomic analysis, and cells used were always less than 20 passages from the stocks tested for purity.

Whole genomic analysis

RNA was extracted from 3 independent collections of SKOV3ip1 and SKOV3TRip2 cells at 80% confluence with the RNeasy Mini kit (Qiagen). It was subjected to microarray analysis using the Illumina HumanRef-8 Expression BeadChip, which targets ~24,500 well-annotated transcripts. Microarray data were normalized by the cubic-spline method (24) using the Illumina BeadStudio software. The significance of differentially expressed genes was determined by Student's t test followed by correction for false discovery (25). A heat map was generated using Cluster 3.0 and Java TreeView software. The array data have been registered with GEO (accession #GSE23779) for public access.

Western blot analysis

Cultured cell lysates were collected in modified radioimmunoprecipitation assay lysis buffer with protease inhibitor cocktail (Roche) and subjected to immunoblot analysis by standard techniques (26) using anti-ALDH1A1 antibody (BD Biosciences) at 1:1,000 dilution overnight at 4°C, or anti–β-actin antibody (Sigma Chemical) at 1:2,000.

Immunohistochemical staining and clinical correlations

Immunohistochemical (IHC) analysis was done on formalin-fixed, paraffin-embedded samples, using standard techniques (26). For ALDH1A1, antigen retrieval was in citrate buffer for 45 minutes in an atmospheric pressure steamer, using anti-ALDH1A1 antibody (BD Biosciences) at 1:500 dilution in Cyto-Q reagent (Innovex Biosciences) overnight at 4°C. Primary antibody detection was with Mach 4 HRP polymer (Biocare Medical) for 20 minutes at room temperature, followed by diaminobenzidine incubation. After IHC staining, the number of tumor cells positive for ALDH1A1 was counted and expressed as a percentage of all tumor cells by an examiner blinded to clinical outcome. Patient samples were categorized as having low (<1%), intermediate (1%–20%), or high (21%–100%) ALDH1A1 expression. The IHC analysis was done on samples collected at primary debulking surgery on 65 untreated patients with stage III–IV, high-grade papillary serous adenocarcinoma; with institutional review board approval, clinical information was collected. Progression-free and overall survival were plotted with the Kaplan–Meier method for patients in each group of ALDH1A1 expression and compared with the log-rank statistic by using PASW 17.0.

For dual staining of ALDH1A1 and CD68 (for macrophages), staining for ALHD1A1 was done first as previously, followed by exposure to anti-CD68 antibody (1:4,000; Dako) and goat anti-mouse-AP (Jackson Immunoresearch). AP was developed with Ferangi Blue chromagen kit (Biocare Medical). For dual staining of ALDH1A1 and hypoxic tumor regions, mice bearing SKOV3TRip2 xenografts were injected with 60 mg/kg of Hypoxyprobe-1 reagent (HPI, Inc.). Tumor sections in FFPE were subjected to antigen retrieval as above, followed by exposure to fluorescein isothiocyanate (FITC)-conjugated anti-hypoxyprobe-1 mouse antibody (1:50) overnight at 4°C. This was detected with HRP-conjugated anti-FITC antibody (1:500, Jackson Immunoresearch) and DAB resolution. Endogenous murine

Published OnlineFirst October 1, 2010; DOI:10.1158/1535-7163.MCT-10-0563

IgG was then blocked with anti-mouse IgG F(ab')2 fragments (Jackson ImmunoResearch), and ALDH1A1 stained as above using AP-conjugated anti-mouse IgG and Ferangi Blue chromagen.

ALDEFLUOR assay and tumorigenicity in limiting dilutions

Active ALDH1A1 was identified with the ALDEFLUOR assay according to manufacturer's instructions (StemCell Technologies). The ALDH1A1-positive population was defined by cells with increased FITC signal, with gates determined by diethylaminobenzaldehyde (DEAB)-treated cells (DEAB being an inhibitor of ALDH1A1 activity). For tumorigenicity experiments, the ALDEFLUOR-positive population from A2780cp20 cells were sorted with a FACS Aria II flow cytometer (BD Biosciences) and reanalyzed to confirm at least 95% positivity. Collected cells were washed and resuspended in Ca^{2+}- and Mg^{2+}-free Hanks' balanced salt solution (HBSS; Gibco) and injected intraperitoneally into NOD-SCID mice in limiting dilutions . Mice were followed for 1 year or until tumors formed, then sacrificed and tumor confirmed histologically. For flow cytometric analysis of these tumors, xenografts were dissociated mechanically with a scalpel, passed through a 70-mm filter to collect single-cell suspensions, with the remaining clumped cells incubated in 0.5 mg/mL of collagenase and 0.0369 mg/mL of hyaluronidase (Calbiochem) for 30 minutes at 37°C. These chemically digested cells were again filtered through a 70 μm filter, added to the initial collection and subjected to the ALDEFLUOR assay. ALDEFLUOR-positive cells or negative cells were then injected into additional mice ($n = 5$) to examine maintenance of tumorigenicity.

Primary xenograft development

With institutional IRB and IACUC approval, excess of freshly collected omental metastases from advanced stage ovarian cancer patients were acquired after tissue required for diagnosis and management had been sequestered. 3 to 4-mm^3 sections were cut and implanted subcutaneously on the dorsal aspect of NOD-SCID mice. Adjacent sections were submitted for histologic analysis to confirm tumor. Tumors were measured in 2 dimensions twice per week. After progressive growth was noted, mice with formed tumors were treated with vehicle or cisplatin (7.5 mg/kg weekly by intraperitoneal administration). Mice were treated for 8 weeks and then sacrificed, and tumors were harvested.

SiRNA downregulation *in vitro*

To examine downregulation of ALDH1A1 with siRNA, cells were exposed to 2.5 μg/mL of control siRNA (target sequence 5′-AATTCTCCGAACGTGTCACGT-3′; Sigma), or 1 of 3 tested ALDH1A1-targeting constructs (SASI_Hs01_00244055, 00244056, or 00303091; Sigma), at a 1:3 siRNA (μg) to Lipofectamine 2000 (μL) ratio. Lipofectamine 2000 and siRNA were incubated for 20 minutes at room temperature, added to cells in serum-free RPMI to incubate for 6 hours, followed by the addition of 15% FBS/RMPI thereafter. Transfected cells were grown at 37°C for 48 to 72 hours and then harvested for Western blot.

Assessment of cell viability with chemotherapy IC_{50} and cell-cycle analysis

To a 96-well plate, 2,000 cells per well were exposed to increasing concentrations of docetaxel or cisplatin in triplicates. Viability was assessed by 2-hour incubation with 0.15% MTT (Sigma) and spectrophotometric analysis at OD_{450} (optical density at 450 nm). For effects of siRNA on IC_{50}, cells were incubated with siRNA for 24 hours in 6-well plates and then replated in 96-well plates, and chemotherapy was administered after 12 hours to allow attachment. IC_{50} was determined by finding the dose at which the drug had 50% of its effect and calculated by the following equation: $IC_{50} = [(OD_{450max} - OD_{450min})/2) + OD_{450min}]$. Test of synergy was according to the Loewe additivity model (27) and calculated by the following equation: combination index (CI) = $[D_1/D_{x1}] + [D_2/D_{x2}]$ (where a CI of 1 suggests an additive effect, <1 suggests synergy, and >1 suggests antagonism). For cell-cycle analysis, cells were transfected with siRNA as described previously for 72 hours, trypsinized, washed in PBS, and fixed in 75% ethanol overnight. Cells were then centrifuged, washed twice in PBS, and reconstituted in PBS with 50 μg/mL of propidium iodide. Propidium iodide fluorescence was assessed by flow cytometry, and percentage of cells in each cycle was calculated by the cell-cycle analysis module for FlowJo.

Orthotopic ovarian cancer model and *in vivo* delivery of siRNA

For orthotopic therapy experiments using ovarian cancer cell lines, female athymic nude mice (NCr-nu) were purchased from the National Cancer Institute and cared for in accordance with guidelines of the American Association for Accreditation of Laboratory Animal Care. For all *in vivo* experiments, trypsinized cells were suspended in HBSS and 10^6 cells injected intraperitoneally into 40 mice per experiment. After 1 week, mice were randomized to: a) control siRNA/DOPC, b) control siRNA/DOPC plus chemotherapy, c) ALDH1A1-targeting siRNA/DOPC, or d) chemotherapy plus ALDH1A1-targeting siRNA/DOPC. SiRNA/DOPC dose was 5 μg twice per week in a volume of 100 μL intraperitoneally. Chemotherapy doses were docetaxel 35 μg intraperitoneally weekly for SKOV3TRip2, or cisplatin 160 μg intraperitoneally weekly for A2780cp20. Mice were treated for 4 weeks before sacrifice and tumor collection. SiRNA was incorporated into 1,2-dioleoyl-*sn*-glycero-3-phosphatidylcholine (DOPC) neutral nanoliposomes as previously described (28), lyophilized, and reconstituted in 0.9% saline for administration.

Published OnlineFirst October 1, 2010; DOI:10.1158/1535-7163.MCT-10-0563

Statistical analysis

Comparisons between treatment groups of tumor weight was carried out with the 2-tailed Student's *t* test, if tests of data normality were met. Those represented by alternate distribution were examined by Mann–Whitney *U* statistic. Differences between groups were considered statistically significant at $P < 0.05$. The number of mice per group ($n = 10$) was chosen as directed by a power analysis to detect a 50% decrease in tumor growth with β error of 0.2. Progression-free and overall survival in patients with 3 categories of ALDH1A1 staining were compared by plotting with the Kaplan–Meier method and assessing for statistical differences with the log-rank statistic, using PASW 17.0 software.

Results

Expression profiling of chemoresistant ovarian cancer cell lines

To discover genes mediating taxane resistance, expression profiling of parental SKOV3ip1 and taxane-resistant SKOV3TRip2 cells was done with microarray analysis using the Illumina HumanRef-8 Expression BeadChip. The SKOV3TRip2 cell line was previously generated through progressive exposure to paclitaxel (designated SKOV3TR; 23) and then passaged intraperitoneally in mice for 2 generations to select populations with enhanced tumorigenicity. Similarly, SKOV3ip1 were derived from SKOV3 parental cells to select for cells with enhanced tumorigenicity. We found 34 genes to be upregulated more than 10-fold in SKOV3TRip2 (Fig. 1), among which was ALDH1A1, with a 92.7-fold increase ($P = 0.0025$). Twenty genes were more than 10-fold increased in SKOV3ip1. SKOV3TRip2 cells were confirmed to have approximately 3,000-fold increased resistance to docetaxel, as measured by MTT IC_{50} (62.5 nmol/L vs. 0.02 nmol/L; Fig. 2A).

ALDH1A1 expression in ovarian cancer cell lines

To confirm an increase in ALDH1A1 expression/activity in SKOV3TRip2 and examine expression in other ovarian cancer cell lines, 4 pairs of parental and chemoresistant cell lines were examined: SKOV3ip1/SKOV3-TRip2; HeyA8/HeyA8MDR (multidrug resistant); A2780ip2/A2780cp20 (10-fold increased cisplatin resistance); and IGROV-AF1/IGROV-cp20 (5-fold increased cisplatin resistance). In addition, an immortalized, nontransformed cell line derived from normal ovarian surface epithelium, HIO-180, was examined. We found that expression of total ALDH1A1, as measured by Western blot analysis, was in each case higher in the chemoresistant cell line, with the exception of HeyA8/HeyA8MDR, in which ALDH1A1 was low to absent in both (Fig. 2B). To examine whether ALDH1A1 was not only present but also active, we subjected cells to flow cytometric analysis using the ALDEFLUOR assay. This functional assay predominantly identifies active ALDH1A1 by conversion of a chemical to a fluorochrome. The presence of a subpopulation of ALDH1A1-active cells could be readily identified in SKOV3TRip2 (58% of the total population) and A2780cp20 (2.2%) but not in their parental cell line (Fig. 2C). Furthermore, the strong shift in fluorescent signal in some cells suggests that there was not simply a general increase in expression in all cells but rather separate populations of ALDH1A1-positive and -negative cells. This was confirmed by immunohistochemistry, which showed distinct populations of ALDH1A1-positive or -negative cells in A2780cp20 and SKOV3TRip2 cells but not in the parental A2780ip2 and SKOV3ip1 cells in culture (Fig. 2D). Finally, we observed that this heterogeneous profile was maintained in tumors. After intraperitoneal injection of SKOV3TRip2 cells into nude mice and collection of the resulting orthotopic tumor implants, IHC staining of for ALDH1A1 showed both positive and negative ALDH1A1 subpopulations (Fig. 2E). To examine whether this heterogeneity in expression was due to differential expression in hypoxic regions, a tumor-bearing mouse was injected with hypoxyprobe reagent and sacrificed after 30 minutes. The tumor was costained with ALDH1A1 and antihypoxyprobe antibody. We found that the ALDH1A1-positive cells were not preferentially localized to hypoxic regions in the tumor, with only 1.5% of ALDH1A1-positive cells concurrently positive for hypoxyprobe and only 3.3% of hypoxyprobe-positive cells also positive for ALDH1A1 ($P < 0.01$; Fig. 2F).

ALDH1A1 expression in human ovarian cancer specimens

To determine the pattern of ALDH1A1 expression and possible correlations with chemoresistance in patients, we next examined ALDH1A1 expression in 65 untreated, high-grade papillary serous stage III–IV ovarian cancer patient specimens (patient characteristics in Table 1). We found a wide range of expression patterns (Fig. 3A). There was no ALDH1A1 in tumor cells in 27.1% of samples. ALDH1A1 expression was noted in 1% to 20% of cells in 44% of tumors, representing the largest cohort of expression patterns. As in xenografts from cell lines, expression was typically strong in some cells and negative in others, signifying distinct heterogeneity in the tumor. There was no distinct histologic pattern to the location of the positive cells (such as around vasculature or on the leading edge of the tumor), but positive cells did tend to cluster together. The remaining tumors (28.9%) all had between 21% and 100% staining, with 10% of all patients having strong ALDH1A1 expression in nearly 100% of their tumor cells. To confirm that ALDH1A1 expression was not being mistakenly identified in tumor-infiltrating macrophages, several snap-frozen samples were dual stained for ALDH1A1 and CD68. Although images are not as detailed as those from paraffin-embedded samples, dual staining clearly shows that the majority of macrophages (blue) are ALDH1A1 negative and therefore the heterogeneous ALDH1A1 positivity in tumors is not simply due to detection of macrophage infiltration (Fig. 3B).

Published OnlineFirst October 1, 2010; DOI:10.1158/1535-7163.MCT-10-0563

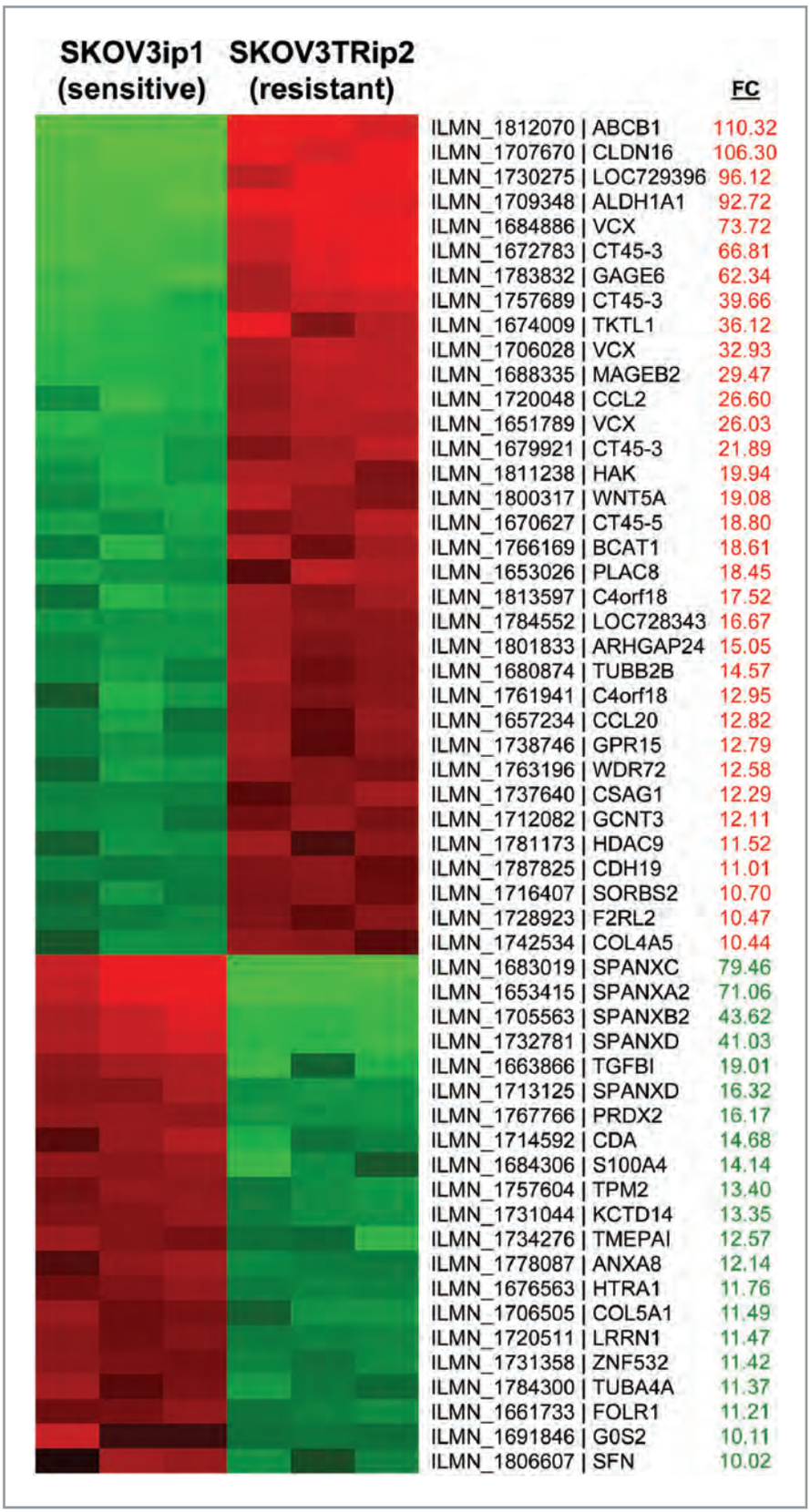

Figure 1. Comparison of whole genome expression profiling between SKOV3TRip2 and SKOV3ip1 cell lines. Total RNA from the SKOV3TRip2 and SKOV3ip1 cell lines were subjected to whole genome expression profiling using the Illumina platform. The genes with a greater than 10-fold increase in SKOV3TRip2 are shown in red, whereas those with a greater than 10-fold increase in SKOV3ip1 are shown in green. FC, fold change.

Published OnlineFirst October 1, 2010; DOI:10.1158/1535-7163.MCT-10-0563

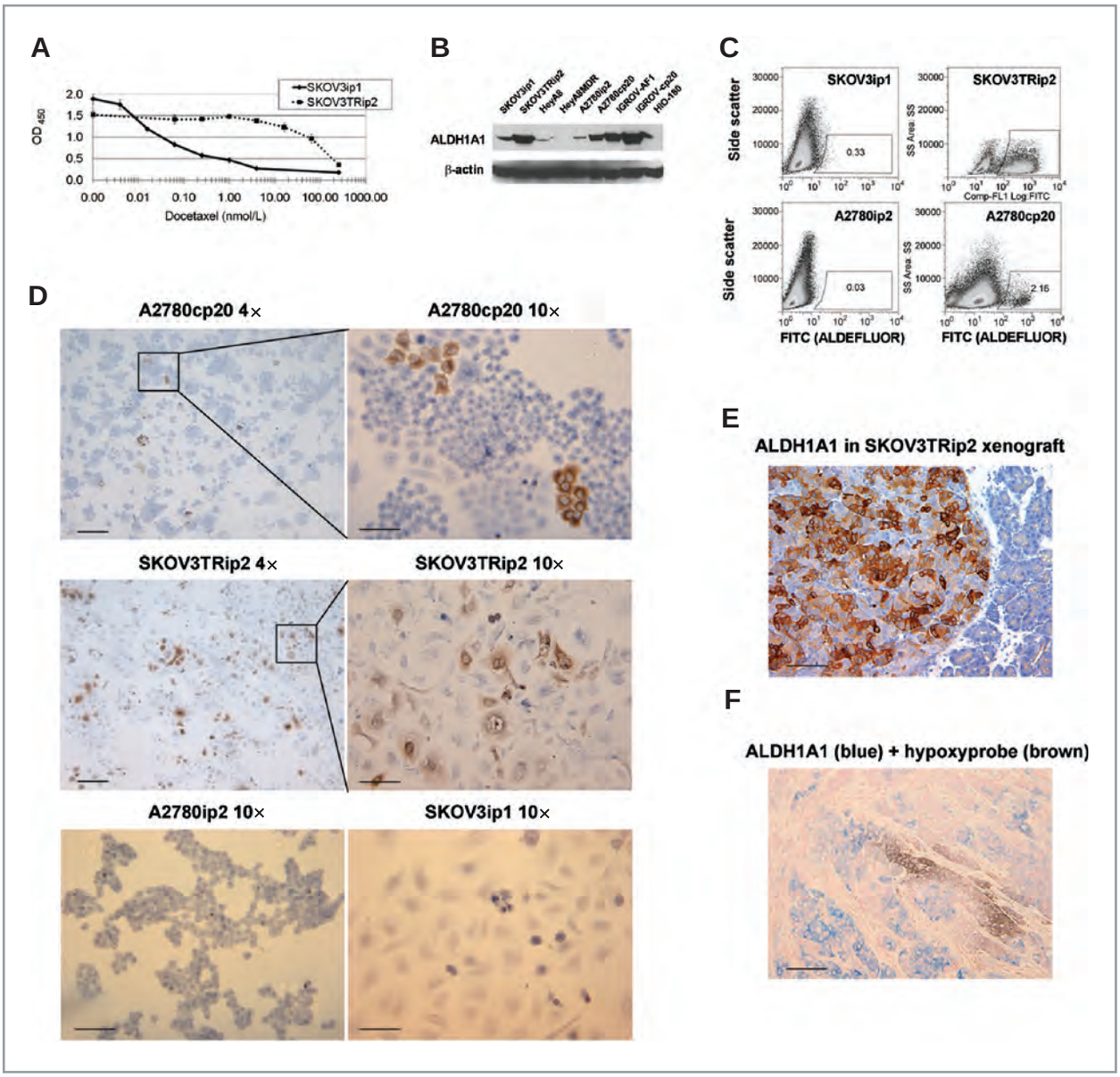

Figure 2. ALDH1A1 expression in ovarian cancer cell lines. A, as measured with the MTT viability assay, the SKOV3TRip2 ovarian cancer cell line has a docetaxel IC_{50} approximately 3,000-fold higher than that of its parental SKOV3ip1 cell line. B, expression of ALDH1A1 by Western blot in 4 pairs of chemosensitive and chemoresistant ovarian cancer cell lines and the nontransformed HIO-180 normal ovarian surface epithelium line. In all cases except HeyA8/HeyA8MDR, in which both lines had minimal expression, the chemoresistant line had increased ALDH1A1 expression. C, as measured by the ALDEFLUOR assay, the A2780cp20 (cisplatin resistant) and SKOV3TRip2 (taxane resistant) also contained a higher percentage of cells with functional ALDH1A1. D, this was confirmed by the IHC analysis for ALDH1A1 on these cell lines *in vitro* in which individual cells appeared either negative or strongly positive, demonstrating heterogeneity of ALDH1A1 expression in the cell line population. A low-power (4×) view gives an appreciation for the distinct colonies of ALDH1A1-positive cells, whereas examination at high power (10×) shows the definitive ALDH1A1-positive or -negative nature of individual A2780cp20 and SKOV3TRip2 cells but an absence of ALDH1A1 in parental A2780ip2 and SKOV3ip1 lines. E, this heterogeneity is also present in tumor xenografts, as seen by the IHC analysis for ALDH1A1 in SKOV3TRip2 tumors grown in mice (intraperitoneal location is confirmed by the presence of normal pancreatic tissue on the right side of the slide). F, ALDH1A1 expression is not limited to hypoxic cells, as shown in xenografts collected from mice given the hypoxyprobe reagent and subjected to the co-IHC analysis for ALDH1A1 (in blue) and the hypoxyprobe by-product (in brown). Scale bars represent 50 μm in 10× views, 100 μm in 4× views (E, F).

Correlation of ALDH1A1 expression with clinical outcomes

To determine whether ALDH1A1 expression correlated with clinical outcomes, we compared progression-free survival and overall survival from patient samples described earlier (and in Table 1) in cohorts with no ALDH1A1 expression, 1% to 20% expression, and greater than 20% expression, as this grouping allowed similar

Published OnlineFirst October 1, 2010; DOI:10.1158/1535-7163.MCT-10-0563

Table 1. Characteristics of patients tested for ALHD1A1 expression ($n = 65$)

Characteristic	Percentage or average (range)
Age at diagnosis	62.2 (34–89)
Caucasian race	71%
Pretreated with chemotherapy	0%
Stage	
III	74%
IV	26%
Ca125	3,071 (161–9,600)
Ascites	87%
Optimal debulking	74%
Papillary serous histology	100%
Platinum/taxane primary therapy	96%
Progression-free survival, mo	14.2 (1.7–108)
Overall survival, y	2.5 (0.2–11.8)
ALDH1A1 staining	
Absent	27.1%
1%–20% of cells	44.0%
21%–100% of cells	28.9%

Abbreviation: Ca125, cancer antigen 125

numbers between groups. Patients with greater than 20% ALDH1A1-positive cells had a shorter median progression-free survival (6.1 months) than those with 1% to 20% ALDH1A1-positive cells (8.2 months) or those with no ALDH1A1-positive cells (13.8 months), which was statistically significant according to the log-rank test ($P = 0.035$; Fig. 3C). Overall survival, which reflects resistance to multiple chemotherapeutic agents used in the recurrent setting, showed a trend toward a poor outcome with increasing ALDH1A1 expression (median overall survival 1.09 vs. 1.84 vs. 2.32 years), but the trend was not statistically significant ($P = 0.33$; Supplementary Fig. 1).

Preferential survival of ALDH1A1-positive cells with cisplatin treatment

To determine whether the ALDH1A1-positive cells have preferential survival in the tumor microenvironment with platinum treatment, we established mouse xenografts from primary patient samples by subcutaneously implanting a freshly collected tumor specimen into NOD-SCID mice. A subcutaneous rather than orthotopic model was used so that tumor growth and response could be accurately measured. Once tumors were established and growing, and achieved a size of approximately 1 cm^3, intraperitoneal administration of 7.5 μg/kg of cisplatin weekly was initiated whereas only vehicle was administered to controls (Fig. 3D). When tumors grew to a size of 2 cm^3 in controls, having remained stable with cisplatin treatment, they were harvested and sections stained for ALDH1A1 expression. Baseline expression of ALDH1A1 in the implanted tumor was seen in approximately 1% of cancer cells and similar levels were found in growing xenografts in untreated mice (Fig. 3E). A significant increase in the percentage of ALDH1A1-positive cells was, however, noted in cisplatin-treated xenografts to 38% ($P < 0.001$; Fig. 3E). Consistent with this, the ALDEFLUOR assay on the dissociated tumor showed that 0.6% of cells from untreated tumors were ALDEFLUOR positive whereas 17.6% of cells from cisplatin-treated tumors were ALDEFLUOR positive. Because the treated xenograft in this case did not regress, but rather remained stable in size, cisplatin exposure may have induced ALDH1A1 expression in surviving cells in addition to preferential killing of ALDH1A1-negative cells.

Tumor-initiating capacity of ALDH1A1-positive ovarian cancer cells

In breast and other cancers, the ALDH1A1-active cancer cells have been shown to represent a tumor-initiating population (10–19). To determine whether this were the case in ovarian cancer, we sorted ALDH1A1-positive and -negative populations from the A2780cp20 cell line using the ALDEFLUOR assay and injected cells intraperitoneally into NOD-SCID mice in limiting dilutions to determine tumor-initiating potential. As summarized in Table 2, ALDEFLUOR-positive cells exhibited increased tumorigenic potential, with 100% tumor initiation after the injection of 100,000, 25,000, or 5,000 cells, and 1 tumor was established after the injection of 1,000 cells. ALDEFLUOR-negative cells could form tumors, although at a lower rate: 2 of 5 mice formed tumors after the injection of 25,000 or 100,000 cells and no tumors formed after the injection of 5,000 or 1,000 cells. Mice were followed for 1 year after injection and thorough necropsies were performed in remaining mice to confirm that tumors failed to develop. The TD_{50}, or dose of cells required to permit tumor formation in 50% of animals, was 50-fold lower with ALDEFLUOR-positive cells. Perhaps, more striking was the makeup of these tumors. One requirement of a tumor-initiating population is that it has the capacity to give rise to heterogeneous tumors, composed of both stem cell and non–stem cell populations, therefore

Table 2. Tumorigenicity of ALDEFLUOR-positive and negative cells

A2780cp20 cells injected intraperitoneally	1,000,000	250,000	100,000	25,000	5,000	1,000	Serial transplantation rate
ALDEFLUOR negative	5/5	4/5	2/5	2/5	0/5	0/5	0/5
ALDEFLUOR positive			5/5	5/5	5/5	1/5	5/5

Published OnlineFirst October 1, 2010; DOI:10.1158/1535-7163.MCT-10-0563

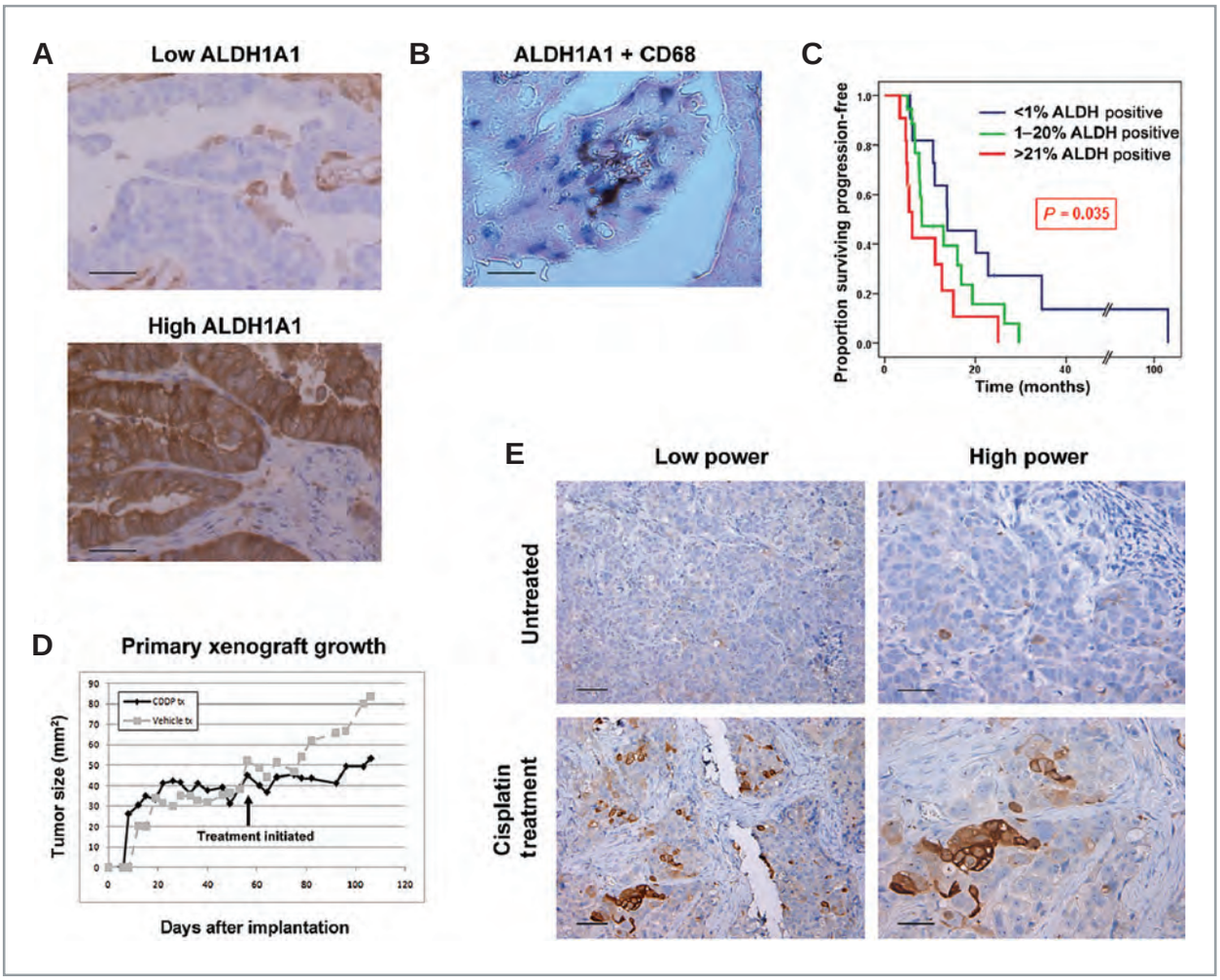

Figure 3. ALDH1A1 expression in ovarian cancer patients. ALDH1A1 was assessed by the IHC analysis in 65 high-grade stage III–IV papillary serous ovarian cancer patients. A, several expression patterns were seen, including absent, spotty (e.g., Low ALDH), and diffuse (High ALDH) staining. Consistent with staining in cell lines, both strongly positive and negative populations were noted. B, to confirm the spotty ALDH1A1 pattern was not identifying infiltrating macrophages, the co-IHC analysis on frozen tissue for ALDH1A1 (brown) and CD68 (a pan-macrophage marker, blue) was done. C, patients were stratified into less than 1%, 1%–20%, and greater than 20% ALDH1A1 expression, and progression-free and overall survival was plotted by the Kaplan–Meier method and tested for statistical significance by the log-rank test. There was a significantly shorter progression-free survival in patients with increasing ALDH1A1 expression. D, mice with established primary subcutaneous xenografts were treated with vehicle or cisplatin for 5 weeks. E, tumors from these mice were harvested and subjected to IHC analysis for ALDH1A1. Tumors treated with cisplatin showed a significant increase in the number of ALDH1A1-positive tumors cells. Magnification at low and high powers is shown. Scale bars represent 50 mm in panels A, B, and High-power images of E, and 100 mm in Low-power images of E.

demonstrating multipotent differentiation potential. This was noted in tumors that formed after the injection of ALDEFLUOR-positive cells. In all 16 of these tumors, a strongly positive ALDH1A1 population was noted in the minority of the sample, on average 4.7% of the tumor (range 2.4%–6.1%; Fig. 4A). However, no ALDEFLUOR-positive cells were found in the tumors that formed after the injection of ALDH1A1-negative cells (Fig. 4B). This was confirmed by the IHC analysis (Fig. 4C and D). This argues against the idea that tumors are formed because of contamination with ALDEFLUOR-positive cells or that ALDH1A1 expression is simply induced by the tumor microenvironment regardless of the capacity of the cells.

This difference in the capacity to generate ALDEFLUOR-positive cells was also noted *in vitro*. SKOV3TRip2 cells sorted into ALDEFLUOR-positive and -negative populations were cultured separately, and the ALDEFLUOR assay was done on the different populations at 24, 48, and 72 hours (Fig. 4E and F). Of the ALDEFLUOR-positive cells, the population gradually reverted to 75.3%, 54.2%, and 51.4% ALDEFLUOR-positive cells, respectively, for each time point. However, the ALDEFLUOR-negative cells could not produce any ALDEFLUOR-positive cells.

To confirm that the ALDEFLUOR-positive cells from tumors maintained tumorigenicity, these populations

Published OnlineFirst October 1, 2010; DOI:10.1158/1535-7163.MCT-10-0563

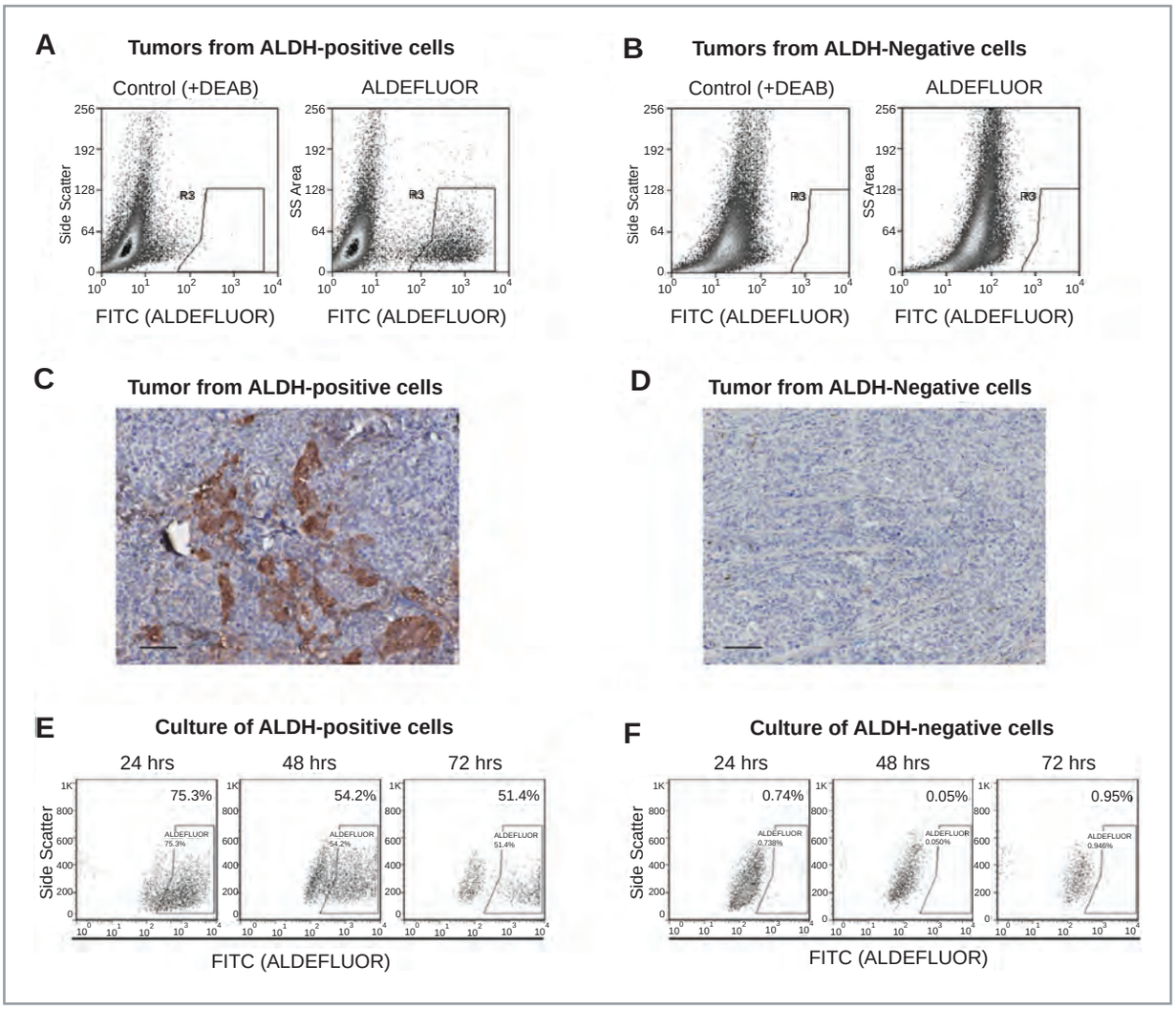

Figure 4. ALDH1A1 populations in A2780cp20 xenografts. Intraperitoneal tumors that developed after the injection of ALDEFLUOR-positive or -negative A2780cp20 cells were assessed for ALDH1A1 composition. A, tumors that formed after the injection of purely ALDEFLUOR-positive cells showed both ALDEFLUOR-positive and -negative populations and recapitulated the tumor-initiating cells phenotype of having a small (2.4%–6.1%) percentage of ALDEFLUOR-positive cells. B, interestingly, tumors that formed after the injection of purely ALDEFLUOR-negative cells contained only ALDEFLUOR-negative cells, showing an absence of capacity for differentiation, at least in terms of ALDEFLUOR positivity. C and D, this expression discrepancy was also noted on the immunohistochemical analysis for ALDH1A1 from these samples. Scale bars represent 100 μm. Similarly, *in vitro*, SKOV3TRip2 ALDEFLUOR-positive cells give rise to both ALDEFLUOR-positive and -negative cells, (E) reestablishing baseline levels at 48 hours, whereas ALDEFLUOR-negative cells cannot give rise to ALDEFLUOR-positive cells (F).

were sorted and reinjected intraperitoneally into mice and continued to form tumors at 100% rate with 25,000 cells injected. However, ALDEFLUOR-negative cells from the tumors forming after ALDEFLUOR-negative cells were injected did not form tumors. Taken together, these studies show that ALDEFLUOR-positive cells have increased but not absolute tumorigenicity, but they do have a differentiation capacity and maintenance of the tumorigenic phenotype that is absent in ALDEFLUOR-negative cells.

In an effort to determine whether ALDEFLUOR-positive cells, freshly collected from ovarian cancer patients, have similar tumorigenicity, we have sorted ALDEFLUOR-positive and -negative cells from 5 separate ovarian cancer patients, dissociating tumors metastatic to the omentum at the time of primary debulking surgery. In this cohort, 1.5% to 17.8% of cells were ALDEFLUOR positive. A total of 25,000 ALDEFLUOR-positive cells, 100,000 ALDEFLUOR-negative cells, or 100,000 unsorted cells were injected intraperitoneally into 5 mice per group per patient. Unfortunately, no tumors formed in any mice, highlighting the difficulty of tumorigenicity studies in primary ovarian cancer samples dissociated to single cell suspensions.

To preliminarily determine whether there is an overlap between the ALDEFLUOR-positive population and other

Published OnlineFirst October 1, 2010; DOI:10.1158/1535-7163.MCT-10-0563

markers of putative stem cells in ovarian cancer, these 5 samples were also profiled for CD44, c-kit, and CD133. We were not able to identify a convincing positive c-kit population from any sample. CD133-positive cells made up an average of 3.1% of total tumor cells (range, 0.6%–5.7%) and were greater than 80% of ALDEFLUOR positive in all 5 samples (mean, 86.7%; range, 81.5%–100%). CD44 was more commonly expressed, representing an average of 45.7% of tumors (but with a very broad range of 2.4%–98.2%). Of the CD44-positive cells, 75.4% were also ALDEFLUOR positive (range, 46.6%–88.8%). Similarly, the SKOV3TRip2 line has 82% CD44-positive cells, and of these, 74% were ALDEFLUOR positive. Although a great number of samples will need to be examined to fully delineate whether multiple marker–positive cells can more accurately define the most pure tumorigenic cell, there is certainly overlap in marker expression. There are both double-positive CD44/ALDEFLUOR and CD133/ALDEFLUOR-positive populations that may prove more discerning as cancer stem cell populations, and ongoing studies could assess this distinction. Interestingly, the A2780cp20 cell line is completely negative for CD44 and the HeyA8 cell line is negative for ALDH1A1/ALDEFLUOR, despite the fact that both are highly tumorigenic. This highlights the fact that these cannot be the sole mediators of tumorigenicity in mice.

Downregulation of ALDH1A1 sensitizes ovarian cancer cells to chemotherapy

Given the association of ALDH1A1 expression with chemoresistant cell lines and a decreased progression-free survival in ovarian cancer patients, we asked whether downregulation of ALDH1A1 could sensitize resistant cells to chemotherapy. Two different siRNA constructs were identified that reduced ALDH1A1 expression by greater than 80% (Fig. 5A). Reduction in the ALDEFLUOR population was confirmed (Fig. 5B). SKOV3TRip2 or A2780cp20 cells were exposed to ALDH1A1-targeting siRNA (ALDH1A1 siRNA) or control siRNA for 24 hours before replating and adding increasing concentrations of docetaxel or cisplatin, respectively. Cell viability 4 days after the addition of chemotherapy was assessed with the MTT assay. In SKOV3TRip2 cells, siRNA-ALDH1A1 alone reduced viability by 49% (Fig. 5C; $P < 0.001$). Downregulation of ALDH1A1 also reduced the docetaxel IC_{50} from 178 to 82 nmol/L. In A2780cp20, the effects of ALDH1A1 downregulation alone were modest (Fig. 5D; reduced viability by 15.9%, $P = 0.040$) but sensitization to cisplatin was considerable, with a decrease in the IC_{50} from 5.1 to 2.0 μmol/L. Tests for synergy suggest moderate synergy in each cell line (CI = 0.82 for SKOV3TRip2 and 0.75 for A2780cp20). The contrasting effects of ALDH1A1-siRNA alone are consistent with the number of ALDH1A1-active cells in these cell lines, with SKOV3TRip2 cell lines having 50% to 60% of ALDEFLUOR-positive cells and A2780cp20 having just 2% of 3%. To determine how ALDH1A1 downregulation alone may affect cell growth, cell-cycle analysis was done in a separate experiment. We found that ALDH1A1 downregulation induced an accumulation of SKOV3TRip2 cells in S and G_2 phases ($P < 0.001$; compared with control siRNA) but had only minimal effects on the cell cycle of A2780cp20 cells (Fig. 5E).

There are no known inhibitors of ALDH1A1 for *in vivo* studies. Therefore, we used a method for delivery of siRNA *in vivo*, using DOPC nanoparticles. We and others (28–32) have previously shown delivery of siRNA incorporated into DOPC nanoliposomes to the tumor parenchyma with subsequent target downregulation. In this study, nude mice were injected intraperitoneally with either SKOV3TRip2 or A2780cp20 cells and randomized to 4 treatment groups to begin 1 week after cell injection: a) control siRNA in DOPC, delivered intraperitoneally twice per week; b) docetaxel 35 mg, delivered intraperitoneally weekly (for SKOV3TRip2 model) or cisplatin 160 μg, delivered intraperitoneally weekly (for A2780cp20 model); c) ALDH1A1-siRNA in DOPC, intraperitoneally twice per week; or d) ALDH1A1-siRNA in DOPC plus docetaxel (for SKOV3TRip2) or cisplatin (for A2780cp20). After 4 weeks of treatment, mice were sacrificed and total tumor weight recorded. The IHC analysis confirmed reduced ALDH1A1 expression with ALDH1A1-siRNA/DOPC treatment compared with controls but not with chemotherapy alone (Supplementary Fig. 2; too little tissue was available to examine with the ALDEFLUOR assay). In SKOV3TRip2 xenografts (Fig. 5F), there was a nonsignificant reduction of 37.0% in tumor growth with docetaxel treatment ($P = 0.17$) and of 25.0% with ALDH1A1 siRNA treatment ($P = 0.38$) compared with control siRNA/DOPC. The observation that ALDH1A1 downregulation alone significantly decreased SKOV3TRip2 growth *in vitro* but was less pronounced *in vivo* suggests that tumor microenvironment factors such as supporting stromal cells may be able to protect cells from ALDH1A1 depletion. However, the combination of ALDH1A1 siRNA and docetaxel resulted in significantly reduced growth by 93.6% compared with control siRNA ($P < 0.001$), by 89.8% compared with docetaxel plus control siRNA ($P = 0.003$), and by 91.4% compared with ALDH1A1 siRNA ($P = 0.002$). In A2780cp20 (Fig. 5G), there was a similar nonsignificant reduction of 43.9% in tumor weight with cisplatin alone ($P = 0.32$) and of 57.0%with ALDH1A1 siRNA treatment ($P = 0.19$). These effects may be even less significant than the mean tumor weights suggest, given the presence of 2 especially large tumors in the control siRNA group. However, again combined therapy showed a sensitization to chemotherapy with ALDH1A1 siRNA, with combination therapy reducing growth by 85.0% compared with control siRNA ($P = 0.048$), by 73.4% compared with cisplatin plus control siRNA ($P = 0.013$), and by 65.3% compared with ALDH1A1 siRNA alone ($P = 0.039$). Given the minimal effects of each single agent and the consistent finding of significant improvement with combined therapy, these data suggest a synergy between

Published OnlineFirst October 1, 2010; DOI:10.1158/1535-7163.MCT-10-0563

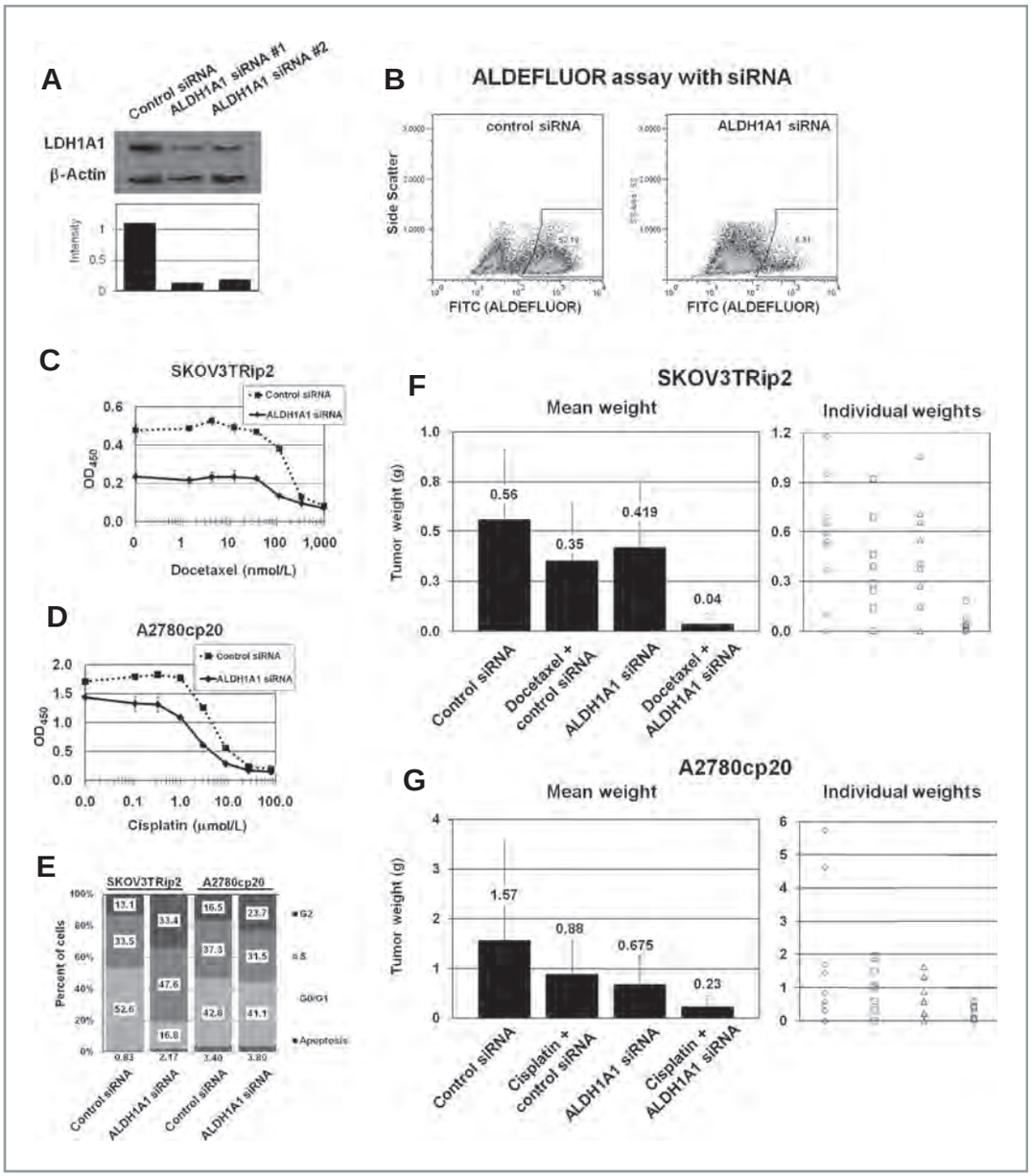

Figure 5. Efficacy of ALDH1A1 downregulation with siRNA *in vitro* and *in vivo*. Identification of siRNA constructs that decrease ALDH1A1 expression was confirmed by Western blotting (A) and by flow cytometry (B) using the ALDEFLUOR assay in the SKOV3TRip2 cell line. C, downregulation of ALDH1A1 with siRNA 48 hours prior to the treatment of SKOV3TRip2 cells with increasing doses of docetaxel showed a sensitization effect, decreasing IC_{50} from 178 to 82 nmol/L. siRNA alone also showed an effect, with decreased viability by 49%. D, in the A2780cp20 cell line, downregulation of ALDH1A1 alone had minimal effect but sensitized cells to cisplatin, decreasing IC_{50} from 5.1 to 2.0 μmol/L. E, cell-cycle analysis shows that ALDH1A1 downregulation induces accumulation of cells in S and G_2 phases in SKOV3TRip2, with little effect on A2780cp20. F, *in vivo*, mice injected intraperitoneally with SKOV3TRip2 cells were treated with ALDH1A1-siRNA incorporated in DOPC nanoparticles, docetaxel/control siRNA in DOPC, or the combination and compared with mice treated with control siRNA in DOPC. Mice treated with either of the single agents had minimal effect, but the combination showed a significant reduction compared with treatment with control siRNA (94% reduction in tumor growth; $P < 0.001$) or either of the single agents (90%–91% reduction; $P < 0.005$). G, similarly, mice injected with A2780cp20 cells showed a minimal, nonsignificant reduction in growth with cisplatin or ALDH1A1-siRNA in DOPC, but combination therapy was statistically superior to either of the single agents (65%–73% reduction; $P < 0.04$) or control siRNA (85% reduction; $P = 0.048$). Mean tumor weight and individual tumor sizes are presented.

ALDH1A1 downregulation and both taxane and platinum chemotherapeutic agents, though formal dose-finding experiments would be required to definitively prove synergy.

Discussion

We have found that ALDH1A1 expression and activity are increased in chemoresistant ovarian cancer cell lines

Published OnlineFirst October 1, 2010; DOI:10.1158/1535-7163.MCT-10-0563

and in *in situ* primary ovarian cancer xenografts treated with cisplatin. Expression of ALDH1A1 is frequent in ovarian tumors, and patients with low ALDH1A1 expression levels have a more favorable outcome than those with more ALDH1A1-positive cells. ALDEFLUOR-positive cells have increased (but not absolute) tumorigenicity compared with ALDEFLUOR-negative cells and have a differentiating capacity that is not present in the ALDEFLUOR-negative population. Most important, downregulation of ALDH1A1 expression sensitized normally chemoresistant tumors to both docetaxel and cisplatin both *in vitro* and in an orthotopic mouse model of ovarian cancer.

The search for tumor-initiating cells in ovarian cancer has resulted in observations that the $CD44^+/c\text{-}kit^+$ population has an approximately 5,000-fold increase in tumorigenicity, with tumors forming after the injection of as few as 100 cells from primary tumor, xenograft, or spheroid heterogeneous populations (5), and that the $CD133^+$ population has approximately 20-fold increased tumorigenicity, with tumor formation with as few as 100 to 500 cells from murine xenografts, and tumor formation 4 times faster with $CD133^+$ cells (7). Furthermore, the increased tumorigenicity of $CD133^+$ cells can be inhibited by interfering with binding between CD44 and its ligand hyaluronic acid (6). Other investigators have found equal rates of tumor formation among $CD133^+$ and $CD133^-$ cells from the A2780 cell line, but a faster growth rate in $CD133^+$ cells (8). The side population (SP) cells from the MOVCAR cell line also formed tumors more frequently and appeared 3 to 4 weeks sooner than tumors derived from non-SP cells (9). In all of these studies, as in ours, the tumors resulting from the putative tumor-initiating cell population contained both tumor-initiating cell and non-tumor-initiating cell populations, demonstrating multipotentiality. Interestingly, we have seen that cells comprising tumors formed from ALDH1A1-negative cells lack the capacity to generate ALDH1A1-positive cells and do not continue to propagate tumors over multiple generations, suggesting that their multipotentiality is limited. This lack of differentiating capacity has also been noted in ALDEFLUOR-negative cells from breast cancer cell lines (33).

The most appropriate source of tumor cells for tumorigenicity experiments is of some debate. Although it is desirable to use samples freshly collected from primary tumors, sorting these samples and establishing primary xenografts have proven problematic. Ovarian cancer xenografts and cells lines have traditionally been challenging to establish from primary samples. All previously reported studies of ovarian tumor-initiating cells have used selected cells of some sort, either from xenografts of varying generations or from cells grown in differentiation-inhibiting media (to form tumor spheres), to serve as a compromise between freshly collected specimens and cell lines. However, those cells that form tumors in mice even in the first generation almost certainly represent some select portion of the original tumor. That these xenografts still contain only a small percentage of tumor-initiating cells speaks either to the appropriateness of this approach or to the testament that the tumor-forming cells are multipotent, give rise to tumor-initiating cell-negative populations, and remain relatively rare. Use of cell lines is often discouraged because of their homogenous nature. But clearly, even within cell lines, there is heterogeneity in ALDH1A1 expression, as shown by the detection of distinct populations by flow cytometric and IHC analyses (Fig. 2). Distinct ALDEFLUOR-positive and -negative populations have also been found in several breast cancer cell lines, with ALDEFLUOR-positive cells having increased tumorigenicity and differing molecular signatures (33). Therefore, our finding that the ALDEFLUOR-positive population in cell lines has increased tumorigenicity may reflect the more aggressive phenotype of ALDH1A1-active cells but does not represent proof that this population is important to *in situ* ovarian cancers. Evidence that patients with increasing ALDH1A1 expression have poor outcomes suggests this association, but additional tumorigenicity experiments from freshly collected tumors would more appropriately define the ALDEFLUOR population as clinically significant tumor-initiating cells.

The importance of tumorigenicity in defining cancer stem cells has also been debated. Although tumor formation with 100 to 500 ALDEFLUOR-positive cells and a lack of tumor formation with the injection of 10^5 ALDEFLUOR-negative cells definitely reflect an aggressive phenotype, the biologic processes required for xenograft formation—survival under stressful experimental conditions, adhesion, time to proliferation, and variations in host immunocompetence—may not reflect the true population that cancer stem cell research seeks to identify. Our ultimate goal should be to identify the subpopulations in parent tumors that survive chemotherapy and therefore are more likely to cause recurrence. Stem cells that survive chemotherapy should exhibit chemoresistance to be clinically relevant. In breast cancer, for example, the $CD44^+/CD24^-$ population is highly tumorigenic. However, Tanei et al., who studied tissue obtained before and after neoadjuvant chemotherapy, found that despite a positive response to treatment, the proportion of $CD44^+/CD24^-$-negative cells was unchanged. In these samples, however, the ALDH1A1-positive population was significantly increased (34).

ALDH1A1 has previously been proposed to play a role in chemoresistance, having been noted to be higher in proteomic profiling of IGROV platinum-resistant ovarian cancer cells (35), in genomic profiling of multidrug-resistant gastric carcinoma (36), and in cells resistant to cyclophosphamide (37, 38), oxazaphosphorines (39), and now docetaxel and cisplatin. ALDH1A1 oxidizes many intracellular aldehydes into carboxylic acids (40), detoxifying many of the free oxygen radicals generated by chemotherapeutic agents. It stands to reason that a stem cell population should be resistant to multiple chemotherapeutic

Published OnlineFirst October 1, 2010; DOI:10.1158/1535-7163.MCT-10-0563

agents rather than being specific to one class. This also follows clinically, in that most ovarian cancer patients who develop resistance to platinum agents have resistance to multiple agents (2). ALDH1A1 has been shown to be associated with BRCA1 in breast cancer, in that knockdown of BRCA1 increases the ALDEFLUOR population and ALDEFLUOR-positive cells preferentially contain BRCA1 loss of heterozygosity (41). These findings could also be important to BRCA-mediated ovarian cancer. Despite this body of evidence for the importance of ALDH1A1, it is not fully understood whether any of the additional ALDH1 isoforms are important to stem cell biology. In our study, ALDH1A1 can be specifically identified with isotype-specific antibodies (as used for the IHC analysis and Western blotting). However, the more important and consistently used identifier of a stem cell population is the ALDEFLUOR assay, which, although primarily dependent on ALDH1A1, may also identify ALDH1A2 and ALDH1A3 isotypes [(42) and unpublished data by Stem Cell Technologies]. As a therapeutic agent, we have seen positive effects by targeting ALDH1A1 with siRNA, but to maximize the efficacy of therapeutics, the contribution of these additional isotypes will need to be defined with additional studies.

Although our finding of a poor outcome in patients with high ALDH1A1 expression agrees with similar investigations in breast cancer (12, 13) and ovarian cancer (20), one interesting report found that a high ALDH1A1 expression level actually confers a positive prognosis in ovarian cancer (43). This cohort also contained patients with absent, scattered, and diffuse staining. However, this cohort included patients with stage I and II disease and low-grade tumors, and ALDH1A1 expression was higher in these patients [confirming findings from a previous report (44)]. Furthermore, with multivariate analysis, only stage correlated with survival; ALDH1A1 expression no longer predicted outcomes. In ovarian cancer, there is a well-recognized dichotomy in carcinogenesis and pathobiology (45), whereby low-grade tumors (which are more often diagnosed at stage I or II) are paradoxically more chemoresistant but have prolonged survival due to slow growth. Given these collective data, and the several mechanisms by which ALDH1A1 has been shown to contribute to chemoresistance, it may be that ALDH1A1 is more frequently expressed in low-grade tumors but participates in chemoresistance to both high-grade and low-grade subtypes.

We have shown that the ALDH1A1-positive population has properties of cancer stem cells, is associated with taxane and platinum resistance, and can be resensitized to chemotherapy with downregulation of ALDH1A1 *in vitro* and *in vivo*. Therefore, ALDH1A1 is not just a marker of an aggressive population but also a mediator of the phenotype and a viable target for therapy. As better models are developed to more purely define the true chemoresistant population in *de novo* patient tumors, the ALDH1A1 population, either alone or in combination with other markers and mediators of resistance, may represent a population that must be targeted to achieve increased response rates and survival in ovarian cancer patients.

Disclosure of Potential Conflicts of Interest

No potential conflicts of interest were disclosed.

Grant Support

Funding support provided by the Reproductive Scientist Development Program through the Ovarian Cancer Research Fund and the National Institutes of Health (NIH; K12 HD00849), the Department of Defense Ovarian Cancer Research Academy, a Career Development Award from the UT MD Anderson Cancer Center Specialized Program of Research Excellence in ovarian cancer (CA083639), and the Gynecologic Cancer Foundation to C.N.L.; NIH (CA109298 and CA110793, P50 CA083639; CA128797, RC2GM092599), Program Project Development Grant from the Ovarian Cancer Research Fund, the Marcus Foundation, and the Betty Ann Ashe Murray Distinguished Professorship to A.K.S.

Received 06/16/2010; revised 09/03/2010; accepted 09/17/2010; published OnlineFirst 10/01/2010.

References

1. Jemal A, Siegel R, Ward E, Hao Y, Xu J, Thun MJ. Cancer statistics, 2009. CA Cancer J Clin 2009;59:225–49.
2. Hoskins W, Perez C, Young R, Barakat R, Markman M, Randall M. Principles and Practice of Gynecologic Oncology. 4th ed.Philadelphia: Lippincott Williams & Wilkins; 2005.
3. Rosen JM, Jordan CT. The increasing complexity of the cancer stem cell paradigm. Science 2009;324:1670–3.
4. Dalerba P, Cho RW, Clarke MF. Cancer stem cells: models and concepts. Annu Rev Med 2007;58:267–84.
5. Zhang S, Balch C, Chan MW, Lai HC, Matei D, Schilder JM, et al. Identification and characterization of ovarian cancer-initiating cells from primary human tumors. Cancer Res 2008;68:4311–20.
6. Slomiany MG, Dai L, Tolliver LB, Grass GD, Zeng Y, Toole BP. Inhibition of functional hyaluronan-CD44 interactions in CD133-positive primary human ovarian carcinoma cells by small hyaluronan oligosaccharides. Clin Cancer Res 2009;15:7593–601.
7. Curley MD, Therrien VA, Cummings CL, Sergent PA, Koulouris CR, Friel AM, et al. CD133 expression defines a tumor initiating cell population in primary human ovarian cancer. Stem Cells 2009;27(12):2875–83.
8. Baba T, Convery PA, Matsumura N, Whitaker RS, Kondoh E, Perry T, et al. Epigenetic regulation of CD133 and tumorigenicity of CD133$^+$ ovarian cancer cells. Oncogene 2009;28(2):209–18.
9. Szotek PP, Pieretti-Vanmarcke R, Masiakos PT, Dinulescu DM, Connolly D, Foster R, et al. Ovarian cancer side population defines cells with stem cell-like characteristics and Mullerian Inhibiting Substance responsiveness. Proc Natl Acad Sci U S A 2006;103:11154–9.
10. Moreb JS. Aldehyde dehydrogenase as a marker for stem cells. Curr Stem Cell Res Ther 2008;3:237–46.
11. Balicki D. Moving forward in human mammary stem cell biology and breast cancer prognostication using ALDH1. Cell Stem Cell 2007;1:485–7.
12. Ginestier C, Hur MH, Charafe-Jauffret E, Monville F, Dutcher J, Brown M, et al. ALDH1 is a marker of normal and malignant human mammary stem cells and a predictor of poor clinical outcome. Cell Stem Cell 2007;1:555–67.

Published OnlineFirst October 1, 2010; DOI:10.1158/1535-7163.MCT-10-0563

13. Charafe-Jauffret E, Ginestier C, Iovino F, Tarpin C, Diebel M, Esterni B, et al. Aldehyde dehydrogenase 1-positive cancer stem cells mediate metastasis and poor clinical outcome in inflammatory breast cancer. Clin Cancer Res 2010;16:45–55.
14. Croker AK, Goodale D, Chu J, Postenka C, Hedley BD, Hess DA, et al. High aldehyde dehydrogenase and expression of cancer stem cell markers selects for breast cancer cells with enhanced malignant and metastatic ability. J Cell Mol Med 2009;13(8B): 2236–52.
15. Huang EH, Hynes MJ, Zhang T, Ginestier C, Dontu G, Appelman H, et al. Aldehyde dehydrogenase 1 is a marker for normal and malignant human colonic stem cells (SC) and tracks SC overpopulation during colon tumorigenesis. Cancer Res 2009;69:3382–9.
16. Carpentino JE, Hynes MJ, Appelman HD, Zheng T, Steindler DA, Scott EW, et al. Aldehyde dehydrogenase-expressing colon stem cells contribute to tumorigenesis in the transition from colitis to cancer. Cancer Res 2009;69:8208–15.
17. Dembinski JL, Krauss S. Characterization and functional analysis of a slow cycling stem cell-like subpopulation in pancreas adenocarcinoma. Clin Exp Metastasis 2009;26:611–23.
18. Ucar D, Cogle CR, Zucali JR, Ostmark B, Scott EW, Zori R, et al. Aldehyde dehydrogenase activity as a functional marker for lung cancer. Chem Biol Interact 2009;178:48–55.
19. Ma S, Chan KW, Hu L, Lee TK, Wo JY, Ng IO, et al. Identification and characterization of tumorigenic liver cancer stem/progenitor cells. Gastroenterology 2007;132:2542–56.
20. Deng S, Yang X, Lassus H, Liang S, Kaur S, Ye Q, et al. Distinct expression levels and patterns of stem cell marker, aldehyde dehydrogenase isoform 1 (ALDH1), in human epithelial cancers. PLoS One 2010;5:e10277.
21. Buick RN, Pullano R, Trent JM. Comparative properties of five human ovarian adenocarcinoma cell lines. Cancer Res 1985;45:3668–76.
22. Yoneda J, Kuniyasu H, Crispens MA, Price JE, Bucana CD, Fidler IJ. Expression of angiogenesis-related genes and progression of human ovarian carcinomas in nude mice. J Natl Cancer Inst 1998;90:447–54.
23. Duan Z, Feller AJ, Toh HC, Makastorsis T, Seiden MV. TRAG-3, a novel gene, isolated from a taxol-resistant ovarian carcinoma cell line. Gene 1999;229:75–81.
24. Illumina I. BeadStudio Normalization Algorithms for Gene Expression Data. Technical note: Illumina® RNA analysis 2007. Available from: http://www.illumina.com/Documents/products/technotes/technote_beadstudio_normalization.pdf (accessed July 1, 2010).
25. Benjamini Y, Drai D, Elmer G, Kafkafi N, Golani I. Controlling the false discovery rate in behavior genetics research. Behav Brain Res 2001;125:279–84.
26. Landen CN Jr, Lu C, Han LY, Coffman KT, Bruckheimer E, Halder J, et al. Efficacy and antivascular effects of EphA2 reduction with an agonistic antibody in ovarian cancer. J Natl Cancer Inst 2006;98:1558–70.
27. Straetemans R, O'Brien T, Wouters L, Van Dun J, Janicot M, Bijnens L, et al. Design and analysis of drug combination experiments. Biom J 2005;47:299–308.
28. Landen CN Jr, Chavez-Reyes A, Bucana C, Schmandt R, Deavers MT, Lopez-Berestein G, et al. Therapeutic EphA2 gene targeting *in vivo* using neutral liposomal small interfering RNA delivery. Cancer Res 2005;65:6910–8.
29. Gray MJ, Dallas NA, Van Buren G, Xia L, Yang AD, Somcio RJ, et al. Therapeutic targeting of Id2 reduces growth of human colorectal carcinoma in the murine liver. Oncogene 2008;27:7192–200.
30. Halder J, Kamat AA, Landen CN Jr, Han LY, Lutgendorf SK, Lin YG, et al. Focal adhesion kinase targeting using *in vivo* short interfering RNA delivery in neutral liposomes for ovarian carcinoma therapy. Clin Cancer Res 2006;12:4916–24.
31. Kamat AA, Feng S, Agoulnik IU, Kheradmand F, Bogatcheva NV, Coffey D, et al. The role of relaxin in endometrial cancer. Cancer Biol Ther 2006;5:71–7.
32. Villares GJ, Zigler M, Wang H, Melnikova VO, Wu H, Friedman R, et al. Targeting melanoma growth and metastasis with systemic delivery of liposome-incorporated protease-activated receptor-1 small interfering RNA. Cancer Res 2008;68:9078–86.
33. Charafe-Jauffret E, Ginestier C, Iovino F, Wicinski J, Cervera N, Finetti P, et al. Breast cancer cell lines contain functional cancer stem cells with metastatic capacity and a distinct molecular signature. Cancer Res 2009;69:1302–13.
34. Tanei T, Morimoto K, Shimazu K, Kim SJ, Tanji Y, Taguchi T, et al. Association of breast cancer stem cells identified by aldehyde dehydrogenase 1 expression with resistance to sequential paclitaxel and epirubicin-based chemotherapy for breast cancers. Clin Cancer Res 2009;15:4234–41.
35. Le Moguen K, Lincet H, Marcelo P, Lemoisson E, Heutte N, Duval M, et al. A proteomic kinetic analysis of IGROV1 ovarian carcinoma cell line response to cisplatin treatment. Proteomics 2007;7:4090–101.
36. Ludwig A, Dietel M, Lage H. Identification of differentially expressed genes in classical and atypical multidrug-resistant gastric carcinoma cells. Anticancer Res 2002;22:3213–21.
37. Russo JE, Hilton J. Characterization of cytosolic aldehyde dehydrogenase from cyclophosphamide resistant L1210 cells. Cancer Res 1988;48:2963–8.
38. Yoshida A, Dave V, Han H, Scanlon KJ. Enhanced transcription of the cytosolic ALDH gene in cyclophosphamide resistant human carcinoma cells. Adv Exp Med Biol 1993;328:63–72.
39. Kohn FR, Landkamer GJ, Manthey CL, Ramsay NK, Sladek NE. Effect of aldehyde dehydrogenase inhibitors on the *ex vivo* sensitivity of human multipotent and committed hematopoietic progenitor cells and malignant blood cells to oxazaphosphorines. Cancer Res 1987;47:3180–5.
40. Riveros-Rosas H, Julian-Sanchez A, Pina E. Enzymology of ethanol and acetaldehyde metabolism in mammals. Arch Med Res 1997;28:453–71.
41. Liu S, Ginestier C, Charafe-Jauffret E, Foco H, Kleer CG, Merajver SD, et al. BRCA1 regulates human mammary stem/progenitor cell fate. Proc Natl Acad Sci U S A 2008;105:1680–5.
42. Yokota A, Takeuchi H, Maeda N, Ohoka Y, Kato C, Song SY, et al. GM-CSF and IL-4 synergistically trigger dendritic cells to acquire retinoic acid-producing capacity. Int Immunol 2009;21:361–77.
43. Chang B, Liu G, Xue F, Rosen DG, Xiao L, Wang X, et al. ALDH1 expression correlates with favorable prognosis in ovarian cancers. Mod Pathol 2009;22:817–23.
44. Tanner B, Hengstler JG, Dietrich B, Henrich M, Steinberg P, Weikel W, et al. Glutathione, glutathione *S*-transferase alpha and pi, and aldehyde dehydrogenase content in relationship to drug resistance in ovarian cancer. Gynecol Oncol 1997;65:54–62.
45. Landen CN Jr, Birrer MJ, Sood AK. Early events in the pathogenesis of epithelial ovarian cancer. J Clin Oncol 2008;26:995–1005.

Published OnlineFirst December 5, 2011; DOI:10.1158/1078-0432.CCR-11-2188

Clinical Cancer Research

Stem Cell Pathways Contribute to Clinical Chemoresistance in Ovarian Cancer

Adam D. Steg, Kerri S. Bevis, Ashwini A. Katre, et al.

Clin Cancer Res 2012;18:869-881. Published OnlineFirst December 5, 2011.

Published OnlineFirst December 5, 2011; DOI:10.1158/1078-0432.CCR-11-2188

Cancer Therapy: Clinical

Clinical Cancer Research

Stem Cell Pathways Contribute to Clinical Chemoresistance in Ovarian Cancer

Adam D. Steg[1], Kerri S. Bevis[1], Ashwini A. Katre[1], Angela Ziebarth[1], Zachary C. Dobbin[1], Ronald D. Alvarez[1], Kui Zhang[2], Michael Conner[3], and Charles N. Landen[1]

Abstract

Purpose: Within heterogeneous tumors, subpopulations often labeled cancer stem cells (CSC) have been identified that have enhanced tumorigenicity and chemoresistance in *ex vivo* models. However, whether these populations are more capable of surviving chemotherapy in *de novo* tumors is unknown.

Experimental Design: We examined 45 matched primary/recurrent tumor pairs of high-grade ovarian adenocarcinomas for expression of CSC markers ALDH1A1, CD44, and CD133 using immunohistochemistry. Tumors collected immediately after completion of primary therapy were then laser capture microdissected and subjected to a quantitative PCR array examining stem cell biology pathways (Hedgehog, Notch, TGF-β, and Wnt). Select genes of interest were validated as important targets using siRNA-mediated downregulation.

Results: Primary samples were composed of low densities of ALDH1A1, CD44, and CD133. Tumors collected immediately after primary therapy were more densely composed of each marker, whereas samples collected at first recurrence, before initiating secondary therapy, were composed of similar percentages of each marker as their primary tumor. In tumors collected from recurrent platinum-resistant patients, only CD133 was significantly increased. Of stem cell pathway members examined, 14% were significantly overexpressed in recurrent compared with matched primary tumors. Knockdown of genes of interest, including endoglin/CD105 and the hedgehog mediators Gli1 and Gli2, led to decreased ovarian cancer cell viability, with Gli2 showing a novel contribution to cisplatin resistance.

Conclusions: These data indicate that ovarian tumors are enriched with CSCs and stem cell pathway mediators, especially at the completion of primary therapy. This suggests that stem cell subpopulations contribute to tumor chemoresistance and ultimately recurrent disease. *Clin Cancer Res; 18(3); 869–81. ©2011 AACR.*

Introduction

Ovarian cancer is the leading cause of death from a gynecologic malignancy. Although ovarian cancer is among the most chemosensitive malignancies at the time of initial treatment (surgery and taxane/platinum-based chemotherapy), most patients will ultimately develop tumor recurrence and succumb to chemoresistant disease (1). Evaluation of multiple chemotherapy agents in several combinations in the last 20 years has yielded modest improvements in progression-free survival but no increases in durable cures. This clinical course suggests that a population of tumor cells has either inherent or acquired resistance to chemotherapy that allows survival with initial therapy and ultimately leads to recurrence. Targeting the cellular pathways involved in this resistance may provide new treatment modalities for ovarian cancer.

In several hematologic and solid tumors, subpopulations of cells termed cancer stem cells (CSC) or tumor-initiating cells (TIC) have been identified as representing the most tumorigenic and treatment-resistant cells within a heterogeneous tumor mass. Usually defined by their enhanced ability to generate murine xenografts and give rise to heterogeneous tumors that are composed of both CSC and non-CSC populations, these cells may also be more chemoresistant and depend on unique biologic processes compared with the majority of tumor cells (2, 3). In ovarian cancer, many of these properties have been identified in populations of CD44-positive cells (4, 5), CD133-positive cells (6–8), Hoechst-excluding cells (the side population; ref. 9), and aldehyde dehydrogenase (ALDH1A1)-positive cells (10–13) and are associated with poor clinical

Authors' Affiliations: Departments of [1]Obstetrics and Gynecology, [2]Biostatistics, and [3]Pathology, University of Alabama at Birmingham, Birmingham, Alabama

Note: Supplementary data for this article are available at Clinical Cancer Research Online (http://clincancerres.aacrjournals.org/).

Corresponding Author: Charles N. Landen, Department of Obstetrics and Gynecology, The University of Alabama at Birmingham, 1825 University Boulevard, 505 Shelby Building, Birmingham, AL 35294. Phone: 205-934-0473; Fax: 205-934-0474; E-mail: clanden@uab.edu

doi: 10.1158/1078-0432.CCR-11-2188

Published OnlineFirst December 5, 2011; DOI:10.1158/1078-0432.CCR-11-2188

Translational Relevance

Most patients with ovarian cancer will have an excellent response to initial surgical debulking and chemotherapy, but about 75% of patients will later recur and succumb to disease. Primarily on the basis of *ex vivo* models, subpopulations of cancer cells, often described as cancer stem cells, have been hypothesized to represent the most tumorigenic and treatment-resistant cells within a heterogeneous tumor mass. Using a unique cohort of matched primary/recurrent ovarian tumors, we have shown that the expression of putative cancer stem cell markers ALDH1A1, CD44, and CD133 and several additional mediators of stem cell pathways are upregulated in recurrent, chemoresistant disease compared with primary tumor. Further development revealed novel mechanisms of the TGF-β coreceptor endoglin (CD105) and the Gli2 hedgehog transcription factor in platinum resistance. Our findings highlight the importance of stem cell pathways in ovarian cancer recurrence and chemoresistance and show that therapies targeting these pathways may reverse platinum resistance in ovarian cancer.

outcomes. It is acknowledged that these markers are not identifiers of pure populations with all capabilities of conventional stem cells but rather enrich for a population with some stem cell properties.

Whether or not these populations actually have preferential survival in *de novo* tumors and thus contribute to recurrent disease is not known. An increased density of these populations in recurrent or chemoresistant tumors would suggest their importance to the clinical course of ovarian cancer and suggest that these populations would have to be targeted to achieve durable cures. In the current study, we used a unique cohort of matched primary/recurrent ovarian cancer specimens to determine whether putative CSC subpopulations comprise a larger percentage of recurrent tumors and to examine other known mediators of stem cell biology that might correlate with contributors to recurrence. In addition, novel genes were revealed to be highly expressed in recurrent samples, specifically endoglin (CD105) and the Hedgehog mediator Gli2, and were targeted in validation studies to confirm that stem cell pathway members represent novel therapeutic targets in ovarian cancer.

Methods

Immunohistochemical staining and clinical correlations

Immunohistochemical (IHC) analysis was conducted using standard techniques (14) on samples collected from matched primary and recurrent tumors taken from 45 patients with ovarian adenocarcinoma, and with Institutional Review Board approval, clinical information was collected. Pathology was confirmed and formalin-fixed, paraffin-embedded (FFPE) slides were cut at 5 or 10 μm. Antigen retrieval was carried out in citrate buffer (pH 6.0) for 45 minutes in an atmospheric pressure steamer. Slides were then stained using antibodies against ALDH1A1 (Clone 44; BD Biosciences), CD44 (Clone 2F10; R&D Systems), or CD133 (Clone C24B9; Cell Signaling Technology) at 1:500 dilution in Cyto-Q reagent (Innovex Biosciences) overnight at 4°C. Primary antibody detection was achieved with Mach 4 HRP polymer (Biocare Medical) for 20 minutes at room temperature, followed by 3,3′-diaminobenzidine (DAB) incubation. After IHC staining, the number of tumor cells positive for ALDH1A1, CD44, or CD133 were counted by two independent examiners (and a third if there was >20% discrepancy) blinded to the setting in which the tumor was collected (primary or recurrent) and expressed as a percentage of all tumor cells. To be consistent with prior identification of putative CSCs identified through surface expression with flow cytometry, in the case of CD44 and CD133, only strong expression at the surface membrane was considered positive. Intensity was not scored separately, staining was considered only positive or negative, with the primary endpoint percentage of positive tumor cells across the entire slide. The average number of positive cells for each marker among the 45 primary samples was compared with the average among recurrent samples, with additional subgroup analyses conducted as described in the Results section. A subgroup analysis of IHC staining using an antibody against endoglin (Sigma) was also conducted.

Laser capture microdissection

Ten-micrometer thick FFPE sections were prepared from 12 matched pairs of samples from patients with ovarian adenocarcinoma, in whom the recurrent tumors had been collected within 3 months of completion of primary therapy. Sections were rapidly stained with hematoxylin and eosin. Three to five thousand tumor epithelial cells were microdissected from each sample using a PixCell II Laser Capture Microdissection system (Arcturus Engineering). Care was taken to ensure that no stromal cells were collected (see Supplementary Fig. S1). RNA was extracted using the RecoverAll Total Nucleic Acid Isolation Kit (Applied Biosystems) optimized for FFPE samples.

RT^2 profiler PCR array

RNA extracted from microdissected samples was converted to cDNA and amplified using the RT^2 FFPE PreAMP cDNA Synthesis Kit (SABiosciences). Quality of cDNA was confirmed with the Human RT^2 RNA QC PCR Array (SABiosciences), which tests for RNA integrity, inhibitors of reverse transcription and PCR amplification, and genomic and general DNA contamination (15). Gene expression was then analyzed in these samples using the Human Stem Cell Signaling RT^2 Profiler PCR Array (SABiosciences), which profiles the expression of 84 genes involved in pluripotent cell maintenance and differentiation (16). Functional gene groupings consist of the Hedgehog, Notch,

Published OnlineFirst December 5, 2011; DOI:10.1158/1078-0432.CCR-11-2188

TGF-β, and Wnt signaling pathways. PCR amplification was conducted on an ABI Prism 7900HT sequence detection system, and gene expression was calculated using the comparative C_T method as previously described (17).

Cell lines and culture

The ovarian cancer cell lines A2780ip2, A2780cp20, ES2, HeyA8, HeyA8MDR, IGROV-AF1, OvCar-3, and SKOV3ip1 (18–27) were maintained in RPMI-1640 medium supplemented with 10% FBS (Hyclone). All cell lines were routinely screened for *Mycoplasma* species (GenProbe detection kit; Fisher) with experiments carried out at 70 to 80% confluent cultures. Purity of cell lines was confirmed with short tandem repeat genomic analysis, and only cells less than 20 passages from stocks were used in experiments.

RNA extraction from cell lines

Total RNA was isolated from ovarian cancer cell lines using TRIzol reagent (Invitrogen) per manufacturer's instructions. RNA was then DNase treated and purified using the RNEasy Mini Kit (QIAGEN). RNA was eluted in 50 μL of RNase-free water and stored at −80°C. The concentration of all RNA samples was quantified by spectrophotometric absorbance at 260/280 nm using an Epoch microplate spectrophotometer (BioTek Instruments).

Reverse transcription and quantitative PCR

Prior to reverse transcription, all RNA samples were diluted to 20 ng/μL using RNase-free water. The cDNA was prepared using the High Capacity cDNA Reverse Transcription Kit (Applied Biosystems). The resulting cDNA samples were analyzed using quantitative PCR. Primer and probe sets for *ABCG2* (Hs01053790_m1), *ALDH1A1* (Hs00946916_m1), *CD44* (Hs01075861_m1), *CD133* (Hs01009259_m1), *GLI1* (Hs00171790_m1), *GLI2* (Hs00257977_m1), and *RPLP0* (Hs99999902_m1; housekeeping gene) were obtained from Applied Biosystems; primers for *endoglin* (*ENG*; PPH01140F) were obtained from SABiosciences and used according to manufacturer's instructions. PCR amplification was conducted on an ABI Prism 7900HT sequence detection system, and gene expression was calculated using the comparative C_T method.

siRNA transfection

To examine knockdown of endoglin, Gli1, or Gli2 with siRNA, cells were exposed to control siRNA (target sequence: 5′-UUCUCCGAACGUGUCACGU-3′; Sigma), one of 2 tested endoglin-targeting constructs (ENG_A siRNA: 5′-CAAUGAGGCGGUGGCAAU-3′ or ENG_B siRNA: 5′-CAGAAACAGUCCAUUGUGA-3′; Sigma), one of 2 tested Gli1-targeting constructs (GLI1_A siRNA: 5′-CUACUGAUACUCUGGGAUA-3′ or GLI1_B siRNA: 5′-GCAAAUAGGGCUUCACAUA-3′), or one of 2 tested Gli2-targeting constructs (GLI2_A siRNA: 5′-CGAUUGACAUGCGACACCA-3′ or GLI2_B siRNA: 5′-GUACCAUUACGAGCCUCAU-3′) at a 1:3 siRNA (pmol) to Lipofectamine 2000 (μL) ratio. Lipofectamine and siRNA were incubated for 20 minutes at room temperature, added to cells in serum-free RPMI to incubate for 6 to 8 hours, followed by 10% FBS/RMPI thereafter. Transfected cells were grown at 37°C for an additional 48 hours and then harvested for quantitative PCR or Western blot analysis.

Western blot analysis

Cultured cell lysates were collected in modified radioimmunoprecipitation assay (RIPA) lysis buffer with protease inhibitor cocktail (Roche) and subjected to immunoblot analysis by standard techniques (14) using anti-endoglin antibody (Sigma) at 1:500 dilution overnight at 4°C; or anti-β-actin antibody (Clone AC-15, Sigma) at 1:20,000 dilution for 1 hour at room temperature, which was used to monitor equal sample loading. After washing, blots were incubated with goat anti-rabbit (for endoglin) or goat anti-mouse (for β-actin) secondary antibodies (Bio-Rad) conjugated with horseradish peroxidase. Visualization was conducted by the Enhanced Chemiluminescence Method (Pierce Thermo Scientific).

Assessment of cell viability and cell-cycle analysis following siRNA-mediated knockdown

For effects of siRNA-mediated downregulation on cell viability, cells were first transfected with siRNA (5 μg) for 24 hours in 6-well plates (2.5×10^5 cells per well), trypsinized, and then replated on a 96-well plate at 2,000 cells per well. After 4 to 5 days, cell viability was assessed by optical density measurements at 570 nm using 0.15% MTT (Sigma) in PBS. For cell-cycle analysis, 5×10^5 cells in a 60-mm dish were transfected with siRNAs and then cultured in RPMI/10% FBS at 37°C for an additional 48 hours. Cells were then trypsinized, washed in PBS, and fixed in 100% ethanol overnight. Cells were then centrifuged, washed in PBS, and resuspended in PBS containing 0.1% Triton X-100 (v/v), 200 μg/mL DNase-free RNase A, and 20 μg/mL propidium iodide (PI). PI fluorescence was assessed by flow cytometry, and the percentage of cells in sub-G_0, G_0–G_1, S, and G_2–M phases was calculated by the cell-cycle analysis module for Flow Cytometry Analysis Software (FlowJo v.7.6.1). For effects of siRNA-mediated downregulation on cisplatin IC_{50}, cells were first transfected with siRNA (5 μg) in 6-well plates, trypsinized, and then replated on a 96-well plate at 2,000 cells per well, followed by addition of chemotherapy after attachment. IC_{50} was determined by finding the dose at which the drug had 50% of its effect, calculated by the equation $[(OD_{570max} - OD_{570min})/2) + OD_{570min}]$.

Statistical analysis

Comparisons of continuous variables were made using a two-tailed Student *t* test, if assumptions of data normality were met. Those represented by alternate distribution were examined using a nonparametric Mann–Whitney *U* test. Differences between groups were considered statistically significant at $P < 0.05$. Error bars represent SD unless otherwise stated.

Published OnlineFirst December 5, 2011; DOI:10.1158/1078-0432.CCR-11-2188

Results

ALDH1A1, CD44, and CD133 expression in primary human ovarian cancer specimens

We identified a cohort of 45 patients with either papillary serous or endometrioid high-grade ovarian cancer for whom tumor specimens were collected at primary therapy and at the time of recurrent disease. The clinical characteristics of these patients are described in Supplementary Table S1 and represent the typical clinical profiles of patients with ovarian cancer. All patients were initially treated with combination platinum (either cisplatin or carboplatin) and taxane (either paclitaxel or docetaxel) by intravenous infusion. We first examined baseline expression of ALDH1A1, CD44, and CD133, the markers most consistently showing a putative CSC population in ovarian cancer. The percentage of positive ALDH1A1, CD44, and CD133 cells in primary samples averaged 23.4%, 6.2%, and 7.1%, respectively (Fig. 1A). Representations of high and low distribution patterns are shown in Fig. 1B and for CD44 and CD133 high-power views in Fig. 1C. For all 3 proteins examined, staining was typically strong in some cells and negative in others, rather than having a range of intensity across all tumor cells, signifying distinct heterogeneity within the tumor. There was no distinct pattern to the location of the positive cells (such as around vasculature, or on the leading edge of the tumor) but positive cells did tend to cluster together. Staining was appropriately noted intracellularly for ALDH1A1 and on the cell membrane for CD44 and CD133. Interestingly, CD133 expression was usually noted at cell–cell borders rather than circumferentially, suggesting a polarity to expression and possible participation in cell–cell interactions (Fig. 1C).

Change in expression of ALDH1A1, CD44, and CD133 from primary to recurrent ovarian cancer

To determine whether recurrent ovarian tumors have altered expression of ALDH1A1, CD44, and CD133, we compared the average number of positive cells for each marker among the 45 primary samples to that of the recurrent samples taken from the same patients (Fig. 1D). There was a modest increase in ALDH1A1-positive cells (from 23.4% to 29.2%, $P = 0.28$) and CD44-positive cells (from 6.2% to 11%, $P = 0.11$); however, CD133-positive cells were significantly higher (from 7.1% to 29.6%, $P = 0.0004$) in recurrent than in primary samples. To appreciate the change in each subpopulation for each patient, in addition to the mean of the entire group, the change for each tumor is graphically presented in Fig. 1E. For ALDH1A1 and CD44, both increases and decreases were noted for different patients. However, for CD133, the change was almost always an increase. The percentage of CD133-positive cells increased by more than 2-fold in 58% of recurrent samples than in matched primary samples.

Subgroup analysis of ALDH1A1, CD44, and CD133 based on setting of recurrent tumor collection

If the CSC hypothesis is clinically significant, then surviving cells would be expected to give rise again to both resistant CSCs and differentiated chemosensitive cells. Clinically this is seen as most patients will again have a response to treatment at first recurrence. Therefore, we examined the pairs on the basis of when their recurrent tumor was collected: (i) in patients who were clinically without evidence of disease but had other indications for surgery conducted within 3 months of completion of primary therapy, termed persistent tumor; (ii) in patients who recurred more than 6 months after completion of primary therapy and had tumors collected prior to second-line chemotherapy, termed untreated recurrence; and (iii) in the setting of recurrent, chemoresistant disease, termed treated recurrence. Among persistent tumors, there was an even more pronounced increase in ALDH1A1-positive cells (from 29.7% to 54.9%, $P = 0.018$), CD44-positive cells (from 8.3% to 21.2%, $P = 0.16$), and CD133-positive cells (from 6.6% to 53.9%, $P = 0.001$; Fig. 2A). In contrast, samples collected at first recurrence before initiating secondary therapy were composed of similar percentages of each marker as their primary tumor (Fig. 2B), suggesting that the tumor was repopulated with marker-negative differentiated cells. In tumors collected from recurrent platinum-resistant patients, only CD133 was significantly increased in expression (from 6.3% to 34.5%, $P = 0.027$; Fig. 2C). The percentage of CD133-positive cells increased by more than 2-fold in 50% of treated recurrence samples than in matched primary.

Table 1 illustrates the changes in ALDH1A1, CD44, and CD133 staining from primary to persistent tumor in individual patients. Overall, the percentage of ALDH1A1-, CD44-, and CD133-positive cells increased by more than 2-fold in 64%, 67%, and 89% of persistent tumor specimens, respectively, than in matched primary samples. While the expression of at least 2 of the 3 markers was elevated in the majority of specimens, only 4 patients had increased expression of all 3 markers. This suggests that certain mediators may be more active than others in different patients, and there may be other markers of treatment-resistant cells yet to be identified.

Expression of genes involved in human stem cell signaling is increased in recurrent compared with matched primary ovarian tumors

Building on the model that tumor samples present at the completion of primary therapy represent the cells responsible for recurrent disease and are therefore most relevant for study, we laser capture microdissected tumor cells from the 12 patients with persistent tumor analyzed above (Supplementary Fig. S1). Gene expression of putative CSC markers (*ALDH1A1*, *CD44*, *CD133*, and *ABCG2*) as well as 84 genes involved in pluripotent cell maintenance and differentiation was analyzed in these matched samples by qPCR or qPCR array. As shown in Table 2, expression of *ALDH1A1* (2.5-fold, $P = 0.23$) and *CD44* (4.1-fold, $P = 0.0023$) was

Published OnlineFirst December 5, 2011; DOI:10.1158/1078-0432.CCR-11-2188

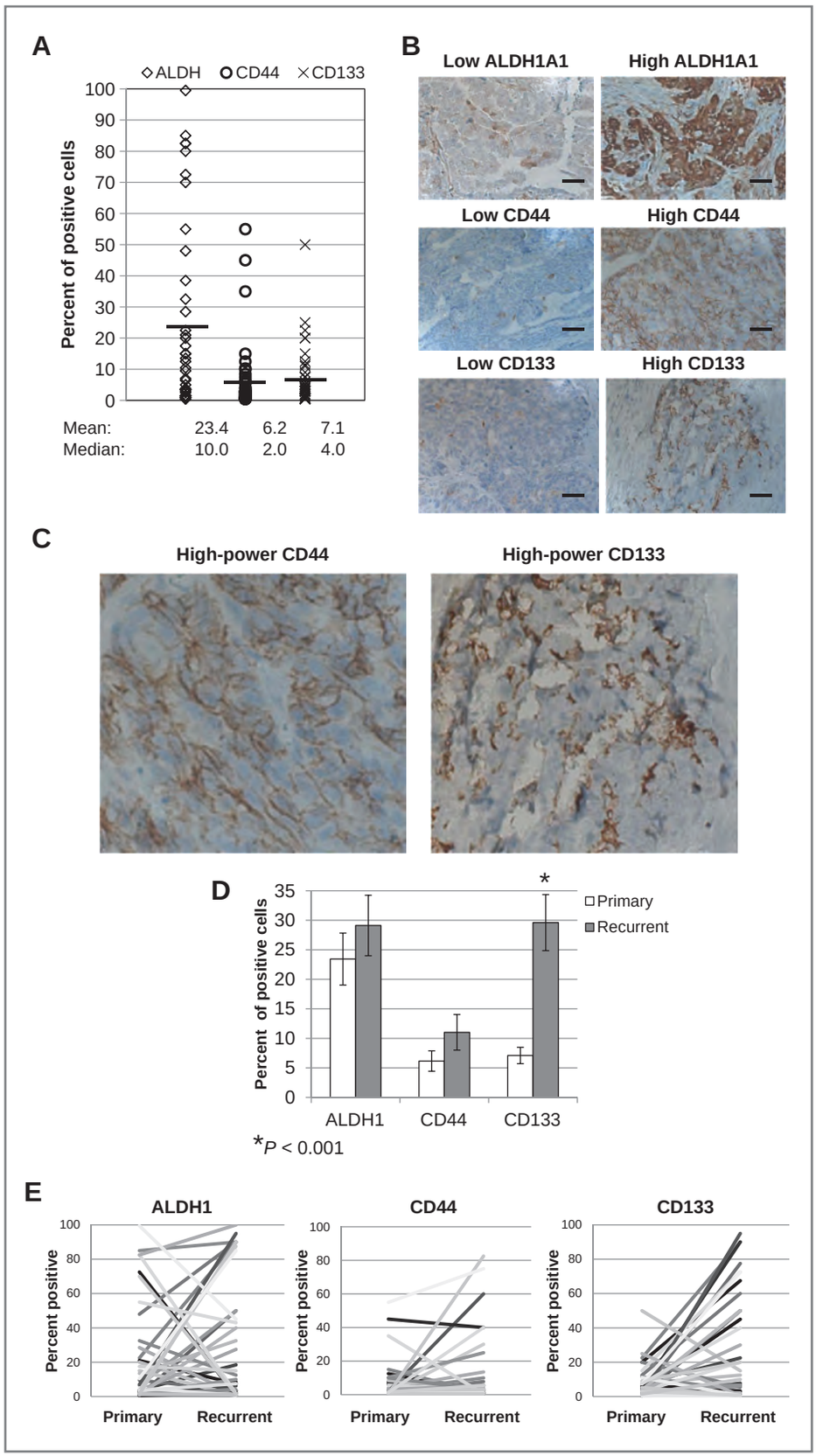

Figure 1. Change in expression of ALDH1A1, CD44, and CD133 from primary to recurrent ovarian cancer. A, ALDH1A1, CD44, and CD133 expression in 45 high-grade ovarian adenocarcinomas was examined using immunohistochemistry. The estimated percentage of positive cells for each sample, with mean (black bars) and median are shown. B, for all 3 proteins examined, staining was heterogeneous, rather than diffusely positive. Examples of high and low frequency expression for each are shown (black bar, 100 μm). C, a higher magnification of CD44 and CD133 expression in primary ovarian cancer specimens, showing cell surface expression. D, the average number of positive cells for ALDH1A1, CD44, and CD133 among the 45 primary samples was compared with the average among matched recurrent samples. Only CD133 was significantly higher in recurrent samples. Error bars represent SEM. *, $P < 0.001$. E, to evaluate the change in each subpopulation for each patient, in addition to the mean of the entire group, the change for each tumor is shown in individual graphs.

Published OnlineFirst December 5, 2011; DOI:10.1158/1078-0432.CCR-11-2188

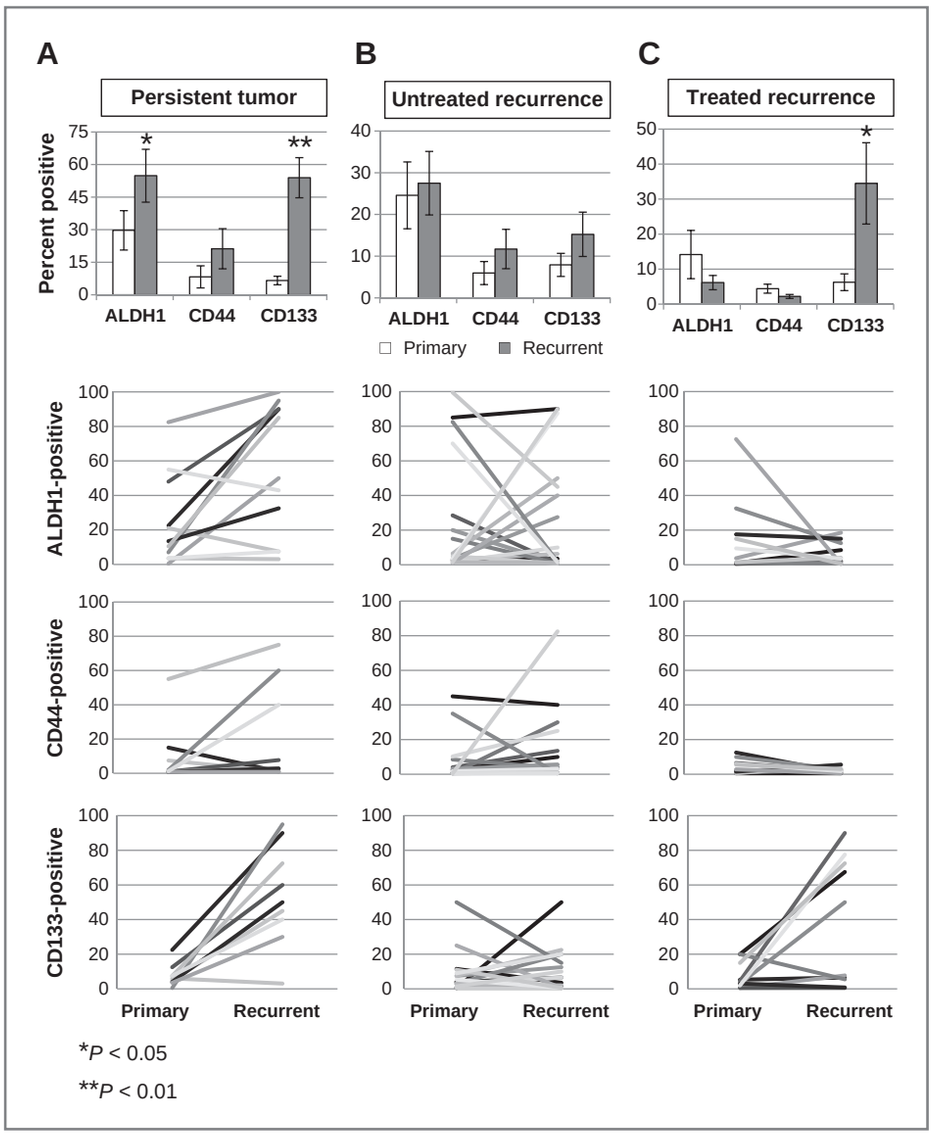

Figure 2. Subgroup analysis of ALDH1A1, CD44, and CD133 based on setting of recurrent tumor collection. Expression of ALDH1A1, CD44, and CD133 was broken down into subcategories based on the setting in which the recurrent tumor was retrieved. A, ALDH1A1, CD44, and CD133 expression was higher in samples collected immediately after the completion of primary therapy (persistent tumor; $n = 12$). B, samples collected at first recurrence before initiating secondary therapy (untreated recurrence; $n = 20$) were composed of similar percentages of each marker. C, in tumors collected from recurrent, platinum-resistant patients (treated recurrence; $n = 13$), only CD133 was increased in expression. Error bars represent SEM. *, $P < 0.05$; **, $P < 0.01$.

elevated in persistent tumors compared with matched primary samples, similar to IHC analysis. Expression of breast cancer resistance protein (*ABCG2*/*BCRP*), a well-characterized drug efflux transporter that has been associated with stem cell phenotype (9, 28), was also increased in persistent tumors (7.7-fold, $P = 0.0163$). Attempts to optimize experimental conditions to examine BCRP by immunohistochemistry failed and therefore we could not validate this increase at the protein level. CD133 mRNA expression was virtually undetectable in both primary and persistent tumor samples. This suggests that increased CD133 protein expression in recurrent tumors noted by immunohistochemistry may be due to posttranscriptional or posttranslational regulation.

Of the 84 genes examined by the Human Stem Cell Signaling RT^2 Profiler Array (16), we found that 12 of these genes (14%) were significantly increased in persistent compared with matched primary tumor. Members of the TGF-β superfamily signaling pathway (*ENG*, *ZEB2*, *LTBP4*, *TGFBR2*, *RGMA*, *ACVR1B*, and *SMAD2*) were most commonly significantly increased as well as members of the Hedgehog (*GLI1* and *GLI2*), Notch (*PSEN2*), and Wnt (*FZD9* and *BCL9L*) pathways. Of particular interest, the TGF-β coreceptor endoglin (*ENG*) was, on average, 3.77-fold ($P = 0.0023$) higher in persistent tumors and more than 2-fold higher in 9 of the 12 samples. All of the tumors, either primary or recurrent, expressed endoglin. This protein is a recognized marker for angiogenesis, primarily expressed on endothelial cells (29, 30), but increased expression specific to tumor cells in our laser-microdissected tissues suggest that it may play a role in tumor cell chemoresistance and could be targeted for therapy. IHC staining of these specimens for endoglin expression confirmed that recurrent tumors had a greater density of

Published OnlineFirst December 5, 2011; DOI:10.1158/1078-0432.CCR-11-2188

Table 1. Changes in ALDH1A1, CD44, and CD133 staining from primary to persistent ovarian tumor

Patient	ALDH1A1[a]	CD44[a]	CD133[a]
502	↑	↓	↑
505	↑	NM	NM
510	↓	↓	↑
511	↑	↑	↑
522	NC	↑	NC
525	↑	↑	↑
535	↑	↑	↑
540	NC	NC	↑
544	↑	NM	NM
548	↑	↑	↑
549	NC	↑	↑

Abbreviations: NC, density of cells did not change by more than 2-fold; NM, not measured because of insufficient tumor.
[a]An increase or decrease more than 2-fold designated by arrow.

endoglin positivity than in the matched primary tumor and that expression was definitively present in tumor cells not just the in vasculature (Fig. 3A). In addition, endoglin and CD133 expression significantly correlated ($r = 0.62$, $P = 0.006$), as did Gli1 and CD133 expression ($r = 0.54$, $P = 0.022$), suggesting that the increase in CD133 positivity observed in recurrent compared with matched primary tumors is accompanied by an increase in markers of stem cell signaling.

Endoglin is expressed in ovarian cancer cell lines and its downregulation leads to decreased cell viability

To further explore the potential role of endoglin in ovarian cancer, we first examined gene expression in cell lines. These included ES2, IGROV-AF1, OvCar-3, SKOV3ip1 and 2 pairs of parental and chemoresistant ovarian cancer cell lines: A2780ip2/A2780cp20 (20-fold increased cisplatin resistance and 10-fold increased taxane resistance) and HeyA8/HeyA8MDR (500-fold taxane resistant). As shown in Fig. 3B, mRNA expression of endoglin was prominent in ES2, HeyA8, and HeyA8MDR cells. Minimal expression of endoglin was detected in the A2780ip2, A2780cp20, IGROV-AF1, OvCar-3, and SKOV3ip1 cell lines. Protein expression was assessed by Western blot and correlated with mRNA quantification (data not shown).

To determine whether endoglin might be a target for tumor-specific therapy, 2 different siRNA constructs (ENG_A siRNA and ENG_B siRNA) were identified with variable efficacy in reducing endoglin expression (95%–99% reduction with construct A, 50% reduction with construct B), as determined by Western blot (Fig. 3C). ES2 and HeyA8MDR cells transiently transfected with these

Table 2. Quantitative PCR analysis of putative CSC markers and stem cell pathways in matched primary/persistent ovarian cancers (n=12)

Gene name (symbol)	Signaling pathway	Mean		No. of decreased	No. of increased
		Fold change[a]	P[b]	>50%	>2-fold
Putative CSC markers					
Aldehyde dehydrogenase 1A1 (*ALDH1A1*)		2.46	0.2343	3	6
CD44 molecule (*CD44*)		4.08	0.0023	2	9
Prominin 1 (*PROM1/CD133*)		1.11	0.8877	4	5
ATP-binding cassette, sub-family G, member 2 (*ABCG2/BCRP*)		7.65	0.0163	1	5
Human Stem Cell Signaling RT2 Profiler PCR Array					
Endoglin (*ENG*)	TGF-β	3.77	0.0023	0	9
Zinc-finger E-box–binding homeobox 2 (*ZEB2*)	TGF-β	3.66	0.0062	1	9
Presenilin 2 (*PSEN2*)	Notch	3.30	0.0071	0	7
GLI family zinc finger 1 (*GLI1*)	Hedgehog	10.21	0.0076	1	10
GLI family zinc finger 2 (*GLI2*)	Hedgehog	7.61	0.0111	2	9
Latent transforming growth factor-β binding protein 4 (*LTBP4*)	TGF-β	4.69	0.0146	1	9
Transforming growth factor-β receptor II (*TGFBR2*)	TGF-β	2.76	0.0190	0	8
RGM domain family, member A (*RGMA*)	TGF-β	7.84	0.0204	2	9
Activin A receptor, type IB (*ACVR1B*)	TGF-β	2.20	0.0275	0	4
Frizzled homolog 9 (*FZD9*)	Wnt	10.43	0.0393	2	8
SMAD family member 2 (*SMAD2*)	TGF-β	1.79	0.0435	1	6
B-cell CLL/lymphoma 9-like (*BCL9L*)	Wnt	2.06	0.0463	1	6

[a]Persistent compared with primary tumor.
[b]Calculated using paired Student *t* test.

Published OnlineFirst December 5, 2011; DOI:10.1158/1078-0432.CCR-11-2188

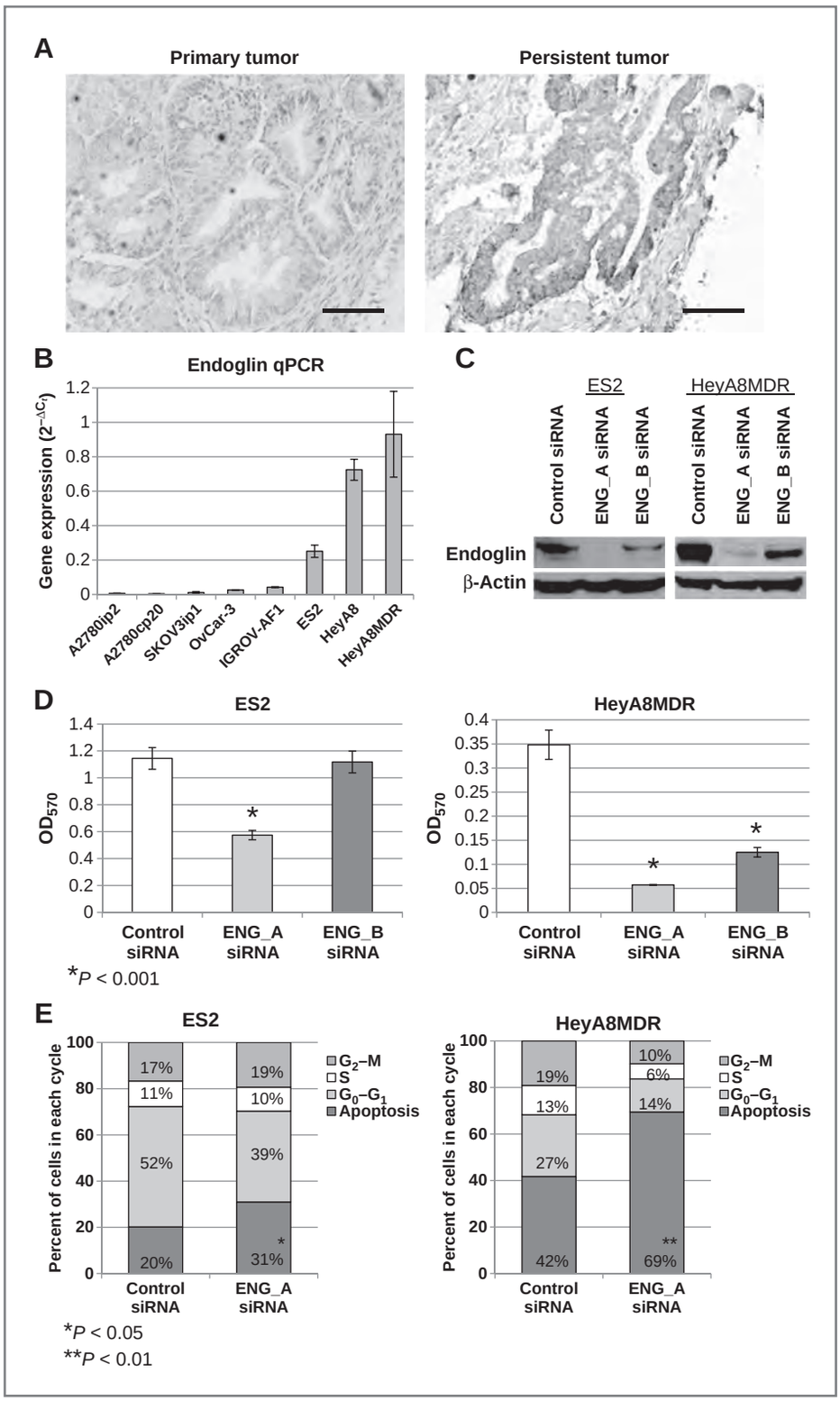

Figure 3. Endoglin is expressed in persistent ovarian tumor and ovarian cancer cell lines, and its downregulation leads to decreased cell viability. A, matched primary/persistent ovarian tumor pairs ($n = 12$) were subjected to IHC analysis of endoglin to evaluate changes in expression. Persistent tumors were found to have a higher density of endoglin staining than in primary specimens. Representative histologic sections are shown for a matched pair (black bar, 100 μm). B, mRNA expression of endoglin was quantified in 8 different ovarian cancer cell lines using quantitative PCR. Gene expression is shown as $\log_2$ transformed ΔC_T values [difference between the C_T value of the gene of interest (*endoglin*) and that of the housekeeping gene (*RPLP0*)]. C, downregulation of endoglin in ES2 and HeyA8MDR cells using 2 different siRNA constructs was determined by Western blot analysis. β-Actin was used as a loading control. D, ES2 and HeyA8MDR cells transiently transfected with anti-endoglin siRNAs had decreased viability as determined by MTT assay. E, cell-cycle analysis (PI staining) revealed that downregulation of endoglin led to an accumulation of both ES2 and HeyA8MDR cells in the sub-G_0 or apoptotic fraction. Data are representative of 3 independent experiments. *, $P < 0.001$.

endoglin-targeting siRNAs showed a significant reduction in viability, as determined by MTT assay (Fig. 3D). This effect on viability correlated with the degree of endoglin downregulation, as ENG_A siRNA reduced cell viability by 50% to 84% (in ES2 and HeyA8MDR, respectively, $P < 0.001$), whereas ENG_B siRNA had no effect on ES2 and a

Published OnlineFirst December 5, 2011; DOI:10.1158/1078-0432.CCR-11-2188

64% reduction in HeyA8MDR ($P < 0.001$). The variability in effects on the 2 cell lines may reflect their dependency on endoglin, as HeyA8MDR cells have 3.7-fold higher endoglin expression than ES2 cells. In addition, ES2 cells may have compensatory pathways active at a baseline that reduce their dependency on endoglin. Additional studies will be required to fully elucidate these mechanisms.

To determine the mechanism by which endoglin downregulation may affect cell viability, cell-cycle analysis was conducted in a separate experiment. ES2 and HeyA8MDR cells were exposed to control or anti-endoglin siRNA (ENG_A), allowed to grow for a total of 72 hours, and examined for DNA content by PI staining (Fig. 3E). In both ES2 and HeyA8MDR, endoglin knockdown resulted in a significant accumulation of cells in the sub-G_0/apoptotic fraction compared with cells transfected with control siRNA (from 20% to 31%; $P < 0.05$ and from 42% to 69%; $P < 0.01$, respectively).

Targeting of Gli1 and Gli2 in ovarian cancer cells

Analysis of stem cell genes upregulated in recurrent tumors reveals both primary mediators of the Hedgehog pathway to be increased after chemotherapy (Table 2). The Hedgehog pathway has previously been implicated in the survival of CSCs (31). To validate its targetability in ovarian cancer, we first examined gene expression of *GLI1* and *GLI2* in the same cell lines as mentioned above. As shown in Fig. 4A, there was no correlation between *GLI1* and *GLI2* expression among the cell lines examined, although all cell lines expressed *GLI1*, *GLI2*, or both. Of note, A2780cp20 cells were found to express *GLI1* 2.05-fold higher and *GLI2* 1.40-fold higher ($P < 0.001$) than their parental line (A2780ip2), suggesting that these Hedgehog pathway members may be involved in mediating platinum resistance.

A2780cp20 ($Gli1^+/Gli2^+$) and ES2 ($Gli1^-/Gli2^+$) cells were subsequently used for examining the biologic effects of Gli1/2 knockdown. Downregulation of Gli1/2 in these cell lines was achieved using 2 different siRNA constructs as confirmed by quantitative PCR (Fig. 4B). Importantly, each siRNA construct showed selectivity for the *GLI* gene to which it was designed against (i.e., *GLI1* siRNAs had no effect on *GLI2* expression and *GLI2* siRNAs had no effect on *GLI1* expression). As shown in Fig. 4C, knockdown of Gli1 or Gli2 alone significantly decreased A2780cp20 cell viability [by up to 65% ($P < 0.001$) and 61% ($P < 0.001$), respectively], whereas in ES2 cells, knockdown of Gli2, but not Gli1, significantly reduced cell viability (by up to 82%, $P < 0.001$). The lack of an effect of *GLI1* downregulation on ES2 cells would be expected as these cells have little to no detectable *GLI1* expression. Interestingly, an increased sensitivity to cisplatin was observed in both A2780cp20 and ES2 cell lines after knockdown of Gli2, but not Gli1 (Fig. 4C). Cisplatin IC_{50} decreased from 4 to 0.8 μmol/L (5.0-fold change) in A2780cp20 cells and from 0.7 to 0.15 μmol/L (4.7-fold change) in ES2 cells. Taken with the demonstration of increased Gli2 expression in samples collected immediately after platinum-based chemotherapy (Table 2), these data make a compelling argument that Gli2 plays a role in platinum resistance, which can be at least partially overcome with Gli2 downregulation. However, Gli1 only appears to contribute to absolute viability, with no platinum-sensitizing effects.

To determine the mechanism by which Gli1/2 downregulation may affect cell viability and/or platinum sensitivity, cell-cycle analysis was conducted in a separate experiment. A2780cp20 cells were exposed to control, anti-Gli1 (GLI1_B), or anti-Gli2 (GLI2_B) siRNA, allowed to grow for a total of 72 hours, and examined for DNA content by PI staining. As shown in Fig. 4D, downregulation of Gli1 had little effect on the cell-cycle distribution of A2780cp20 cells, with a modest accumulation in the sub-G_0 or apoptotic fraction compared with control siRNA (8%–12%, $P < 0.05$). This suggests that the observed decrease in cell viability following Gli1 knockdown may be due to mechanisms independent of the cell cycle. Alternatively, downregulation of Gli2 had a greater impact, with a 4-fold increase (8%–32%, $P < 0.001$) in induction of apoptosis than in control siRNA. This further suggests that Gli2 plays a critical role in ovarian cancer cell survival.

Discussion

We have found that recurrent tumors are more densely composed of putative CSCs as characterized by ALDH1A1, CD44, and CD133 than their matched primary ovarian cancer specimens, suggesting that their expression is clinically significant and may correlate with residual chemoresistant populations that must be present at the end of primary therapy. Presumably targeting these populations with some other treatment modality would be required to achieve durable cures in patients with ovarian cancer. In addition, we identified several genes from a large panel of 84 genes involved in stem cell biology to be significantly overexpressed in recurrent patient samples, further suggesting that resistant tumors are enriched with genes involved in stem cell pathways. With this methodology, the TGF-β coreceptor endoglin was found to be overexpressed in residual tumor cells and thus important to the chemoresistant cancer cell population. This represents a previously unrecognized function of this gene as a mediator of survival in tumor cells, in addition to its known role in angiogenesis. Moreover, the Hedgehog transcription factor Gli2 was also overexpressed and functional in the chemoresistant population and, with correlative *in vitro* data, was found to play a novel role in platinum resistance.

It is hypothesized that CSCs may be responsible for tumor initiation or recurrent disease. There are many facets of this hypothesis that are still under debate, including what level of stemness such populations may have, how best to identify the true stem cell population, and whether these marker-defined cells are also the ones surviving initial chemotherapy (32). However, there clearly are subpopulations within a heterogeneous tumor that have more aggressive, chemoresistant features than others in *ex vivo* and now *de novo* models (2, 33). This is clinically evident in the

Published OnlineFirst December 5, 2011; DOI:10.1158/1078-0432.CCR-11-2188

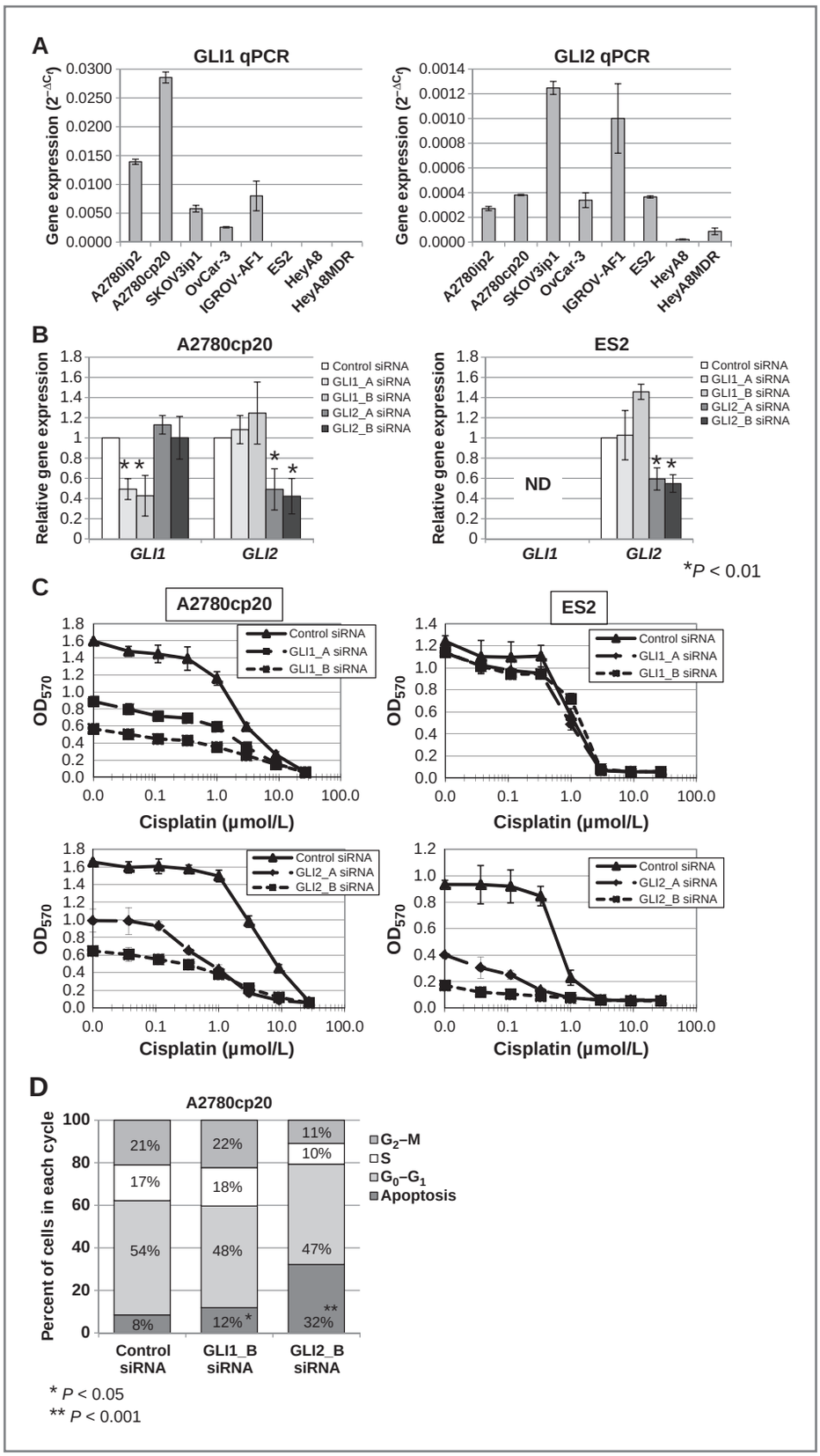

Figure 4. Downregulation of Gli1/2 leads to decreased cell viability and downregulation of Gli2, but not Gli1, sensitizes ovarian cancer cells to cisplatin *in vitro*. A, mRNA expression of *GLI1* and *GLI2* was quantified in 8 different ovarian cancer cell lines using quantitative PCR (qPCR). Gene expression is shown as $\log_2$ transformed ΔC_T values. B, downregulation of Gli1/2 in A2780cp20 and ES2 cells using 2 different siRNA constructs was determined by quantitative PCR. Each siRNA construct showed selectivity for the *GLI* gene to which it was designed against. ND, not detectable; *, $P < 0.01$. C, knockdown of GLI1 or GLI2 alone diminished A2780cp20 cell viability, whereas only knockdown of GLI2 diminished ES2 cell viability as determined by MTT assay. Increased sensitivity to cisplatin (CDDP) was noted in A2780cp20 and ES2 cells transfected with *GLI2* siRNAs, but not *GLI1* siRNAs. D, cell-cycle analysis (PI staining) of A2780cp20 cells exposed to control siRNA, *GLI1* siRNA, or *GLI2* siRNA for a total of 72 hours. Downregulation of Gli2 and, to a lesser extent Gli1, led to an accumulation of cells in the sub-G_0 or apoptotic fraction. Data are representative of 3 independent experiments.

Published OnlineFirst December 5, 2011; DOI:10.1158/1078-0432.CCR-11-2188

observation that patients often have outstanding initial responses to chemotherapy, suggesting that the majority of primary tumor is actually chemosensitive. It is important to note that although we do see an increase in these populations, recurrent tumors are not completely composed of these cells. This indicates that either additional chemoresistant populations are yet to be identified, or these cells have such differentiating capacity that they rapidly produce marker-negative cells, or both. An additional limitation of our analysis is the specific examination of stem cell pathways. Other pathways almost certainly play important roles in mediating survival of the therapy-resistant population; one example being altered DNA repair mechanisms. Recent evidence suggests that ovarian cancers can arise from specific defects in DNA repair pathways, and that inhibitors of the proteins involved in these pathways, such as PARP, could be used to reverse chemoresistance (34), It is reasonable to postulate that CSCs, like normal stem cells, would have enhanced mechanisms of DNA repair, allowing for survival with prolonged exposures to DNA-damaging insults. Analysis of RNA from FFPE samples showed that the extract was of quality appropriate for qPCR analysis, but not enough samples had sufficient quality for full microarray analysis, which could be used in future studies to examine the role of DNA repair or other pathways in mediating chemoresistance. Further characterization of the recurrent chemoresistant tumors with evolving high-throughput methods that can be conducted on FFPE samples, or identification of a cohort of patients with snap frozen tumors, would be required to fully characterize this aggressive population.

Whether the chemoresistant population is composed of predominantly cancer cells with stem cell biology or not, we propose a model of how such a population may comprise the overall tumor during different clinical settings. Because most patients have an initial positive response to chemotherapy, the presenting tumor must be composed of mostly therapy-sensitive cells (TSC), with a small component of therapy-resistant cells (TRC). Treatment selectively kills TSCs, resulting in predominantly TRCs, but in a small enough volume that they are not clinically detectable (persistent tumor). Therefore, the patient is observed, but in about 75% of cases, tumors will recur 18 to 24 months after completion of therapy (with an untreated recurrent tumor). Because of the differentiation capacity of the resistant cells, this tumor has become repopulated with CSC marker–negative differentiated cells and is again heterogeneous, with a significant portion of chemosensitive cells. This would seem to be the case, given the observed 50% response rate seen in patients receiving second-line chemotherapy. However, either because of genetic changes in genetically unstable tumor cells or further selective growth of the therapy-resistant population, ultimately the TRCs dominate, patients get no further response with multiple agents and succumb to tumor burden (treated recurrent tumor). The observed increase in CSC marker staining, particularly ALDH1A1 and CD133, in samples collected immediately at the completion of primary therapy suggests these cells have preferential survival and can go on to give rise to recurrent disease. These cells may represent a population that could be targeted to achieve increased response rates and survival in patients with ovarian cancer.

It is an interesting finding that $CD44^+$ cells were less dense in recurrent tumors than in CD133 and ALDH1, despite multiple studies showing that $CD44^+$ cells have CSC properties. Many of these studies have used CD44 in combination with other markers, such as c-kit (4), MyD88 (5), CD133 (6), and CD24 (35). It is for this reason that we examined CD44 by itself as potentially important, but at the same time may have introduced a limitation by not being able to evaluate dual-positive populations. It is yet to be determined the degree of crossover between individual markers. Likely, the combination of markers will identify a more aggressive population than either alone, as previously shown with CD133 and ALDH1 (11), but it is unknown whether such combinations then exclude other aggressive populations. This disparity, however, highlights the limitations in defining the key population by marker status alone, instead relying on clinical behaviors such as resistance to chemotherapy.

Recent studies have shown that developmental pathways (such as Notch, Wnt, Hedgehog, and TGF-β) play an important role in the self-renewal and maintenance of CSCs and that inhibiting these pathways may provide useful therapeutic strategies both alone and in combination with traditional chemotherapies (36, 37). In our study, genes identified as being significantly overexpressed in persistent tumors included endoglin (a member of the TGF-β superfamily) and the primary mediators of hedgehog transcription, *GLI1* and *GLI2*, among others (Table 2). The most significant and consistent increase in expression from primary to persistent tumor occurred in endoglin (CD105), a TGF-β coreceptor. This molecule interacts with TGF-β receptor II [TGFBR2, which was also significantly increased in persistent tumors (2.76-fold, $P = 0.0190$)], both dependently and independently of the TGF-β ligand (38). This interaction subsequently promotes gene transcription mediated by the Smad family of transcription factors (Smad2 and 4). In contrast, a proteolytically cleaved, secreted form of endoglin, known as soluble endoglin (Sol-Eng) appears to inhibit TGF-β signaling by scavenging circulating TGF-β ligands (39). Endoglin is a well-described marker of angiogenesis whose expression is turned on in growing/sprouting endothelial cells (such as those supplying vasculature to tumors). This characteristic of endoglin has made it a desirable target for antiangiogenic cancer therapy, with monoclonal antibodies being developed for future clinical use (29, 30). Previous studies have shown that endoglin expression in the stroma of ovarian tumors is associated with poor survival (40, 41), but the role of this receptor in cancer cell biology remains largely unexplored. On the basis of our data, it appears that endoglin plays a role in ovarian cancer chemoresistance and recurrence. Moreover, endoglin appears to be important for continued ovarian cancer cell survival as evidenced by our *in vitro* data. In a study conducted by Li and colleagues, it was shown that endoglin

Published OnlineFirst December 5, 2011; DOI:10.1158/1078-0432.CCR-11-2188

prevents apoptosis in endothelial cells undergoing hypoxic stress, either in the presence or absence of TGF-β ligand (42). It could be speculated that endoglin serves a similar antiapoptotic function in tumor epithelial cells and thereby promotes ovarian cancer cell survival. Whether this is due to the promotion of TGF-β signaling or through a TGF-β–independent mechanism remains to be determined. Taken together, these data suggest that inhibiting endoglin could be used to target both the tumor and its developing vasculature, thereby having a potentially greater therapeutic benefit. Additional studies will determine the viability of endoglin as a therapeutic target, as antibodies have been developed that disrupt the interaction of endoglin and TGF-β receptor II (43, 44).

Previous studies have implicated hedgehog signaling in multidrug resistance (45, 46); however, the role of this pathway in resistance to platinum-based compounds remains largely unexplored. While both Gli1 and Gli2 appeared to mediate ovarian cancer cell survival *in vitro*, only downregulation of Gli2 sensitized cells to cisplatin in a synergistic fashion, with a 5-fold reduction in IC_{50} concentrations in two different cell lines. It is suggested that the mechanism underlying this sensitization involves apoptosis. Inhibition of apoptosis is known to mediate cisplatin resistance (47), and Gli2 has previously been shown to serve an antiapoptotic function through transcriptional regulation of apoptotic inhibitor molecules (48–50). In our study, we found that downregulation of Gli2 alone induced apoptosis, and this may have contributed to the increased sensitivity of ovarian cancer cells to cisplatin *in vitro*. Interestingly, downregulation of Gli1 had no effect on cisplatin toxicity. Future studies on the link between Gli2, apoptosis, and cisplatin resistance are warranted.

Collectively, the data presented in this study show that cells with stem cell properties enrich recurrent ovarian tumors, especially in their more chemoresistant forms. The varied density of these subpopulations in different clinical scenarios provides insight into the dynamic heterogeneity during the typical natural history of ovarian cancer progression. Additional stem cell pathways contribute to the continued survival and chemoresistance of ovarian cancer, and targeting these pathways may be necessary to achieve durable clinical response in this disease. In addition, the TGF-β coreceptor endoglin (CD105) and the Hedgehog mediator Gli2 were found to be overexpressed in recurrent ovarian tumors and are promising targets in overcoming chemoresistance.

Disclosure of Potential Conflicts of Interest

No potential conflicts of interest were disclosed.

Grant Support

Funding support was provided by the University of Alabama at Birmingham Center for Clinical and Translational Science (5UL1RR025777), the Reproductive Scientist Development Program through the Ovarian Cancer Research Fund and the NIH (K12 HD00849), and the Department of Defense Ovarian Cancer Research Academy (OC093443).

The costs of publication of this article were defrayed in part by the payment of page charges. This article must therefore be hereby marked *advertisement* in accordance with 18 U.S.C. Section 1734 solely to indicate this fact.

Received August 26, 2011; revised November 8, 2011; accepted November 17, 2011; published OnlineFirst December 5, 2011.

References

1. Bhoola S, Hoskins WJ. Diagnosis and management of epithelial ovarian cancer. Obstet Gynecol 2006;107:1399–410.
2. Rosen JM, Jordan CT. The increasing complexity of the cancer stem cell paradigm. Science 2009;324:1670–3.
3. Dalerba P, Cho RW, Clarke MF. Cancer stem cells: models and concepts. Annu Rev Med 2007;58:267–84.
4. Zhang S, Balch C, Chan MW, Lai HC, Matei D, Schilder JM, et al. Identification and characterization of ovarian cancer-initiating cells from primary human tumors. Cancer Res 2008;68:4311–20.
5. Alvero AB, Montagna MK, Holmberg JC, Craveiro V, Brown DA, Mor G. Targeting the mitochondria activates two independent cell death pathways in the ovarian cancer stem cells. Mol Cancer Ther 2011;10:1385–93.
6. Slomiany MG, Dai L, Tolliver LB, Grass GD, Zeng Y, Toole BP. Inhibition of functional hyaluronan-CD44 interactions in CD133-positive primary human ovarian carcinoma cells by small hyaluronan oligosaccharides. Clin Cancer Res 2009;15:7593–601.
7. Curley MD, Therrien VA, Cummings CL, Sergent PA, Koulouris CR, Friel AM, et al. CD133 expression defines a tumor initiating cell population in primary human ovarian cancer. Stem Cells 2009;27:2875–83.
8. Baba T, Convery PA, Matsumura N, Whitaker RS, Kondoh E, Perry T, et al. Epigenetic regulation of CD133 and tumorigenicity of CD133+ ovarian cancer cells. Oncogene 2009;28:209–18.
9. Szotek PP, Pieretti-Vanmarcke R, Masiakos PT, Dinulescu DM, Connolly D, Foster R, et al. Ovarian cancer side population defines cells with stem cell-like characteristics and Mullerian inhibiting substance responsiveness. Proc Natl Acad Sci U S A 2006;103:11154–9.
10. Landen CN Jr, Goodman B, Katre AA, Steg AD, Nick AM, Stone RL, et al. Targeting aldehyde dehydrogenase cancer stem cells in ovarian cancer. Mol Cancer Ther 2010;9:3186–99.
11. Silva IA, Bai S, McLean K, Yang K, Griffith K, Thomas D, et al. Aldehyde dehydrogenase in combination with CD133 defines angiogenic ovarian cancer stem cells that portend poor patient survival. Cancer Res 2011;71:3991–4001.
12. Kryczek I, Liu S, Roh M, Vatan L, Szeliga W, Wei S, et al. Expression of aldehyde dehydrogenase and CD133 defines ovarian cancer stem cells. Int J Cancer 2012;130:29–39.
13. Deng S, Yang X, Lassus H, Liang S, Kaur S, Ye Q, et al. Distinct expression levels and patterns of stem cell marker, aldehyde dehydrogenase isoform 1 (ALDH1), in human epithelial cancers. PLoS One 2010;5:e10277.
14. Landen CN Jr, Lu C, Han LY, Coffman KT, Bruckheimer E, Halder J, et al. Efficacy and antivascular effects of EphA2 reduction with an agonistic antibody in ovarian cancer. J Natl Cancer Inst 2006;98:1558–70.
15. SABiosciences. Human RT^2 RNA QC PCR Array; 2011. Available from: http://www.sabiosciences.com/rt_pcr_product/HTML/PAHS-999A.html. Accessed on 6/17/2011.
16. SABiosciences. Human Stem Cell Signaling RT^2 Profiler PCR Array; 2011. Available from: http://www.sabiosciences.com/rt_pcr_product/HTML/PAHS-047A.html. Accessed on 6/17/2011.

Published OnlineFirst December 5, 2011; DOI:10.1158/1078-0432.CCR-11-2188

17. Steg A, Wang W, Blanquicett C, Grunda JM, Eltoum IA, Wang K, et al. Multiple gene expression analyses in paraffin-embedded tissues by TaqMan low-density array: application to hedgehog and Wnt pathway analysis in ovarian endometrioid adenocarcinoma. J Mol Diagn 2006;8:76–83.
18. Louie KG, Behrens BC, Kinsella TJ, Hamilton TC, Grotzinger KR, McKoy WM, et al. Radiation survival parameters of antineoplastic drug-sensitive and -resistant human ovarian cancer cell lines and their modification by buthionine sulfoximine. Cancer Res 1985;45:2110–5.
19. Landen CN, Kim TJ, Lin YG, Merritt WM, Kamat AA, Han LY, et al. Tumor-selective response to antibody-mediated targeting of alphavbeta3 integrin in ovarian cancer. Neoplasia 2008;10:1259–67.
20. Halder J, Kamat AA, Landen CN Jr, Han LY, Lutgendorf SK, Lin YG, et al. Focal adhesion kinase targeting using *in vivo* short interfering RNA delivery in neutral liposomes for ovarian carcinoma therapy. Clin Cancer Res 2006;12:4916–24.
21. Lau DH, Ross KL, Sikic BI. Paradoxical increase in DNA cross-linking in a human ovarian carcinoma cell line resistant to cyanomorpholino doxorubicin. Cancer Res 1990;50:4056–60.
22. Buick RN, Pullano R, Trent JM. Comparative properties of five human ovarian adenocarcinoma cell lines. Cancer Res 1985;45:3668–76.
23. Moore DH, Allison B, Look KY, Sutton GP, Bigsby RM. Collagenase expression in ovarian cancer cell lines. Gynecol Oncol 1997;65:78–82.
24. Thaker PH, Yazici S, Nilsson MB, Yokoi K, Tsan RZ, He J, et al. Antivascular therapy for orthotopic human ovarian carcinoma through blockade of the vascular endothelial growth factor and epidermal growth factor receptors. Clin Cancer Res 2005;11:4923–33.
25. Spannuth WA, Mangala LS, Stone RL, Carroll AR, Nishimura M, Shahzad MM, et al. Converging evidence for efficacy from parallel EphB4-targeted approaches in ovarian carcinoma. Mol Cancer Ther 2010;9:2377–88.
26. Hamilton TC, Young RC, McKoy WM, Grotzinger KR, Green JA, Chu EW, et al. Characterization of a human ovarian carcinoma cell line (NIH: OVCAR-3) with androgen and estrogen receptors. Cancer Res 1983;43:5379–89.
27. Yu D, Wolf JK, Scanlon M, Price JE, Hung MC. Enhanced c-erbB-2/neu expression in human ovarian cancer cells correlates with more severe malignancy that can be suppressed by E1A. Cancer Res 1993;53:891–8.
28. Ding XW, Wu JH, Jiang CP. ABCG2: a potential marker of stem cells and novel target in stem cell and cancer therapy. Life Sci 2010;86:631–7.
29. Fonsatti E, Altomonte M, Nicotra MR, Natali PG, Maio M. Endoglin (CD105): a powerful therapeutic target on tumor-associated angiogenetic blood vessels. Oncogene 2003;22:6557–63.
30. Dallas NA, Samuel S, Xia L, Fan F, Gray MJ, Lim SJ, et al. Endoglin (CD105): a marker of tumor vasculature and potential target for therapy. Clin Cancer Res 2008;14:1931–7.
31. Merchant AA, Matsui W. Targeting Hedgehog–a cancer stem cell pathway. Clin Cancer Res 2010;16:3130–40.
32. Hill RP. Identifying cancer stem cells in solid tumors: case not proven. Cancer Res 2006;66:1891–5; discussion 1890.
33. Sneddon JB, Werb Z. Location, location, location: the cancer stem cell niche. Cell Stem Cell 2007;1:607–11.
34. Annunziata CM, O'Shaughnessy J. Poly (ADP-ribose) polymerase as a novel therapeutic target in cancer. Clin Cancer Res 2010;16:4517–26.
35. Wei X, Dombkowski D, Meirelles K, Pieretti-Vanmarcke R, Szotek PP, Chang HL, et al. Mullerian inhibiting substance preferentially inhibits stem/progenitors in human ovarian cancer cell lines compared with chemotherapeutics. Proc Natl Acad Sci U S A 2010;107:18874–9.
36. Takebe N, Harris PJ, Warren RQ, Ivy SP. Targeting cancer stem cells by inhibiting Wnt, Notch, and Hedgehog pathways. Nat Rev Clin Oncol 2011;8:97–106.
37. Singh A, Settleman J. EMT, cancer stem cells and drug resistance: an emerging axis of evil in the war on cancer. Oncogene 2010;29:4741–51.
38. Barbara NP, Wrana JL, Letarte M. Endoglin is an accessory protein that interacts with the signaling receptor complex of multiple members of the transforming growth factor-beta superfamily. J Biol Chem 1999;274:584–94.
39. Perez-Gomez E, Del Castillo G, Juan Francisco S, Lopez-Novoa JM, Bernabeu C, Quintanilla M. The role of the TGF-β coreceptor endoglin in cancer. Sci World J 2010;10:2367–84.
40. Henriksen R, Gobl A, Wilander E, Oberg K, Miyazono K, Funa K. Expression and prognostic significance of TGF-beta isotypes, latent TGF-beta 1 binding protein, TGF-beta type I and type II receptors, and endoglin in normal ovary and ovarian neoplasms. Lab Invest 1995;73:213–20.
41. Taskiran C, Erdem O, Onan A, Arisoy O, Acar A, Vural C, et al. The prognostic value of endoglin (CD105) expression in ovarian carcinoma. Int J Gynecol Cancer 2006;16:1789–93.
42. Li C, Issa R, Kumar P, Hampson IN, Lopez-Novoa JM, Bernabeu C, et al. CD105 prevents apoptosis in hypoxic endothelial cells. J Cell Sci 2003;116:2677–85.
43. Shiozaki K, Harada N, Greco WR, Haba A, Uneda S, Tsai H, et al. Antiangiogenic chimeric anti-endoglin (CD105) antibody: pharmacokinetics and immunogenicity in nonhuman primates and effects of doxorubicin. Cancer Immunol Immunother 2006;55:140–50.
44. Seon BK, Haba A, Matsuno F, Takahashi N, Tsujie M, She X, et al. Endoglin-targeted cancer therapy. Curr Drug Deliv 2011;8:135–43.
45. Sims-Mourtada J, Izzo JG, Ajani J, Chao KS. Sonic Hedgehog promotes multiple drug resistance by regulation of drug transport. Oncogene 2007;26:5674–9.
46. Singh RR, Kunkalla K, Qu C, Schlette E, Neelapu SS, Samaniego F, et al. ABCG2 is a direct transcriptional target of hedgehog signaling and involved in stroma-induced drug tolerance in diffuse large B-cell lymphoma. Oncogene. 2011 May 30. [Epub ahead of print].
47. Siddik ZH. Cisplatin: mode of cytotoxic action and molecular basis of resistance. Oncogene 2003;22:7265–79.
48. Regl G, Kasper M, Schnidar H, Eichberger T, Neill GW, Philpott MP, et al. Activation of the BCL2 promoter in response to Hedgehog/GLI signal transduction is predominantly mediated by GLI2. Cancer Res 2004;64:7724–31.
49. Kump E, Ji J, Wernli M, Hausermann P, Erb P. Gli2 upregulates cFlip and renders basal cell carcinoma cells resistant to death ligand-mediated apoptosis. Oncogene 2008;27:3856–64.
50. Narita S, So A, Ettinger S, Hayashi N, Muramaki M, Fazli L, et al. GLI2 knockdown using an antisense oligonucleotide induces apoptosis and chemosensitizes cells to paclitaxel in androgen-independent prostate cancer. Clin Cancer Res 2008;14:5769–77.

Published OnlineFirst July 13, 2011; DOI:10.1158/1078-0432.CCR-11-0432

Clinical Cancer Research

Targeting the Notch Ligand Jagged1 in Both Tumor Cells and Stroma in Ovarian Cancer

Adam D. Steg, Ashwini A. Katre, Blake Goodman, et al.

Clin Cancer Res 2011;17:5674-5685. Published OnlineFirst July 13, 2011.

Published OnlineFirst July 13, 2011; DOI:10.1158/1078-0432.CCR-11-0432

Cancer Therapy: Preclinical

Clinical Cancer Research

Targeting the Notch Ligand Jagged1 in Both Tumor Cells and Stroma in Ovarian Cancer

Adam D. Steg[1], Ashwini A. Katre[1], Blake Goodman[2], Hee-Dong Han[2,5], Alpa M. Nick[2], Rebecca L. Stone[2], Robert L. Coleman[2], Ronald D. Alvarez[1], Gabriel Lopez-Berestein[3,5], Anil K. Sood[2,4,5], and Charles N. Landen[1]

Abstract

Purpose: Jagged1, a Notch ligand, is expressed on both tumor epithelial and endothelial cells and therefore may be amenable to dual targeting of the tumor stroma and malignant cell compartments of the tumor microenvironment.

Experimental Design: We describe *in vitro* effects of targeting of Jagged1 on ovarian cancer cells and *in vivo* effects of independent targeting of stromal and malignant cell Jagged1 using species-specific human or murine siRNA constructs incorporated into chitosan nanoparticles and delivered intravenously in an orthotopic mouse model.

Results: Jagged1 expression was prominent in SKOV3ip1 and IGROV-AF1, and significantly overexpressed in SKOV3TRip2, a taxane-resistant SKOV3 subclone. Jagged1 silencing with siRNA decreased cell viability and reversed taxane chemoresistance. In two different orthotopic ovarian cancer models, treatment with anti-human Jagged1 siRNA-CH reduced growth by 54.4% to 58.3% and with anti-murine Jagged1 siRNA-CH reduced growth by 41.7% to 48.8%. The combination of both species-specific constructs reduced tumor weight by 87.5% to 93.1% and sensitized SKOV3TRip2 tumors to docetaxel *in vivo*. Tumors showed reduced microvessel density with anti-murine Jagged1 constructs and decreased proliferation with anti-human Jagged1 siRNAs-CH. In addition, we show that Jagged1 downregulation does not sensitize cells to taxanes through a reduction in *MDR1* expression, but at least in part by cross-talk with the GLI2 mediator of the Hedgehog pathway.

Conclusions: Jagged1 plays dual roles in cancer progression through an angiogenic function in tumor endothelial cells and through proliferation and chemoresistance in tumor cells. Dual inhibition represents an attractive therapeutic strategy for ovarian and potentially other malignancies. *Clin Cancer Res; 17(17); 5674–85. ©2011 AACR.*

Introduction

Ovarian cancer is the leading cause of death from a gynecologic malignancy. Although ovarian cancer is among the most chemosensitive malignancies at the time of initial treatment (surgery and taxane/platinum-based chemotherapy), most patients will develop tumor recurrence and succumb to chemoresistant disease (1). Evaluation of multiple chemotherapy agents in several combinations in the last 20 years has yielded modest improvements in progression-free survival, but no increases in durable cures. The clinical course suggests that a population of tumor cells has either inherent or acquired resistance to chemotherapy that allows survival with initial therapy and ultimately leads to recurrence. Targeting the cellular pathways involved in this resistance may provide new treatment modalities for ovarian cancer.

The Notch pathway plays an important role in cell growth and differentiation during embryonic development (2). Mature Notch receptors (Notch1; refs. 2–4) consist of an extracellular and transmembrane unit. Upon binding to ligands (Jagged1, 2 and delta-like ligand (DLL) 1, 3, and 4) on the surface of neighboring cells, the Notch extracellular unit is dissociated from the transmembrane unit, which is then endocytosed into ligand-expressing cells. Further cleavage of the transmembrane unit by "a disintegrin and metalloprotease" proteins (ADAM10 and/or 17) and γ-secretase produces an active intracellular fragment that translocates to the nucleus, where it forms a transcriptional complex with CSL, mastermind-like proteins (MAML1, 2, and 3), and p300. Transcriptional mediators of Notch signaling include members of the HES and HEY family. Recent reports have implicated Notch signaling in multiple

Authors' Affiliations: [1]Department of Obstetrics and Gynecology, University of Alabama at Birmingham, Birmingham, Alabama; and Departments of [2]Gynecologic Oncology, [3]Experimental Therapeutics, and [4]Cancer Biology, and [5]Center for RNA Interference and Non-Coding RNA, U.T.M.D. Anderson Cancer Center, Houston, Texas

Corresponding Author: Charles N. Landen, Department of Obstetrics and Gynecology, The University of Alabama at Birmingham, 1825 University Boulevard, 505 Shelby Building, Birmingham, AL 35294. Phone: 205-934-0473; Fax: 205-934-0474; E-mail: clanden@uab.edu

doi: 10.1158/1078-0432.CCR-11-0432

Published OnlineFirst July 13, 2011; DOI:10.1158/1078-0432.CCR-11-0432

Translational Relevance

Most ovarian cancer patients will have an excellent response to initial surgical debulking and chemotherapy, but about 75% of patients will later recur and succumb to disease. There is likely a privileged population with either inherent or acquired resistance to chemotherapy, and finding therapies against this population is essential to achieving long-term disease control. Among many potential pathways implicated in survival of these populations is the Notch pathway, and the Notch ligand Jagged1, which can be expressed on both tumor endothelial cells and tumor cells. We have showed that Jagged1 plays important roles in both compartments of the tumor—chemoresistance in tumor cells and angiogenesis in stroma. Furthermore, targeting Jagged1 independently on endothelial cells leads to reduced angiogenesis and, on tumor cells, reduces proliferation and reverses taxane resistance. A novel mechanism of Jagged1 signaling through the Hedgehog pathway is also described. Our findings highlight that dual targeting of each compartment of the tumor microenvironment (stromal and malignant cells) is an important principle underlying therapy, and that therapies specifically against Jagged1 may improve response rates and outcomes in ovarian cancer.

malignancies (3), including ovarian cancer (4–7), and suggest that this pathway may be especially important in maintaining the subpopulation of cancer cells with stem cell properties (8) as well as conferring resistance to chemotherapies (9, 10). The Notch ligand Jagged1 is frequently overexpressed on both ovarian cancer cells (6) and tumor-associated endothelial cells (11), suggesting that selectively targeting this protein may present a novel therapeutic strategy to target both stromal and tumor cells in ovarian cancer. The Notch pathway is highly implicated in normal and tumor-associated angiogenesis (12–14). Moreover, studies have shown that Jagged1 can activate gene expression (15) and transform kidney epithelial cells (16) without involvement of Notch signaling, indicating that Jagged1 may have its own signaling function that is important to tumorigenesis independent of the canonical Notch pathway.

As most studies have focused on the effects of inhibiting the Notch receptor and its downstream signaling, specific inhibition of Jagged1 has not been fully explored, which is especially important given potential Notch-independent effects of Jagged1. In addition, it is not known whether the greater *in vivo* contribution of Notch inhibition is through its antiangiogenic mechanism or specific activity against malignant cells. In this study, we sought to determine the effects of targeting Jagged1 on the viability and taxane and platinum chemoresistance of ovarian cancer cells and tumor-associated stroma, independently and concurrently. Utilizing a novel methodology for delivering siRNA *in vivo*, we independently target Jagged1 in stromal cells with anti-murine siRNA and Jagged1 in malignant cells with anti-human siRNA and show that Jagged1 plays important roles in tumor angiogenesis and chemoresistance and is an attractive target for therapy.

Materials and Methods

Cell lines and culture

The ovarian cancer cell lines A2780ip2, A2780cp20, HeyA8, HeyA8MDR, IGROV-AF1, SKOV3ip1, and SKOV3-TRip2 (17, 18) were maintained in RPMI-1640 medium supplemented with 10% FBS (Hyclone). A2780cp20 (platinum resistant), HeyA8MDR (taxane resistant), and SKOV3TRip2 (taxane resistant, a kind gift of Dr. Michael Seiden (19), were generated by sequential exposure to increasing concentrations of chemotherapy. HeyA8MDR and SKOV3TRip2 were maintained with the addition of 150 ng/mL of paclitaxel. The murine ovarian endothelial cell (MOEC) line was established from the immortomouse, which harbors temperature-sensitive SV40 large T antigen overexpression (20). MOEC cells allowed for the evaluation of murine-specific Jagged1 expression. All cell lines were routinely screened for *Mycoplasma* species (GenProbe detection kit; Fisher) with experiments carried out at 70% to 80% confluent cultures. Purity of cell lines was confirmed with short tandem repeat genomic analysis, and only cells less than 20 passages from stocks were used in experiments.

RNA extraction and reverse transcription

Total RNA was isolated from ovarian cancer cell lines by using Trizol reagent (Invitrogen) per manufacturer's instructions. RNA was then DNase treated and purified by using the RNeasy Mini Kit (QIAGEN). RNA was eluted in 50 μL of RNase-free water and stored at −80°C. The concentration of all RNA samples was quantified by spectrophotometric absorbance at 260/280 nm by using an Eppendorf BioPhotometer plus. Prior to cDNA synthesis, all RNA samples were diluted to 20 ng/μL using RNase-free water. cDNA was prepared by using the High Capacity cDNA Reverse Transcription Kit (Applied Biosystems). The resulting cDNA samples were analyzed using quantitative PCR.

Quantitative PCR

Primer and probe sets for *GLI1* (Hs00171790_m1), *GLI2* (Hs00257977_m1), *HES1* (Hs00172878_m1), *HEY1* (Hs00232618_m1), *JAG1* (Hs01070032_m1), *MDR1* (Hs00184500_m1), *NOTCH1* (Hs00413187_m1), *NOTCH3* (Hs01128541_m1), and *RPLP0* (Hs99999902_m1; housekeeping gene) were obtained from Applied Biosystems and used according to manufacturer's instructions. PCR amplification was carried out on an ABI Prism 7900HT sequence detection system, and gene expression was calculated by using the comparative cycling threshold (C_t) method as previously described (21). Briefly, this technique uses the formula $2^{-\Delta\Delta C_t}$ to

Published OnlineFirst July 13, 2011; DOI:10.1158/1078-0432.CCR-11-0432

calculate the expression of target genes normalized to a calibrator. The C_t indicates the cycle number at which the amount of amplified target reaches a fixed threshold. C_t values range from 0 to 40 (the latter representing the default upper limit PCR cycle number that defines failure to detect a signal).

Western blot analysis

Cultured cell lysates were collected in modified radioimmunoprecipitation assay lysis buffer with protease inhibitor cocktail (Roche) and subjected to immunoblot analysis by standard techniques (22) using anti-Jagged1 antibody (28H8; Cell Signaling Technology) at 1:1,000 dilution overnight at 4°C, PARP antibody (7D3-6; BD Biosciences) at 1:1,000 dilution overnight at 4°C, anti-Cleaved Notch1 antibody (Cell Signaling Technology) at 1:1,000 dilution overnight at 4°C, anti-Notch3 antibody (M-134; Santa Cruz Biotechnology) at 1:200 dilution overnight at 4°C, anti-Gli2 antibody (Sigma) at 1:500 dilution overnight at 4°C, or anti–β-actin antibody (AC-15; Sigma) at 1:20,000 dilution for 1 hour at room temperature (RT), which was used to monitor equal sample loading. After washing, blots were incubated with goat anti-rabbit (for Jagged1, Notch1, Notch3, and Gli2) or goat anti-mouse (for PARP and β-actin) secondary antibodies (Bio-Rad) conjugated with horseradish peroxidase. Visualization was carried out by the enhanced chemiluminescence method (Pierce Thermo Scientific).

siRNA transfection

To examine downregulation of Jagged1, Gli2, Notch1, or Notch3 with siRNA, cells were exposed to control siRNA (target sequence: 5′-UUCUCCGAACGUGUCACGU-3′; Sigma) or one of 2 tested Jagged1-targeting constructs (JAG1_A: 5′-GAAUGUGAGGCCAAACCUU-3′ or JAG1_B: 5′-CCUGUAACAUAGCCCGAAA-3′; Sigma) or one of 2 tested Gli2-targeting constructs (GLI2_A: 5′-GUACCAUUACGAGCCUCAU-3′ or GLI2_B: 5′-CCUUCAAGGCGCAGUACAU-3′; Sigma) or a Notch1-targeting construct (5′-GUGUGAAUCCAACCCUUGU-3′; Sigma) or a Notch3-targeting construct (5′-GGUAGUAAUGCUGGAGAUU-3′; Sigma) at a 1:3 siRNA (μg) to lipofectamine 2,000 (μL) ratio. Lipofectamine and siRNA were incubated for 20 minutes at RT, added to cells in serum-free RPMI to incubate for 6 hours, followed by 10% FBS/RMPI thereafter. Transfected cells were grown at 37°C for 48 to 72 hours and then harvested for viable cell counting, quantitative PCR, or Western blot analysis.

Assessment of cell viability with chemotherapy IC_{50} and cell-cycle analysis

To a 96-well plate, 2,000 cells/well were exposed to increasing concentrations of docetaxel in triplicate. Viability was assessed with 0.15% MTT (Sigma). For effects of siRNA-mediated downregulation on docetaxel IC50, cells were first transfected with siRNA (5 μg) for 24 hours in 6-well plates, then trypsinized, and re-plated at 2,000 cells per well, followed by addition of chemotherapy after attachment. IC_{50} was determined by finding the dose at which the drug had 50% of its effect, calculated by the equation $[(OD450_{MAX} - OD450_{MIN})/2 + OD450_{MIN}]$. Test of synergy was carried out by the Loewe additivity model (23), calculated by the equation $CI = (D_1/D_{x1}) + (D_2/D_{x2})$, where a CI (combination index) of 1 suggests an additive effect, less than 1 suggests synergy, and more than 1 suggests antagonism. For cell-cycle analysis, cells were transfected with siRNA for 72 hours, trypsinized, and fixed in 75% ethanol overnight. Cells were then centrifuged, washed 2× in PBS, and reconstituted in PBS with 50 μg/mL propidium iodide (PI). PI fluorescence was assessed by flow cytometry, and the percentage of cells in sub-G_0, G_0–G_1, S, and G_2–M phases were calculated by the cell-cycle analysis module for Flow Cytometry Analysis Software (FlowJo v.7.6.1).

Orthotopic ovarian cancer model and *in vivo* delivery of siRNA

For orthotopic therapy experiments using ovarian cancer cell lines, female athymic nude mice (NCr-nu) were purchased from the National Cancer Institute after Institution Animal Care and Use Committee approval of protocols, and cared for in accordance with guidelines of the American Association for Accreditation of Laboratory Animal Care. For all *in vivo* experiments, trypsinized cells were resuspended in 10% FBS-containing RPMI, washed with PBS, and suspended in serum-free Hanks' balanced salt solution at a concentration of 5×10^6 cells/mL, and 1×10^6 cells (IGROV-AF1 or SKOV3TRip2) were injected IP in 200 μL into 40 mice per experiment. After 1 week, mice ($n = 10$ per group) were randomized to treatment with (i) 10 μg control siRNA, (ii) 5 μg murine-specific anti-Jagged1 siRNA (target sequence: 5′-CAGUAAUGACACUAUUCAA-3′, Sigma) plus 5 μg control siRNA, (iii) 5 μg human-specific anti-Jagged1 siRNA (same as JAG1_B siRNA) plus 5 μg control siRNA, or (iv) 5 μg of both species-specific siRNA constructs. In another experiment, mice bearing SKOV3TRip2 tumors were randomized to treatment with (i) 10 μg control siRNA, (ii) 10 μg control siRNA plus docetaxel, (iii) both species-specific anti-Jagged1 siRNA constructs (5 μg each), or (iv) both species-specific constructs (5 μg each) plus docetaxel. In a separate experiment, mice bearing SKOV3TRip2 tumors were randomized to treatment with (i) 10 μg control siRNA plus docetaxel, (ii) 5 μg human-specific anti-Jagged1 siRNA plus 5 μg control siRNA plus docetaxel; (iii) 5 μg murine-specific anti-Jagged1 siRNA plus 5 μg control siRNA plus docetaxel, or (iv) both species-specific constructs (5 μg each) plus docetaxel. siRNA constructs were incorporated in chitosan nanoparticles as previously described (24, 25) and administered IV twice per week in a volume of 100 μL. Docetaxel was administered IP at a dose of 35 μg weekly. Mice were treated for 4 to 6 weeks before sacrifice and tumor collection.

Immunohistochemical staining

Resected tumors frozen in Tissue-Tek OCT compound (Sakura) were used for immunohistochemical (IHC) analysis of microvessel density (MVD) by using anti-CD31

Published OnlineFirst July 13, 2011; DOI:10.1158/1078-0432.CCR-11-0432

antibodies (Cell Signaling Technology). Analysis of cell proliferation was determined by IHC carried out on formalin-fixed paraffin-embedded tumors with anti-PCNA (proliferating cell nuclear antigen) antibodies (Cell Signaling Technology). Detection of CD31 and PCNA were carried out as previously described (26). To quantify MVD and cell proliferation, 5 random fields were recorded for each tumor at 100× magnification. A vessel was defined as CD31 staining with a visible associated lumen. PCNA staining was considered positive if the entire nucleus was strongly positive. Terminal deoxynucleotidyl transferase–mediated dUTP nick end labeling (TUNEL) was carried out as previously described to determine cell apoptosis (27). Quantification of apoptosis was calculated by determining the number of apoptotic cells in 5 random fields for each tumor at 200× magnification. All staining was quantified by 2 investigators in a blinded fashion. Images were assessed and quantified without modification; however, for publication of PCNA figures, contrast was enhanced to an entire image by using the "Auto Contrast" tool in Photoshop to avoid bias.

Statistical analysis

Comparisons of gene expression, PI fluorescence, mean tumor weight, and mean MVD, PCNA, and TUNEL$^+$ cells were analyzed by using a 2-tailed Student's *t* test, if assumptions of data normality were met. Those represented by alternate distribution were examined by using a nonparametric Mann–Whitney *U* test. Differences between groups were considered statistically significant at $P < 0.05$. Error bars represent standard deviation unless otherwise stated. Number of mice per group ($n = 10$) was chosen as directed by a power analysis to detect a 50% decrease in tumor growth with beta error of 0.2.

Results

Jagged1 expression in ovarian cancer cell lines

We first examined Jagged1 expression (both mRNA and protein) in IGROV-AF1 and 3 pairs of parental and chemoresistant ovarian cancer cell lines: A2780ip2/A2780cp20 (20-fold increased cisplatin resistance and 10-fold increased taxane resistance), HeyA8/HeyA8MDR (500-fold taxane resistant), and SKOV3ip1/SKOV3TRip2 (1,000-fold taxane resistant). mRNA expression of Jagged1, as measured by quantitative PCR, was prominent in IGROV-AF1, SKOV3ip1, and SKOV3TRip2 with little to no expression in the A2780ip2/A2780cp20 and HeyA8/HeyA8MDR lines (Fig. 1A). Western blot analysis showed similar Jagged1 expression as that obtained using qPCR (Fig. 1B). Interestingly, Jagged1 mRNA expression was 4.6-fold higher ($P < 0.05$) in the taxane-resistant SKOV3TRip2 line compared with its parental cell line, SKOV3ip1.

Downregulation of Jagged1 decreases viability and reverses taxane resistance in ovarian cancer cells *in vitro*

To determine whether Jagged1 downregulation affects ovarian cancer cell viability *in vitro*, IGROV-AF1 and

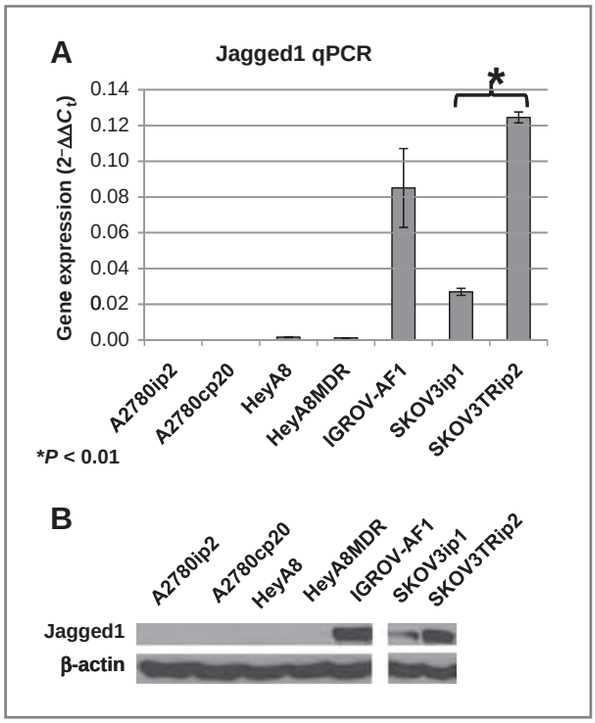

Figure 1. Jagged1 expression in ovarian cancer cell lines. A, mRNA expression of Jagged1 was quantified in IGROV-AF1 and three pairs of chemosensitive and chemoresistant ovarian cancer cell lines using quantitative PCR. Gene expression is shown as $\log_2$ transformed ΔC_t values [difference between the C_t value of the gene of interest (Jagged1) and that of the housekeeping gene (RPLP0)]. *, $P < 0.01$. B, protein expression of Jagged1 was also measured using Western blot analysis. β-actin was used as a loading control. Blot is representative of 3 independent experiments.

SKOV3TRip2 cells were transiently transfected with 2 different siRNA constructs against Jagged1 (JAG1_A or JAG1_B siRNA). JAG1_B siRNA decreased Jagged1 expression to a greater extent than JAG1_A siRNA in both IGROV-AF1 and SKOV3TRip2 cells, as determined by Western blot (Fig. 2A). Concordantly, JAG1_B siRNA had the greatest effect on cell viability for both IGROV-AF1 (37.7% reduction, $P < 0.05$) and SKOV3TRip2 (71.5% reduction, $P < 0.001$) cells (Fig. 2B, data points on *y*-axis). Given the increased expression of Jagged1 in the taxane-resistant SKOV3TRip2 line, we asked whether downregulation of Jagged1 could sensitize resistant cells to chemotherapy. IGROV-AF1 and SKOV3TRip2 cells were transiently transfected with Jagged1-targeting siRNAs or control siRNA for 24 hours and exposed to increasing concentrations of docetaxel. Cell viability was assessed by MTT assay 4 days after the addition of docetaxel. As shown in Figure 2B, downregulation of Jagged1 did not increase the sensitivity of IGROV-AF1 cells to docetaxel (IC_{50}: ~2 nmol/L); however, downregulation of Jagged1 reduced the docetaxel IC_{50} from 40 to 10.2 nmol/L in SKOV3TRip2 cells. Overcoming taxane resistance in the SKOV3TRip2 line but not in the already-sensitive IGROV-AF1 line suggests that the mechanism by which Jagged1 contributes to taxane resistance

Published OnlineFirst July 13, 2011; DOI:10.1158/1078-0432.CCR-11-0432

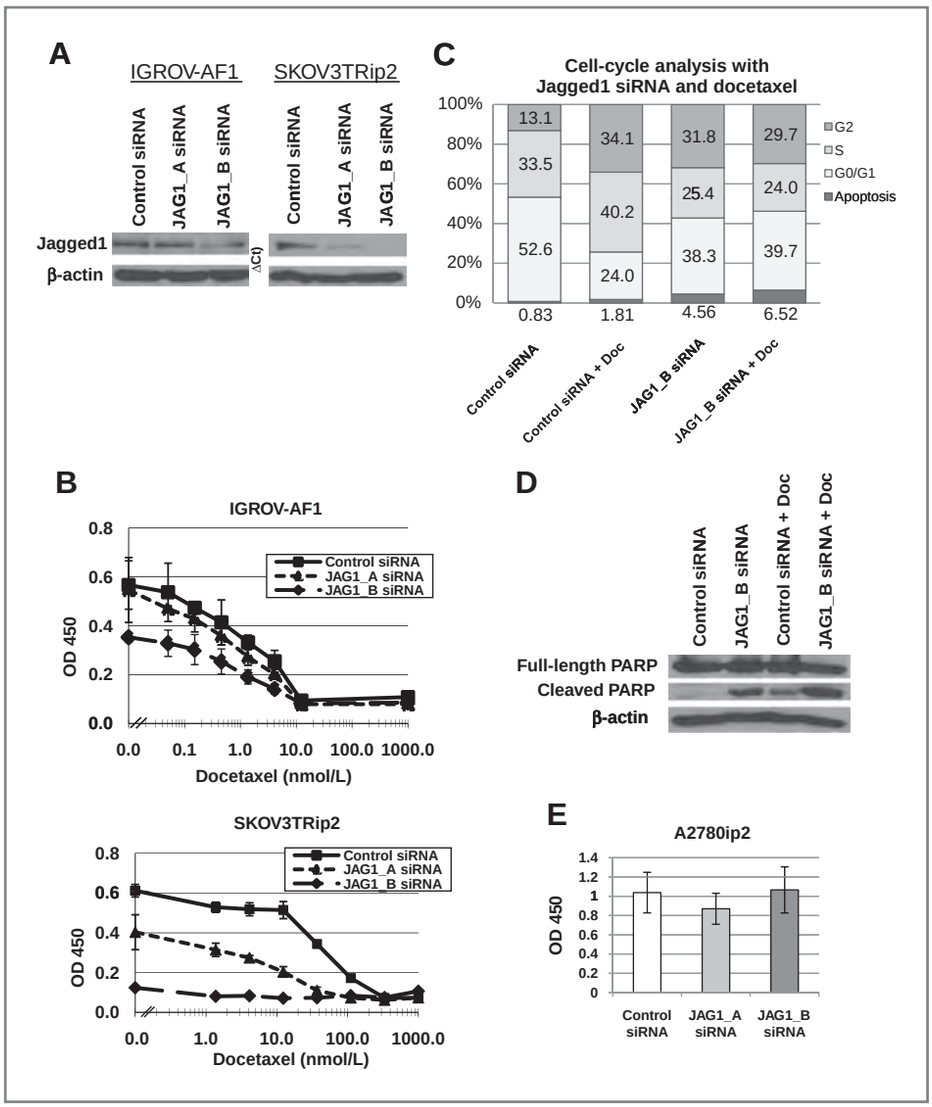

Figure 2. Downregulation of Jagged1 decreases viability and sensitizes to docetaxel in ovarian cancer cells. A, downregulation of Jagged1 in IGROV-AF1 and SKOV3TRip2 cells using 2 different siRNA constructs was determined by Western blot analysis. B, IGROV-AF1 and SKOV3TRip2 cells transiently transfected with anti-Jagged1 siRNAs had decreased viability; SKOV3TRip2 cells were sensitized to docetaxel (Doc) following Jagged1 knockdown. C, cell-cycle analysis showed that Jagged1 downregulation (alone and in combination with docetaxel) induces an accumulation of SKOV3TRip2 cells in the sub-G_0 phase, indicative of cells undergoing apoptosis, and the G_2–M phase. D, PARP cleavage, an indicator of apoptosis, was also observed in SKOV3TRip2 cells exposed to Jagged1 siRNA (alone or in combination with docetaxel), as determined by Western blot analysis. Blots are representative of 3 independent experiments. E, Jagged1 siRNAs had no effect on the viability of A2780ip2 cells, which do not express Jagged1.

are the same as those responsible for acquired taxane resistance, rather than an additive effect that might be seen in any cell line. Tests for synergy indicate a CI of 0.77, suggesting moderate synergy in the SKOV3TRip2 line. To determine the mechanism by which Jagged1 downregulation may affect cell growth, cell-cycle analysis was carried out in a separate experiment. SKOV3TRip2 cells were exposed to control or anti-Jagged1 siRNA for 24 hours, followed by vehicle or docetaxel at IC_{50} levels for another 48 hours. Jagged1 downregulation alone and in combination with docetaxel induced a small but statistically significant increase in apoptosis ($P < 0.001$, compared with control siRNA; $P < 0.01$, compared with docetaxel alone) and an accumulation of SKOV3TRip2 cells in the G_2–M phase ($P < 0.001$, compared with control siRNA; Fig. 2C). Induction of apoptosis was confirmed by the presence of PARP cleavage in SKOV3TRip2 cells exposed to Jagged1 siRNA (Fig. 2D). Jagged1 siRNAs had no sensitizing effect to carboplatin in SKOV3TRip2 and A2780cp20 cells (data not shown) and had no significant effect on the viability of Jagged1-negative A2780ip2 cells (Fig. 2E).

Human versus murine *in vivo* downregulation of Jagged1

We have previously shown that Jagged1 and other Notch family members are overexpressed in tumor-associated endothelial cells, and that Jagged1 downregulation prevented tube formation of HUVEC cells *in vitro* (11). Given the effects of Jagged1 downregulation on tumor cells as well, we sought to determine the relative effects of targeting Jagged1 in the stromal and malignant cell compartments individually. In addition, inhibition of both compartments would simulate effects that would be expected in patients. There are no known inhibitors of Jagged1 for *in vivo* studies. Therefore, we utilized a method for delivery of siRNA *in vivo* by using chitosan nanoparticles. siRNA holds the

Published OnlineFirst July 13, 2011; DOI:10.1158/1078-0432.CCR-11-0432

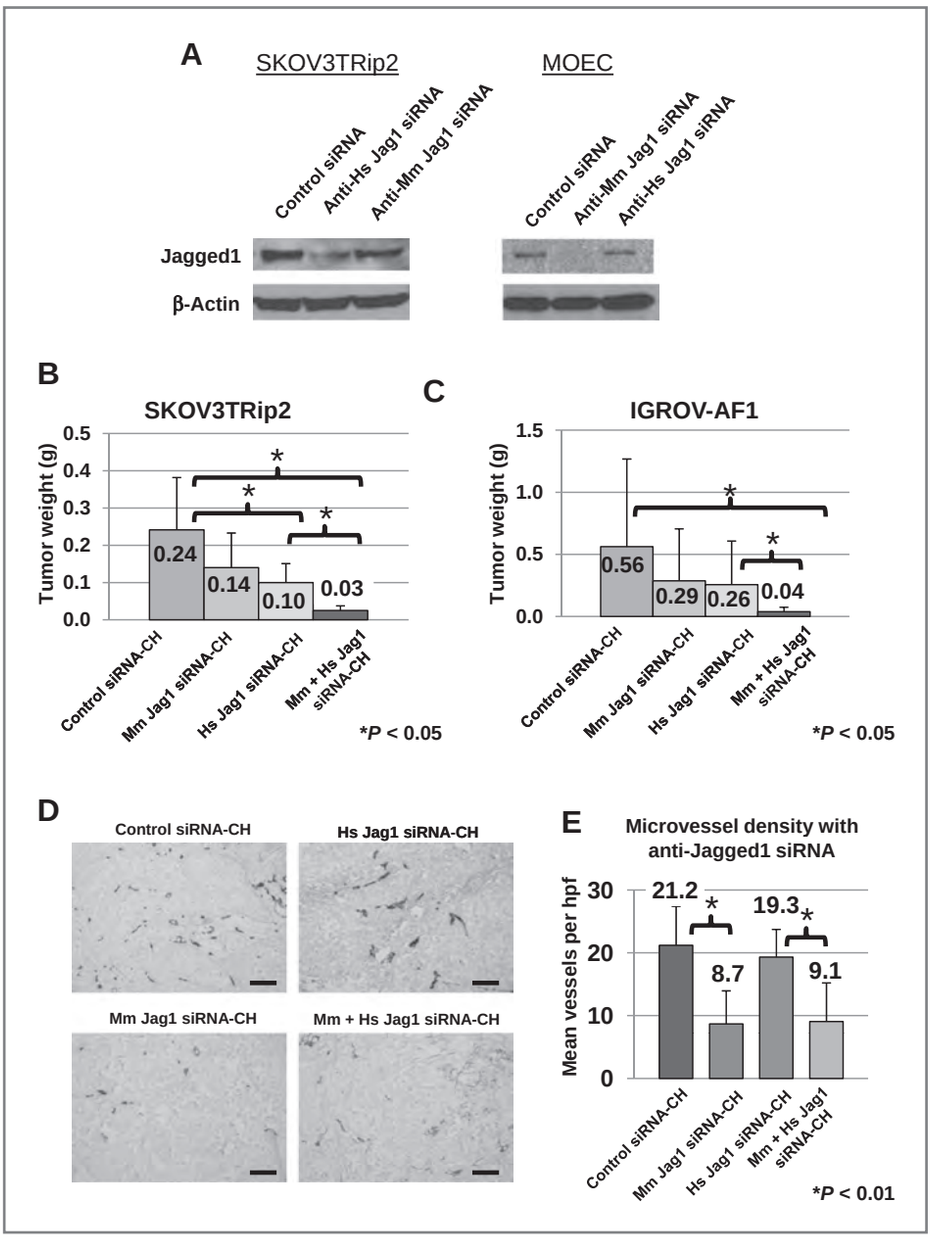

Figure 3. Human versus murine *in vivo* downregulation of Jagged1. A, species-specific downregulation of Jagged1 in human SKOV3TRip2 and mouse MOEC cell lines was determined by Western blot analysis. B, mice injected intraperitoneally with SKOV3TRip2 cells were treated with siRNAs incorporated in chitosan (CH) nanoparticles. Mice treated with the combination showed a significant reduction in tumor weight compared with treatment with control siRNA or either single species-specific Jagged1 siRNA. C, similarly, mice injected with IGROV-AF1 cells had significantly decreased tumor weight after treatment with combination murine- and human-Jagged1 siRNAs compared with control siRNA or either single species-specific siRNA. Mean tumor weights with SD are presented. D, SKOV3TRip2 tumors were subjected to IHC analysis of CD31 to evaluate MVD. Xenografts treated with anti-murine Jagged1 siRNA had significantly decreased MVD compared with those treated with control siRNA. Representative histologic sections are shown for the various treatment groups (black bar, 100 μm) with mean and SD values across each treatment group shown in the adjoining graph (E). Cntrl, control; Hs, human; Mm, murine; siRNA-CH, siRNA in chitosan nanoparticles. *, $P < 0.05$.

additional advantage of inhibiting both Notch-dependent and Notch-independent effects mediated by Jagged1 through bidirectional signaling. We have previously shown that twice weekly administration of siRNA incorporated into biodegradable chitosan nanoparticles results in siRNA delivery to the tumor parenchyma with subsequent target downregulation in both stromal and malignant tumor cells (24, 25, 28, 29). In this study, nude mice were injected intraperitoneally with either SKOV3TRip2 or IGROV-AF1 cells and randomized to four treatment groups: (i) control siRNA, (ii) murine-specific anti-Jagged1 siRNA, (iii) human-specific anti-Jagged1 siRNA, or (iv) both species-specific constructs. The specificity of each Jagged1 siRNA construct against the human or murine species was first showed *in vitro* by using human SKOV3TRip2 and murine MOEC cell lines by Western blot analysis (Fig. 3A). For *in vivo* studies, siRNAs were incorporated into chitosan nanoparticles and administered IV twice per week. After 4 weeks of treatment, all mice were sacrificed and total tumor weight recorded. In SKOV3TRip2 xenografts (Fig. 3B), there was a reduction in tumor growth with anti-murine Jagged1 siRNA-CH (41.7%, $P = 0.089$) compared with control siRNA, and human-specific anti-Jagged1 siRNA-CH significantly reduced tumor weight by 58.3% ($P = 0.042$). The combination of both species-specific constructs resulted in significantly reduced tumor weight by 87.5% compared

Published OnlineFirst July 13, 2011; DOI:10.1158/1078-0432.CCR-11-0432

with control siRNA ($P = 0.019$). This represented an 82.1% reduction compared with murine siRNA-CH alone ($P = 0.13$) and a 70% reduction compared with human siRNA-CH alone ($P = 0.03$). Similarly, in IGROV-AF1 xenografts (Fig. 3C), there was a moderate reduction in tumor weight with just murine-specific anti-Jagged1 siRNA-CH (48.8%, $P = 0.24$) or human-specific anti-Jagged1 siRNA-CH (54.4%, $P = 0.27$) compared with control siRNA. However, treatment with combined species-specific anti-Jagged1 siRNAs-CH again resulted in a significant decrease in tumor weight by 93.1% compared with control siRNA-CH ($P = 0.008$), by 84.9% compared with anti-human Jagged1 siRNA-CH alone ($P = 0.0046$), and by 86.5% compared with anti-murine Jagged1 alone ($P = 0.012$). There was not a statistically significant reduction in the number of nodules in each group, suggesting that the primary mechanism of reduced tumor size is reduced growth, rather than implantation and uptake of the tumor implants.

Given the Notch pathway's implication in angiogenesis, IHC analysis of CD31 was carried out to evaluate MVD to determine whether species-specific targeting of Jagged1 has antiangiogenic effects. As shown in representative sections in Figure 3D, MVD was significantly reduced in SKOV3-TRip2 tumors treated with anti-murine Jagged1 siRNA-CH (alone or in combination with anti-human Jagged1 siRNA-CH) compared with those treated with control siRNA (from 21.2 to 8.7 vessels per hpf, Figure 3E, $P < 0.01$). Anti-human Jagged1 siRNA-CH alone had no significant effect on MVD.

Taxane sensitization with dual-compartment Jagged1 downregulation *in vivo*

To determine the effect of Jagged1 downregulation on taxane sensitivity *in vivo*, nude mice were injected intraperitoneally with SKOV3TRip2 cells and randomized to four treatment groups (to begin 1 week after cell injection): (i) control siRNA-CH, (ii) control siRNA-CH + docetaxel, (iii) combined human and mouse-specific anti-Jagged1 siRNAs-CH, or (iv) combined human and murine-specific anti-Jagged1 siRNAs-CH + docetaxel. After 5 weeks of treatment, mice were sacrificed and total tumor weight recorded. As shown in Figure 4A, control siRNA-CH + docetaxel treatment had no effect on SKOV3TRip2 tumor weight. In contrast, treatment with combined human and mouse-specific anti-Jagged1 siRNAs-CH significantly reduced tumor weight (by 78.4%) compared with control siRNA-CH + docetaxel ($P = 0.038$). In addition, the combination of species-specific anti-Jagged1 siRNAs-CH and docetaxel further decreased tumor weight by 94.8% compared with control siRNA-CH + docetaxel ($P = 0.017$) and by 76.0% compared with dual-compartment Jagged1 downregulation alone ($P = 0.04$).

To determine whether decreases in SKOV3TRip2 tumor weights following Jagged1 downregulation (alone and in combination with docetaxel) were because of decreased cell proliferation, apoptosis, or both, IHC analysis of PCNA and TUNEL staining was carried out. Proliferation rates were significantly decreased in tumors treated with anti-human Jagged1 siRNA-CH, whether anti-human siRNA was used alone, in combination with anti-murine Jagged1 siRNA-CH, or in combination with anti-murine Jagged1 siRNA-CH plus docetaxel (23.3%, 11.4%, and 5.8%, respectively) compared with both control siRNA-CH (72.5%) or control siRNA-CH plus docetaxel (69.4%, $P < 0.001$; Fig. 4B and C). Rates of apoptosis were not significantly different for the treatment groups ranging from 3.9% to 6.6% (data not shown). The small percentage of cells undergoing apoptosis following Jagged1 downregulation (both *in vitro* and *in vivo*) suggest that decreased cell proliferation, rather than apoptosis, largely contributes to Jagged1 knockdown effects.

To determine whether increased taxane sensitivity observed with combined species-specific anti-Jagged1 siRNAs is because of effects on tumor cells, murine stromal cells, or both, SKOV3TRip2 xenografts were treated with docetaxel plus control siRNA-CH, anti-human Jagged1 siRNA-CH, anti-murine Jagged1 siRNA-CH, or combined anti-human/anti-murine Jagged1 siRNA-CH. As shown in Figure 4D, anti-murine Jagged1 siRNA-CH plus docetaxel had no effect on SKOV3TRip2 tumor weight compared with control siRNA-CH plus docetaxel. In contrast, treatment with either anti-human Jagged1 siRNA-CH plus docetaxel or anti-human/anti-murine Jagged1 siRNA-CH plus docetaxel significantly decreased tumor weight (by 79.8%, $P = 0.001$ and 74.6%, $P = 0.003$, respectively). These data would suggest that unlike its role in angiogenesis, Jagged1's role in taxane resistance is a characteristic of tumor cells, rather than transmitted through signals from the tumor stroma.

Jagged1 downregulation contributes to decreased ovarian cancer cell viability in part through downregulation of Gli2

To confirm that Jagged1 targeting was working through the Notch pathway, we evaluated mRNA levels of the Hes1 and Hey1 transcription factors, known downstream mediators of Notch signaling, by quantitative PCR. Surprisingly, downregulation of Jagged1 resulted in a modest increase in both *HES1* (1.7-fold, $P = 0.27$) and *HEY1* (1.8-fold, $P = 0.22$), rather than a decrease that would be expected from targeting Notch signaling (Fig. 5A). Therefore, alternate pathways of effect were sought. The primary mediator of taxane resistance in general, and in the SKOV3TRip2 cell line specifically, is expression of *MDR1*, with 110-fold increased expression compared with parental SKOV3ip1 (30). Therefore, we first examined whether Jagged1 downregulation reduced *MDR1* expression. Paradoxically, decreasing Jagged1 with transient siRNA actually led to a nearly significant 1.75-fold increase ($P = 0.06$) in *MDR1* expression (Fig. 5B). To explore other potential mechanisms, we examined the Hedgehog signaling pathway (in particular, the downstream effectors *GLI1* and *GLI2*) because of its involvement in stem cell maintenance, similar to the Notch pathway. Previous investigators have noted links between stem cell signaling pathways, such as the Notch and Wnt pathways (31) and the Notch and

Published OnlineFirst July 13, 2011; DOI:10.1158/1078-0432.CCR-11-0432

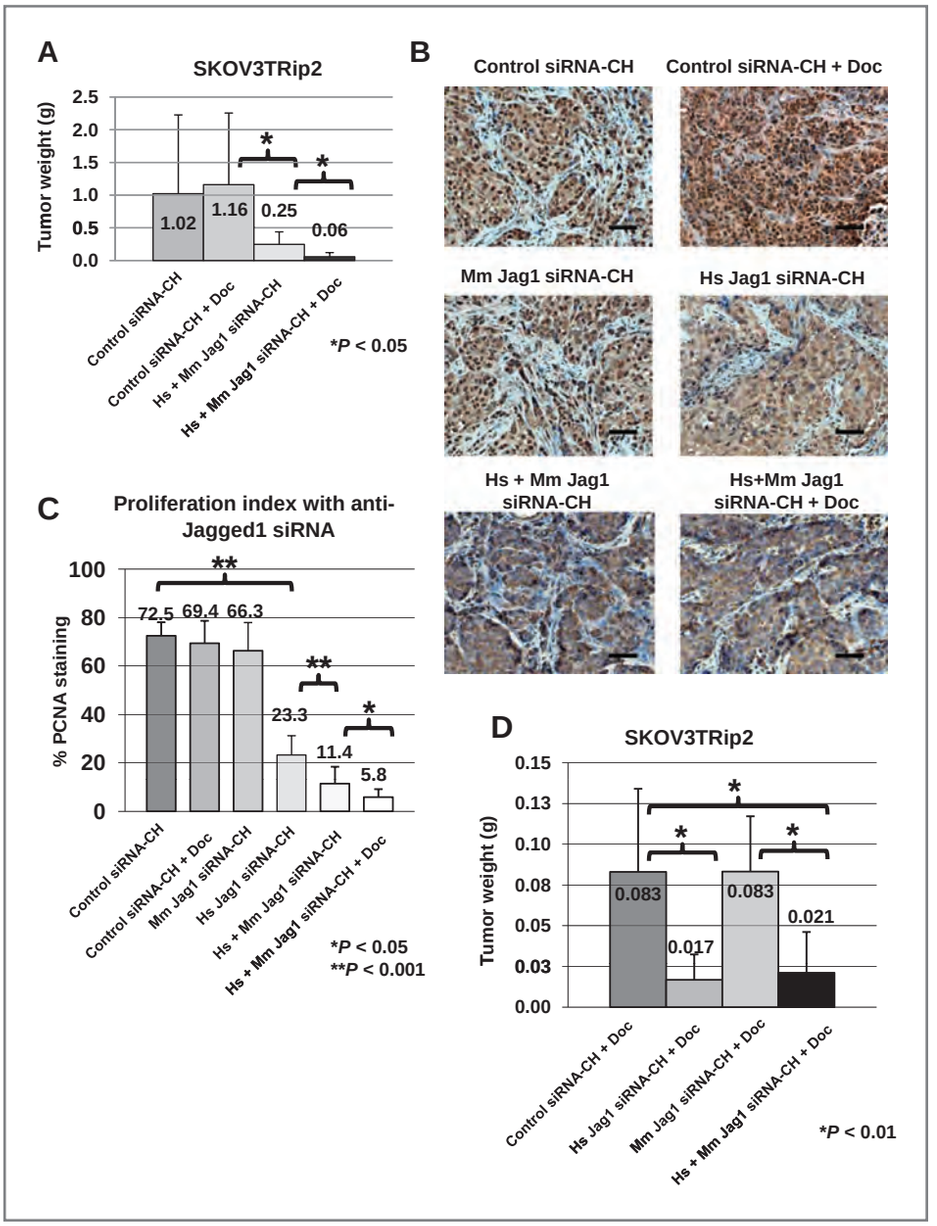

Figure 4. Taxane sensitization with dual-compartment Jagged1 downregulation *in vivo*. A, mice injected intraperitoneally with SKOV3TRip2 cells were treated with either control siRNA, control siRNA + docetaxel, combined human- and murine-Jagged1 siRNAs, or combined Jagged1 siRNAs + docetaxel. All siRNA constructs were incorporated in chitosan (CH) nanoparticles. Mice treated with the combination species-specific Jagged1 siRNAs + docetaxel showed a significant reduction in tumor weight compared with treatment with either Jagged1 siRNAs or docetaxel alone. Mean tumor weights with SD are presented. *, $P < 0.05$. B, SKOV3TRip2 tumors were subjected to IHC analysis of PCNA to evaluate cell proliferation. Xenografts treated with anti-human Jagged1 siRNA or combined species-specific Jagged1 siRNAs (alone and in combination with docetaxel) had significantly decreased proliferation rates compared with those treated with control siRNA or control siRNA plus docetaxel. Representative histologic sections are shown (B) for the various treatment groups (black bar, 100 μm) with mean and SD values across each treatment group shown in the adjoining graph (C). *, $P < 0.05$, **, $P < 0.001$. D, mice injected intraperitoneally with SKOV3TRip2 cells were treated with docetaxel plus either control siRNA, anti-human Jagged1 siRNA, anti-murine Jagged1 siRNA, or combined human- and murine-Jagged1 siRNAs. All siRNA constructs were incorporated in chitosan nanoparticles. Mice treated with anti-human and not anti-mouse Jagged1 siRNA showed a significant reduction in tumor weight in combination with docetaxel. Mean tumor weights with SD are presented. *, $P < 0.01$.

Hedgehog pathways (32). Expression of *GLI1* was not significantly affected by Jagged1 siRNA compared with control siRNA; however, *GLI2* expression was significantly reduced (by 2.20-fold, $P = 0.0016$) following Jagged1 downregulation (Fig. 5B). In addition, it was found that *JAG1* and *GLI2* (but not *GLI1*) gene expression levels significantly correlated among the ovarian cancer cell lines examined in this study ($r = 0.81$, $P = 0.0273$).

Published OnlineFirst July 13, 2011; DOI:10.1158/1078-0432.CCR-11-0432

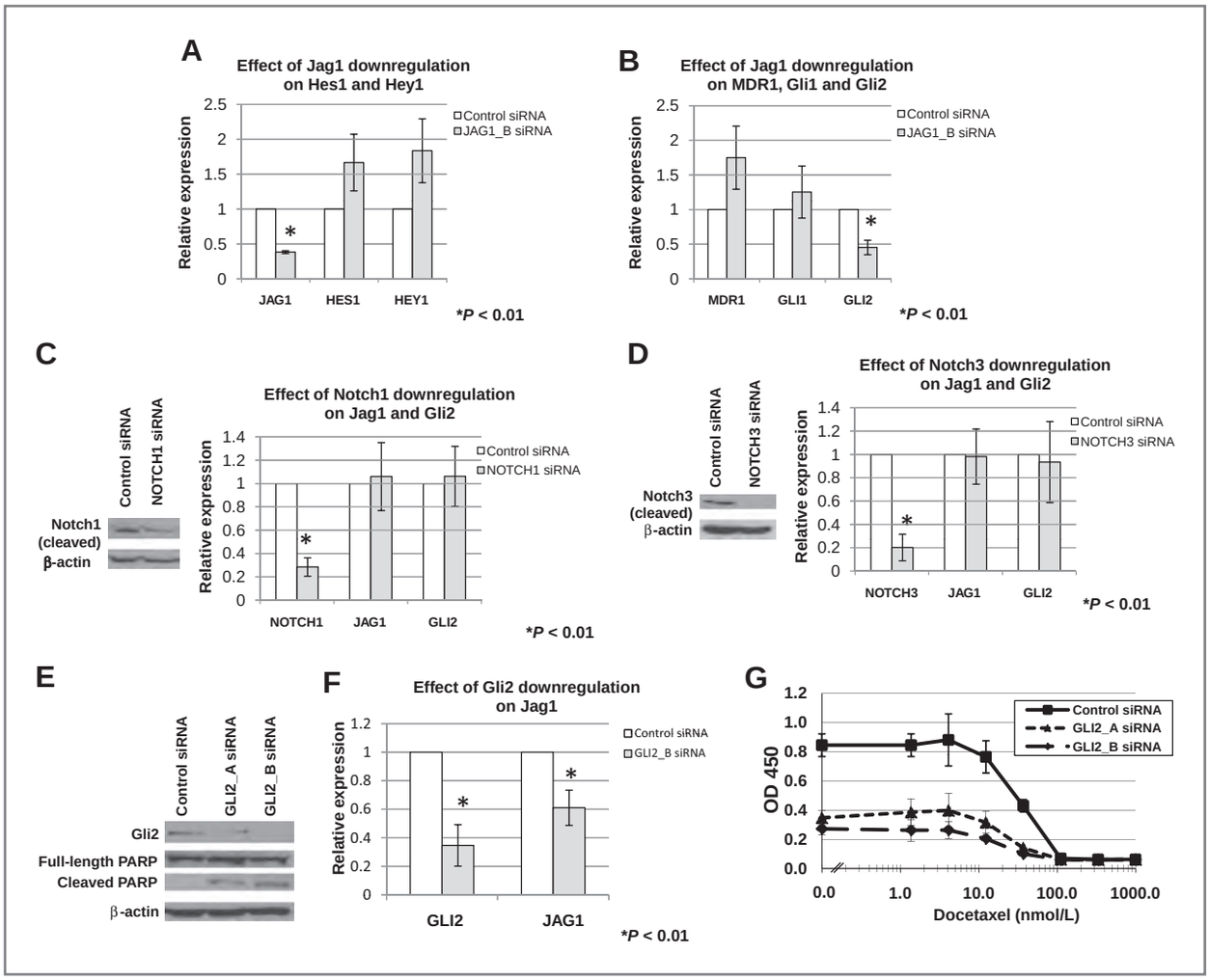

Figure 5. Gli2 reduction following Jagged1 downregulation contributes to decreased ovarian cancer cell viability and taxane sensitization. SKOV3TRip2 cells were transiently transfected with control siRNA or anti-Jagged1 siRNA for 72 hours and examined for gene expression by using quantitative PCR. A, Notch signaling targets *HES1* and *HEY1* were moderately increased as a result of Jagged1 downregulation. Error bars represent SEM. B, expression of *GLI2*, but not *MDR1* or *GLI1*, was significantly decreased following Jagged1 downregulation. C, knockdown of Notch1 did not affect *JAG1* or *GLI2* expression. D, knockdown of Notch3 also had no effect on *JAG1* or *GLI2* expression. E, PARP cleavage was observed in SKOV3TRip2 cells transfected with Gli2 siRNAs, as determined by Western blot (representative of 3 independent experiments). F, expression of *JAG1* was significantly decreased following Gli2 downregulation. G, knockdown of Gli2 by using 2 different siRNA constructs decreased viability and increased sensitivity to docetaxel in SKOV3TRip2 cells. *, $P < 0.01$.

To further explore this potentially unique relationship between Jagged1 and the hedgehog transcription factor Gli2, we first examined whether this mechanism was Notch dependent because downregulation of Jagged1 appeared to have no effect on Notch downstream targets. To this end, we knocked down expression of Notch1 and Notch3, key Notch receptors implicated in stem cell maintenance and ovarian cancer (5, 33), and examined *JAG1* and *GLI2* gene expression. As shown in Figure 5C and D, downregulation of either Notch1 or Notch3 had no effect on *JAG1* or *GLI2* expression, suggesting that Jagged1 influences Gli2 in a Notch-independent fashion. To examine the downstream effects of reduced *GLI2* expression, we selectively targeted Gli2 using two different siRNA constructs (Fig. 5E). First, we examined effects of apoptosis with Gli2 knockdown and noted significant induction of PARP cleavage compared with control siRNA (Fig. 5E). Interestingly, we found that Gli2 downregulation in turn significantly decreased *JAG1* expression (1.64-fold, $P = 0.0028$, Fig. 5F), further suggesting a link between these signaling peptides. To determine if Gli2 plays a role in Jagged1-mediated taxane sensitization, SKOV3TRip2 cells were transiently transfected with Gli2-targeting siRNAs or control siRNA for 24 hours before the addition of increasing concentrations of docetaxel. Gli2 siRNAs alone reduced cell viability by up to 68% (Fig. 5G, $P < 0.001$), but reduced the docetaxel IC_{50} only slightly from 40 to 29 nmol/L. Because the taxane sensitizing effects of Gli2 targeting are not as pronounced as Jagged1 targeting alone, it seems that both Gli2 and

Published OnlineFirst July 13, 2011; DOI:10.1158/1078-0432.CCR-11-0432

additional Notch-independent pathways are at work in taxane resistance.

Discussion

In this study, we found that targeting Jagged1 in tumor cells induces apoptosis, reduces cell viability, and reverses taxane resistance in ovarian cancer cells both *in vitro* and *in vivo*, at least in part through downregulation of the Hedgehog mediator *GLI2*. In addition, knockdown of Jagged1 in tumor stromal cells reduces tumor growth through an antiangiogenic mechanism. The participation of Jagged1 in both stromal and malignant cell compartments makes it an attractive target for therapy and shows the utility of a model whereby these compartments can be targeted independently to delineate the various contributions of different cells in the tumor microenvironment.

Previous studies have shown aberrant expression of the Notch pathway in ovarian cancer (4–7). In particular, Jagged1 was found to be the primary Notch ligand expressed in ovarian cancer cells compared with Jagged2 and DLL1, 3, and 4 (6). Jagged1 was also found to be overexpressed in endothelial cells purified from ovarian cancers compared with normal ovaries (11). Taken together, these studies indicate that Jagged1 would be a desirable therapeutic target in ovarian cancer, both from an antitumor and antiangiogenic standpoint. In our study, we found that downregulation of Jagged1 resulted in decreased ovarian cancer cell viability *in vitro*, most likely mediated through reduced cell proliferation and, to a lesser extent, induction of apoptosis. Our study is the first to show that targeting Jagged1 diminishes tumor burden *in vivo*. Because there are no known inhibitors of Jagged1, we used chitosan nanoparticles to deliver Jagged1 siRNAs in tumor-bearing mice. These positively charged nanoparticles allow for the transport of siRNA across cellular membranes and are biodegradable, biocompatible, and have low immunogenicity (34, 35). Targeting Jagged1 using this delivery system may also avoid the dose-limiting toxicities inherent to systemic Notch inhibitors such as gamma-secretase inhibitors (36). Selective targeting of Jagged1 by using chitosan greatly decreased tumor burden and increased taxane sensitivity in orthotopic ovarian cancer mouse models. These results, combined with our observations *in vitro*, indicate that Jagged1 plays an important role in ovarian cancer cell survival. Whether these effects occur entirely through Notch signaling remains an open question. It has been suggested by Choi and colleagues (6) and others (15, 16) that Jagged1 may have its own signaling function that is independent of the canonical Notch pathway. Indeed, the lack of a decrease in the expression of Notch downstream targets, *HES1* and *HEY1*, following Jagged1 downregulation in our study supports this mechanism. This potentially unique Notch-independent function of Jagged1 in human cancers, however, has yet to be fully explored.

The interaction between cancer cells and the surrounding stroma is increasingly becoming a focus of study in cancer research due to its role in tumor progression. This tumor-associated stroma is composed primarily of endothelial cells, which are necessary for tumor angiogenesis, and fibroblasts, which can secrete growth factors to the adjacent cancer cells. Recent reports suggest that Notch signaling can occur between tumor and stromal cells in some malignancies (37, 38), indicating that targeting the Notch-ligand interaction in endothelial cells can have therapeutic applications. In addition, studies have shown that Jagged1 expression is crucial for normal vascular development during embryogenesis and that mutations of the *JAGGED1* gene can cause Alagille syndrome, a disease characterized by, among other deformities, congenital heart defects (39, 40). In our study, we found that selectively targeting Jagged1 in the tumor stroma significantly reduced MVD (as measured by CD31) and, when combined with Jagged1 antagonism in cancer cells, the overall antitumor effect was greater than either anti-Jagged1 method alone. These data suggest that, unlike most cancer-associated targets which are expressed in only one compartment of the tumor, inhibiting Jagged1 activity could be used to target both the tumor and its developing vasculature, thereby having a potentially greater therapeutic benefit.

Chemoresistance remains a persistent obstacle in the treatment of ovarian cancer. Although the clinical behavior of ovarian cancer suggests that most cancer cells are initially sensitive to chemotherapy, they subsequently either develop resistance or contain a population of cells that are inherently resistant. The latter hypothesis is consistent with what has become known as cancer stem cells or cancer initiating cells (CIC). These CICs are commonly believed to have enhanced tumorigenicity, differentiation capacity, and resistance to chemotherapy in comparison with non-CICs. It is because of these features that CICs have been examined for molecular pathways and markers that could be targeted for therapeutic purposes. Recent studies have shown that the ancient developmental pathways Hedgehog, Wnt, and Notch play important roles in the maintenance of CICs and that inhibiting these pathways may provide enhanced chemosensitivity when combined with traditional chemotherapies (8, 41–43). In our study, we sought to determine the mechanism whereby Jagged1, a known target of Wnt/β-catenin signaling (44, 45) and a Notch ligand, might sensitize ovarian cancer cells to docetaxel. We chose to focus on the hedgehog pathway because of its involvement in CIC maintenance and multidrug resistance (46–49). Interestingly, expression of *GLI2*, a hedgehog transcriptional effector, was significantly decreased following Jagged1 knockdown whereas expression of *GLI1* and *MDR1* was not. This relationship, one that seems to be Notch independent, between Jagged1 and Gli2 was also found to work both ways as knockdown of Gli2 diminished Jagged1 expression. Moreover, selective targeting of Gli2 using siRNA constructs decreased viability and increased sensitivity of ovarian cancer cells to docetaxel, although to a lesser degree than Jagged1 knockdown. These results suggest that inhibition of Gli2 contributes to the cell death and chemosensitization resulting from Jagged1

Published OnlineFirst July 13, 2011; DOI:10.1158/1078-0432.CCR-11-0432

knockdown with other, as yet undefined, mechanisms likely playing a role as well. This connection between Jagged1 and Gli2 has not been previously identified and may have important therapeutic implications because targeting both Notch and Hedgehog, especially in combination with chemotherapy, is increasingly being advocated for the treatment of a variety of malignancies (3, 8, 50).

Collectively, the data presented in this study show that the Notch ligand Jagged1 contributes to taxane resistance, and targeting Jagged1 in ovarian cancer cells as well as in surrounding stroma significantly reduces growth through antiproliferative, apoptotic, antiangiogenic, and taxane-sensitizing effects. With the ability to identify subsets of cancer patients with Jagged1 overexpression, antagonism of this signaling molecule could ultimately provide a useful therapeutic strategy for ovarian cancer.

Disclosure of Potential Conflicts of Interest

No potential conflicts of interest were disclosed.

Grant Support

This work was supported by the Reproductive Scientist Development Program through the Ovarian Cancer Research Fund and the NIH (K12 HD00849), the Gynecologic Cancer Foundation, and the Department of Defense Ovarian Cancer Research Academy (OC093443) to C.N. Landen; and NIH (CA10929801, P50 CA083639, CA128797, RC2GM092599, U54 CA151668), and the Ovarian Cancer Research Fund, Inc. (Program Project Development Grant) grants to A.K. Sood.

The costs of publication of this article were defrayed in part by the payment of page charges. This article must therefore be hereby marked *advertisement* in accordance with 18 U.S.C. Section 1734 solely to indicate this fact.

Received February 16, 2011; revised June 28, 2011; accepted July 1, 2011; published OnlineFirst July 13, 2011.

References

1. Bhoola S, Hoskins WJ. Diagnosis and management of epithelial ovarian cancer. Obstet Gynecol 2006;107:1399–410.
2. Fortini ME. Notch signaling: the core pathway and its posttranslational regulation. Dev Cell 2009;16:633–47.
3. Wang Z, Li Y, Banerjee S, Sarkar FH. Emerging role of Notch in stem cells and cancer. Cancer Lett 2009;279:8–12.
4. Hopfer O, Zwahlen D, Fey MF, Aebi S. The Notch pathway in ovarian carcinomas and adenomas. Br J Cancer 2005;93:709–18.
5. Park JT, Li M, Nakayama K, Mao TL, Davidson B, Zhang Z, et al. Notch3 gene amplification in ovarian cancer. Cancer Res 2006;66:6312–8.
6. Choi JH, Park JT, Davidson B, Morin PJ, Shih Ie M, Wang TL. Jagged-1 and Notch3 juxtacrine loop regulates ovarian tumor growth and adhesion. Cancer Res 2008;68:5716–23.
7. Jung SG, Kwon YD, Song JA, Back MJ, Lee SY, Lee C, et al. Prognostic significance of Notch 3 gene expression in ovarian serous carcinoma. Cancer Sci 2010;101:1977–83.
8. Pannuti A, Foreman K, Rizzo P, Osipo C, Golde T, Osborne B, et al. Targeting Notch to target cancer stem cells. Clin Cancer Res 2010;16:3141–52.
9. Zhang S, Balch C, Chan MW, Lai HC, Matei D, Schilder JM, et al. Identification and characterization of ovarian cancer-initiating cells from primary human tumors. Cancer Res 2008;68:4311–20.
10. Park JT, Chen X, Trope CG, Davidson B, Shih Ie M, Wang TL. Notch3 overexpression is related to the recurrence of ovarian cancer and confers resistance to carboplatin. Am J Pathol 2010;177:1087–94.
11. Lu C, Bonome T, Li Y, Kamat AA, Han LY, Schmandt R, et al. Gene alterations identified by expression profiling in tumor-associated endothelial cells from invasive ovarian carcinoma. Cancer Res 2007;67:1757–68.
12. Yan M, Plowman GD. Delta-like 4/Notch signaling and its therapeutic implications. Clin Cancer Res 2007;13:7243–6.
13. Phng LK, Gerhardt H. Angiogenesis: a team effort coordinated by notch. Dev Cell 2009;16:196–208.
14. Li JL, Harris AL. Notch signaling from tumor cells: a new mechanism of angiogenesis. Cancer Cell 2005;8:1–3.
15. LaVoie MJ, Selkoe DJ. The Notch ligands, Jagged and Delta, are sequentially processed by alpha-secretase and presenilin/gamma-secretase and release signaling fragments. J Biol Chem 2003;278:34427–37.
16. Ascano JM, Beverly LJ, Capobianco AJ. The C-terminal PDZ-ligand of JAGGED1 is essential for cellular transformation. J Biol Chem 2003;278:8771–9.
17. Buick RN, Pullano R, Trent JM. Comparative properties of five human ovarian adenocarcinoma cell lines. Cancer Res 1985;45:3668–76.
18. Yoneda J, Kuniyasu H, Crispens MA, Price JE, Bucana CD, Fidler IJ. Expression of angiogenesis-related genes and progression of human ovarian carcinomas in nude mice. J Natl Cancer Inst 1998;90:447–54.
19. Duan Z, Feller AJ, Toh HC, Makastorsis T, Seiden MV. TRAG-3, a novel gene, isolated from a taxol-resistant ovarian carcinoma cell line. Gene 1999;229:75–81.
20. Langley RR, Ramirez KM, Tsan RZ, Van Arsdall M, Nilsson MB, Fidler IJ. Tissue-specific microvascular endothelial cell lines from H-2K(b)-tsA58 mice for studies of angiogenesis and metastasis. Cancer Res 2003;63:2971–6.
21. Steg A, Wang W, Blanquicett C, Grunda JM, Eltoum IA, Wang K, et al. Multiple gene expression analyses in paraffin-embedded tissues by TaqMan low-density array: application to hedgehog and Wnt pathway analysis in ovarian endometrioid adenocarcinoma. J Mol Diagn 2006;8:76–83.
22. Landen CN Jr, Lu C, Han LY, Coffman KT, Bruckheimer E, Halder J, et al. Efficacy and antivascular effects of EphA2 reduction with an agonistic antibody in ovarian cancer. J Natl Cancer Inst 2006;98:1558–70.
23. Straetemans R, O'Brien T, Wouters L, Van Dun J, Janicot M, Bijnens L, et al. Design and analysis of drug combination experiments. Biom J 2005;47:299–308.
24. Han HD, Mangala LS, Lee JW, Shahzad MM, Kim HS, Shen D, et al. Targeted gene silencing using RGD-labeled chitosan nanoparticles. Clin Cancer Res 2010;16:3910–22.
25. Lu C, Han HD, Mangala LS, Ali-Fehmi R, Newton CS, Ozbun L, et al. Regulation of tumor angiogenesis by EZH2. Cancer Cell 2010;18:185–97.
26. Kim SJ, Uehara H, Karashima T, Shepherd DL, Killion JJ, Fidler IJ. Blockade of epidermal growth factor receptor signaling in tumor cells and tumor-associated endothelial cells for therapy of androgen-independent human prostate cancer growing in the bone of nude mice. Clin Cancer Res 2003;9:1200–10.
27. Baker CH, Kedar D, McCarty MF, Tsan R, Weber KL, Bucana CD, et al. Blockade of epidermal growth factor receptor signaling on tumor cells and tumor-associated endothelial cells for therapy of human carcinomas. Am J Pathol 2002;161:929–38.
28. Cai YQ, Chen SR, Han HD, Sood AK, Lopez-Berestein G, Pan HL. Role of M2, M3, and M4 muscarinic receptor subtypes in the spinal cholinergic control of nociception revealed using siRNA in rats. J Neurochem 2009;111:1000–10.
29. Feng S, Agoulnik I, Truong A, Li Z, Creighton CJ, Kaftanovskaya EM, et al. Suppression of relaxin receptor RXFP1 decreases prostate cancer growth and metastasis. Endocr Relat Cancer 2010;17:1021–33.
30. Landen CN, Goodman BW, Katre AA, Steg AD, Nick AM, Stone R, et al. Targeting aldehyde dehydrogenase cancer stem cells in ovarian cancer. Mol Cancer Ther 2010;9:3186–99.

Published OnlineFirst July 13, 2011; DOI:10.1158/1078-0432.CCR-11-0432

31. Rodilla V, Villanueva A, Obrador-Hevia A, Robert-Moreno A, Fernandez-Majada V, Grilli A, et al. Jagged1 is the pathological link between Wnt and Notch pathways in colorectal cancer. Proc Natl Acad Sci U S A 2009;106:6315–20.
32. Schreck KC, Taylor P, Marchionni L, Gopalakrishnan V, Bar EE, Gaiano N, et al. The Notch target Hes1 directly modulates Gli1 expression and Hedgehog signaling: a potential mechanism of therapeutic resistance. Clin Cancer Res 2010;16:6060–70.
33. Gao MQ, Choi YP, Kang S, Youn JH, Cho NH. $CD24^{+}$ cells from hierarchically organized ovarian cancer are enriched in cancer stem cells. Oncogene 2010;29:2672–80.
34. Katas H, Alpar HO. Development and characterisation of chitosan nanoparticles for siRNA delivery. J Control Release 2006;115:216–25.
35. Liu X, Howard KA, Dong M, Andersen MO, Rahbek UL, Johnsen MG, et al. The influence of polymeric properties on chitosan/siRNA nanoparticle formulation and gene silencing. Biomaterials 2007;28:1280–8.
36. Wong GT, Manfra D, Poulet FM, Zhang Q, Josien H, Bara T, et al. Chronic treatment with the gamma-secretase inhibitor LY-411,575 inhibits beta-amyloid peptide production and alters lymphopoiesis and intestinal cell differentiation. J Biol Chem 2004;279:12876–82.
37. Jundt F, Probsting KS, Anagnostopoulos I, Muehlinghaus G, Chatterjee M, Mathas S, et al. Jagged1-induced Notch signaling drives proliferation of multiple myeloma cells. Blood 2004;103:3511–5.
38. Zeng Q, Li S, Chepeha DB, Giordano TJ, Li J, Zhang H, et al. Crosstalk between tumor and endothelial cells promotes tumor angiogenesis by MAPK activation of Notch signaling. Cancer Cell 2005;8:13–23.
39. Zimrin AB, Pepper MS, McMahon GA, Nguyen F, Montesano R, Maciag T. An antisense oligonucleotide to the notch ligand jagged enhances fibroblast growth factor-induced angiogenesis in vitro. J Biol Chem 1996;271:32499–502.
40. Crosnier C, Attie-Bitach T, Encha-Razavi F, Audollent S, Soudy F, Hadchouel M, et al. JAGGED1 gene expression during human embryogenesis elucidates the wide phenotypic spectrum of Alagille syndrome. Hepatology 2000;32:574–81.
41. Merchant AA, Matsui W. Targeting Hedgehog–a cancer stem cell pathway. Clin Cancer Res 2010;16:3130–40.
42. Takahashi-Yanaga F, Kahn M. Targeting Wnt signaling: can we safely eradicate cancer stem cells?Clin Cancer Res 2010;16:3153–62.
43. Rizzo P, Osipo C, Foreman K, Golde T, Osborne B, Miele L. Rational targeting of Notch signaling in cancer. Oncogene 2008;27:5124–31.
44. Katoh M, Notch ligand, JAG1, is evolutionarily conserved target of canonical WNT signaling pathway in progenitor cells. Int J Mol Med 2006;17:681–5.
45. Chen X, Stoeck A, Lee SJ, Shih IM, Wang MM, Wang TL. Jagged1 expression regulated by Notch3 and Wnt/β-catenin signaling pathways in ovarian cancer. Oncotarget 2010;1:210–8.
46. Sims-Mourtada J, Izzo JG, Ajani J, Chao KS. Sonic Hedgehog promotes multiple drug resistance by regulation of drug transport. Oncogene 2007;26:5674–9.
47. Narita S, So A, Ettinger S, Hayashi N, Muramaki M, Fazli L, et al. GLI2 knockdown using an antisense oligonucleotide induces apoptosis and chemosensitizes cells to paclitaxel in androgen-independent prostate cancer. Clin Cancer Res 2008;14:5769–77.
48. Mine T, Matsueda S, Gao H, Li Y, Wong KK, Peoples GE, et al. Created Gli-1 duplex short-RNA (i-Gli-RNA) eliminates CD44 Hi progenitors of taxol-resistant ovarian cancer cells. Oncol Rep 2010;23:1537–43.
49. Mimeault M, Johansson SL, Henichart JP, Depreux P, Batra SK. Cytotoxic effects induced by docetaxel, gefitinib, and cyclopamine on side population and nonside population cell fractions from human invasive prostate cancer cells. Mol Cancer Ther 2010;9:617–30.
50. Ulasov IV, Nandi S, Dey M, Sonabend AM, Lesniak MS. Inhibition of Sonic hedgehog and Notch pathways enhances sensitivity of CD133 (+) glioma stem cells to temozolomide therapy. Mol Med 2010;17:103–12.

Preclinical Development

Molecular Cancer Therapeutics

Smoothened Antagonists Reverse Taxane Resistance in Ovarian Cancer

Adam D. Steg, Ashwini A. Katre, Kerri S. Bevis, Angela Ziebarth, Zachary C. Dobbin, Monjri M. Shah, Ronald D. Alvarez, and Charles N. Landen

Abstract

The hedgehog (HH) pathway has been implicated in the formation and maintenance of a variety of malignancies, including ovarian cancer; however, it is unknown whether HH signaling is involved in ovarian cancer chemoresistance. The goal of this study was to determine the effects of antagonizing the HH receptor, Smoothened (Smo), on chemotherapy response in ovarian cancer. Expression of HH pathway members was assessed in three pairs of parental and chemotherapy-resistant ovarian cancer cell lines (A2780ip2/A2780cp20, SKOV3ip1/SKOV3TRip2, HeyA8/HeyA8MDR) using quantitative PCR and Western blot analysis. Cell lines were exposed to increasing concentrations of two different Smo antagonists (cyclopamine, LDE225) alone and in combination with carboplatin or paclitaxel. Selective knockdown of Smo, Gli1, or Gli2 was achieved using siRNA constructs. Cell viability was assessed by MTT assay. A2780cp20 and SKOV3TRip2 orthotopic xenografts were treated with vehicle, LDE225, paclitaxel, or combination therapy. Chemoresistant cell lines showed higher expression (>2-fold, $P < 0.05$) of HH signaling components compared with their respective parental lines. Smo antagonists sensitized chemotherapy-resistant cell lines to paclitaxel, but not to carboplatin. LDE225 treatment also increased sensitivity of ALDH-positive cells to paclitaxel. A2780cp20 and SKOV3TRip2 xenografts treated with combined LDE225 and paclitaxel had significantly less tumor burden than those treated with vehicle or either agent alone. Increased taxane sensitivity seems to be mediated by a decrease in P-glycoprotein (MDR1) expression. Selective knockdown of Smo, Gli1, or Gli2 all increased taxane sensitivity. Smo antagonists reverse taxane resistance in chemoresistant ovarian cancer models, suggesting combined anti-HH and chemotherapies could provide a useful therapeutic strategy for ovarian cancer. *Mol Cancer Ther; 1–11. ©2012 AACR.*

Introduction

Ovarian cancer is the leading cause of death from a gynecologic malignancy. Although ovarian cancer is among the most chemosensitive malignancies at the time of initial treatment (surgery and taxane/platinum-based chemotherapy), most patients will develop tumor recurrence and succumb to chemoresistant disease (1). Evaluation of multiple chemotherapy agents in several combinations in the last 20 years has yielded modest improvements in progression-free survival, but no increase in durable cures. This clinical course suggests that a population of tumor cells has either inherent or acquired resistance to chemotherapy that allows survival with initial therapy and ultimately leads to recurrence. Targeting the cellular pathways involved in this resistance may provide new treatment modalities for ovarian cancer.

The Hedgehog (HH) pathway plays an important role in cell growth and differentiation during embryonic development (2). There are 3 known mammalian HH ligands—Sonic, Indian, and Desert. These ligands are secreted peptides that bind to the transmembrane Patched (Ptch) receptor. In the absence of HH ligand, Ptch serves as a negative regulator of Smoothened (Smo), a G-protein–coupled receptor. In the presence of HH ligand, Ptch repression of Smo is abolished, leading to downstream activation of the Gli family of transcription factors (Gli1, refs. 2, 3). Gli transcription factors translocate from the cytoplasm to the nucleus, where they bind DNA and activate transcription of HH target genes, including *PTCH1* and *GLI1*, the expression of which are frequently measured to evaluate the presence or absence of HH pathway activity (3, 4). Gli homologues have distinct, but overlapping functions; Gli1 serves only as a transcriptional activator, whereas Gli2 and Gli3 are capable of both activating and repressing HH gene transcription.

Recent reports have implicated HH signaling in multiple malignancies (5, 6), including ovarian cancer (7–9), and suggest this pathway may be especially important in maintaining the subpopulation of cancer cells with stem

Authors' Affiliation: Department of Obstetrics and Gynecology, University of Alabama at Birmingham, Birmingham, Alabama

Corresponding Author: Charles N. Landen, Department of Obstetrics and Gynecology, The University of Alabama at Birmingham, 1825 University Boulevard, 505 Shelby Building, Birmingham, AL 35294. Phone: 205-934-0473; Fax: 205-934-0474; E-mail: clanden@uab.edu

doi: 10.1158/1535-7163.MCT-11-1058

cell properties (10, 11) as well as conferring resistance to chemotherapies (12, 13). Inhibition of the HH signaling pathway, therefore, has become a desirable therapeutic strategy for the treatment of various cancers. Cyclopamine, a steroidal alkaloid derived from the lily plant *Veratrum californicum*, was the first compound identified that inactivates HH signaling by antagonizing Smo function (14–16). Since this discovery, pharmaceutical companies have synthesized more selective Smo antagonists, including NVP-LDE225 (17), which is currently being investigated in clinical trials (11).

The effects of Smo antagonists, both alone and in combination with chemotherapies, remains an active area of study in cancer research. Examination of combination effects is potentially important, given the hypothesized role of stem cell pathways in chemoresistance. However, the mechanisms by which HH inhibition might sensitize cells to chemotherapy, and whether such an approach would be effective in ovarian cancer, are not known. In our study, we sought to determine the effects of Smo antagonists on the viability of ovarian cancer cells, both alone and in combination with chemotherapy. We show that Smo antagonists have activity alone, but more dramatically can reverse taxane resistance in ovarian cancer, both *in vitro* and *in vivo*, through modulation of the multidrug resistance mediator, P-glycoprotein (MDR1). These findings provide new insight into HH signaling, its contribution to an aggressive subpopulation of cells, and new opportunities for clinical development.

Materials and Methods

Reagents and cell culture

Cyclopamine was purchased from Toronto Research Chemicals and dissolved in 95% ethanol to create a 10 mmol/L stock solution. NVP-LDE225 (LDE225) was kindly provided by Novartis Pharma AG and dissolved in dimethyl sulfoxide (DMSO) to create a 10 mmol/L stock solution. The ovarian cancer cell lines A2780ip2, A2780cp20, HeyA8, HeyA8MDR, SKOV3ip1, and SKOV3TRip2 (18–23) were maintained in RPMI-1640 medium supplemented with 10% FBS (Hyclone). A2780cp20 (platinum- and taxane-resistant), HeyA8MDR (taxane-resistant), and SKOV3TRip2 (taxane-resistant, a kind gift of Dr Michael Seiden; ref. 24) were generated by sequential exposure to increasing concentrations of chemotherapy (25). HeyA8MDR and SKOV3TRip2 were maintained with the addition of 150 ng/mL of paclitaxel. All cell lines were routinely screened for *Mycoplasma* species (GenProbe detection kit; Fisher) with experiments done at 70% to 80% confluent cultures. Purity of cell lines was confirmed with STR genomic analysis, and only cells less than 20 passages from stocks were used in experiments.

RNA extraction and reverse transcription

Total RNA was isolated from ovarian cancer cell lines using TRIzol reagent (Invitrogen) per manufacturer's instructions. RNA was then DNase treated and purified using the RNeasy Mini Kit (QIAGEN). RNA was eluted in 50 μL of RNase-free water and stored at −80°C. The concentration of all RNA samples was quantified by spectrophotometric absorbance at 260/280 nm using an Eppendorf BioPhotometer plus. Before cDNA synthesis, all RNA samples were diluted to 20 ng/μL using RNase-free water. cDNA was prepared using the High Capacity cDNA Reverse Transcription Kit (Applied Biosystems). The resulting cDNA samples were analyzed using quantitative PCR (qPCR).

Quantitative PCR

Primer and probe sets for *Desert HH* (Hs0036806_m1), *GLI1* (Hs00171790_m1), *GLI2* (Hs00257977_m1), *Indian HH* (Hs00745531_s1), *MDR1* (Hs00184500_m1), *PTCH1* (Hs00181117_m1), *SMO* (Hs00170665_m1), *Sonic HH* (Hs), and *RPLP0* (Hs99999902_m1; housekeeping gene) were obtained from Applied Biosystems and used according to manufacturer's instructions. PCR amplification was conducted on an ABI Prism 7900HT sequence detection system and gene expression was calculated using the comparative C_T method as previously described (26). Briefly, this technique uses the formula $2^{-\Delta\Delta C}{}_T$ to calculate the expression of target genes normalized to a calibrator. The cycling threshold (C_T) indicates the cycle number at which the amount of amplified target reaches a fixed threshold. C_T values range from 0 to 40 (the latter representing the default upper limit PCR cycle number that defines failure to detect a signal).

Western blot analysis

Cultured cell lysates were collected in modified radioimmunoprecipitation assay lysis buffer with protease inhibitor cocktail (Roche) and subjected to immunoblot analysis by standard techniques (25) using anti-Gli1 antibody (Cell Signaling Technology) at 1:1,000 dilution overnight at 4°C, anti-Smo antibody (LifeSpan Biosciences) at 1:1,000 dilution overnight at 4°C, or anti-β-actin antibody (AC-15, Sigma-Aldrich) at 1:20,000 dilution for 1 hour at room temperature (RT), which was used to monitor equal sample loading. After washing, blots were incubated with goat anti-rabbit (for Gli1 and Smo) or goat anti-mouse (for β-actin) secondary antibodies (Bio-Rad) conjugated with horseradish peroxidase. Visualization was done by the enhanced chemiluminescence method (Pierce Thermo Scientific).

siRNA transfection

To examine downregulation of Smo, Gli1, or Gli2 individually with siRNA, cells were exposed to control siRNA (target sequence: 5′-UUCUCCGAACGUGUCACGU-3′, Sigma-Aldrich), one of 2 tested Smo-targeting constructs (siRNA1: 5′-GAGGAGUCAUGACUCUGUUCUCCAU-3′ or siRNA2: 5′-UGACCUCAAUGAGCCCUCAGCU-GAU-3′; Invitrogen), one of 2 tested Gli1-targeting constructs (siRNA1: 5′-CUACUGAUACUCUGGGAUA-3′ or siRNA2: 5′-GCAAAUAGGGCUUCACAUA-3′;

Sigma-Aldrich), or one of 2 tested Gli2-targeting constructs (siRNA1: 5′-GACAUGAGCUCCAUGCUCA-3′ or siRNA2: 5′-CGAUUGACAUGCGACACCA-3′; Sigma-Aldrich) at a 1:3 siRNA (μg) to Lipofectamine 2000 (μL) ratio. Lipofectamine and siRNA were incubated for 20 minutes at RT, added to cells in serum-free RPMI to incubate for up to 8 hours, followed by 10% FBS/RMPI thereafter. Transfected cells were grown at 37°C for 48 to 72 hours and then harvested for qPCR or Western blot analysis.

Assessment of cell viability and cell-cycle analysis

To a 96-well plate, 2,000 cells/well were exposed to increasing concentrations of cyclopamine or LDE225, alone or in combination with carboplatin or paclitaxel, in triplicate. Viability was assessed with 0.15% MTT (Sigma-Aldrich). For effects of siRNA-mediated downregulation on paclitaxel IC_{50}, cells were first transfected with siRNA (5 μg) for 24 hours in 6-well plates, then trypsinized and replated at 2,000 cells per well, followed by addition of chemotherapy after attachment. IC_{50} of the agent of interest was determined by finding the dose at which the drug had 50% of its effect, calculated by the equation $[(OD450_{MAX} - OD450_{MIN})/2) + OD450_{MIN}]$. For cell-cycle analysis, cells were treated with vehicle alone, paclitaxel alone, LDE225 alone, or combined LDE225 and paclitaxel for 72 hours, trypsinized, and fixed in 100% ethanol overnight. Cells were then centrifuged, washed in PBS, and resuspended in PBS containing 0.1% Triton X-100 (v/v), 200 μg/mL DNase-free RNase A, and 20 μg/mL propidium iodide (PI). PI fluorescence was assessed by flow cytometry and the percentage of cells in sub-G_0, G_0–G_1, S-, and G_2–M phases was calculated by the cell-cycle analysis module for Flow Cytometry Analysis Software (FlowJo v.7.6.1).

ALDEFLUOR assay

Active aldehyde dehydrogenase (ALDH) was identified with the ALDEFLUOR assay according to manufacturer's instructions (StemCell Technologies). The ALDH-positive population was defined by cells with increased FITC signal absent in DEAB-treated cells, as previously described (27). ALDEFLUOR-positive and -negative populations from SKOV3Trip2 cells were sorted with a FACS Aria II flow cytometer (BD Biosciences), and collected cells were seeded onto a 96-well plate at a concentration of 2,000 cells/well. After overnight attachment, cells were then exposed to either DMSO or 5 μmol/L LDE225, alone or in combination with increasing concentrations of paclitaxel. Viability was assessed with 0.15% MTT (Sigma-Aldrich).

Orthotopic ovarian cancer model

For orthotopic therapy experiments using ovarian cancer cell lines, female athymic nude mice (NCr-nu) were purchased from the National Cancer Institute (Frederick, MD, USA) after Institution Animal Care and Use Committee approval of protocols, and cared for in accordance with guidelines of the American Association for Accreditation of Laboratory Animal Care. For all *in vivo* experiments, trypsinized cells were resuspended in 10% FBS-containing RPMI, washed with PBS, and suspended in serum-free HBSS at a concentration of 5×10^6 cells/mL, and 1×10^6 cells (A2780cp20 or SKOV3TRip2) were injected IP in 200 μL into 40 mice per experiment. After 1 week, mice ($n = 10$ per group) were randomized to treatment with (a) vehicle alone (0.5% methyl cellulose/0.5% Tween 80 in sterile water), (b) vehicle plus paclitaxel 75 μg, (c) LDE225 alone (60 mg/kg), or (d) combined LDE225 and paclitaxel. Vehicle and LDE225 were administered by gavage once daily and paclitaxel was administered i.p. weekly. Mice were treated for 4 weeks (A2780cp20) or 6 weeks (SKOV3TRip2, which grow more slowly) before sacrifice and tumor collection. All tumors were excised and weighed in total.

Statistical analysis

Comparisons of gene expression, cell viability, PI fluorescence, and mean tumor weight were analyzed using a 2-tailed Student *t* test, if assumptions of data normality were met. Those represented by alternate distribution were examined using a nonparametric Mann–Whitney *U* test. Differences between groups were considered statistically significant at $P < 0.05$. Error bars represent standard deviation unless otherwise stated. Number of mice per group ($n = 10$) was chosen as directed by a power analysis to detect a 50% decrease in tumor growth with β error of 0.2.

Results

Expression of HH pathway members in chemosensitive and chemoresistant ovarian cancer cell lines

We first examined mRNA expression of HH ligands [Sonic (*SHH*), Indian (*IHH*), Desert (*DHH*)], receptors (*PTCH1*, *SMO*), and transcription factors (*GLI1*, *GLI2*) in 3 pairs of parental and chemoresistant ovarian cancer cell lines: A2780ip2/A2780cp20 (20-fold increased cisplatin resistance and 10-fold increased taxane resistance), HeyA8/HeyA8MDR (500-fold taxane resistant), and SKOV3ip1/SKOV3TRip2 (1000-fold taxane resistant). As shown in Fig. 1A, mRNA levels of *SHH* were significantly higher in A2780cp20 (17.4-fold, $P < 0.05$) and SKOV3-TRip2 (2.4-fold, $P < 0.05$) cells compared with parental. *IHH* was also higher (3.5-fold, $P < 0.05$) in SKOV3TRip2 cells with *DHH* expression remaining unchanged or decreased in chemoresistant cell lines compared with parental. mRNA levels of *PTCH1* were significantly higher (2.1-fold, $P < 0.05$) in SKOV3TRip2 compared with parental SKOV3ip1 cells; however, no significant changes in *SMO* expression were observed between chemoresistant and chemosensitive cell lines (Fig. 1B). Protein expression of Smo was confirmed in all cell lines tested and did not always correlate with expression at the mRNA level (Fig. 1C). *GLI1* mRNA expression was significantly

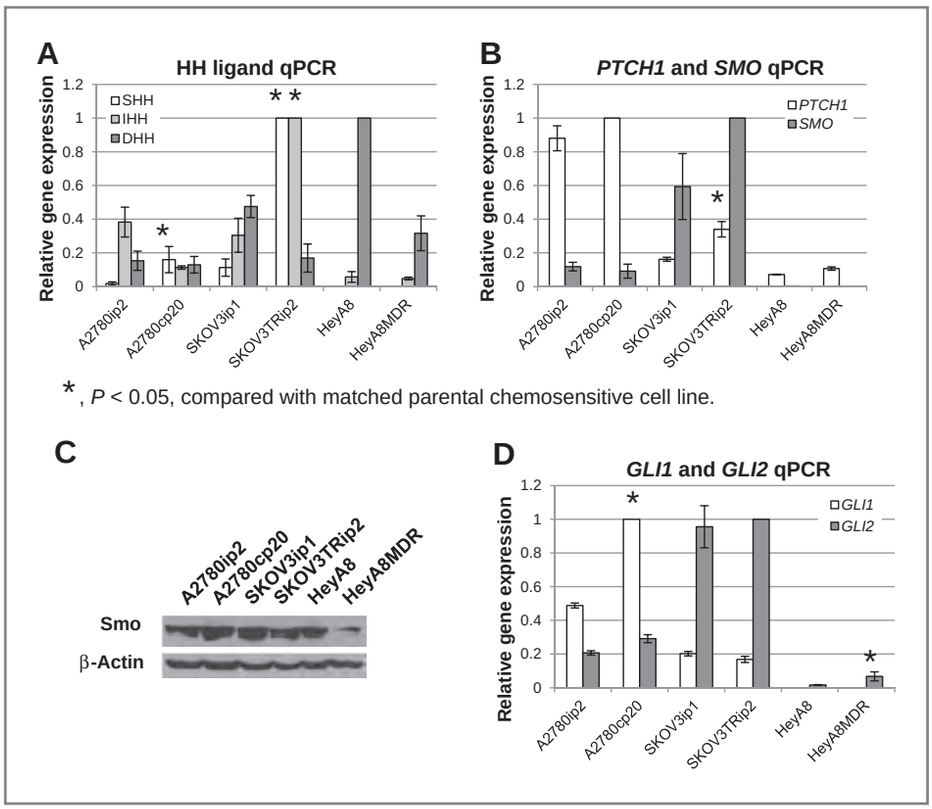

Figure 1. Expression of HH signaling components in chemosensitive and chemoresistant ovarian cancer cell lines. Gene expression was calculated relative to the sample/cell line with the highest expression of a particular gene. A, mRNA expression of HH ligands, Sonic (*SHH*), Indian (*IHH*), and Desert (*DHH*). B, mRNA expression of HH receptors, *PTCH1* and *SMO*. C, protein expression of Smo was also measured using Western blot analysis. β-Actin was used as a loading control. D, mRNA expression of HH transcription factors, *GLI1* and *GLI2*. Data are representative of 3 independent experiments. *, $P < 0.05$, compared with parental chemosensitive cell line.

higher (2.0-fold, $P < 0.05$) in A2780cp20 compared with parental A2780ip2 cells and *GLI2* mRNA expression was significantly higher (4.1-fold, $P < 0.05$) in HeyA8MDR compared with parental HeyA8 cells, although at very low levels in both (Fig. 1D). These results show that HH signaling is often higher in chemoresistant matched ovarian cancer cell lines.

Smo antagonists diminish cell viability and HH gene expression in ovarian cancer cell lines

Having observed Smo expression (both mRNA and protein) in both chemosensitive and chemoresistant ovarian cancer cell lines, we next examined response to the Smo antagonists cyclopamine and LDE225 among these cell lines. The chemical structure of LDE225 is shown in Fig. 2A. As shown in Table 1, cyclopamine IC_{50}s varied from 7.5 μmol/L (A2780ip2) to 19 μmol/L (SKOV3TRip2) and LDE225 IC_{50}s varied from 7.5 μmol/L (A2780cp20) to 24 μmol/L (SKOV3ip1). Interestingly, chemoresistant cell lines were more sensitive (up to 2.25-fold, $P < 0.05$) to LDE225 compared with their chemosensitive counterparts. Chemoresistant cell lines were also more sensitive to LDE225 than cyclopamine. To confirm that decreased cell viability was associated with diminished HH pathway activity, A2780cp20 cells were exposed to increasing concentrations of LDE225 (1, 5, and 10 μmol/L) for 72 hours and gene expression of HH target genes *PTCH1*, *GLI1*, and *GLI2* was analyzed by qPCR. A dose-dependent decrease in the expression of all 3 genes was observed with a maximum reduction of 39%, 43%, and 32% ($P < 0.05$), respectively, after exposure to 10 μmol/L LDE225 (Fig. 2B). Protein expression of the HH transcriptional activator Gli1 was also reduced in a dose-dependent manner after LDE225 treatment (Fig. 2C). Taken together, these data show the efficacy and HH-specific activity of LDE225 in multiple chemoresistant cell lines.

Smo antagonism reverses taxane resistance in chemoresistant ovarian cancer cell lines both *in vitro* and *in vivo*

Having observed increased expression of HH signaling components and response to Smo antagonists in chemoresistant ovarian cancer cell lines, we sought to determine whether targeting the HH pathway could increase sensitivity to carboplatin and paclitaxel, chemotherapy agents most commonly used in the treatment of ovarian cancer. Neither cyclopamine nor LDE225 affected response to carboplatin among the chemoresistant cell lines examined (data not shown). However, as shown in Table 1, both Smo antagonists significantly increased the sensitivity of all 3 chemoresistant cell lines to paclitaxel (by up to 27- and 20-fold, respectively; $P < 0.05$). Increased sensitivity to paclitaxel after combination with cyclopamine or LDE225 even occurred at low doses that were not effective alone (5 μmol/L cyclopamine, Fig. 3A and 1 μmol/L

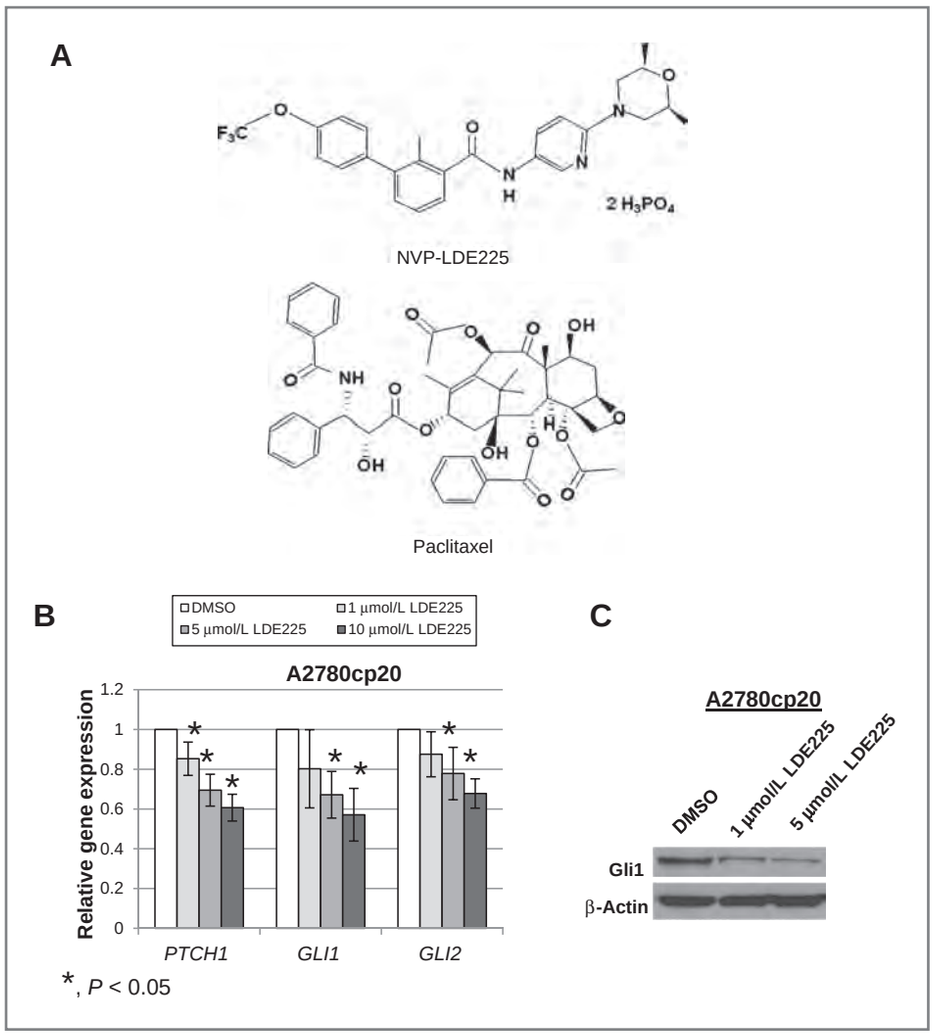

Figure 2. LDE225 reduces HH pathway activity in chemoresistant ovarian cancer cells. A, chemical structures of NVP-LDE225 and paclitaxel. B, gene expression of *PTCH1*, *GLI1*, and *GLI2* was examined in A2780cp20 cells after exposure to increasing concentrations of LDE225 using qPCR. *, $P < 0.05$, compared with DMSO vehicle control. C, protein expression of Gli1 in A2780cp20 cells after exposure to increasing concentrations of LDE225 was measured using Western blot analysis to confirm mRNA results. β-Actin was used as a loading control. Data are representative of 3 independent experiments.

LDE225, Fig. 3B). To determine the mechanism by which Smo antagonism combined with paclitaxel affects cell growth, we carried out cell-cycle analysis on A2780cp20 cells that were treated with DMSO alone (vehicle control), paclitaxel alone (30 nmol/L), LDE225 alone (5 μmol/L), or combined paclitaxel and LDE225 for 72 hours. As shown in Fig. 3C, combination treatment resulted in a greater accumulation of cells in the sub-G_0/apoptotic, S-, and G_2–M phases compared with control or either treatment alone. These data suggest that LDE225 enhances cell-cycle

Table 1. Ovarian cancer cell line response to Smo antagonists, alone and in combination with paclitaxel

	Mean IC_{50}, μmol/L		Mean paclitaxel IC_{50}, nmol/L			
Cell line	**Cyclopamine**	**LDE225**	**Control**	**w/Cyclopamine (5 μmol/L)**	**w/LDE225 (5 μmol/L)**	***P***
A2780ip2	7.5	12	4	1.5	2.6	NS
A2780cp20	10	7.5	30	1.3	1.5	<0.05
SKOV3ip1	14	24	6	3	5.5	NS
SKOV3TRip2	19	12	400	15	120	<0.05
HeyA8	12	18	7	4.2	6.5	NS
HeyA8MDR	13	8	650	50	115	<0.05

Abbreviation: NS, not significant.

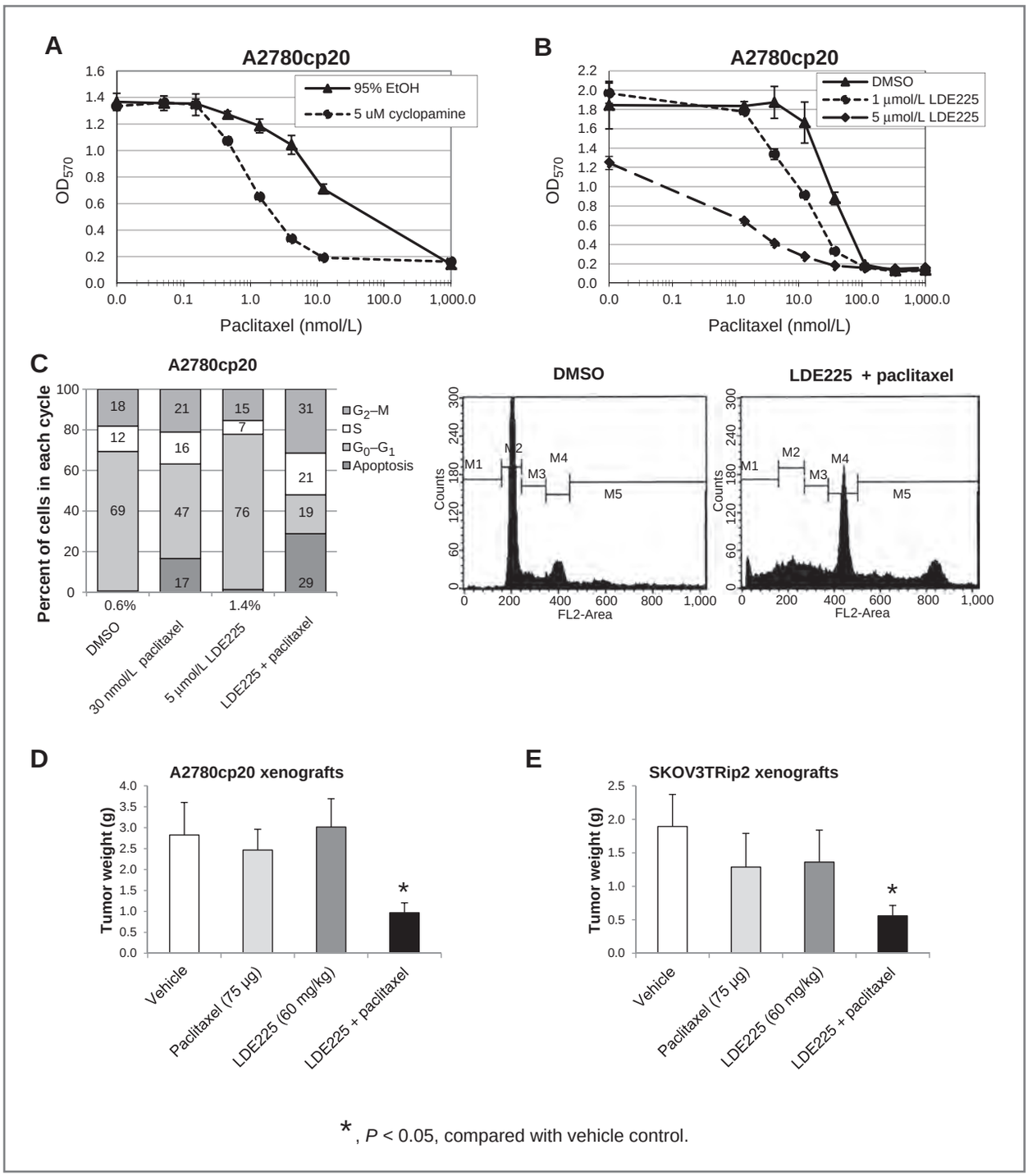

Figure 3. Smo antagonism reverses taxane resistance in chemoresistant ovarian cancer cell lines both *in vitro* and *in vivo*. A, A2780cp20 cells were exposed to either 95% ethanol (EtOH, vehicle control) or cyclopamine (5 μmol/L) in combination with increasing concentrations of paclitaxel. Cell viability was determined by MTT assay. B, A2780cp20 cells were exposed to either DMSO (vehicle control) or LDE225 (1 and 5 μmol/L) in combination with increasing concentrations of paclitaxel. Cell viability was determined by MTT assay. C, cell-cycle analysis was conducted on A2780cp20 cells treated with DMSO alone, paclitaxel alone, LDE225 alone, or combined paclitaxel and LDE225 using propidium iodide (PI) staining. Representative histograms of DMSO- and combination-treated cells are shown on the right. Data are representative of 3 independent experiments. D, mice injected intraperitoneally with A2780cp20 cells were treated with vehicle alone, paclitaxel alone, LDE225 alone, or combined paclitaxel + LDE225. E, mice injected intraperitoneally with SKOV3TRip2 cells were treated with either vehicle alone, paclitaxel alone, LDE225 alone, or combined paclitaxel + LDE225. For both xenograft models, mice treated with the combination paclitaxel + LDE225 showed a significant reduction in tumor weight compared with treatment with vehicle alone. Mean tumor weights with standard error are presented. *, $P < 0.05$, compared with vehicle control.

arrest and cell death induced by the microtubule-stabilizing effects of paclitaxel.

To determine if LDE225 can similarly reverse taxane resistance *in vivo*, an orthotopic mouse model using chemoresistant cell lines was used. Nude mice were injected intraperitoneally with either A2780cp20 or SKOV3TRip2 cells and randomized to 4 treatment groups: (a) vehicle alone, (b) paclitaxel alone (75 μg weekly), (c) LDE225 alone (60 mg/kg daily), or (d) combined paclitaxel and LDE225. When control mice started to become moribund with tumor burden, all mice were sacrificed and total tumor weights recorded. In the A2780cp20 model (Fig. 3D), there was no significant reduction in tumor growth with either paclitaxel or LDE225 alone. However, the combination of paclitaxel and LDE225 resulted in significantly reduced tumor weight, by 65.7% compared with vehicle alone ($P = 0.028$). This represented a 60.7% reduction compared with paclitaxel alone ($P = 0.014$) and a 68% reduction compared with LDE225 alone ($P = 0.010$), again showing synergy of paclitaxel and LDE225. Similar results were observed in SKOV3TRip2 xenografts (Fig. 3E). Neither paclitaxel nor LDE225 alone had a statistically significant impact on tumor growth, whereas combination treatment significantly reduced tumor weight, by 70.4% compared with vehicle alone ($P = 0.015$). This represented a 56.6% reduction compared with paclitaxel alone ($P = 0.18$) and a 58.8% reduction compared with LDE225 alone ($P = 0.13$), although neither was statistically significant.

LDE225 sensitizes chemoresistant ovarian cancer cells to paclitaxel by downregulating MDR1 expression and sensitizes both ALDH-negative and -positive ovarian cancer cells to paclitaxel

The primary mediator of taxane resistance in general, and in the chemoresistant cell lines examined in this study (27), is the expression of the drug efflux protein, P-glycoprotein (ABCB1/MDR1). To identify the mechanism underlying taxane sensitization after Smo antagonism, we next examined whether LDE225 could modulate *MDR1* gene expression. In A2780cp20 cells exposed to LDE225 alone, paclitaxel alone, and combined LDE225 + paclitaxel for 72 hours, it was observed that LDE225 decreased *MDR1* expression (by up to 49.2%, $P < 0.05$), whereas paclitaxel actually led to a compensatory *increase* in *MDR1* expression (2.88-fold, $P < 0.05$) compared with vehicle control (Fig. 4A). This compensatory increase in *MDR1* was alleviated by LDE225 in a dose-dependent manner (up to a 59.9% decrease, $P < 0.05$), showing that this compound increases sensitivity to paclitaxel, at least in part, by downregulating *MDR1*. Similar results were observed in SKOV3TRip2 cells (Fig. 4B); LDE225 decreased *MDR1* expression both alone (by up to 36.4%, $P < 0.05$ compared with vehicle control) and in combination with paclitaxel (by up to 50.8%, $P < 0.05$ compared with paclitaxel alone). In this cell line, a compensatory increase in *MDR1* was not observed with paclitaxel alone, likely because *MDR1* is already expressed at extremely high levels (140-fold more than in A2780cp20) in this 1,000-fold taxane-resistant cell line (27). To determine if similar modulation of *MDR1* occurs *in vivo*, RNA isolated from A2780cp20 tumors (from Fig. 3D) was examined. In agreement with the *in vitro* data, LDE225 alone significantly reduced *MDR1* expression (by 35.2%, $P < 0.05$) and paclitaxel alone significantly increased *MDR1* expression (2.55-fold, $P < 0.05$) compared with vehicle control (Fig. 4C). In addition, combination treatment significantly reduced *MDR1* expression compared with paclitaxel alone (by 48.8%, $P < 0.05$), blunting this compensatory rise.

In addition to our examination of MDR1 expression after LDE225 treatment, we also examined βIII-tubulin and stathmin, proteins that have been associated with microtubule regulation and resistance to taxanes (28). It was found that neither of these proteins was affected by LDE225 treatment *in vitro* (as determined by Western blot analysis, data not shown). Taken together, these data support a mechanism whereby LDE225 causes the downregulation of *MDR1* expression, which then leads to increased uptake of paclitaxel within chemoresistant cells, rather than potentiating the microtubule stabilizing effect of this compound.

We have previously shown that ALDH activity is associated with enhanced tumorigenicity and chemoresistance in ovarian cancer, and may define one of potentially many cancer cell populations with stem cell-like features (27, 29). To determine whether cancer stem cells (CSCs) might play a role in taxane sensitization after LDE225 treatment, we collected ALDH-negative and -positive cell populations from the SKOV3TRip2 cell line, and exposed them to combined LDE225 and paclitaxel. As shown in Fig. 4D, it was found that ALDH-negative and -positive SKOV3TRip2 cells showed a similar decrease in viability after LDE225 treatment alone (21.4% vs. 16.8%, respectively), compared with DMSO control. In addition, sensitivity to paclitaxel (as determined by IC_{50}) was similarly increased after combination treatment in ALDH-negative and -positive cells (5.1-fold vs. 4.0-fold change in IC_{50}, respectively). These results indicate that the more tumorigenic ALDH-positive cells are just as susceptible to LDE225 treatment as ALDH-negative cells, and that HH inhibition can sensitize both populations to taxane therapy. Whether other putative CSC populations such as CD133, CD44, and the side population, with which there is some (but not complete) crossover with the ALDH population (30), can also be sensitized to taxanes will be the subject of future investigations.

Knockdown of Smo diminishes HH pathway activity, reduces viability, and reverses taxane resistance in ovarian cancer cells

To determine whether LDE225 reverses taxane resistance through inhibition of Smo alone or off-target effects, we selectively targeted HH pathway members using siRNAs and observed effects on HH pathway activity and paclitaxel response. As shown in Fig. 5A, knockdown

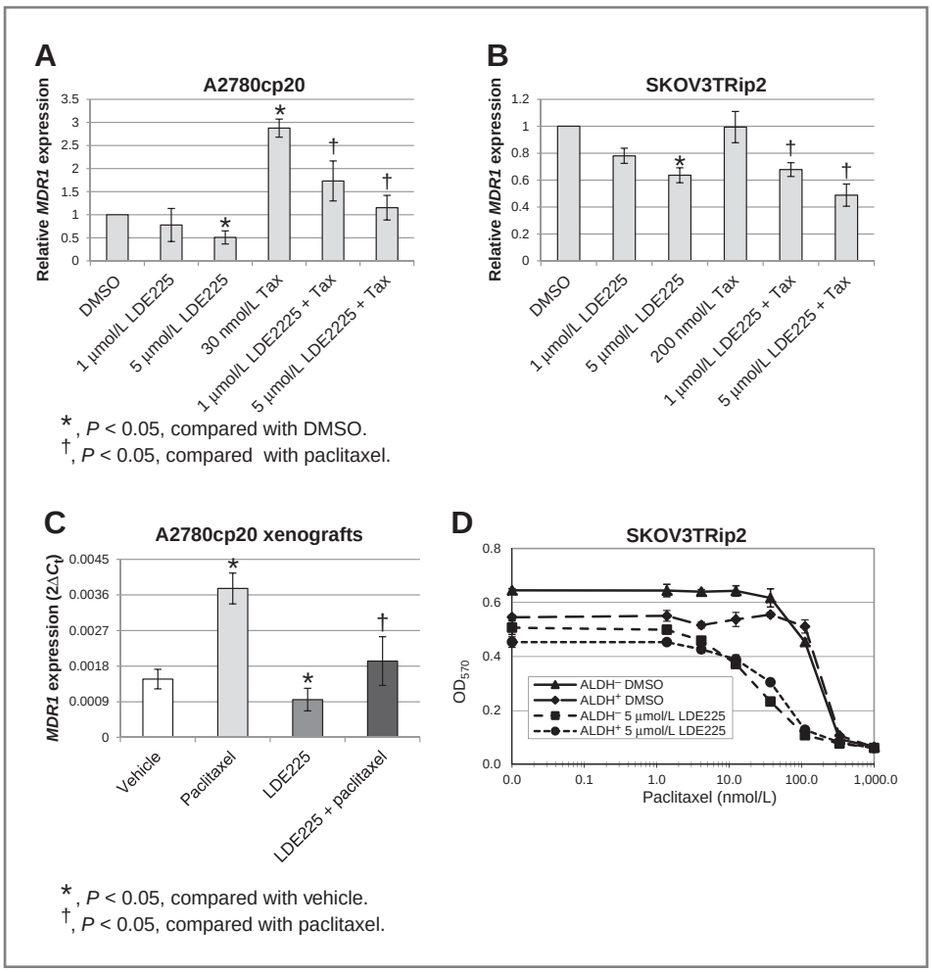

Figure 4. LDE225 sensitizes chemoresistant ovarian cancer cells to paclitaxel by downregulating MDR1 expression and sensitizes both ALDH-negative and -positive ovarian cancer cells to paclitaxel. A, A2780cp20 cells were exposed to DMSO, LDE225 (1 or 5 μmol/L), paclitaxel (Tax, 30 nmol/L), or combined LDE225 + paclitaxel for 72 hours and examined for *MDR1* gene expression. *, $P < 0.05$, compared with DMSO; †, $P < 0.05$, compared with paclitaxel alone. B, SKOV3TRip2 cells were exposed to DMSO, LDE225 (1 or 5 μmol/L), paclitaxel (Tax, 200 nmol/L), or combined LDE225 + paclitaxel for 72 hours and examined for *MDR1* gene expression. *, $P < 0.05$, compared with DMSO; †, $P < 0.05$, compared with paclitaxel alone. Data are representative of 3 independent experiments. C, A2780cp20 xenografts ($n = 5$ per group) treated with vehicle alone, paclitaxel alone, LDE225 alone, or combined LDE225 + paclitaxel were resected after 4 weeks of therapy and examined for *MDR1* gene expression. Mean expression with SE are presented. *, $P < 0.05$, compared with vehicle; †, $P < 0.05$, compared with paclitaxel alone. D, SKOV3TRip2 cells were sorted into aldehyde dehydrogenase–negative (ALDH−) and -positive (ALDH+) populations, using the ALDEFLUOR assay, and then exposed to either DMSO or 5 μmol/L LDE225, both alone and in combination with increasing concentrations of paclitaxel. Cell viability was determined by MTT assay.

of Smo was achieved both at the mRNA and protein level. As expected, this downregulation led to a significant decrease in HH target genes *PTCH1* (66.6%, $P < 0.01$), *GLI1* (86.5%, $P < 0.01$), and *GLI2* (62.0%, $P < 0.01$). Individual knockdown of HH mediators Smo, Gli1, or Gli2 using 2 distinct siRNA constructs for each gene led to increased sensitivity to paclitaxel (Fig. 5B–D). In particular, Smo knockdown decreased paclitaxel IC_{50} by up to 11.7-fold; Gli1 knockdown, up to 3.5-fold; and Gli2 knockdown, up to 5.9-fold. In agreement with cyclopamine and LDE225 biologic effects, knockdown of Smo, Gli1, or Gli2 alone significantly decreased cell viability (by up to 73.5%, 57.6%, and 26.5%, respectively, $P < 0.01$) compared with control siRNA. Collectively, these data suggest that HH signaling promotes ovarian cancer cell survival and mediates taxane resistance.

Discussion

In this study, we found that HH pathway signaling components are overexpressed in chemoresistant ovarian cancer cells. Moreover, targeting the HH pathway decreased ovarian cancer cell viability and sensitized chemoresistant ovarian cancer cells to paclitaxel therapy through decreased *MDR1* expression. The participation of HH signaling in ovarian cancer cell survival and chemotherapy resistance makes it an attractive target for therapy, especially because most patients with ovarian

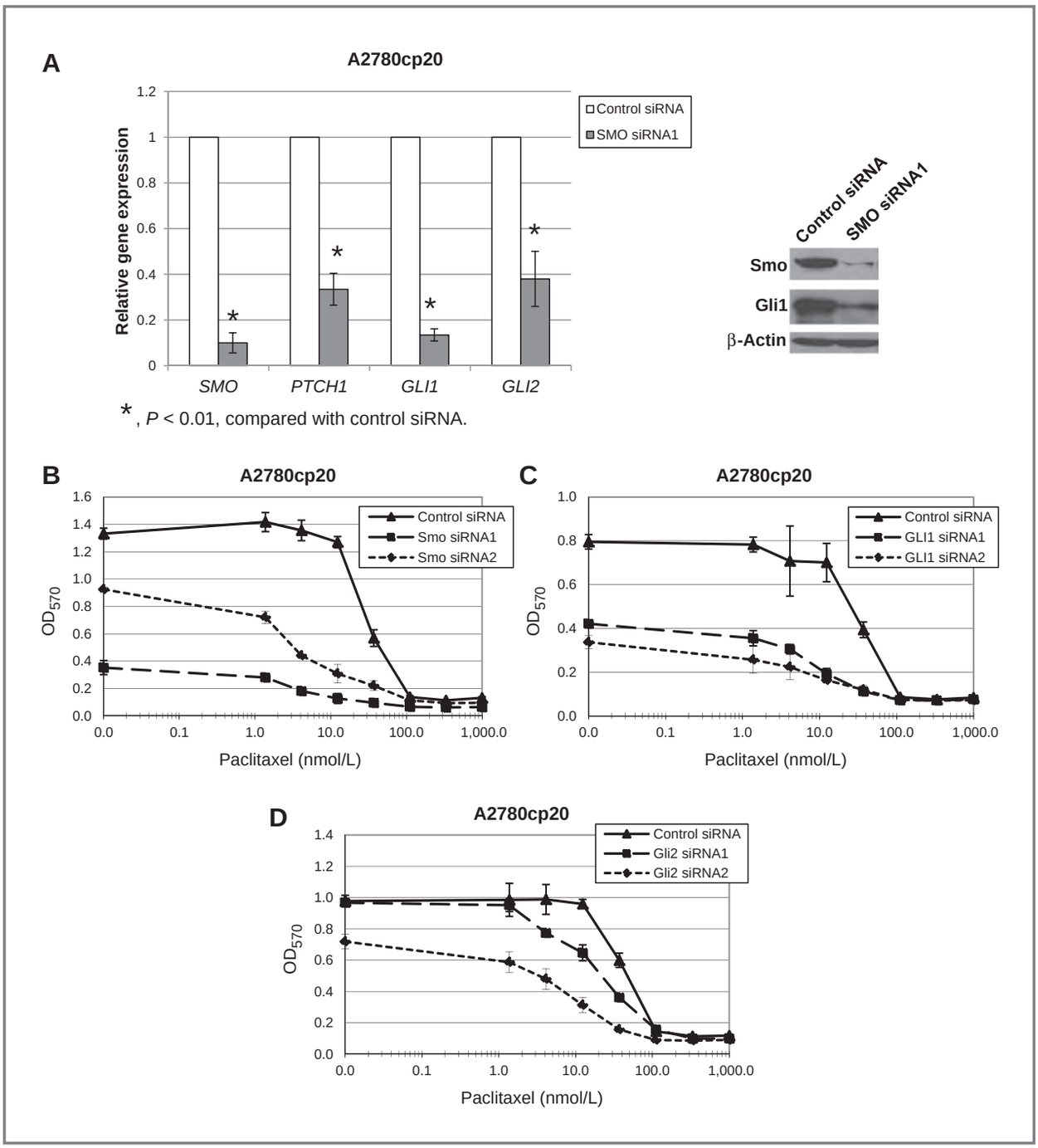

Figure 5. Knockdown of Smo diminishes HH pathway activity, reduces viability, and reverses taxane resistance in ovarian cancer cells. A, A2780cp20 cells were exposed to either control or Smo siRNA for 72 hours and examined for mRNA expression of HH pathway mediators *SMO*, *PTCH1*, *GLI1*, and *GLI2*. *, $P < 0.01$, compared with control siRNA. Protein expression of Smo and Gli (inset) was also measured using Western blot analysis to confirm mRNA results. β-Actin was used as a loading control. A2780cp20 cells were transfected with either control siRNA or 2 distinct siRNA constructs designed against Smo (B), Gli1 (C), or Gli2 (D) and exposed to increasing concentrations of paclitaxel. Cell viability was determined by MTT assay. Data are representative of 3 independent experiments.

cancer develop tumor recurrence and succumb to chemoresistant disease.

Currently, it has not been shown what role HH signaling might play in mediating ovarian cancer chemoresistance, a persistent obstacle in the treatment of this disease. Although the clinical behavior of ovarian cancer suggests that most cancer cells are initially sensitive to chemotherapy, they subsequently either develop resistance or

contain a population of cells that are inherently resistant. The latter hypothesis is consistent with what has become known as tumor initiating cells or CSCs. These CSCs are commonly believed to have enhanced tumorigenicity, differentiation capacity, and resistance to chemotherapy in comparison with non-CSCs. It is because of these features that CSCs have been examined for molecular pathways and markers that could be targeted for therapeutic purposes. Recent studies have suggested that developmental pathways, including HH, play important roles in the maintenance of CSCs (10/11) and that inhibiting these pathways may provide enhanced chemosensitivity when combined with traditional chemotherapies. In our study, we sought to define a role for HH signaling in ovarian cancer chemoresistance. Both *in vitro* and *in vivo*, we observed significant sensitization to paclitaxel after Smo antagonism (LDE225) in taxane-resistant ovarian cancer cells. This sensitization was also present in ALDH-positive cells, a subpopulation of cancer cells with enhanced tumorigenicity and chemoresistance. The mechanism underlying this sensitization seems to involve downregulation of P-glycoprotein (ABCB1/MDR1), a well-characterized mediator of multidrug resistance. By downregulating *MDR1* expression, uptake of paclitaxel by cancer cells would be increased, resulting in a greater response to the chemotherapeutic agent. This mechanism would explain why Smo antagonists did not sensitize chemoresistant cells to carboplatin, because this compound is not a substrate for the P-glycoprotein drug efflux pump. In addition, this model of HH inhibition and chemosensitization agrees with a previous study done by Sims-Mourtada and colleagues, in which it was showed that cyclopamine sensitized prostate cancer cells to a variety of chemotherapy agents *in vitro* (including the taxane docetaxel), through modulation of MDR1 expression (12). The observation that Smo antagonism did not sensitize cells to platinum therapy highlights the specificity of this effect.

Previous studies have showed aberrant expression of the HH pathway in primary specimens of ovarian cancer compared with normal ovarian epithelium (7–9), including a study that found elevated Gli1 expression is associated with decreased survival (9). These studies have also showed decreased ovarian cancer cell growth/viability after treatment with the Smo antagonist cyclopamine, results that our study supports. We have previously shown that *GLI1* and *GLI2* mRNA levels were significantly higher in cancer cells isolated from persistent/chemoresistant tumors compared with those isolated from matched primary tumors (29). Smo expression was also increased (3.7-fold) in persistent tumors; however, this increase was not statistically significant. Patients from whom persistent tumors were obtained had failed both taxane and platinum chemotherapies, making it difficult to determine whether this increase in HH pathway genes is a taxane-specific effect. The *in vitro* data presented in this study, however, would suggest that Smo, as well as Gli1 and Gli2, are associated with taxane resistance. In our initial experiments examining the effects of targeting HH alone, either with Smo antagonists or RNAi, ovarian cancer cell viability was significantly decreased *in vitro*, indicating that the HH pathway is important for ovarian cancer survival. However, this effect did not seem to translate to our xenograft models, in which the Smo antagonist LDE225 had no significant impact on tumor growth when used alone, even in models with relatively high Gli1 expression. These findings suggest that survival pathways are activated in the murine tumor microenvironment that allows resistance to HH antagonist monotherapy. Given the recognized importance of crosstalk between the tumor stromal cells and malignant cells in the HH pathway (6), and the failure of this model to target both murine and human compartments, more efficacy may be noted with monotherapy in humans.

Collectively, the data presented in this study show that increased expression of HH signaling components is associated with taxane resistance, which can be overcome by targeting multiple effectors of the HH signaling pathway. With the ability to identify subsets of patients with cancer with HH pathway overexpression, antagonism of HH signaling in combination with taxane therapy could ultimately provide a useful therapeutic strategy for recurrent, chemoresistant ovarian cancer.

Disclosure of Potential Conflicts of Interest

No potential conflicts of interest were disclosed.

Authors' Contributions

Conception and design: A.D. Steg, C.N. Landen
Development of methodology: A.D. Steg, C.N. Landen
Acquisition of data (provided animals, acquired and managed patients, provided facilities, etc.): A.D. Steg, A.A. Katre, K.S. Bevis, A. Ziebarth, Z. C. Dobbin, M.M. Shah, C.N. Landen
Analysis and interpretation of data (e.g., statistical analysis, biostatistics, computational analysis): A.D. Steg, C.N. Landen
Writing, review, and/or revision of the manuscript: A.D. Steg, A. Ziebarth, R.D. Alvarez, C.N. Landen
Administrative, technical, or material support (i.e., reporting or organizing data, constructing databases): A.A. Katre, Z.C. Dobbin, C.N. Landen
Study supervision: C.N. Landen

Acknowledgments

NVP-LDE225 was kindly provided by Novartis Pharma AG.

Grant Support

This work was supported by the University of Alabama at Birmingham Center for Clinical and Translational Science (5UL1RR025777, C.N. Landen), the Reproductive Scientist Development Program through the Ovarian Cancer Research Fund and the NIH (K12 HD00849, C.N. Landen), and the Gynecologic Cancer Foundation and the Department of Defense Ovarian Cancer Research Academy (OC093443, C.N. Landen).

The costs of publication of this article were defrayed in part by the payment of page charges. This article must therefore be hereby marked *advertisement* in accordance with 18 U.S.C. Section 1734 solely to indicate this fact.

Received December 28, 2011; revised April 3, 2012; accepted April 18, 2012; published OnlineFirst May 2, 2012.

References

1. Bhoola S, Hoskins WJ. Diagnosis and management of epithelial ovarian cancer. Obstet Gynecol 2006;107:1399–410.
2. Hooper JE, Scott MP. Communicating with Hedgehogs. Nat Rev 2005;6:306–17.
3. Ruiz i Altaba A, Mas C, Stecca B. The Gli code: an information nexus regulating cell fate, stemness and cancer. Trends Cell Biol 2007;17: 438–47.
4. Stecca B, Ruiz IAA. Context-dependent regulation of the GLI code in cancer by HEDGEHOG and non-HEDGEHOG signals. J Mol Cell Biol 2010;2:84–95.
5. Pasca di Magliano M, Hebrok M. Hedgehog signalling in cancer formation and maintenance. Nat Rev Cancer 2003;3:903–11.
6. Theunissen JW, de Sauvage FJ. Paracrine Hedgehog signaling in cancer. Cancer Res 2009;69:6007–10.
7. Chen X, Horiuchi A, Kikuchi N, Osada R, Yoshida J, Shiozawa T, et al. Hedgehog signal pathway is activated in ovarian carcinomas, correlating with cell proliferation: it's inhibition leads to growth suppression and apoptosis. Cancer Sci 2007;98:68–76.
8. Bhattacharya R, Kwon J, Ali B, Wang E, Patra S, Shridhar V, et al. Role of hedgehog signaling in ovarian cancer. Clin Cancer Res 2008;14: 7659–66.
9. Liao X, Siu MK, Au CW, Wong ES, Chan HY, Ip PP, et al. Aberrant activation of hedgehog signaling pathway in ovarian cancers: effect on prognosis, cell invasion and differentiation. Carcinogenesis 2009;30: 131–40.
10. Ruiz i Altaba A. Therapeutic inhibition of Hedgehog-GLI signaling in cancer: epithelial, stromal, or stem cell targets? Cancer Cell 2008;14: 281–3.
11. Merchant AA, Matsui W. Targeting Hedgehog—a cancer stem cell pathway. Clin Cancer Res 2010;16:3130–40.
12. Sims-Mourtada J, Izzo JG, Ajani J, Chao KS. Sonic Hedgehog promotes multiple drug resistance by regulation of drug transport. Oncogene 2007;26:5674–9.
13. Singh RR, Kunkalla K, Qu C, Schlette E, Neelapu SS, Samaniego F, et al. ABCG2 is a direct transcriptional target of hedgehog signaling and involved in stroma-induced drug tolerance in diffuse large B-cell lymphoma. Oncogene 2011;30:4874–86.
14. Binns W, James LF, Shupe JL, Everett G. A congenital Cyclopian-type malformation in lambs induced by maternal ingestion of a range plant, *Veratrum californicum*. Am J Vet Res 1963;24:1164–75.
15. Cooper MK, Porter JA, Young KE, Beachy PA. Teratogen-mediated inhibition of target tissue response to Shh signaling. Science 1998;280:1603–7.
16. Chen JK, Taipale J, Cooper MK, Beachy PA. Inhibition of Hedgehog signaling by direct binding of cyclopamine to Smoothened. Gen Dev 2002;16:2743–8.
17. Buonamici S, Williams J, Morrissey M, Wang A, Guo R, Vattay A, et al. Interfering with resistance to smoothened antagonists by inhibition of the PI3K pathway in medulloblastoma. Sci Transl Med 2010;2:51ra70.
18. Louie KG, Behrens BC, Kinsella TJ, Hamilton TC, Grotzinger KR, McKoy WM, et al. Radiation survival parameters of antineoplastic drug-sensitive and -resistant human ovarian cancer cell lines and their modification by buthionine sulfoximine. Cancer Res 1985;45: 2110–5.
19. Landen CN, Kim TJ, Lin YG, Merritt WM, Kamat AA, Han LY, et al. Tumor-selective response to antibody-mediated targeting of alphavbeta3 integrin in ovarian cancer. Neoplasia 2008;10:1259–67.
20. Halder J, Kamat AA, Landen CN Jr, Han LY, Lutgendorf SK, Lin YG, et al. Focal adhesion kinase targeting using *in vivo* short interfering RNA delivery in neutral liposomes for ovarian carcinoma therapy. Clin Cancer Res 2006;12:4916–24.
21. Buick RN, Pullano R, Trent JM. Comparative properties of five human ovarian adenocarcinoma cell lines. Cancer Res 1985;45:3668–76.
22. Moore DH, Allison B, Look KY, Sutton GP, Bigsby RM. Collagenase expression in ovarian cancer cell lines. Gynecol Oncol 1997;65:78–82.
23. Yu D, Wolf JK, Scanlon M, Price JE, Hung MC. Enhanced c-erbB-2/neu expression in human ovarian cancer cells correlates with more severe malignancy that can be suppressed by E1A. Cancer Res 1993;53: 891–8.
24. Duan Z, Feller AJ, Toh HC, Makastorsis T, Seiden MV. TRAG-3, a novel gene, isolated from a taxol-resistant ovarian carcinoma cell line. Gene 1999;229:75–81.
25. Landen CN Jr, Lu C, Han LY, Coffman KT, Bruckheimer E, Halder J, et al. Efficacy and antivascular effects of EphA2 reduction with an agonistic antibody in ovarian cancer. J Natl Cancer Inst 2006;98:1558–70.
26. Steg A, Wang W, Blanquicett C, Grunda JM, Eltoum IA, Wang K, et al. Multiple gene expression analyses in paraffin-embedded tissues by TaqMan low-density array: application to hedgehog and Wnt pathway analysis in ovarian endometrioid adenocarcinoma. J Mol Diagn 2006;8:76–83.
27. Landen CN Jr, Goodman B, Katre AA, Steg AD, Nick AM, Stone RL, et al. Targeting aldehyde dehydrogenase cancer stem cells in ovarian cancer. Mol Cancer Ther 2010;9:3186–99.
28. Kavallaris M. Microtubules and resistance to tubulin-binding agents. Nat Rev Cancer 2010;10:194–204.
29. Steg AD, Bevis KS, Katre AA, Ziebarth A, Dobbin ZC, Alvarez RD, et al. Stem cell pathways contribute to clinical chemoresistance in ovarian cancer. Clin Cancer Res 2012;18:869–81.
30. Silva IA, Bai S, McLean K, Yang K, Griffith K, Thomas D, et al. Aldehyde dehydrogenase in combination with CD133 defines angiogenic ovarian cancer stem cells that portend poor patient survival. Cancer Res 2011;71:3991–4001.

Clinical Cancer Research

Endoglin (CD105) contributes to platinum resistance and is a target for tumor-specific therapy in epithelial ovarian cancer

Angela Ziebarth, Somaira Nowsheen, Adam D. Steg, et al.

Clin Cancer Res Published OnlineFirst November 12, 2012.

Endoglin (CD105) contributes to platinum resistance and is a target for tumor-specific therapy in epithelial ovarian cancer

Angela J. Ziebarth[1], Somaira Nowsheen[2], Adam D. Steg[1], Monjri M. Shah[1], Ashwini A. Katre[1], Zachary C. Dobbin[1], Hee-Dong Han[3], Gabriel Lopez-Berestein[3,4,5], Anil K. Sood[4,5,6], Michael Conner[7], Eddy S. Yang[2], and Charles N. Landen[1*]

[1] Department of Obstetrics and Gynecology, University of Alabama at Birmingham, Birmingham, AL 35294
[2] Department of Radiation Oncology, University of Alabama at Birmingham, Birmingham, AL 35294
[3] Center for RNA Interference and Non-Coding RNA, [4]Departments of Experimental Therapeutics, [5]Cancer Biology, and [6]Gynecologic Oncology & Reproductive Medicine, U.T.M.D. Anderson Cancer Center, Houston, TX 77030
[7] Department of Pathology, University of Alabama at Birmingham, Birmingham, AL 35294

Running Title: Cytotoxic induction of DNA damage with endoglin targeting

Keywords: Endoglin, CD105, platinum resistance, ovarian cancer, siRNA, cancer stem cells

*Correspondence: Charles N. Landen, Jr., MD, MS
Associate Professor
Department of Obstetrics and Gynecology
The University of Alabama at Birmingham
176F RM 10250
619 19th Street South
Birmingham, AL 35249
Work: 205-934-4986
Fax: 205-975-6174
clanden@uab.edu

Acknowledgements: Funding support provided in part by the University of Alabama at Birmingham Center for Clinical and Translational Science (5UL1RR025777), the Reproductive Scientist Development Program through the Ovarian Cancer Research Fund and the National Institutes of Health (K12 HD00849), and the Department of Defense Ovarian Cancer Research Academy (OC093443), the Ovarian Cancer Research Fund, U54 CA151668, P50 CA083639, and the RGK Foundation.

Statement of Translational Relevance: Ovarian cancer remains the most lethal gynecologic malignancy, largely due to its high rate of chemoresistant recurrence. Endoglin (CD105) is overexpressed on tumor-associated endothelial cells and is a target for anti-angiogenic therapy, but expression on tumor cells has only been recently demonstrated. In the current study, we demonstrate that endoglin is actually predominantly expressed in the cytoplasm of malignant cells, and downregulating endoglin promotes apoptosis, induces DNA damage, and sensitizes cells to platinum therapy *in vitro* and *in vivo*. This occurs through effects on numerous DNA repair genes, most prominently BARD1. The novel demonstration of efficacy in targeting tumor cells themselves, in addition to the previously-recognized effects of targeting vasculature, make this therapeutic an attractive mechanism to target both compartments of the tumor microenvironment.

Abstract:

Purpose: Endoglin (ENG, CD105) is a membranous protein overexpressed in tumor-associated endothelial cells, chemoresistant populations of ovarian cancer cells, and potentially stem cells. Our objective was to evaluate the effects and mechanisms of targeting endoglin in ovarian cancer.

Experimental Design: Global and membranous endoglin expression was evaluated in multiple ovarian cancer lines. *In vitro*, the effects of siRNA-mediated endoglin knockdown with and without chemotherapy were evaluated by MTT assay, cell-cycle analysis, alkaline comet assay, γ-H2AX foci formation, and qPCR. In an orthotopic mouse model, endoglin was targeted with chitosan-encapsulated siRNA with and without carboplatin.

Results: Endoglin expression was surprisingly predominantly cytoplasmic, with a small population of surface-positive cells. Endoglin inhibition decreased cell viability, increased apoptosis, induced double-stranded DNA damage, and increased cisplatin sensitivity. Targeting endoglin downregulates expression of numerous DNA repair genes, including BARD1, H2AFX, NBN, NTHL1, and SIRT1. BARD1 was also associated with platinum resistance, and was induced by platinum exposure. *In vivo*, anti-endoglin treatment decreased tumor weight in both ES2 and HeyA8MDR models when compared to control (35-41% reduction, $p<0.05$). Endoglin inhibition with carboplatin was associated with even greater inhibitory effect when compared to control (58-62% reduction, $p<0.001$).

Conclusions: Endoglin downregulation promotes apoptosis, induces significant DNA damage through modulation of numerous DNA repair genes, and improves platinum sensitivity both *in vivo* and *in vitro.* Anti-endoglin therapy would allow dual treatment of both tumor angiogenesis

and a subset of aggressive tumor cells expressing endoglin and is being actively pursued as therapy in ovarian cancer.

Introduction

Epithelial ovarian carcinoma (EOC) remains the most lethal gynecologic malignancy.[1] While initial response to first-line therapy (consisting of surgical cytoreduction and combination platinum/taxane therapy) is usually effective, the majority of patients will ultimately recur with chemotherapy-resistant cancer and succumb to disease. This emphasizes the need for novel therapies aimed at targeting the population of cancer cells most resistant to initial therapy.

Endoglin (ENG) is a 180kDa disulfide-linked homodimer transmembrane protein most prominently expressed on proliferating endothelial cells. It is a well-characterized angiogenic marker that is upregulated during angiogenesis, and is overexpressed in vascular endothelium in malignancies including ovarian, leukemia, gastrointestinal stromal tumors (GIST), melanoma, and laryngeal cancers, but is rarely expressed in non-endothelial cells.[2-3] It is a co-receptor of TGFBR2 that binds TGF-B and is an important mediator of fetal vascular/endothelial development.[4] Recently, anti-angiogenic agents have received extensive attention as new therapeutic modalities, and CD105 has become an additional target by which intratumoral angiogenesis may be targeted.[5-6] However, endoglin may serve in a capacity beyond angiogenesis alone. Studies in GIST[7] and breast cancer[8] suggest that endoglin is upregulated not only in tumor endothelial cells, but also in actual tumor cells, and is associated with poor prognosis. Soluble endoglin has also been noted in ovarian cancer ascites,[9] and increased endoglin expression in ovarian cancer endothelial cells is associated with poor prognosis.[10] Additionally, we have recently shown that while endoglin is rarely expressed in primary ovarian cancer cells, it is frequently expressed in recurrent platinum-resistant tumor cells, as compared to the primary untreated tumor.[11] These findings suggest a broader role of endoglin in tumor cell biology beyond that of endothelial expression alone. The goal of our current study is to evaluate

the effects of targeting tumor-specific endoglin in ovarian cancer both *in vitro* and *in vivo* and explore the mechanisms by which endoglin may contribute to chemoresistance.

Methods and Materials

Evaluation of endoglin expression in ovarian cancer cell lines. Multiple ovarian cancer cell lines were evaluated for the presence of endoglin, including HeyA8, HeyA8MDR, ES2, A2780ip2, A2780cp20, A2780cp55, SKOV3ip1, SKOV3TRp2, IGROV-AF1, and HIO-180. Cells were maintained in RPMI-1640 medium with 10% fetal bovine serum (FBS) (Hyclone, Logan, UT). The taxane-resistant cell line HeyA8MDR was maintained in the same media with the addition of 150 ng/ml of paclitaxel. Cell lines were routinely screened for Mycoplasma (GenProbe detection kit; Fisher, Itasca, IL) and all experiments performed on 70-80% confluent cultures. Cells less than 20 passages from confirmation of genotype by STR analysis were used.

Cell lysates were collected in modified radioimmunoprecipitation assay lysis buffer with protease inhibitor cocktail (Roche, Manheim, Germany). Immunoblot analysis was performed using rabbit anti-endoglin antibody (Sigma, St. Louis, MO) at 1:500 dilution overnight at 4°C. A loading control was performed with mouse anti-β-actin antibody (Clone AC-15, Sigma) at 1:20,000 dilution for 1 hour at RT. After washing, membranes were incubated in HRP-conjugated goat anti-rabbit (for Endoglin) or goat anti-mouse (for β-actin) secondary antibodies (Bio-Rad, Hercules, CA). Visualization was performed by enhanced chemiluminescence (Pierce Thermo Scientific, Rockford, IL).

Immunohistochemistry. Cell lines in culture were washed with ice cold PBS twice, then fixed by applying 100% ice cold methanol for 10 min. Cells were rehydrated with PBS. Endogenous

peroxidase was blocked with 3% H2O2 in methanol for 15min at RT. The slides were incubated in 10% normal goat serum for 1 hr at RT. The primary anti-endoglin antibody (Sigma HPA011862) was diluted in 10% normal goat serum at 1:50. The slides were kept at 4°C overnight. Biotin-labeled secondary antibody was applied on cells at the concentration of 1:2000 for 1hr at RT, followed by avidin-biotin peroxidase buffer. DAB (3,3'-diaminobenzidine) was used as chromophore to detect the staining. To visualize endoglin expression in tumor sections, formalin-fixed paraffin-embedded tissue was cut in sections of 5uM thickness. Slides were warmed for 15 minutes and sequentially deparaffinized. Antigen retrieval was carried out in Citrate buffer (pH6.0) in a pressure cooker at high pressure for 5 min. Endogenous peroxidase was quenched by 3% H2O2 in methanol for 15 min. Slides were incubated in 10% normal goat serum for 1hr at RT. Slides were then incubated (4°C, Overnight) in antibody against endoglin (Sigma HPA011862) in 10% normal goat serum at 1:200 dilution. Detection was carried out using biotin labeled secondary antibody against rabbit at dilution of 1:2000 incubated at RT for 1 hr, followed by avidin-biotin peroxidase buffer. DAB (3,3'-diaminobenzidine) was used as chromophore.

Flow cytometry. After trypsinisation and centrifugation, the cell pellet was washed and resuspended in washing buffer (PBS containing 2% FBS and 0.1% sodium azide).$1x10^7$ cells were resuspended in 50µls of 10% goat buffer for 1hr kept on ice. Cells were incubated in antibody against endoglin 1:100 (Sigma HPA011862) in 10% goat serum for 1hr on ice. Alexa-488-conjugated anti rabbit antibody was applied on cells for 30 minutes and incubated on ice. The cells were washed twice in PBS and analyzed by FACS.

Endoglin Downregulation by siRNA transfection: In order to determine the effects of endoglin downregulation in ovarian cancer cells, transient knockdown was accomplished with anti-endoglin siRNA. Lipofectamine 2000 (Invitrogen) transfection was performed on Hey8MDR and ES2 cell lines using control siRNA (target sequence: 5'-UUCUCCGAACGUGUCACGU-3', Sigma) lacking known human or mouse targets, or one of two different Endoglin-targeting constructs (5'-CAAUGAGGCGGUGGCAAU-3' ["ENG_A"} or 5'-CAGAAACAGUCCAUUGUGA-3' ["ENG_B"], Sigma). These anti-human sequences have no more than 8 consecutive bp homology with murine CD105 (by BLASTN) and therefore should not affect murine endoglin expression. Lipofectamine was added to 5μg siRNA at a 3:1 v/v ratio (or as otherwise specified, as in Figure 1E) were incubated for 20 min at RT, added to cells in serum-free RPMI to incubate for 12 hours in 6- well plates, then maintained in 10% FBS/RPMI for an additional 12 hours, trypsinized and re-plated on a 96-well plate at a concentration of 2,000 cells per well. Cells were treated with vehicle or increasing doses of carboplatin or paclitaxel to generate an IC 50 curve. After 5 days, cells were washed and incubated with MTT reagent (Sigma) for 2 hours at 37°C. Media was then removed, cells dissolved in DMSO, and optical density measurements at 570 nm read with a spectrophotometer. The IC50 was the chemotherapy concentration giving the OD_{IC50} reading, calculated by the formula $OD_{IC50} = [(OD_{MAX} - OD_{MIN})/2 + OD_{MIN}]$. Assays were repeated in triplicate.

Apoptosis analysis. Analysis of apoptosis was performed with the Annexin V assay combined with propidium iodide (PI, eBiosciences #88-8005-74). ES2 and HeyA8MDR cells were transfected with either control siRNA or anti-endoglin siRNA in serum-free RPMI growth media for 12 hours, followed by maintenance in 10% FBS/RMPI. Cells were trypsinized 96 hours

following transfection, washed twice in PBS, and then resuspended in 200μL 1x binding buffer containing 5μL of Annexin V. 10μL of PI was added, cells were incubated for 10 minutes at RT in the dark. Fluorescent signal (FITC and PI) in cells were analyzed by FACS and data were analyzed with FlowJo v.7.6.1 (Ashland, OR).

Alkaline comet assay. ES2 cells (n=400,000 in 6-well plate) were transfected with endoglin and control siRNA. Twenty-four hours following transfection, cells were exposed to cisplatin without supplemental SVF at a concentration of 1μM (the approximate IC80 level for this line) for either 1 or 4 hours, carefully rinsed to remove the drug, and cultured in regular media. Vehicle or control siRNA were included in all experiments. At the indicated time points, cells were collected and subjected to alkaline comet assay according to the manufacturer's instructions (catalog # 4250-050-K; Trevigen). Briefly, cells were combined with low melting agarose onto CometSlides (Trevigen). After lysis, cells were subjected to electrophoresis and stained with SYBR green. Subsequently, cells were visualized using fluorescent microscopy (Carl Zeiss, Thornwood, NY). At least 200 comet images were analyzed for each time point using Comet Score software (version 1.5; TriTek Corp.). The number of tail-positive cells with small and large nuclei was manually counted by an examiner blinded to treatment group, and expressed as a percentage of all cells evaluated. Experiments were repeated in triplicate.

γ-H2AX foci formation. ES2 cell lines were cultured and seeded on sterile cover slips. Twenty-four hours following transfection with control or anti-endoglin siRNA, cells were exposed to 1μM cisplatin for either 1 or 4 hours, carefully rinsed to remove the drug, and cultured in regular media. Following the treatment period, IHC was performed as previously described[12-13] with

slight modification for foci staining. Briefly, cells were rinsed in phosphate buffered saline (PBS) and incubated for 5 minutes at 4°C in ice-cold cytoskeleton buffer (10mM Hepes/KOH, pH 7.4, 300mM sucrose, 100mM NaCl, 3mM MgCl2) supplemented with 1mM PMSF, 0.5mM sodium vanadate and proteasome inhibitor (Sigma, 1:100 dilution) followed by fixation in 70% ethanol for 15 minutes. The cells were blocked and incubated with primary antibody (1:500 dilution, anti-phosphoH2AX Ser139, Millipore, catalog # MI-07-164). The secondary antibody was anti-rabbit Alexa Fluor 488–conjugated antibody (1:2000 dilution; Invitrogen). DAPI (Invitrogen, catalog # D21490) was used for nuclear staining. The cover slips were subsequently mounted onto slides with mounting media (Aqua poly mount, Polysciences, Inc. catalog # 18606) and analyzed via fluorescence microscopy (Carl Zeiss, Thornwood, NY). Positive and negative controls were included on all experiments. A total of 500 cells were assessed. For foci quantification, cells with greater than 10 foci were counted as positive according to the standard procedure. Experiments were repeated in triplicate.

RNA extraction from cell lines. Total RNA was isolated from ovarian cancer cell lines using Trizol reagent (Invitrogen, Carlsbad, CA) per manufacturer's instructions. RNA was then DNase treated and purified using the RNeasy Mini Kit (QIAGEN, Hilden, Germany). RNA was eluted in 50 μL of RNase-free water and stored at -80°C. The concentration of all RNA samples was quantified by spectrophotometric absorbance at 260/280 nm using an Epoch Microplate Spectrophotometer (BioTek Instruments, Winooski, VT).

DNA repair qPCR array. ES2 and HeyA8 cells in culture were exposed to siRNA against endoglin in Lipofectamine 2000 as described above. After 48 hours, cells were collected and

mRNA extracted. Two replicates per cell line were performed. These four samples were then subjected to a quantitative PCR array consisting of 84 genes from DNA damage/repair pathways (plus additional housekeeping genes; the RT2 Profiler PCR Array Human DNA Damage Signaling Pathway, SA Biosciences Cat# PAHS-209Z, performed per manufacturer's instructions). Briefly, extracted RNA was converted to cDNA and amplified using the RT^2 FFPE PreAMP cDNA Synthesis Kit (SABiosciences, Frederick, MD). Quality of cDNA was confirmed with the Human RT^2 RNA QC PCR Array (SABiosciences). Gene expression was analyzed using the Human DNA Damage Signaling Pathway RT^2 Profiler PCR Array (SABiosciences), which profiles the expression of 84 genes involved in pluripotent cell maintenance and differentiation[14]. Functional gene groupings consist of the ATM/ATR signaling, nucleotide excision repair, base-excision repair, mismatch repair, double strand break repair, apoptosis, and cell cycle checkpoint regulators. PCR amplification was performed on an ABI Prism 7900HT sequence detection system and gene expression was calculated using the comparative C_T method[15].

Reverse transcription and quantitative PCR. Extracted RNA samples were diluted to 20 ng/μL using RNase-free water. cDNA was prepared using the High Capacity cDNA Reverse Transcription Kit (Applied Biosystems). The resulting cDNA samples were analyzed using quantitative PCR. Primer and probe sets for *ENG* (PPH01140F) *ATM* (PPH00325C), *BARD1* (PPH09451A), *DDIT3* (PPH00310A), *H2AFX* (PPH12636B), *NBN* (PPH00946C), *NTHL1* (PPH02720A), *PPP1R15A* (PPH02081E), *SIRT1* (PPH02188A), *ATP7B* (PPH06148A), and *RPLP0* (Hs99999902_m1, housekeeping gene) were obtained from SABiosciences and used according to manufacturer's instructions. PCR amplification was performed on an ABI Prism

7900HT sequence detection system and gene expression was calculated using the comparative C_T method.

Orthotopic Mouse Model. Female athymic nude mice (nu-nu) were obtained from the National Cancer Institute Frederick Cancer Research and Development Center (Frederick, MD). Mice were cared for in accordance with American Association for Accreditation of Laboratory Animal Care guidelines, the United States Health Services Commissioned Corps "Policy on Human Care and Use of Laboratory Animals," and University of Alabama at Birmingham Institutional Animal Care and Use Committee policies. ES2 tumors were established by intraperitoneal (IP) injection of $1x10^6$ cells suspended in 200μL of serum free RPMI media. Hey8MDR tumors were established in a similar way, using $5x10^5$ cells. To evaluate the effectiveness of endoglin-targeted therapy *in vivo,* siRNA was incorporated into chitosan nanoparticles as previously described.[16-17] Therapy was initiated 1 week after tumor cell injection. Mice were randomized to one of four treatments (n=10 per group): a) control siRNA alone (150 ug/kg twice weekly injected IV), b) control siRNA with IP carboplatin (160 mg), c) anti-endoglin siRNA (150 ug/kg twice weekly) alone, or d) anti-endoglin siRNA with carboplatin. All treatments were suspended in 100 μL 0.9% normal saline (NS). Mice were monitored for adverse effects, and all treatment groups sacrificed when control mice became uncomfortable with tumor burden. ES2 tumors behaved aggressively, and were harvested following 2 weeks of treatment. Hey8MDR tumors were harvested after 3 weeks of therapy. Mouse weight, ascites volume, tumor weight and distribution of tumor were recorded. Representative tumor samples were obtained from 5 mice in each treatment group, formalin-fixed, paraffin-embedded, and cut into 5 micron sections for evaluation of Proliferating Cell Nuclear Antigen (PCNA), Terminal deoxynucleotidyl transferase

mediated dUTP Nick End Labeling assay (TUNEL), γ H2AX (phosphorylation of Histone 2A protein) and 53BP1 (a mediator of the DNA damage checkpoint).

Tumor PCNA Immunohistochemistry and TUNEL. Sections were deparaffinized and re-hydrated, and antigen retrieval was performed with citrate buffer (pH 6.0) in pressure cooker for 5 minutes. Endogenous peroxidase activity was quenched with 3% hydrogen peroxide solution in methanol for 15 minutes. Sections were blocked with CytoQ immune diluent and block and probed with PCNA primary antibody (PCNA-PC10, Cell signaling Technology, 1:5000 dilution) at 4°C overnight. Sections were washed and incubated with the Mach 3 mouse HRP polymer system. After rinsing, the sections were incubated with DAB chromophoric solution (Scytek Labs, Utah, USA) for 5 min at room temperature, then counterstained with Gill's hematoxylin (Ricca chemicals). Four 40x microscopic fields were counted from each section, averaged over 5 mice in each treatment group, and expressed as a percentage of the total number of tumor cells. Apoptosis was determined by TUNEL assay with a colorimetric apoptotic cell detection kit (Promega), per manufacturer's instruction. As with PCNA IHC, 4 microscopic fields at 40x magnification were evaluated from each section. Stained cells were recorded as a percentage of the total number of tumor cells.

Tumor γH2AX and 53BP1 IHC. Formalin fixed tissues were heated at 60°C for 1hr and rehydrated according to standard protocol. Subsequently, the tissues were permeabilized in 0.5% Triton X-PBS for 10 min, blocked in 2% BSA-0.1% Triton-X-PBS for 1 hr, and incubated with primary antibodies (1:500 dilution, anti phospho H2AX Ser139, Millipore, catalog # MI-07-164; 1:500 dilution, anti-53BP1, Novus Biologicals, catalog # NB100-304). The secondary antibody

was anti-rabbit Alexa Fluor 488–conjugated antibody (1:2000 dilution; Invitrogen). DAPI (Invitrogen, catalog # D21490) was used for nuclear staining. The slides were subsequently mounted using mounting media (Aqua poly mount, Polysciences, Inc. catalog # 18606) and analyzed via fluorescence microscopy (Carl Zeiss, Thornwood, NY). Positive and negative controls were included on all experiments. A total of 500 cells were assessed. For foci quantification, cells with greater than 10 foci were counted as positive according to the standard procedure. Experiments were repeated in triplicate. Data show the mean and SEM.

Statistics. Analysis of normally distributed continuous variable was performed using a two-tailed Student's t-test. Those data with alternate distribution were examined using a nonparametric Mann-Whitney U test. A $p<0.05$ was considered statistically significant.

Results

Effects of endoglin downregulation on cell viability and platinum sensitivity. Endoglin is expressed by multiple ovarian cancer cell lines (Figure 1A), most prominently in HeyA8, HeyA8MDR, and ES2 cells. Weak expression was detected in the HIO-180, A2780ip2, A2780cp20, SKOV3ip1, SKOV3TRp2, and IGROV-AF1 cell lines. This was previously demonstrated at the mRNA level by quantitative PCR[11]. To confirm that expression was predominantly at the cell surface, consistent with its function as a co-receptor for TGFβ, we performed immunohistochemistry on the ES2 and HeyA8MDR cell lines. Surprisingly, the predominant staining was noted n the perinuclear cytoplasm (Figure 1B). This was confirmed by flow cytometry, where interestingly not only was membranous staining rare, but there was a very distinct separate population with 100-fold fluorescent intensity (rather than a global shift among

all cells), consistent with a separate small population of cells with strong endoglin surface expression (Figure 1C). This population represented 6.0% of HeyA8MDR and 5.4% of ES2 cells. On close examination of IHC on cultured cells, a minority of the cells could be seen to have strong membranous expression of CD105 (arrows, Figure 1B). A separate endoglin-positive population has previously been noted in renal cell carcinoma cells, which did exhibit stem-cell properties.[18] However, these data are conclusive that the majority of endoglin expression in ovarian cancer is cytoplasmic, suggesting a role other than just as a co-receptor for TGF-beta.

To determine whether siRNA-mediated downregulation of endoglin had significant effects on viability and chemosensitivity, two different siRNA constructs (ENG_A siRNA and ENG_B siRNA) were examined. Both effectively reduced endoglin expression at 48 hours at the mRNA (Figure 1D) and protein level[11]). Both were previously shown to reduce cell viability[11]. To determine the mechanism by which endoglin knockdown reduced viability, evaluation of apoptosis was performed by the TUNEL assay. Annexin V/PI co-fluorescent staining performed 48 hours following transfection indicated significantly fewer viable cells in those treated with anti-endoglin siRNA than those treated with control siRNA (47.2% vs. 65.1%, $p<0.05$). A sample flow cytometry plot and a graph of average over three experiments are shown in Figure 1D. Those treated with anti-endoglin siRNA had increased percentages of cells in both early apoptosis (21.5% vs. 17.9%, $p<0.05$) and late apoptosis (18.9% vs. 12.0%, $p<0.05$). Effects were more pronounced when combined with cisplatin. In order to determine whether Endoglin knockdown had an effect on viability in combination with chemotherapy, cells were exposed to siRNA, then re-plated after 24 hours, and incubated with increasing concentrations of cisplatin or paclitaxel. Because endoglin downregulation alone was associated with substantial cell death in the HeyA8MDR model, knockdown was performed with several dilutions of siRNA in an effort

to more clearly delineate effects on platinum sensitivity. In both ES2 (normal IC50 for cisplatin = 0.7μM) and HeyA8MDR (normal IC50 for cisplatin = 0.65μM) models, increased cisplatin chemosensitivity was noted (up to 4-fold and 2-fold reduction in IC50, respectively, Figure 1E). Similar experiments were performed with paclitaxel, which did not show an increased sensitization with endoglin downregulation (data not shown).

Downregulation of endoglin induces DNA damage *in vitro*. Because platinum toxicity is mediated primarily through induction of DNA damage, we evaluated whether the enhanced cisplatin sensitivity from endoglin knockdown was a result of increased DNA damage. DNA damaging agents can induce both single-stranded breaks (SSBs) and double stranded breaks (DSBs) which can lead to initiation of apoptotic pathways. DNA damage in the ES2 line was first assessed via an alkaline comet assay, which detects both SSB and DSB. As quantified in Figure 2A, increased DNA damage over 24 hours was observed with cisplatin, endoglin downregulation with siRNA, and the combination (although combination therapy was not significantly increased compared to either single-agent treatment). A representative section demonstrating common effects on nearly all cells is shown (Figure 2B). Because a long comet tail can be the result of either DNA damage without death or apoptosis-associated DNA release, the nucleus size was also quantified. A small nucleus would be associated with apoptosis, whereas a long comet tail associated with a normal (larger) nucleus would indicate just DNA damage. As shown in Figure 2C for cells treated for 24 hours, those cells with a long tail present predominantly still had a large nucleus. Because most toxic effects on viability noted previously were assessed at 48 hours or longer, this DNA damage may be a precursor to apoptosis

induction. But it does demonstrate that DNA damage is the inciting event, rather than a result of apoptosis triggered by other mechanisms.

To further characterize the specific nature of DNA damage, development of foci of activated γ-H2AX was performed (Figure 2D). ES2 cells were employed, due to the rapid toxicity and cell death noted with endoglin downregulation with HeyA8. Phosphorylation of the histone protein H2AX on serine 139 (γ-H2AX) occurs at sites flanking DNA DSBs. The phosphorylation of thousands of H2AX molecules forms a focus in the chromatin flanking the DSB site that can be detected *in situ*. A higher proportion of cells with persistent γ-H2AX foci was noted with endoglin downregulation, to an even greater extent than cisplatin alone. The combination of cisplatin and endoglin downregulation induced more DSB repair than either agent alone. Collectively, these data suggest that a primary mechanism of DNA damage after endoglin downregulation is through induction of double-strand breaks in DNA.

Endoglin-targeting DNA damage is through effects on multiple mediators of DNA repair. In order to determine the mechanism by which downregulation of endoglin induces DNA damage, we first subjected both ES2 and HeyA8MDR cells treated with control siRNA or endoglin-siRNA for 48 hours to a qPCR-based array of 84 genes participating in DNA damage and repair pathways. This exploratory analysis found multiple genes that were either downregulated or upregulated in response to decreased endoglin, some of which were only associated with changes in one cell line (Supplemental Table 1). Select genes were then chosen for confirmatory assessment with qPCR (Figure 3). Genes for these analyses were selected based on the degree to which they were altered, the associated p-value, and whether the change was noted in both cell lines. With endoglin downregulation, significant concurrent downregulation

was noted by qPCR in H2AFX (36-43%), BARD1 (47-71%), NBN (38-41%), NTHL1 (39-53%), and SIRT1 (34-49%). A significant induction of mRNA was noted in DDIT3 (1.9-2.6-fold) and PPP1R15A (1.27-1.74-fold). There was no single DNA repair pathway subclass that comprised all affected genes, but consistent with data from the γ-H2AX assay, most were participants in either the double stranded break repair (BARD1, H2AFX, NBN) or nucleotide excision repair (SIRT1, NTHL1).

The downregulation of BARD1 was particularly interesting. BARD1 is an oncogenic regulator of BRCA1, and downregulation would be expected to result in export of BRCA1 from the nucleus and impairment of DNA repair. Furthermore, BARD1 was noted to be significantly *upregulated* in chemoresistant tumor samples from patients, compared to their primary tumors.[11] BARD1 expression is prominent in ES2 and HeyA8MDR, which follows if it is under transcriptional regulation by endoglin. Therefore, we examined BARD1 induction in response to platinum treatment in a progressively platinum-resistant triad of cell lines derived from A2780: A2780ip2 (which generates IP tumors more consistently than the parental line but is chemosensitive), A2780cp20 (having a platinum IC50 of 20μM), and A2780cp55 (with an IC50 of 55μM). The A2780cp20 and cp55 lines are stably platinum-resistant, and not chronically maintained in platinum. BARD1 expression is minimal in the parental A2780ip2 line, but increases at baseline ("Untreated") with each degree of platinum resistance (Figure 3B). Additionally, when exposed to an IC50 concentration of carboplatin, BARD1 mRNA production is significant increased in both A2780ip2 and A2780cp20. Levels were unchanged with carboplatin exposure in A2780cp55, likely due to its high baseline expression. A significant reduction in BARD1 with endoglin downregulation and an induction of BARD1 in response to platinum exposure strongly implicate this gene and its control on BRCA1 as a major mechanism

through which endoglin downregulation may lead to DNA damage, apoptosis, and sensitivity to platinum.

In addition to enhanced DNA repair mechanisms, a major mechanism of platinum resistance is through increased export of platinum agents through copper transporters such as ATP7B.[19] Therefore we also examined the effects of endoglin downregulation on ATP7B by qPCR. SiRNA-mediated targeting of endoglin resulted in a significant downregulation of ATP7B (by 20-24%, $p<0.05$, Figure 3C). While significant, this was not to the same extent many DNA repair genes were induced or activated.

Evaluation of tumor growth with anti-endoglin treatment in an orthotopic murine model.

In order to determine if endoglin downregulation was an effective therapy *in vivo*, an orthotopic murine model was utilized using human specific anti-endoglin siRNA delivered within a chitosan nanoparticle. Chitosan (CH) is a natural nanoparticle that has been previously demonstrated to result in efficient delivery of siRNA to tumor after IV administration, with subsequent protein downregulation and gene-specific modulation.[16, 20-22] Because the siRNA delivered is specific to the human endoglin mRNA, any observed effect would be expected to be due to targeting the tumor cells, rather than the vasculature, which would require murine-specific siRNA. ES2 and HeyA8MDR cells were injected IP, and treatment was started 1 week later with a) control siRNA-CH alone, b) control siRNA-CH plus carboplatin, c) anti-endoglin siRNA-CH alone, or d) anti-endoglin siRNA-CH plus carboplatin. Carboplatin was used instead of cisplatin because of its preferable side-effect profile *in vivo*, which has led to its choice as standard of care in ovarian cancer patients. Tumors demonstrated reduced growth both with endoglin downregulation alone and in combination with platinum. In the ES2 model (Figure 4A), mice

treated with carboplatin had similar tumor burden to control (p=0.555), an expected result due to the highly platinum-resistant nature of the ES2 cell line, which is derived from a patient with clear cell carcinoma. Mice treated with anti-endoglin siRNA alone had a significantly reduced tumor weight, by 35.6% (p=0.014). Combined END-siRNA-CH with carboplatin was more effective that either agent alone, with a 57.7% reduction in tumor weight compared to control (p<0.001). Furthermore, combination therapy was more effective than siRNA-endoglin-CH alone, with an additional 34.3% reduction (p=0.033) In the HeyA8MDR model (Figure 4B), mice treated with carboplatin, endoglin-siRNA-CH, or combination therapy had significantly less tumor weight when compared to control (34% reduction p=0.027, 41.2% reduction p=0.002, and 61.2% reduction p<0.01, respectively). Those treated with carboplatin and control siRNA-CH had similar tumor burden reduction as those treated with endoglin-siRNA-CH (p=0.628). Combination therapy was again more effective than either single-agent carboplatin (additional 40.6% reduction, p=0.069), or endoglin-siRNA alone (34%, p=0.048). In the resected tumors, reduced expression of endoglin was confirmed with immunohistochemistry, in both groups of tumors treated with endoglin-siRNA-CH. Representative sections are pictured (Figure 4C). With both models, there was not a significant difference in mouse weight in any group. The distribution of tumor was also similar in all groups, suggesting there was not a significant effect on particular site of growth, adhesion, or migration.

Endoglin downregulation induces DNA damage and apoptosis *in vivo*. Our *in vitro* findings suggest a role of DNA damage and apoptosis following endoglin downregulation. To validate these findings *in vivo*, tumors from each treatment group described above were examined for proliferation, apoptosis, and induction of DNA damage. PCNA IHC was performed and revealed

no significant differences in percentage of PCNA positive cells, with approximately half of cells being positive in each treatment group (Figure 5A). A lack of effect on progression through the cell cycle and proliferation may explain why combination with taxanes was not synergistic with endoglin downregulation *in vitro*. TUNEL assay was performed to evaluate to detect differences in apoptosis between treatment groups. Control, carboplatin and anti-endoglin siRNA groups were not significantly different. However, the cohort receiving combination therapy had a significantly higher percent of apoptotic cells when compared to control ($p<.001$, Figure 5B). This increase, though statistically significant, is relatively small, which may be due to clearance of dead cells over the course of the 4-week experiment. To determine if DNA damage was still noted in the tumors collected at completion of therapy, fluorescent IHC was performed to evaluate for γ-H2AX as an indicator of *in vivo* DSB. A significantly higher amount of DNA damage was detected in both treatment groups receiving anti-endoglin treatment than either control or single-agent carboplatin treatment (Figure 5C). Additionally, 53BP1 is a mediator of DNA damage response and a tumor suppressor whose accumulation on damaged chromatin promotes DNA repair and enhances DNA damage response signaling. A significantly higher number of 53BP1-positive cells was noted in both cohorts that received anti-endoglin treatment when compared to either control or single-agent platinum (Figure 5D). These data are consistent with *in vitro* studies demonstrating that endoglin downregulation alone leads to DNA damage and apoptosis.

Discussion

Endoglin is overexpressed in solid tumor vasculature and is a reliable marker of angiogenesis.[5] Multiple anti-angiogenic therapies have been studied in ovarian cancer, and anti-

endoglin therapy has been proposed for several cancers in which increased endothelial endoglin expression has been noted.[23] However, to date, few studies address the expression of endoglin on tumor cells and its potential role in cancer progression. Building off our previous findings that Endoglin is increase in recurrent samples when compared to matched primary tumors[11], we have demonstrated that endoglin expression is highly expressed in many ovarian cancer cell lines, and that downregulation results in induction of cell death through induction of DNA damage and a synergistic killing effect with platinum agents both *in vitro* and *in vivo*. These novel findings demonstrate that therapeutics targeting endoglin may affect both the vasculature and malignant cells within the tumor microenvironment.

The primary canonical role of endoglin is as a co-receptor for TGF-beta.[24-26] As such, its expression on endothelial cells is primarily on the cell membrane.[27] However, we interestingly found endoglin expression in ovarian cancer cells was predominantly cytoplasmic, and clustered together in the perinuclear region of the cell. This would suggest that endoglin either has a separate TGF-beta-independent function dependent on nuclear proximity, or trafficking to the cell membrane is an important component of its regulation. Only a small (5-6%), but well-defined population had surface expression. This distinct population would be consistent with a cancer stem cell-like population, as has been previously described in endoglin-positive renal cell carcinoma[18]. Endoglin-positive meningioma cells have similar increased tumorigenicity and capacity to differentiate into adipocytes and osteocytes.[28]

Henriksen et al. evaluated endoglin expression in primary ovarian cancer cells and found that high tumor cell endoglin staining correlated with short overall survival.[29] Another group has shown that cells from cultured ascites that progressed towards a mesenchymal phenotype were high in endoglin.[30] We identified endoglin as a potential target for therapeutics through a screen

of stem cell pathways overexpressed in recurrent ovarian cancer samples. Among members of the TGF-β, Notch, Wnt, and Hedgehog pathways, endoglin was most significantly and consistently overexpressed in recurrent ovarian cancer samples when compared to their matched primaries, suggesting a role in chemoresistance.[11] We specifically examined stem cell pathways to address the question of whether the cancer stem cell population may be responsible for surviving initial chemotherapy. Endoglin has previously been implicated in stem cell biology, having originally been described on hematopoietic progenitor cells[31], and later demonstrated to identify precursor cells capable of tissue-specific differentiation[32-33].

It makes sense that cells with prolonged survival, such as stem/progenitor cells, would reply on pathways to mediate DNA damage. Because of the association noted with increased endoglin expression in platinum (and taxane)-resistant recurrent ovarian cancers,[11] and the contribution of enhanced DNA repair for platinum resistance,[19] we further examined the contribution of endoglin to DNA repair. We have found a previously unknown contribution of endoglin to expression of numerous DNA repair genes. These encompass several subtypes of DNA repair, predominantly double stranded break repair (BARD1, H2AFX, NBN), but also nucleotide excision repair (SIRT1, NTHL1), and cell cycle arrest (DDIT3, PPP1R15A), which may be a reactionary process in order to accomplish DNA repair. Recently BARD1 has been implicated in ovarian cancer pathogenesis for its interaction with BRCA1 and 2. BARD1 and BRCA1 interact with each other through their amino terminal RING finger domains. This interaction is required for BRCA1 stability, as well as for nuclear localization. The BRCA1-BARD1 complex serves as an E3 ubiquitin ligase, which has been noted to have critical activity in both the cell cycle check point through H2AX, NPM and γ-tubulin and in DNA fragmentation.[34-35] Additionally, patients with mutations of both BARD1 and BRCA2 have a

substantially increased risk for development of both breast and ovarian cancer. While BARD 1 has been found to interact and co-localize with BRCA1 at the spindle poles in early mitosis, it also interacts with BRCA2 at late mitosis in the midbody. Therefore BARD1 has been found to sequentially link the function of these[36] two proteins. In our analysis, BARD1 expression was reduced by 50-75% and H2AX expression was reduced 35-50% following endoglin knockdown. endoglin-mediated downregulation of BARD1 and its subsequent effects on BRCA1 and 2 and H2AX may therefore explain why we found substantial decreased cell viability, DNA damage and increased apoptosis.[34]

Silent Information Regulator Type 1 (SIRT1) is a nicotinamide adenine dinucleotide-dependent class III histone deacetylase (HDAC). SIRT1 has is associated with longevity and has been found to act primarily by inhibiting cellular senescence. SIRT1 is up-regulated in tumor cell lines and human tumors, and may be involved in tumorigenesis.[36] It has also been found to be over-expressed in chemoresistant tumors of cancer patients. SIRT1 inhibition leads to decrease in MDR1 expression and increase in drug sensitivity in ovarian cancer cell lines.[37] Our research suggests that Endogin knockdown was associated with a 30-50% reduction in SIRT1. This inhibition may help account for the increased platinum sensitivity we found with endoglin downregulation.

In regards to therapeutic development in cancer patients, delivery of siRNA constructs has the potential to offer long duration of target inhibition as well as reduced toxicity compared other approaches.[16, 20, 38-44] However, development of a delivery modality for siRNA constructs remains the rate-limiting step in translational research. Early delivery modalities included delivery of “naked” siRNA. Later attempts included high-pressure siRNA injections and intratumoral injections, neither of which has demonstrated substantial success. The development

of chitosan encapsulation and nanoliposomes to deliver siRNA has become widely accepted in translational studies and is and promising as a therapeutic modality as modifications to enhance in vivo delivery progress.[22] SiRNA mediated therapeutics are being used in ongoing trials with patients with macular degeneration, AIDS, malignant melanoma, acute renal failure, hepatitis B, and now in cancer patients, where phase I trials are in development. One particular advantage of siRNA-based therapeutics over conventional treatment modalities would apply to endoglin-based targeting. If indeed the cytoplasmic portion of endoglin is important to chemoresistance, downregulation of production at the mRNA level may be more effective than antibody-based targeting currently aimed at inhibiting angiogenesis.[45-46]

Because of the rarity of endoglin expression in normal tissues, anti-endoglin therapy has the potential to offer tumor-directed therapy in addition to anti-angiogenic therapy. Anti-endoglin therapy is being explored as a therapeutic in several cancers as an anti-angiogenic agent. In ovarian cancer, endoglin-targeted therapies may offer the additional advantage of targeting tumor cells overexpressing endoglin, including platinum-resistant tumors. Its effects on BRCA1 and 2 and H2AX through BARD1 downregulation, and its association with SIRT1 downregulation contribute to DNA damage repair and enhancement of platinum sensitivity. Our data strongly suggest that endoglin-targeted therapy has the potential to improve platinum sensitivity through induction of DNA damage and should be actively pursued as a potential therapy in the treatment of ovarian cancer.

REFERENCES

1. Siegel R, Naishadham D, Jemal A. Cancer statistics, 2012. CA: A Cancer Journal for Clinicians. 2012;62(1):10-29.
2. Perez-Gomez E, Del Castillo G, Juan Francisco S, Lopez-Novoa JM, Bernabeu C, Quintanilla M. The role of the TGF-beta coreceptor endoglin in cancer. ScientificWorldJournal. 2010;10:2367-84.
3. Marioni G, Staffieri A, Manzato E, Ralli G, Lionello M, Giacomelli L, et al. A higher CD105-assessed microvessel density and worse prognosis in elderly patients with laryngeal carcinoma. Arch Otolaryngol Head Neck Surg. 2011 Feb;137(2):175-80.
4. Barbara NP, Wrana JL, Letarte M. Endoglin is an accessory protein that interacts with the signaling receptor complex of multiple members of the transforming growth factor-beta superfamily. J Biol Chem. 1999 Jan 8;274(2):584-94.
5. Dallas NA, Samuel S, Xia L, Fan F, Gray MJ, Lim SJ, et al. Endoglin (CD105): a marker of tumor vasculature and potential target for therapy. Clin Cancer Res. 2008 Apr 1;14(7):1931-7.
6. Fonsatti E, Altomonte M, Arslan P, Maio M. Endoglin (CD105): a target for anti-angiogenetic cancer therapy. Curr Drug Targets. 2003 May;4(4):291-6.
7. Gromova P, Rubin BP, Thys A, Cullus P, Erneux C, Vanderwinden JM. ENDOGLIN/CD105 is expressed in KIT positive cells in the gut and in gastrointestinal stromal tumors. J Cell Mol Med. 2011 Mar 24.
8. Davidson B, Stavnes HT, Forsund M, Berner A, Staff AC. CD105 (Endoglin) expression in breast carcinoma effusions is a marker of poor survival. Breast. 2010 Dec;19(6):493-8.
9. Bock AJ, Tuft Stavnes H, Kaern J, Berner A, Staff AC, Davidson B. Endoglin (CD105) expression in ovarian serous carcinoma effusions is related to chemotherapy status. Tumour Biol. 2011 Feb 26.
10. Taskiran C, Erdem O, Onan A, Arisoy O, Acar A, Vural C, et al. The prognostic value of endoglin (CD105) expression in ovarian carcinoma. Int J Gynecol Cancer. 2006 Sep-Oct;16(5):1789-93.
11. Steg AD, Bevis KS, Katre AA, Ziebarth A, Dobbin ZC, Alvarez RD, et al. Stem cell pathways contribute to clinical chemoresistance in ovarian cancer. Clin Cancer Res. 2012 Feb 1;18(3):869-81.
12. Wang H, Yang ES, Jiang J, Nowsheen S, Xia F. DNA damage-induced cytotoxicity is dissociated from BRCA1's DNA repair function but is dependent on its cytosolic accumulation. Cancer Res. 2010 Aug 1;70(15):6258-67.
13. Yang ES, Wang H, Jiang G, Nowsheen S, Fu A, Hallahan DE, et al. Lithium-mediated protection of hippocampal cells involves enhancement of DNA-PK-dependent repair in mice. J Clin Invest. 2009 May;119(5):1124-35.
14. SABiosciences. DNA Damage Signaling Pathway PCR Array. 2011 [cited; Available from: http://www.sabiosciences.com/rt_pcr_product/HTML/PAHS-029Z.html
15. Steg A, Wang W, Blanquicett C, Grunda JM, Eltoum IA, Wang K, et al. Multiple gene expression analyses in paraffin-embedded tissues by TaqMan low-density array: Application to hedgehog and Wnt pathway analysis in ovarian endometrioid adenocarcinoma. J Mol Diagn. 2006 Feb;8(1):76-83.

16. Han HD, Mangala LS, Lee JW, Shahzad MM, Kim HS, Shen D, et al. Targeted gene silencing using RGD-labeled chitosan nanoparticles. Clin Cancer Res. 2010 Aug 1;16(15):3910-22.
17. Lu C, Han HD, Mangala LS, Ali-Fehmi R, Newton CS, Ozbun L, et al. Regulation of tumor angiogenesis by EZH2. Cancer Cell. 2010 Aug 9;18(2):185-97.
18. Bussolati B, Bruno S, Grange C, Ferrando U, Camussi G. Identification of a tumor-initiating stem cell population in human renal carcinomas. FASEB J. 2008 Oct;22(10):3696-705.
19. Shahzad MM, Lopez-Berestein G, Sood AK. Novel strategies for reversing platinum resistance. Drug Resist Updat. 2009 Dec;12(6):148-52.
20. Steg AD, Katre AA, Goodman BW, Han HD, Nick AM, Stone RL, et al. Targeting the Notch Ligand Jagged1 in Both Tumor Cells and Stroma in Ovarian Cancer. Clin Cancer Res. 2011 Jul 13.
21. Nick AM, Stone RL, Armaiz-Pena G, Ozpolat B, Tekedereli I, Graybill WS, et al. Silencing of p130cas in ovarian carcinoma: a novel mechanism for tumor cell death. J Natl Cancer Inst. 2011 Nov 2;103(21):1596-612.
22. Pecot CV, Calin GA, Coleman RL, Lopez-Berestein G, Sood AK. RNA interference in the clinic: challenges and future directions. Nat Rev Cancer. 2011 Jan;11(1):59-67.
23. ten Dijke P, Goumans MJ, Pardali E. Endoglin in angiogenesis and vascular diseases. Angiogenesis. 2008;11(1):79-89.
24. Koleva RI, Conley BA, Romero D, Riley KS, Marto JA, Lux A, et al. Endoglin structure and function: Determinants of endoglin phosphorylation by transforming growth factor-beta receptors. J Biol Chem. 2006 Sep 1;281(35):25110-23.
25. Rodriguez-Barbero A, Obreo J, Alvarez-Munoz P, Pandiella A, Bernabeu C, Lopez-Novoa JM. Endoglin modulation of TGF-beta1-induced collagen synthesis is dependent on ERK1/2 MAPK activation. Cell Physiol Biochem. 2006;18(1-3):135-42.
26. She X, Matsuno F, Harada N, Tsai H, Seon BK. Synergy between anti-endoglin (CD105) monoclonal antibodies and TGF-beta in suppression of growth of human endothelial cells. Int J Cancer. 2004 Jan 10;108(2):251-7.
27. Yoshitomi H, Kobayashi S, Ohtsuka M, Kimura F, Shimizu H, Yoshidome H, et al. Specific expression of endoglin (CD105) in endothelial cells of intratumoral blood and lymphatic vessels in pancreatic cancer. Pancreas. 2008 Oct;37(3):275-81.
28. Hu D, Wang X, Mao Y, Zhou L. Identification of CD105 (endoglin)-positive stem-like cells in rhabdoid meningioma. J Neurooncol. 2012 Feb;106(3):505-17.
29. Henriksen R, Gobl A, Wilander E, Oberg K, Miyazono K, Funa K. Expression and prognostic significance of TGF-beta isotypes, latent TGF-beta 1 binding protein, TGF-beta type I and type II receptors, and endoglin in normal ovary and ovarian neoplasms. Lab Invest. 1995 Aug;73(2):213-20.
30. Ho CM, Chang SF, Hsiao CC, Chien TY, Shih DT. Isolation and characterization of stromal progenitor cells from ascites of patients with epithelial ovarian adenocarcinoma. J Biomed Sci. 2012;19:23.
31. Pierelli L, Bonanno G, Rutella S, Marone M, Scambia G, Leone G. CD105 (endoglin) expression on hematopoietic stem/progenitor cells. Leuk Lymphoma. 2001 Nov-Dec;42(6):1195-206.
32. Aslan H, Zilberman Y, Kandel L, Liebergall M, Oskouian RJ, Gazit D, et al. Osteogenic differentiation of noncultured immunoisolated bone marrow-derived CD105+ cells. Stem Cells. 2006 Jul;24(7):1728-37.

33. Jiang T, Liu W, Lv X, Sun H, Zhang L, Liu Y, et al. Potent in vitro chondrogenesis of CD105 enriched human adipose-derived stem cells. Biomaterials. 2010 May;31(13):3564-71.
34. Irminger-Finger I. BARD1, a possible biomarker for breast and ovarian cancer. Gynecol Oncol. 2010 May;117(2):211-5.
35. Irminger-Finger I, Busquets S, Calabrio F, Lopez-Soriano FJ, Argiles JM. BARD1 content correlates with increased DNA fragmentation associated with muscle wasting in tumour-bearing rats. Oncol Rep. 2006 Jun;15(6):1425-8.
36. Jang KY, Kim KS, Hwang SH, Kwon KS, Kim KR, Park HS, et al. Expression and prognostic significance of SIRT1 in ovarian epithelial tumours. Pathology. 2009;41(4):366-71.
37. Chu F, Chou PM, Zheng X, Mirkin BL, Rebbaa A. Control of multidrug resistance gene mdr1 and cancer resistance to chemotherapy by the longevity gene sirt1. Cancer Res. 2005 Nov 15;65(22):10183-7.
38. Salva E, Kabasakal L, Eren F, Ozkan N, Cakalagaoglu F, Akbuga J. Local delivery of chitosan/VEGF siRNA nanoplexes reduces angiogenesis and growth of breast cancer in vivo. Nucleic Acid Ther. 2012 Feb;22(1):40-8.
39. Han HD, Mora EM, Roh JW, Nishimura M, Lee SJ, Stone RL, et al. Chitosan hydrogel for localized gene silencing. Cancer Biol Ther. 2011 May 1;11(9):839-45.
40. Rudzinski WE, Aminabhavi TM. Chitosan as a carrier for targeted delivery of small interfering RNA. Int J Pharm. 2010 Oct 31;399(1-2):1-11.
41. Mao S, Sun W, Kissel T. Chitosan-based formulations for delivery of DNA and siRNA. Adv Drug Deliv Rev. 2010 Jan 31;62(1):12-27.
42. Feng S, Agoulnik IU, Truong A, Li Z, Creighton CJ, Kaftanovskaya EM, et al. Suppression of relaxin receptor RXFP1 decreases prostate cancer growth and metastasis. Endocr Relat Cancer. 2010;17(4):1021-33.
43. Dass CR, Choong PF. The use of chitosan formulations in cancer therapy. J Microencapsul. 2008 Jun;25(4):275-9.
44. Howard KA, Rahbek UL, Liu X, Damgaard CK, Glud SZ, Andersen MO, et al. RNA interference in vitro and in vivo using a novel chitosan/siRNA nanoparticle system. Mol Ther. 2006 Oct;14(4):476-84.
45. Rosen LS, Hurwitz HI, Wong MK, Goldman J, Mendelson DS, Figg WD, et al. A Phase I First-in-Human Study of TRC105 (Anti-Endoglin Antibody) in Patients with Advanced Cancer. Clin Cancer Res. 2012 Sep 1;18(17):4820-9.
46. Tsujie M, Tsujie T, Toi H, Uneda S, Shiozaki K, Tsai H, et al. Anti-tumor activity of an anti-endoglin monoclonal antibody is enhanced in immunocompetent mice. Int J Cancer. 2008 May 15;122(10):2266-73.

FIGURE LEGENDS

FIGURE 1. A) Endoglin expression in multiple ovarian cancer cell lines, as measured by Western blot. B) As assessed by IHC, endoglin expression is predominantly cytoplasmic, though some cells with strong membranous staining are noted (arrows). C) A small but distinct endoglin-positive population is seen by flow cytometry. D) Endoglin was effectively downregulated with siRNA. By TUNEL assay, Annexin V/PI co-fluorescence demonstrate a decrease in viable cells, and an increase in both early and late apoptosis, both alone and in combination with cisplatin. E) Cells treated with increasing doses of cisplatin after endoglin downregulation were also assessed by MTT, with the OD570 reflecting the absorbance produced by viable cells. Endoglin downregulation resulted in a significant reduction in cell viability, and increased cisplatin chemosensitivity about 4-fold in ES2 model and 2-fold in HeyA8MDR. Lines denoting the calculated IC50 for control and endoglin-siRNA treatment are shown (grey lines).

FIGURE 2. ES2 cells were evaluated for DNA damage after endoglin targeting. SiRNA-mediated endoglin downregulation induces significant persistent DNA damage, as indicated by alkaline comet assay mean tail moment (A), and visually at 24 hours (B, Original magnification, ×100). This is not a result of immediate apoptosis, as demonstrated by a predominance of large nuclei despite a prominent comet tail (C). Downregulation also induces activation of γ-H2AX foci, a specific measure of double-stranded DNA damage (D). The combination of endoglin downregulation and cisplatin on induction of γ-H2AX foci was greater than either agent alone. Error bars represent SEM.

FIGURE 3. A) ES2 and HeyA8MDR cells were exposed to endoglin-targeting siRNA or control siRNA, mRNA extracted 48 hours later, and subjected to quantitative PCR for selected genes. Each collection was performed in triplicate, and the mean change over housekeeping gene presented. Significant decreases were noted in H2AFX, BARD1, NBN, NTHL1, and SIRT1. Induction of DDIT3 and PPP1R15A was also significant. B) BARD1 mRNA was assessed by qPCR in a triad of progressively platinum-resistant A780 cell lines, and noted to be significantly increased in A2780cp55 at baseline, and in A2780ip2 and A2780cp20 with exposure to carboplatin. C) The copper transporter ATP7B was also modestly, but significantly, reduced with endoglin downregulation.

FIGURE 4. An orthotopic murine model using ES2 and HeyA8MDR cell lines was employed to evaluate treatment with control siRNA-CH alone, control siRNA-CH with carboplatin, anti-endoglin siRNA-CH alone, or anti-endoglin siRNA-CH plus carboplatin. A) In the ES2 model, carboplatin was ineffective, as expected given the platinum-resistant nature of the ES2 cell line. Mice treated with anti-endoglin siRNA-CH alone and combined with carboplatin demonstrated less tumor burden when compared to control or carboplatin alone. Those treated with both anti-endoglin siRNA-CH and carboplatin also demonstrated reduced tumor burden when compared to those endoglin-siRNA-CH alone ($p=0.03$). B) In the HeyA8MDR model, tumors were smaller in mice treated with carboplatin or anti-endoglin siRNA-CH alone, and again combination therapy was more effective than either agent alone ($p<0.05$). C) By qualitative assessment with IHC, endoglin expression was reduced in the tumors treated with endoglin-siRNA-CH therapy.

FIGURE 5. Tumors from each treatment group in our orthotopic mouse model were collected and analyzed by PCNA immunohistochemistry, TUNEL assay, γ-H2AX IHC and 53BP1 IHC. A) There were no significant differences in PCNA IHC, with approximately half of cells being positive. B) There was a significant increase in apoptosis in the cohort receiving combination therapy when compared to control as demonstrated by TUNEL assay. C) Fluorescent IHC was performed to evaluate for γ-H2AX as an indicator of DNA damage. There was a significantly higher amount of DNA damage in both treatment groups receiving anti-endoglin treatment when compared to control or single-agent carboplatin. D) Lastly, 53BP1 is a key protein in the DNA damage checkpoint that was evaluated by IHC. A significantly higher amount of 53BP1 was noted in both cohorts that received anti-endoglin treatment when compared to either control or single-agent carboplatin.

Figure 1.

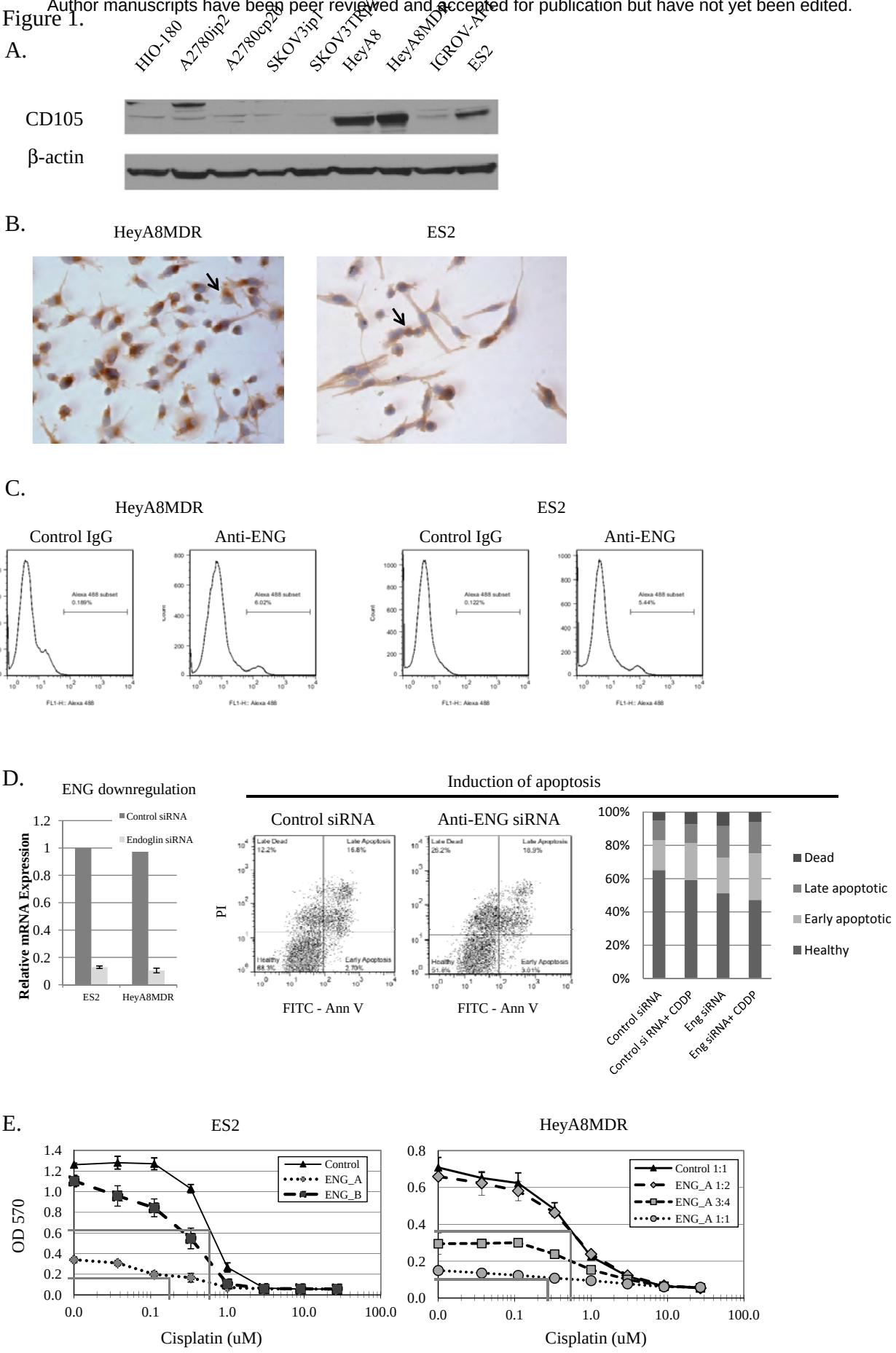

Figure 2.

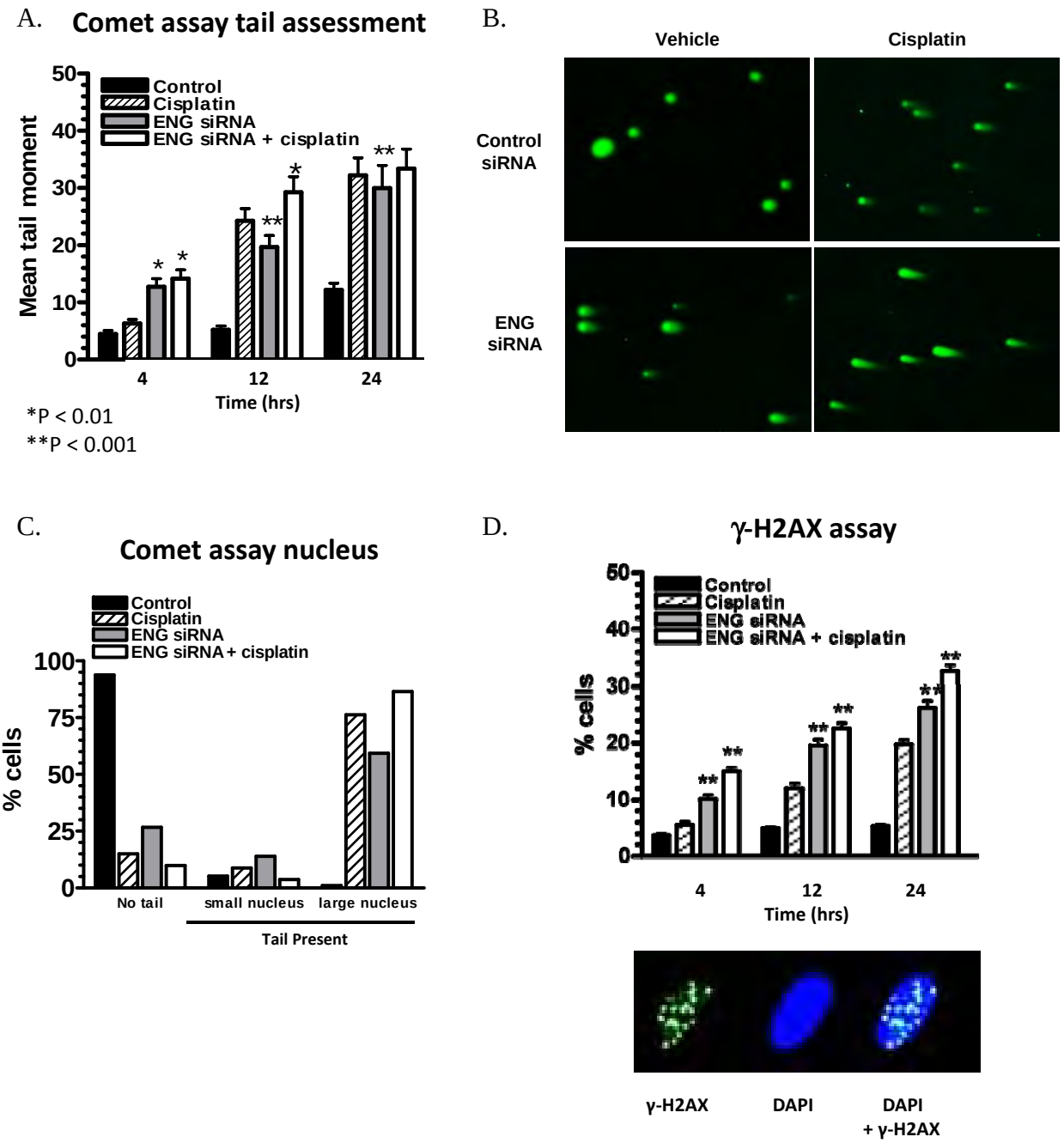

Figure 3.

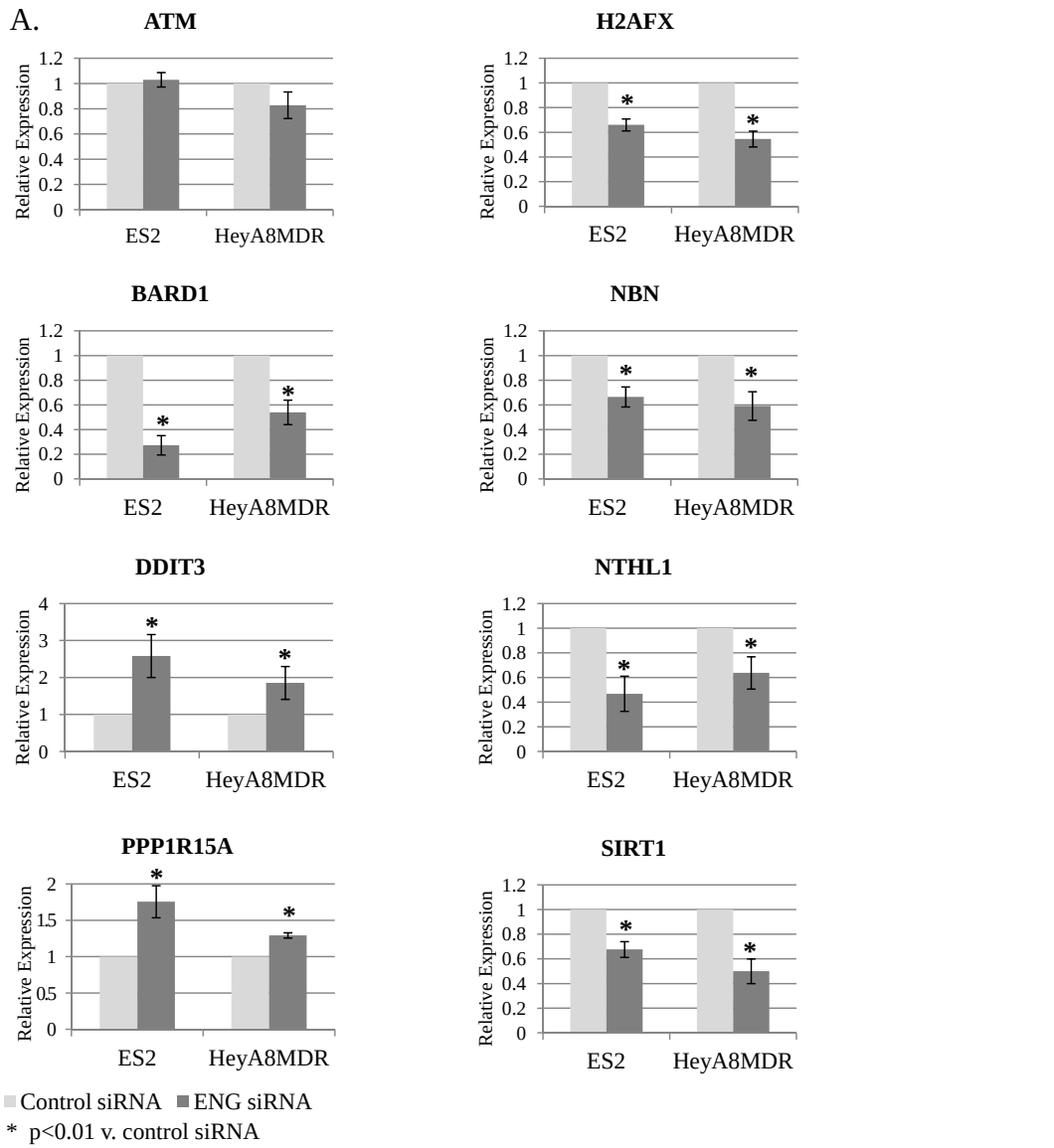

Author Manuscript Published OnlineFirst on November 12, 2012; DOI:10.1158/1078-0432.CCR-12-1045
Author manuscripts have been peer reviewed and accepted for publication but have not yet been edited.

Figure 4.

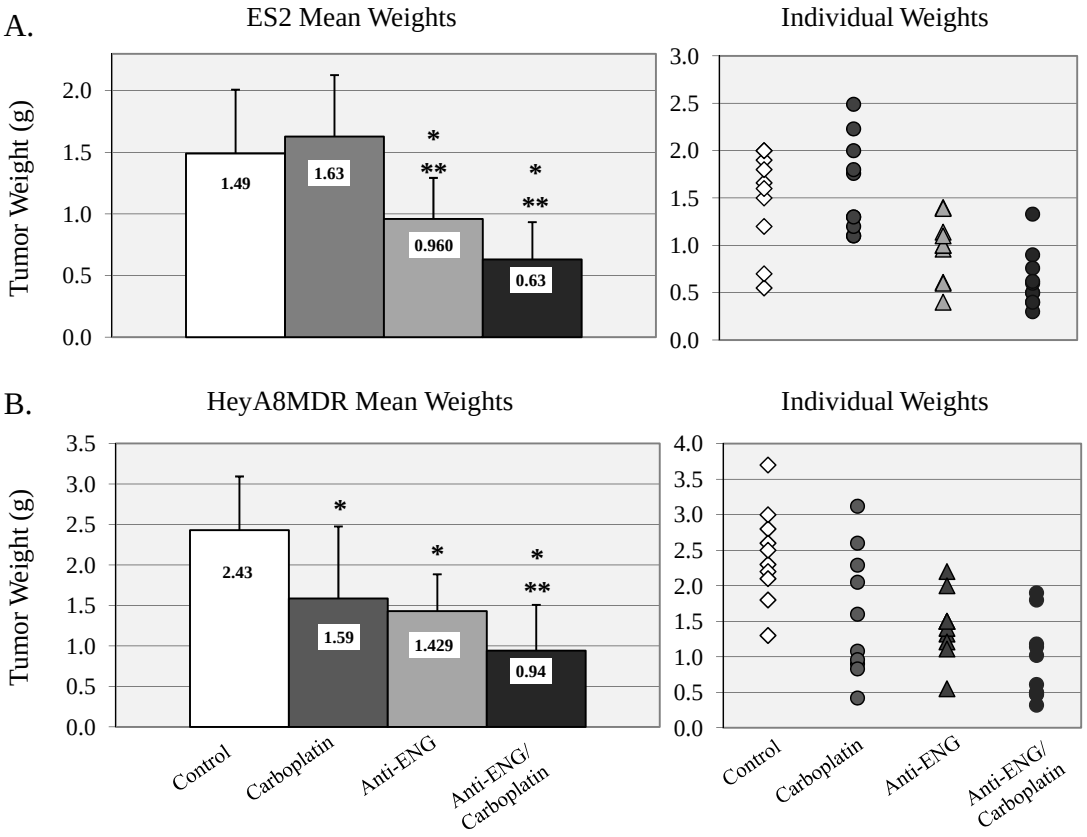

* - p<0.05 v. control
** - p< 0.05 v. carboplatin

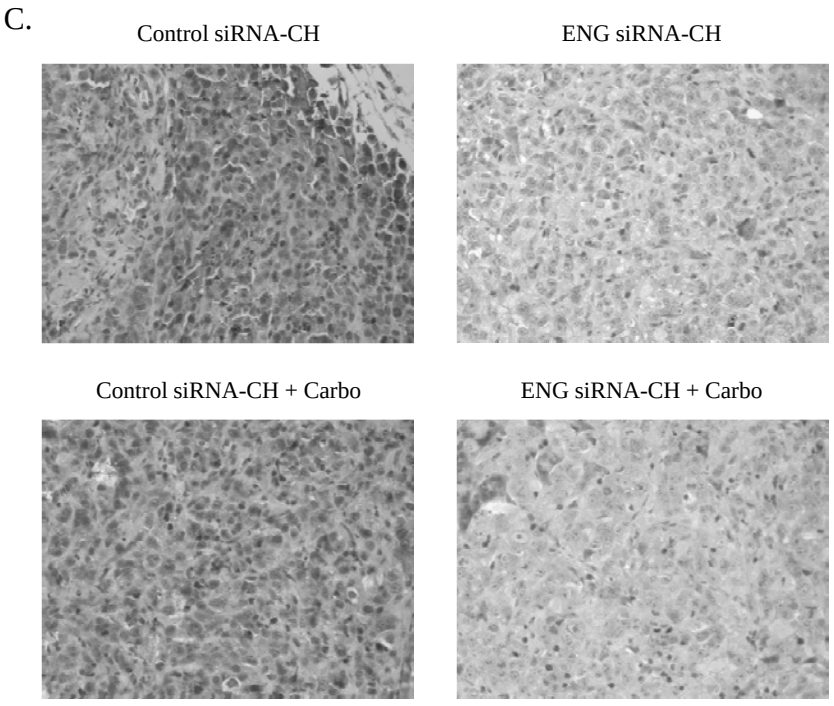

Figure 5.

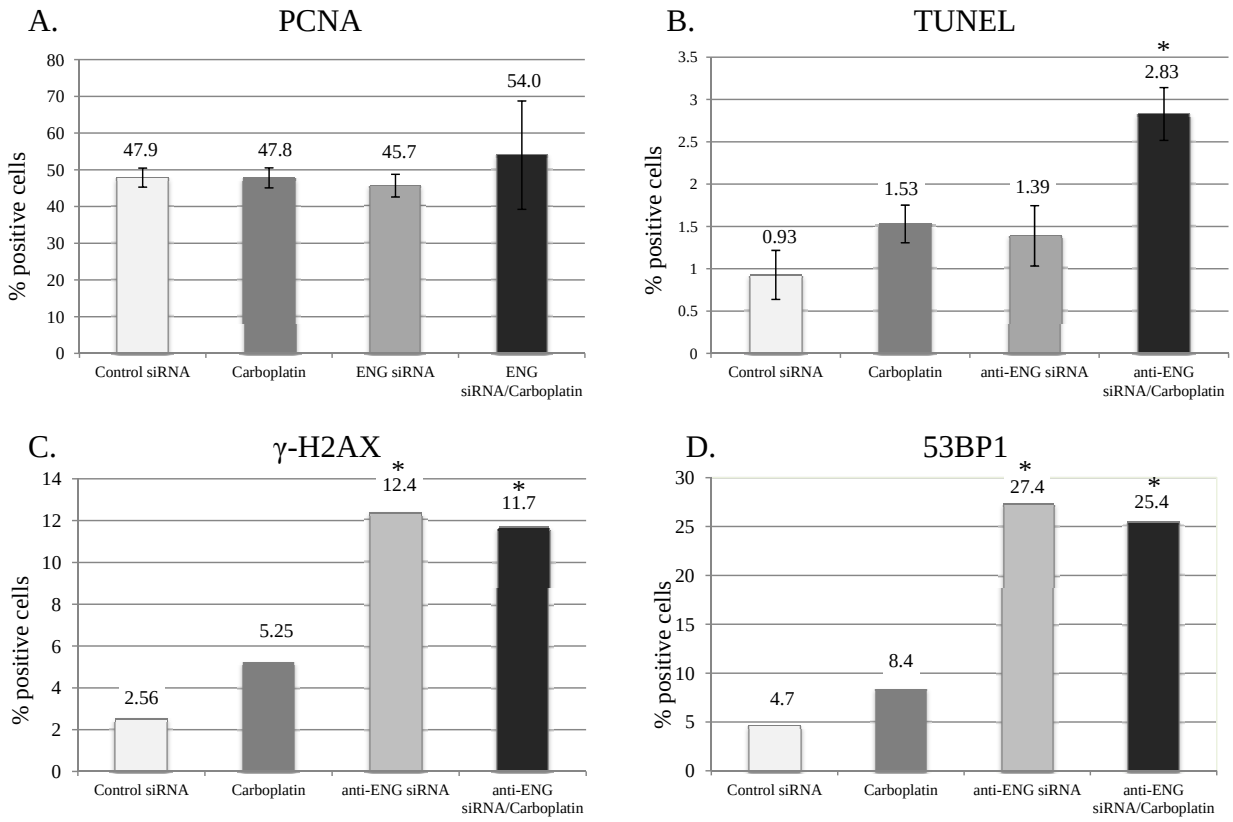

* $P < 0.01$ compared to control

Isolation and Characterization of Potential Cancer Stem Cells from Solid Human Tumors—Potential Applications

Zachary C. Dobbin[1] and Charles N. Landen[1]

[1]Department of Obstetrics and Gynecology, Division of Gynecologic Oncology, University of Alabama at Birmingham, Birmingham, Alabama

ABSTRACT

Cancer stem cells (CSCs) are a subpopulation of cells within a heterogeneous tumor that have enhanced biologic properties, e.g., increased capacity for self-renewal, increased tumorigenicity, enhanced differentiation capacity, and resistance to chemo- and radiotherapies. This unit describes protocols to isolate and characterize potential cancer stem cells from a solid tumor. These involve creating a single-cell suspension from tumor tissue, tagging the cell subpopulations of interest, and sorting them into different populations. The sorted subpopulations can be evaluated for their ability to meet the functional requirements of a CSC, which primarily include increased tumorigenicity in an in vivo xenograft assay. Use of the protocols described in this unit makes it possible to study populations of cells that may have properties of CSCs. *Curr. Protoc. Pharmacol*. 63:14.28.1-14.28.19. © 2013 by John Wiley & Sons, Inc.

Keywords: cancer stem cells • xenograft assay • cell separation and sorting

INTRODUCTION

Cancer stem cells (CSCs) are defined as a specialized subpopulation of cells within a heterogeneous mixture of cancer cells that have enhanced pro-malignant properties. These properties, in various experimental models, include increased tumorigenicity, greater differentiation capacity, and enhanced resistance to radiation and chemotherapy. These cells are also characterized by aggressive migration, invasion, and metastasis, as well as unlimited replicative potential. An important step in identifying these properties is isolation of this cell subpopulation and separation from the other tumor cells so that biologic endpoints can be examined independently. There are two general approaches to distinguishing potential CSCs: (1) by expression of a particular protein of interest, such as CD133, and (2) by functionality. Functional separation entails exposing all the cells in a heterogeneous population to a particular stress, such as chemotherapy or serum-free medium, thereby allowing for differential responses in the various cells to select out the desired population (i.e., chemoresistant cells or tumorspheres, respectively). The most common approach employs one of several methods to separate out a cell population of interest and to test it independently for the stem cell–like phenotype. Described in this unit are protocols to isolate and characterize potential cancer stem cells from primary or xenograft tumor samples, as well as some methods for assessing the properties of this population. In general, the cells are isolated in four steps. For each step there are various approaches used to complete this cell isolation. The first step is the creation of a single-cell suspension of cancer cells; the second is exposure of all cells to a tag that will differentially label those of interest. The third step involves separating the cell subpopulations by flow cytometry or magnetic bead separation. In the final step, the sorted cell populations are interrogated individually for their ability to meet the functional requirements of CSC. These include increased tumorigenicity in an in vivo xenograft

Current Protocols in Pharmacology 14.28.1-14.28.19, December 2013
Published online December 2013 in Wiley Online Library (wileyonlinelibrary.com).
DOI: 10.1002/0471141755.ph1428s63

assay, and demonstration of an increased capacity to give rise to both CSC and non-CSC populations, reproducing the heterogeneity of the original tumor sample.

Like normal stem cells, cancer stem cells are able to undergo self-renewal and to differentiate into any cell found in the heterogeneous tumor. They also have an increased proliferative ability that drives malignant formation (Jordan et al., 2006). The designation CSC is used for consistency in this unit, although the descriptors employed for these cells vary in the literature. Often subpopulations are defined by the functional assay used in their evaluation, such as tumor-initiating cells (TIC) or treatment-resistant cells (TRC). If some properties of a cell subpopulation are indicative of stem cells, but in vivo tumorigenicity is not examined, the cells may be described as cancer stem-like cells (CSLC). Regardless of terminology, this methods detailed in this unit will allow separation of cells for additional study as needed for the experimental question being addressed. There is no specific marker that is universally accepted as a CSC marker. Even for individual tumor types, a certain population may be described as having stem cell properties, although it cannot be concluded that it is the only, or the most reliable, cancer stem cell population in that tissue. Markers often used to define CSC populations include surface expression of CD133 or CD44, and the activity of the ALDH1A1 enzyme (as determined by the ALDEFLUOR assay; STEMCELL Technologies) or the "side population" (SP; see Basic Protocol 3), although many other markers have been used as well (i.e., My88, endoglin, CD24 negativity, and Oct4). When isolating these populations by cell surface marker expression, conclusions are by necessity limited to the specific population being studied. For example, conclusions made regarding a CD133-positive population could, but may not, also apply to other populations within that heterogeneous mass of cells. It is anticipated that in the future more comprehensive methods will be developed and employed that allow for the simultaneous study of multiple cell populations to identify those that are the most "stem-like". Use of the protocols described in the present unit will allow for the isolation and identification of a putative cancer stem cell population that displays many of the characteristics thought to be required of CSC designation and that can be utilized for particular types of studies, such as susceptibility to CSC-specific therapeutics.

The first protocol described is used for obtaining a single-cell suspension of the cancer cells needed for a particular study. This is accomplished using mechanical dissociation, chemical dissociation, or a combination of both (Basic Protocol 1). Two methods of sorting these cell populations are then presented. The first utilizes antibodies to identify CSCs by surface marker expression, after which the cells are separated by flow cytometry (Basic Protocol 2) or magnetic beads (Alternate Protocol 2). The second option isolates cells on the basis of the functional activity of a protein. This includes isolation of the "side population," which is defined as those cells that display an increase in the efflux of Hoechst 33342 dye from the nucleus, which is mediated primarily by the ABCG2 membrane pump (Basic Protocol 3). A similar approach utilizes the ALDEFLUOR assay, which isolates cells with active ALDH1A1 enzyme. As it is performed per the manufacturer's instructions (STEMCELL Technologies), it is not described in detail in this unit. Moreover, protocols are described for assessing the two functional properties generally required to define cancer stem cells. The first of these is an increased tumorigenicity in mice as assessed with a xenograft formation assay (Basic Protocol 4). The second is demonstration that the CSCs have enhanced differentiation capacity. This is accomplished by examining tumor formation in both CSC-positive and CSC-negative populations (Basic Protocol 5).

NOTE: The following procedures must be performed in a Class II biological hazard flow hood or a laminar flow hood.

NOTE: As all solutions and equipment that come in contact with live cells must be sterile, proper aseptic techniques must be employed at all times.

NOTE: All protocols involving patient tissues require IRB approval and donor consent. Protocols employing live animals must first be reviewed and approved by an Institutional Animal Care and Use Committee (IACUC) or must conform to government regulations regarding the care and use of laboratory animals.

MECHANICAL DISSOCIATION OF PRIMARY TUMOR OR MOUSE XENOGRAFTS

BASIC PROTOCOL 1

CSCs constitute a small subset of the cancer cells in a heterogeneous tumor. For this reason, a tumor sample must be dissociated into a single-cell suspension to isolate CSCs from the rest of the cancer cells. Although some utilize marker-positive and -negative populations to accomplish this goal, it is generally believed that for a population to be considered a CSC it must display an increased tumorigenicity and the capacity to reproduce the original human tumor. Detailed in the protocol below is a method for mechanically dissociating a human or mouse xenograft tumor sample.

Materials

At least 1 cm^3 of viable tumor tissue with minimal necrotic component
Serum-free RPMI cell culture medium or medium preferred for the tumor type under analysis
Trypan blue
PBS (optional)

10-cm Petri dish
Tissue forceps
Scalpel with #22 blade
10-, 5-, and 1-ml pipets
16-gauge needles and 3- to 5-ml syringes
70-μm sterile mesh filter (Sefar Filtration)
50-ml conical tube
200- and 100-μm sterile mesh filters (optional; Sefar Filtration)

Additional reagents and equipment for assay of viability by trypan blue exclusion (Strober, 2001)

1. Begin processing tumor as soon as possible after excision to maximize cell viability.

   While ideally the tumor is received immediately after removal from the patient, this is not always possible, as speed of delivery depends on available personnel and the need for pathologic review. Because use of the specimen cannot compromise patient care, collaboration with a surgeon and pathologist who can work together to quickly provide excess tissue is essential. If possible, tissue processing should begin within 30 min of removal, with implantation into mice or culture completed within another 30 to 60 min. Mouse tumors can generally be obtained more quickly, as they are resected immediately after sacrifice and can be identified grossly.

2. After receiving the patient or mouse tissue sample, place the specimen in a 10-cm Petri dish with approximately 1 ml of cold RPMI (or equivalent) medium. Place the dish on ice or an ice pack during dissection.

3. Hold the specimen firmly with tissue forceps. Using the *back* (unsharpened side) of a #22 scalpel blade, scrape the specimen downward, and away, to remove cells from the tumor mass into the dish.

   This should break up the solid mass. As cells are pulled from the tumor mass, strands of connective tissue will be isolated. These should be removed from the collection.

4. Continue scraping the tissue sample until the specimen is too small to hold and there is a sizable "slurry" population in the 10-cm dish.

5. Dissociate the cell slurry.

   a. Repeatedly draw the slurry up into and out of a 10-ml serological pipet. When the slurry passes easily in and out of this pipet, repeat the procedure with a 5-ml pipet, then a 1-ml pipet.

      With this mechanical dissociation procedure, it will eventually be possible to aspirate the slurry into a 16-gauge needle on a 3- or 5-ml syringe.

   b. Using a 3-ml syringe, attach a large-gauge needle (i.e., 16-G) and then gently aspirate the cell slurry into the syringe.

      If only small clumps of cells are needed for later applications, such as injection into mice or for culture, this degree of tissue dissociation is usually sufficient; if so, proceed to step 7. If the objective is to perform flow cytometric analysis, a single-cell suspension is required. For this purpose continue with step 6.

6. Place a 70-μm filter atop a 50-ml conical tube. Slowly deposit the cell suspension using a 5-ml pipet onto the filter. Allow the cell suspension to pass into the collection tube.

   The filter will quickly clog if the suspension still has large debris. In this case, first pass the suspension through 200-μm and 100-μm filters, and then the 70-μm filter.

7. Once the entire the cell suspension is collected, retain 50 μl to use for counting and assessment of viability and centrifuge the remaining sample 10 min at 1500 × *g*, 4°C.

8. While samples are centrifuging, determine the number and viability of cells in the suspension using a hemacytometer and trypan blue exclusion technique (Strober, 2001).

9. Aspirate the medium and resuspend the cellular pellet in the needed amount of cell culture medium or PBS as required for subsequent analysis.

   The resuspension volume is based on the cell density as calculated by trypan blue exclusion.

ALTERNATE PROTOCOL 1

CHEMICAL DISSOCIATION OF PRIMARY TUMOR OR MOUSE XENOGRAFT

The decision whether to use a mechanically based or chemically based dissociation method is primarily a personal preference, but is sometimes guided by tumor density. Avoiding chemical dissociation is advisable, as this approach can be caustic. We have generally experienced reduced cell viability when using chemical dissociation procedures. Some tumor types are more amenable to mechanical dissociation with high viability while others are more appropriate for chemical digestion. This varies not only with tumor type, but also the site of collection and tumors from different patients. Therefore, the decision to perform chemical dissociation is often made on a case-by-case basis, depending on the success of the mechanical dissociation. If the tumor is especially dense, a maximal yield and viability may be provided by starting with chemical dissociation. Alternatively, a combination of chemical and mechanical dissociation can be employed, whereby cells are first mechanically dissociated using Basic Protocol 1, followed by chemical digestion of firm residual tumor that was not dissociated using this approach. With chemical dissociation, an enzyme is used to digest the physical bonds between the tumor cells and the extracellular matrix.

Materials

Tumor fragment
1× PBS
Enzymatic digestion solution (0.25% trypsin/EDTA) with or without hyaluronidase and collagenase (see step 2 note)
RPMI-1640 medium with 10% fetal bovine serum (FBS)
Trypan blue

50-ml, 10-ml (optional), and 15-ml (optional) conical tubes
10-cm Petri dish
#22 scalpel blade and blade handle
Tissue forceps
70-μm sterile mesh filter
10-ml, 5-ml, and 1-ml serological pipets

Additional reagents and equipment for assay of viability by trypan blue exclusion (Strober, 2001)

1. After extraction from the mouse or patient, place the tumor into 10 ml of 1× PBS in a 50-ml conical tube and store on ice until dissociation.

   See note following step 1 of Basic Protocol 1 for information on timing of tumor analysis.

2. Add to the 50-ml conical tube 10 ml of 0.25% trypsin/EDTA with or without hyaluronidase and collagenase.

   If the sample is less than approximately 1 cm^3, use 5 ml of PBS and 5 ml of chemical digestion solution in a 10-ml conical tube.

   To maximize viability, the ideal digestion solution will depend on the cell type. Commonly used digestion solutions include hyaluronidase at 0.05 mg/ml and collagenase at 0.5 mg/ml

3. Deposit tumor onto sterile 10-cm Petri dish. Using the #22 scalpel blade and stabilizing with sterile forceps, initiate dissociation by mincing the tumor sample with a chopping motion, taking care not to crush the tissue.

4. Place the chopped tissue into the conical tube and incubate the sample at 37°C for 20 min.

5. Further dissociate the tumor sample by pipetting the tissue solution up and down using a 10-ml serologic pipet until the tissue passes freely, and then repeat the dissociation process using a 5-ml and then a 1-ml pipet.

6. Neutralize the trypsin-cell solution with 20 ml of RPMI-1640 medium containing 10% FBS (or 10 ml in a 15-ml conical tube).

7. Using a 5-ml pipet, pass the cell suspension through a 70-μm sterile mesh filter placed over a fresh 50-ml conical tube to generate a single-cell suspension.

8. Once the entire cell suspension has been collected, retain 50 μl for cell counting and assessment of viability. Centrifuge the remaining sample 10 min at 1500 × *g*, 4°C.

9. While samples are centrifuging, determine the number and viability of the cells in the suspension using a hemacytometer and trypan blue exclusion (Strober, 2001).

10. Aspirate the medium and resuspend the cellular pellet in an appropriate volume, based on cell density calculated by trypan blue exclusion, of cell culture medium or PBS as needed for later applications.

BASIC PROTOCOL 2

IDENTIFICATION OF CELLS BASED ON SURFACE MARKER EXPRESSION AND SEPARATION BY FLOW CYTOMETRY

Flow cytometry is an important technique for separating putative CSCs from the heterogeneous population of cells isolated from a primary tumor. Sorting with flow cytometry allows the separation of marker-positive cells from the marker-negative cells. If the tumor specimen is derived from a mouse xenograft, it enables separation of murine cells from human tumor cells if that is required, using either an antibody against a tumor-specific antigen to isolate tumor cells or an antibody against the species-specific HLA antigen to separate species-specific cells. Another advantage of flow cytometry is that multiple markers can be used to sort the population simultaneously, allowing potentially positive and negative selection (i.e., inclusion of CD44-positive cells, but exclusion of CD45-positive lymphocytic cells). Multiple tutorials are available online from academic (University of North Carolina and Purdue University) and commercial Web sites (Life Technologies and BD Biosciences), and in *Current Protocols* (Robinson et al., 2013), on the use of flow cytometry for those unfamiliar with the technique. Consult with your flow cytometric core facility for ordering supplies to ensure reagents are appropriate for the instrument. The appropriate analysis of flow cytometric data (Herzenberg et al., 2006) is accomplished using software packages such as FlowJo (Tree Star, Inc) and FCS Express (DeNovo Software).

Materials

Single-cell suspension of cancer cells (Basic Protocol 1)
Phosphate-buffered saline, calcium- and magnesium-free, with 0.1% bovine serum albumin (CMF-PBS/0.1% BSA)
Antibodies for desired surface marker(s) conjugated to a fluorophore (antibodies validated for use in flow cytometry work best; BD Biosciences)
RPMI or cell culture medium of choice containing 0.1% BSA (optional)

5-ml conical polystyrene tubes
Flow cytometer with appropriate channels for the fluorochromes being employed

1. Using a hemacytometer, determine the total number of cells in the single-cell suspension from Basic Protocol 1 and then generate a cell pellet by centrifuging the sample 10 min at 1500 × *g*, 4°C.

2. Aspirate off the supernatant and resuspend the cellular pellet in CMF-PBS/0.1% BSA to a concentration not to exceed 1×10^7 cells/ml.

   For sorting purposes, the cell concentration should be as high as possible to reduce sorting time. However, if the concentration is too high, the flow cytometer may become clogged. This is a function of cell size and extent to which the cells are in a single-cell suspension as opposed to clumps. A good starting point is 5×10^6 cells/ml. For reading, but not sorting, cell density can be reduced, i.e., to 1×10^6 cells/ml, to avoid clogging and to reduce antibody use.

3. Add fluorophore-conjugated antibodies to the sorting sample.

   While the concentration varies by antibody type, it is generally between 1:50 and 1:100, diluted in CMF-PBS/0.1% BSA.

4. Incubate the cell samples with the antibodies for 30 to 45 min at 4°C. Protect from light.

5. Add 4 ml of CMF-PBS/0.1% BSA to each tube and centrifuge for 5 min at 1500 × *g*, 4°C. Carefully discard the supernatant. Repeat this step two additional times to wash the cells.

6. After the last wash, resuspend the cells in a 5-ml conical tube to a maximum of 1×10^7 cells/ml of CMF-PBS/0.1% BSA.

   If it will require a long time (greater than 1 hr) for cytometric analysis or sorting, consider using medium with 0.1% BSA instead of PBS, to maximize viability.

7. Pass a small volume of cells through the flow cytometer to identify the population to be sorted using flow cytometric software.

   Ideally there is a marked separation between negatively stained cells and strongly positive cells. This ensures that sorting by marker positive is reliable. If the signal of the population is normally distributed, and only the "most" positive cells at the end of the bell-shaped curve are marked for isolation, it is important to confirm the cells are in fact more positive than the rest of the population (see step 8).

8. After sorting, run a small sample of the isolated cells through the flow cytometer to confirm that the population is pure.

   Although some signal quenching should be expected, purity should be >95%.

ISOLATING CANCER STEM CELLS USING MAGNETIC BEAD SEPARATION

ALTERNATE PROTOCOL 2

As flow cytometry may not be available, magnetic bead separation can be used as an alternative method for sorting a cell population into putative CSCs. A disadvantage of the magnetic bead approach is that if multiple markers are required for identification of the population of interest, they must be performed in series, rather than concurrently, increasing the time required and potentially decreasing the viability of the final cell sample. However, if large numbers of cells must be sorted to achieve an adequate sample, magnetic bead separation may accomplish this task more quickly than flow cytometry because all cells are processed simultaneously, instead of one at a time. The most important factors when considering any type of sorting procedure are maximizing viability and having as pure a separation as possible. Because sample purity ultimately depends on the quality of the antibody, trial and error may be needed to determine if magnetic bead separation or flow cytometric sorting provides purer samples. Multiple sources of magnetic beads and methods are available, with the most commonly used being the EasySep system (STEMCELL Technologies), Dynabeads (Life Technologies), and magnetic-activated cell sorting (MACS) (Miltenyi Biotec).

Using a principle similar to immunoprecipitation, magnetic bead separation entails the use of antibodies conjugated to a magnetic bead. Cells that have surface markers recognized by antibody are bound to them. Exposing these cells to a magnet separates cells into marker-positive and marker-negative groups. Unlike flow cytometry, only one marker can be used at a time for separating the mixed cell population. If the aim is to isolate a population of putative cancer stem cells that is positive (or negative) for a panel of markers, the procedure must be repeated sequentially until a select cell population remains. If antibodies against a particular marker are not available, some manufacturers have products that will allow any primary antibody to be used (see Support Protocol 1).

This protocol is designed for processing 100 μl to 2.5 ml of cell suspension (up to 5×10^8 cells).

Materials

Single-cell suspension of cancer cells (Basic Protocol 1)
Phosphate-buffered saline, calcium- and magnesium-free with 2% fetal bovine serum and 1 mM EDTA (CMF-PBS/2% FBS/1 mM EDTA)
Species-specific FcR blocking antibody (same species as the FITC- or biotin-conjugated antibody)

FITC-conjugated (or biotin-conjugated) antibody of marker of interest
EasySep FITC (or biotin) selection cocktail (STEMCELL Technologies)
EasySep (or equivalent) magnetic nanoparticles (STEMCELL Technologies)
Medium of choice

12 × 75-mm polystyrene tubes (e.g., Falcon 5-ml round-bottom tubes)
EasySep (or equivalent) magnet (STEMCELL Technologies)

1. Using a hemacytometer, determine the total number of cells in the single-cell suspension from Basic Protocol 1 and then generate a cell pellet by centrifuging the sample 10 min at 1500 × *g*, 4°C.
2. Carefully remove the supernatant and resuspend the cells to a concentration of 1×10^8 cells/ml in CMF-PBS/2% FBS/1 mM EDTA, and transfer them to a 12 × 75-mm polystyrene tube. If the sample contains 10^7 cells or fewer, resuspend them in 100 μl.

   See Support Protocol 1 if a fluorochrome-conjugated antibody is not available for the desired cell surface marker

3. Add species-specific FcR blocking antibody at 100 μl/ml.
4. Add FITC-conjugated (or biotin-conjugated) antibody to a final concentration of 0.3 to 3.0 μg /ml. Mix well and incubate at room temperature for 15 min.

   Titrate FITC- or biotin-conjugated antibody for optimal purity and sample recovery.

   While marker-positive cell recovery increases with higher amounts of antibody labeling, too much antibody can generate false-positive labeling.

5. Add EasySep FITC (or biotin) selection cocktail at 100 μl/ml of cells. Mix well and incubate at room temperature for 15 min.
6. Mix magnetic nanoparticles to ensure uniform suspension by vigorously pipetting 5 to 10 times. Add the nanoparticles at a concentration of 50 μl per ml of cells.
7. Mix the sample well by tapping tube and incubate at room temperature for 10 min.
8. Bring the cell suspension to a total volume of 2.5 ml by adding CMF-PBS/2% FBS/1 mM EDTA. Mix the cells in the tube by gently pipetting up and down 2 to 3 times. Place the tube without a cap into the EasySep magnet and incubate for 5 min.
9. Pick up the magnet and in one smooth motion, invert the magnet and the tube to decant the supernatant fraction into a new tube. Leave the magnet/tube inverted for 2 to 3 sec. Do not shake the magnet to remove drops.
10. Remove the tube from the magnet and add 2.5 ml of CMF-PBS/2% FBS/1 mM EDTA. Mix the cell suspension by pipetting up and down 2 to 3 times. Replace the tube into the EasySep magnet and allow it to incubate for 5 min.
11. Repeat steps 10 and 11, and then step 10 once again, for a total of three 5-min separations in the magnet. Each time collect the negative-selected cells in the same tube.
12. Remove the tube from the magnet after the final separation. Resuspend the cells in the medium of choice at the concentration needed for subsequent use (e.g., injection, culture, collection of protein lysate, extraction of mRNA).

USING THE EasySep "Do-It-Yourself"

SUPPORT PROTOCOL 1

When a commercially available FITC- or biotin-conjugated antibody for use in magnetic bead separations is unavailable, it is possible to prepare the tetrameric antibody complexes needed to bind the target cells to the magnetic beads. While this adds additional steps to the sorting procedure, there is no reason to expect any loss in the yield or purity of the cell collection as compared to sorting with conjugated antibody. This procedure follows that of Alternate Protocol 2, with the additional materials and steps noted.

Additional Materials

Mouse IgG_1 monoclonal antibody for surface marker of interest
Phosphate-buffered saline, calcium- and magnesium-free (CMF-PBS)
EasySep "Do-It-Yourself" Selection Kit (STEMCELL Technologies)

1. Prepare the tetrameric antibody complex by adding 15 μg of the mouse IgG_1 monoclonal antibody dissolved in CMF-PBS into a 1.5-ml polypropylene tube. Record the volume.

   The total volume of the antibody cannot exceed 800 μl.

2. Add 100 μl of component A from the EasySep kit to the tube and mix well by tapping tube.

3. Add 100 μl of component B to the tube and mix well by tapping tube. Place the closed tube into a 37°C incubator (or water bath) for 5 hr or overnight.

4. Bring the tube to a final volume of 1.0 ml by adding the appropriate volume of sterile CMF-PBS.

   The tetrameric antibody complex cocktail should be stable for up to 1 year at 4°C. Do not freeze the cocktail.

5. Using the homemade cocktail, continue the separation of the cell population beginning at step 6 of Alternate Protocol 2.

ISOLATING CANCER STEM CELLS BASED ON HOECHST DYE EXCLUSION: THE SIDE POPULATION (SP)

BASIC PROTOCOL 3

When attempting to identify putative CSCs in either a primary tumor sample or a mouse xenograft tumor, or even a cell line, it is sometimes not known what the surface markers will be for the desired population. Numerous studies have demonstrated that Hoechst 33342 dye can be used in conjunction with flow cytometry to identify the "side-population" of cells that have CSC features. The principle of the Hoechst dye exclusion assay is based on the fact that the fluorescent Hoechst 33342 dye stains DNA. Thus, the fluorescent profile of Hoechst 33342 can identify a minority side population of cells that is highly enriched for markers of hematopoietic stem cells (Goodell et al., 1996). The unique property of the side-population is that these cells eliminate the dye more efficiently than normal cells, resulting in low Hoechst staining (dye exclusion). This enhanced dye efflux is the result of an increase in the activity of multi-drug resistance proteins, primarily ABCG2, which actively transport the Hoechst dye out of the cell nucleus.

Materials

Preferred culture medium
Single-cell suspension of cancer cells (Basic Protocol 1)
Hoechst 33342 dye (Thermo Scientific, cat. no. 62249)
Verapamil (Sigma)
Sterile phosphate-buffered saline, calcium- and magnesium-free (CMF-PBS)

5-ml polystyrene tubes

Additional reagents and equipment for flow cytometry of side population (Goodell, 2005; Petriz, 2013)

1. Maintain the preferred cell culture medium at 37°C before initiating the separation procedure.
2. Using a hemacytometer, determine the total number of cells in the single-cell suspension from Basic Protocol 1 and then generate a cell pellet by centrifuging the sample 10 min at 1500 × *g*, 4°C.
3. Carefully aspirate off the supernatant and resuspend the cells in the 37°C culture medium at a concentration of 1×10^6 cells/ml.
4. Add Hoechst 33342 to the cell suspension to a final concentration of 5 μg/ml. Prepare a separate tube in which verapamil is also added to a final concentration of 50 μM.

   Because verapamil inhibits Hoechst exclusion, it is used to identify the "Hoechst-low" cells.

5. Thoroughly mix the cells and dye by gentle tube tapping, and incubate at 37°C for 90 min. During the incubation period, mix the cells every 15 min with a low-speed vortex.
6. Following incubation, centrifuge the cells 10 min at 1500 × *g*, 4°C to produce a cellular pellet.
7. Remove the supernatant and resuspend the cells in sterile CMF-PBS at 4°C; place in a 5-ml polystyrene tube for flow cytometric analysis.

   At this stage the cells may be separated by flow cytometric sorting.

   The population with low Hoechst staining is identified by noting the location in which cells exposed to verapamil retain strong Hoechst fluorescence.

8. To identify the side population, use an ultraviolet laser on the flow cytometer to excite the Hoechst dye.

   Fluorescence for Hoechst dye is measured at 450 nm (Hoechst blue) and 675 nm (Hoechst red).

9. When passing the sample through the flow cytometer, initially establish a live gate to exclude red blood cells and dead cells present in the sample.

   Personnel at the flow cytometry core should be able to assist with the gating.

10. Sort the side population from the non-side population and keep on ice in sterile 15-ml conical tubes until sorting is complete. Use cells immediately in downstream applications or store frozen at −80°C.

BASIC PROTOCOL 4

DETERMINING TUMORIGENICITY OF PUTATIVE CANCER STEM CELLS

There are many biologic characteristics that might be explored to determine how CSCs differ from the marker-negative population. These include expression profiling, in vitro assays of chemotherapy or radiation resistance, formation of tumor spheres, migration/invasion assays, demonstration of enhanced pluripotency (by examining heterogeneity of subsequent tumors/generations of isolated populations), and others. However, the current gold standard for establishing a population as CSCs is demonstration of enhanced tumorigenicity in murine xenografts. A common approach for measuring this is determination of the amount of cells injected into immunocompromised mice that causes

tumor formation in 50% of the animals. Because of their increased tumorigenicity, CSCs form tumors at a lower cell count as compared to a non-CSC population. While there is no established standard for how much more tumorigenic a population should be to be considered a CSC, in general at least 50- to 100-fold fewer cells (compared to a marker-negative population) should be all that is needed to stimulate tumor formation in 50% of mice. It is also noteworthy that xenograft formation is not solely dependent on the cell population, but also on the mouse strain. Because NOD-SCID mice have an almost complete knock-out of their immune system, they are excellent animals for testing human tumor cells. However, this mouse line is susceptible to spontaneous lymphoma formation, often in less than a year of life. Likewise, IL2 receptor-γ chain-deficient mice, which also lack NK cell function, require fewer cells to establish xenografts. However, because of their severe immunocompromised state these animals are difficult to maintain. When considering the best mouse model for conducting the following studies, it is important to weigh the benefits and risks to each animal model in terms of the study outcome. Taking these factors into consideration, we have generally employed SCID mice as the primary model. Regardless of which model is selected, it is important to have consistency and appropriate controls, with both marker-positive and marker-negative populations examined.

Materials

Putative cancer stem cell and non-CSC populations sorted via Basic Protocol 2, Alternate Protocol 2, Support Protocol 1, or Basic Protocol 3
Preferred cell culture medium (e.g., DMEM), serum-free
Matrigel, preferably without added growth factors (optional; BD Biosciences)
6- to 8-week old SCID mice (e.g., NCI Frederick, Taconic, Charles River Labs, Jackson Labs) of desired gender kept in approved IACUC and ARP conditions
Isoflurane

1-ml syringe
25-gauge needles
Vaporizing anesthesia device (e.g., Drager 19.1, Anesthesia Service and Equipment) with access to clinical-grade oxygen
Betadine scrub
Hair removal equipment (shaver or Nair) if using non-nude mice
Warming equipment, e.g., heat lamp, isothermal pad (Deltaphase Isothermal Pad, Braintree Scientific)

1. Gather sorted cell populations from previous protocols and place them on ice while making preparations for injection.

2. Create serial dilutions of the CSC-positive and non-CSC populations in the preferred serum-free culture medium.

   Ideally tumorigenicity should be examined across a wide range of implanted cell densities, i.e., 1 million cells, followed by 250,000, 100,000, 25,000, 5000, 1000, and finally 100 cells. Often, because of the small proportion of tumor composed of CSCs, obtaining numbers as high as 1 million cells may not be feasible.

3. Prepare a sufficient volume of cell suspension at various concentrations to implant at least 5 mice per dilution and cell population type in the subcutaneous tissue on the flank of the mouse.

   Tumor cells can be injected in different sites depending on the design of the experiment, the tumor cell type, and mouse strain. For example, if studying breast cancer, cells can be easily injected into the mammary fat pads of the mouse and followed for development. For ovarian cancer cells, mice can be injected intraperitoneally. However, in this case it is difficult to follow tumor development, making it necessary to analyze all animals for the amount of tumor formation at the same time, generally when control animals begin

to show signs of distress. Small-animal imaging techniques might be of assistance with this approach if following growth over time is crucial.

4. Remove the Matrigel from the freezer and keep on ice.

   Matrigel solidifies at room temperature.

5. Mix cells for injection and Matrigel together at a 1:1 ratio and draw up into a 1-ml syringe with a 25-gauge needle. Maintain the syringe on ice prior to injecting the mice.

   While mixing cells with Matrigel is optional, it likely improves the rate of tumor formation.

6. Place mice into anesthesia induction chamber and induce anesthesia using 5% isoflurane at a rate of 0.7 liters O_2/min.

   Consult local IACUC regulations regarding anesthetic procedures. There are any number of vaporizing anesthesia devices that can be used. Consult with your local Animal Research Program for possible vendors.

7. Transfer the animal to a nose cone and maintain anesthesia using 1.5 to 2% isoflurane once the mouse is unconscious and does not respond to pain (toe pinch).

8. Clean the skin at the site of injection with a betadine scrub.

   If using fur-bearing mice, it is beneficial to have previously removed the hair over the injection site, either chemically (e.g., Nair) or by shaving.

9. Using one hand to hold taut the skin of the mouse's flank, insert the needle, bevel up, at a shallow angle to avoid penetrating the subcutaneous layer. Inject 200 μl of the Matrigel/cancer cell mixture into the mouse.

   A small bump will appear on the skin if the needle is placed properly in the subcutaneous layer.

10. Place the mouse in a fresh cage using an appropriate warming method (e.g., by heat lamp or isothermal pod) to recover from the anesthesia.

11. Observe mice periodically for tumor formation. Obtain histologic confirmation that the tumor is of the expected cell type (and not a lymphoma, for example).

    Most tumors will form within 3 to 4 months, sometimes as quickly as 1 month. Mice should be observed for at least 6 months before declaring them negative regarding tumor formation.

    If working with a cancer cell line, the time needed for tumor formation will likely be less than when using a primary patient tumor sample. Also, some cancers naturally grow faster than others. Nonetheless, it is important to select a fixed time for the end of the experiment to allow for the calculation of the quantity of cells needed to induce tumor formation in 50% of the animals, in order to make an accurate determination as to whether the cancer stem cell population is more tumorigenic than the non-cancer stem cells.

BASIC PROTOCOL 5

SPHEROID ASSAY OF PUTATIVE CANCER STEM CELLS

Inhibition of cell differentiation is one approach used for the in vitro cultivation of stem cells and progenitor cells. This involves growth on culture plates to which cells cannot attach in a specialized medium containing growth factors that inhibit differentiation. Under these conditions cells generally grow in semi-fused spheroids, floating suspended in the supernatant (Fig. 14.28.1B). This makes them distinguishable from simple aggregates of cells, with which they are often confused (Fig. 14.28.1A). Cells within spheroids are more self-renewing and pluripotent than those that are not. It is also possible that only

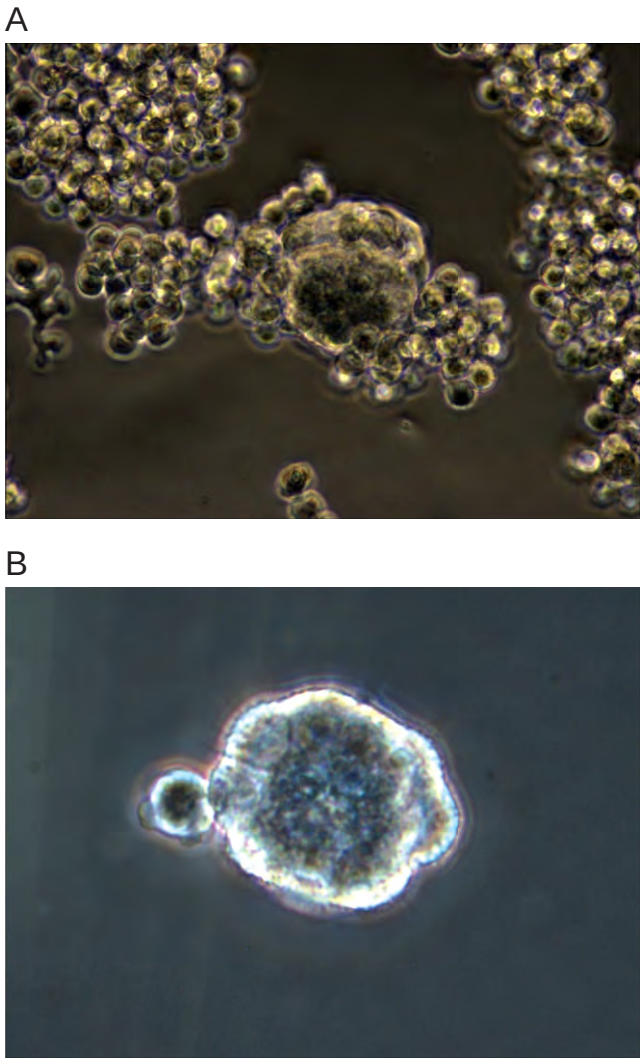

Figure 14.28.1 Spheroid growth in a heterogeneous sample. Unsorted A2780 ovarian cancer cells were plated in serum-free differentiation-inhibiting medium on ultra-low-attachment plates. A spheroid of fused cells is noted to have a different phenotype than the majority of dividing cells, which remain attached as aggregates but not spheroids (**A**). Cells plated as a single cell per well can sometimes form spheroids, which can be maintained for several weeks (**B**).

certain pluripotent cells can develop into spheroids. Originally the only conditions under which primitive neural tissue would grow, and therefore termed the neurosphere method (Reynolds and Weiss, 1996), this approach has been adapted for the propagation of putative cancer stem cells as well. Although this method is convenient for studying stem cells in vitro, it is yet to be proven that only cancer stem cells can grow as spheroids, or that cells growing as spheroids definitively originate from a stem cell. The latter characterization is generally confirmed by in vivo tumorigenicity. Nonetheless, because spheroids do display an increased expression of stem cell markers, and a prolonged self-renewal, they are a convenient way to study stem cell biology and response to therapeutics. While not definitive, a finding of enhanced ability to form spheroids suggests that a subpopulation of the tissue sample has stem cell properties. The following protocol is adapted from that originally described for neurosphere growth, which was later used by Dontu and Wicha to establish mammary spheroids (Dontu et al., 2003).

Materials

Heterogeneous cell population, or subpopulation
B-27 supplement, 50× (Gibco #12587-010)
Serum-free medium of choice
Recombinant FGF-basic (Gibco #PHG0021L)
Recombinant EGF (Gibco #PHG0311)
Costar ultra-low-attachment multiple-well plates (Corning #3473)

1. Gather cell subpopulations separated by flow cytometry or magnetic beads, or a mixed population if preferred.
2. Add 2 ml of 50× stock B-27 supplement to 98 ml of serum-free medium of choice for the cell line employed. Add 20 μl of stock 100 μg/ml recombinant FGF-basic and 20 μl of stock 100 μg/ml recombinant EGF.

   This medium is stable for 4 weeks if stored at 4°C.
3. Use 96-well ultra-low-attachment plates to determine the frequency of spheroid formation. Prepare a solution of cells such that, on average, 1 cell is delivered in every other well (for administration of 200 μl per well, this is a concentration of 2.5 cells/ml).
4. Prepare 20 ml of 2.5 cells/ml in the same medium as above. Mix well by pipetting and then add 200 μl to each well. Culture the samples at 37°C.
5. Refresh the wells every 3 to 4 days with 25 μl of FGF-basic and EGF-containing medium prepared in step 2.

   Because this medium loses activity at 37°C after a few days, formed spheroids will often lose their cohesion.
6. Examine plates for spheroid formation daily. Generally, spheroids will begin to form after 7 to 14 days.

   For this example, the endpoint of this study is the percentage of cells (out of a presumed 48) that form spheroids. Alternatively, it is possible to plate 1000 cells in 2 ml in 6-well plates, with the endpoint being the number of spheroids formed per well. Different cell subpopulations, or conditions (such as inhibitors of stem cell pathways or siRNA-mediated downregulation), can be established in each well.

   As spheroids can often be maintained for 3 to 4 weeks, there is ample time to add therapeutics or drug candidates to different spheroid-containing wells to determine toxicity.

COMMENTARY

Background Information

Over the past 40 years, major advances treatment have led to an increase in the 5-year-survival rate of all cancers from 50% to 68% (Siegel et al., 2012), with some types of cancers showing a greater increase in 5-year survival than others. For example, there has been an overall increase in the 5-year survival with breast cancer from 75% in the 1970s to 90% in 2006, with ovarian and brain cancers increasing from 37% to 45% and 24% to 36%, respectively, over the same time period (Siegel et al., 2012). A major reason for cancer deaths is the failure of a tumor to respond to treatment or its recurrence at distant sites from the primary origin. This ability of a cancer to reappear and resist chemotherapy indicates a population of cells that survives the primary therapy and that are ultimately responsible for death. This can be the result of an inherent resistance to chemotherapy or the evolution of cells by additional mutations or environmental factors that lead to development of chemoresistance. Which of these mechanisms predominates is unknown. A subpopulation of cells with enhanced tumorigenicity, self-renewal, and differentiation capacity is termed "cancer stem cells" (CSCs) because their biologic features are similar to normal stem cells. There are three characteristics used to define a CSC population. First, only a minority of the cancer cells within a heterogeneous tumor

have tumorigenic potential when implanted into immunocompromised animals. Second, CSCs can be identified by, for example, expression of surface markers or enhanced biologic activity, such as ALDH1A1 activity, that makes it possible to isolate them from the non-CSC population. Finally, tumors that develop after CSC injection contain both CSC-positive and CSC-negative cells, demonstrating enhanced differentiating capacity (Dalerba et al., 2007a). While it is unknown whether the cells within a presenting tumor that survive initial chemotherapy are the same as the CSCs that are isolated and tested ex vivo, there is evidence suggesting that this may be the case (Steg et al., 2012).

Data supporting the CSC theory were first accumulated in human acute myeloid leukemia (AML) by Lapidot et al. (1994). In this study, the authors were able to identify a subpopulation of cells that were $CD34^+$ and $CD38^-$. These were the only cells that were tumorigenic and had the ability to reproduce the AML phenotype in mice (Lapidot et al., 1994). Indeed, the malignant phenotype could be reproduced with the injection of just a single cancer cell. After this discovery, work began in earnest to identify whether other tumor types contained subpopulations of such cells. The hypothesis developed that if the CSC population could be targeted and eliminated, a tumor could be permanently eradicated. The search for CSCs in solid tumors was conducted using the same approach used for the discovery of CSC in AML. However, with solid tumors, the additional complexity of reducing the dense mass to a single-cell population while retaining viability inhibited progress in identifying such cells. Putative CSCs had previously been identified in gliomas by the observation that "neurospheres" formed from non-malignant neurons contained cells with stem cell properties (Reynolds and Weiss, 1992). When the neurosphere technique was applied to gliomas, a $CD133^+$ subpopulation was identified that met the criteria for CSCs (Galli et al., 2004; Singh et al., 2004). The Singh study was important in demonstrating that only 100 $CD133^+$ cells needed to be injected into the orthotopic location in SCID mice for a tumor to form that reconstituted the entire heterogeneity of a human glioblastoma. Ultimately, CSCs were identified in breast cancer, colon cancer, and ovarian cancer using the same procedure (Dontu et al., 2003; Dalerba et al., 2007b; O'Brien et al., 2007; Zhang et al., 2008).

The protocols described in this unit can be used to isolate a subpopulation from a solid heterogeneous tumor. These methods make it possible to identify, based on either surface marker expression or a functional assay, a subpopulation of cancer cells, and to determine whether they meet the criteria for a CSC. Experiments can then be conducted to determine how the isolated cells differ biologically from the non-CSC population, and what drugs, drug combinations, or novel drug candidates may be effective in eliminating the CSC population. The destruction of the subpopulation of cells surviving initial chemotherapy, whether CSCs or otherwise, is necessary to achieve a lasting cure.

Critical Parameters and Troubleshooting

Among the more important considerations when conducting these assays is the freshness of the tumor specimen, as this is one of the most important determinants of cell viability and of the success in isolating a CSC population. As two types of tumor specimens, one from patients and one from xenografted mice, are considered in these protocols, the ability to procure fresh specimens requires a collaborative and coordinated effort from surgical oncologists, pathologists, and operating room staff. The ability to receive a specimen and begin processing quickly, preferably less than 30 min after removal, will optimize these assays. It is important when creating the single-cell suspension to consider what effect the selected method has on cell viability. If tumors are particularly dense, a chemical dissociation should be considered in addition to the mechanical dissociation in order to break up the tissue more quickly. Often, however, the combined dissociation procedure comes at the expense of the viability of some cells. Optimization is needed at the dissociation step, whether using mechanical or chemical methods, to maximize viability and yield from the tumor sample. Protocols may need to be modified slightly depending on the tumor, as some are denser and therefore require additional processing, while others may come apart more easily, making it unnecessary to employ chemical digestion. For flow cytometry, sorting for the live cells needed for biologic applications (tumor implantation, cell culture, etc.) is a more technically challenging and complex task than just sorting cells for a determination of surface marker expression. Additional time is needed for sorting live cells, during which some signal intensity may be lost. Also,

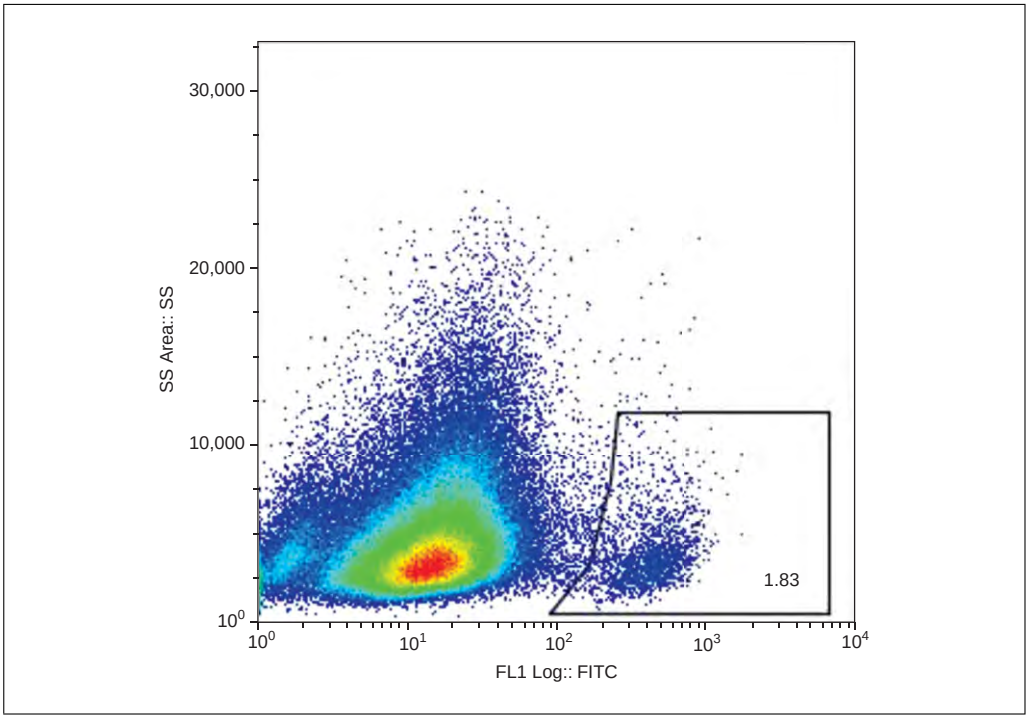

Figure 14.28.2 CD555 expression in a heterogeneous population. Dissociated cells from a freshly collected solid tumor were subjected to flow cytometric analysis after exposure to anti-CD555-FITC antibody. Gating based on the negative control shows that 1.8% of cells are CD555-positive. Side scatter plotted on *y* axis against intensity of FITC signal on *x* axis.

it is important to retest a sorted cell population to ensure the sorting was accurate. A balance must be achieved between a dense concentration of cells to minimize the volume sorted (and minimizing time) while avoiding a suspension that is so dense that it clogs the flow cytometer channels. The investigator should consult with the institutional flow cytometry facility to ensure it will be possible to undertake a live cell sort under sterile conditions to avoid contamination.

Mouse strain is another critical parameter. Experience suggests that SCID mice are ideal for these studies, as these immunocompromised animals combine longevity with a resistance to infection.

Anticipated Results

From 1 g of tumor sample, it should be possible to isolate 7 to 10 million cells with 90% viability. This assumes that the dissociation protocol is optimized for the tissue type that is being examined. In the flow cytometry and magnetic bead separation protocols, the CSC population is usually only <1% to 10% of the total cell population. Caution should be exercised if a freshly isolated cell suspension appears to have a CSC population that is approaching the majority of the cell population. This could indicate that the cell surface marker is too nonselective. In this case, perhaps an antibody could yield a more selective binding profile.

For the in vivo protocol for developing a mouse xenograft in the limited dilution studies, it is frequently noted that CSCs can form tumors with as few as 100 injected cells and can be 25 to 100 times more tumorigenic than non-CSC cells. Published data often suggest higher numbers are needed for tumor formation, which may be a function of overall viability from tumor processing or the mouse model employed. The tumors that develop in the xenograft model should reproduce the phenotype of the originally implanted tumor and be composed of a heterogeneous cell population. A section of all xenografts that develop after both CSC and non-CSC tumor cell injection should be immediately tested by flow cytometry for density of CSCs, or retained for histological analysis to confirm that the xenograft is similar to the originally implanted tumor.

Sample data from CSC determination (Basic Protocol 5)

Hypothesis: Population X identified by expression of hypothetical marker CD555 represents a CSC population.

Result 1: Population identification. Solid tumor samples were collected from the

Table 14.28.1 Growth of CD555-Negative and CD555-Positive Cells in Subcutaneously Injected Mice

	Cells injected						
	1×10^6	2.5×10^5	1×10^5	2.5×10^4	5×10^3	1×10^3	2.5×10^2
CD555-negative	10/10	7/10	1/10	0/10	0/10	0/10	0/10
CD555-positive		10/10	10/10	10/10	10/10	7/10	1/10

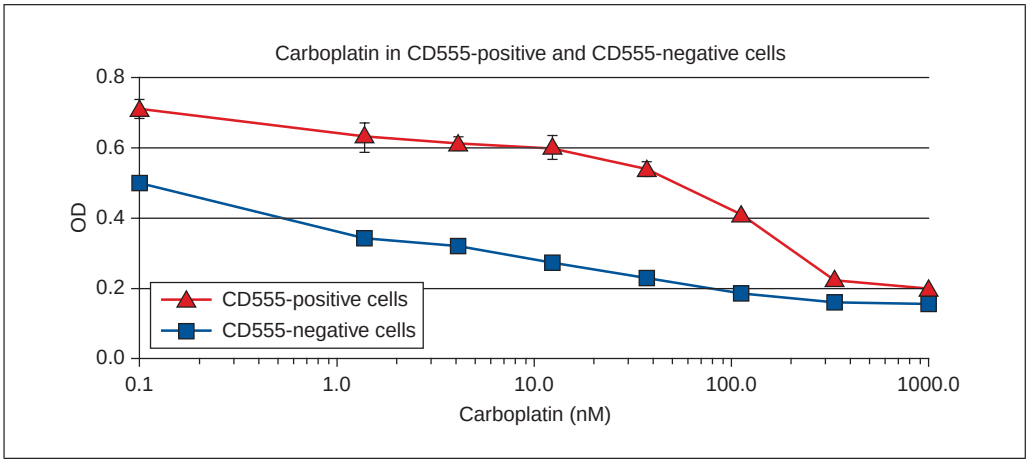

Figure 14.28.3 Platinum resistance in the CD555 population. Dissociated cells were sorted by flow cytometry based on CD555 expression, and plated into 96-well plates, 2000 cells per well. After 6 hr, the medium was replaced with medium with increasing concentrations of carboplatin or vehicle. After 5 days, cells were subjected to MTT. CD555-positive cells were much more resistant, demonstrating a carboplatin IC_{50} value of 82 nM, while CD555-negative cells had an IC_{50} value of 4.4 nM.

operating room and dissociated into single-cell populations. Flow cytometric analysis demonstrated that CD555-positive cells represented a distinct, but small, proportion of the tumor cells (Fig. 14.28.2).

Result 2: Tumorigenicity and Differentiation. In five consecutive cases, tumors were collected and dissociated, and CD555-positive cells were separated from CD555-negative cells by flow cytometric analysis. After sorting, flow cytometric analysis was repeated on the sorted cells to confirm the cells maintained a positive signal. The cells were then injected subcutaneously in limiting dilutions into SCID mice and followed for growth for 3 months. Mice with developing tumors are described in Table 14.28.1. The CD555-positive cells displayed a 250-fold increase in tumorigenicity when compared to CD555-negative cells. That is, it took 250 times more of the negative cells than of the CD555-positive cells to induce tumors in 50% of the cell population. Tumors that formed after injection of CD555 cells were dissociated and subjected to flow cytometry for CD555. These tumors contained both CD555-positive and -negative cells, with the positive cells again making up less than 5% of the tumor.

Result 3: Chemotherapy resistance. CD555-positive and CD555-negative cells were sorted by flow cytometry and plated into 96-well plates, 2000 cells per well, using conventional serum-containing medium. Separate samples were plated into 6-well plates in conventional medium. After 6 hr to allow attachment, the medium was replaced with increasing concentrations of carboplatin, a cytotoxic chemotherapy agent. The cells were allowed to continue to grow for 5 days and then checked for viability using the MTT assay. The CD555-positive cells displayed an increased survival compared to CD555-negative cells (Fig. 14.28.3). Additionally, cells separately plated were analyzed by flow cytometry. Cells originating from CD555-positive cells were 50% CD555-positive and 50% CD555-negative, while the cultured cells from the original CD555-negative cells had reduced proliferation, and were all CD555-negative.

Result 4: Spheroid growth. When A2780 ovarian cancer cells were grown in stem cell–promoting medium (serum-free with

supplemental B-27, FGF-basic, and EGF), several spheroids formed, although some cells only grew in aggregates (Fig. 14.28.1A). The CD-555-positive and -negative cells were separated by flow cytometry and plated onto ultra-low-attachment plates in B-27–supplemented serum-free medium with FGF-basic and EGF. A sample containing 200 μl of a 2.5 cells/ml solution was added to each well of a 96-well plate and placed in a 37°C incubator. One plate was used for CD555-positive cells, and one plate for CD555-negative cells. Upon examination of each well the following day it was found that 40 wells in the CD555-positive plate had an identifiable cell, and 52 wells had an identifiable CD555-negative cell. Every 4 days the medium was refreshed with 25 μl of the stem cell–promoting medium. After 2 weeks, 25 of the CD555-positive cells had formed a spheroid (62.5%, Fig. 14.28.1B), while only four of the CD555-negative cells did so (7.7%).

Time Considerations

The production of a single-cell suspension requires an hour at the most. It can take anywhere from 4 to 14 days for cells in culture to form tumorspheres. During this time, the cells should be kept in the incubator and fresh nutrients added to the medium every 4 days until sphere formation occurs. Once formed, tumorspheres can survive for weeks, although they will dissociate if nutrients are not replaced regularly. Primary cultures of adherent tumor cells usually do not last beyond a few passages in vitro. For the tumor formation studies in the mice, the time varies with cell type and the number of cells injected. Following injection, 2 to 6 months are needed for tumor development, with additional time needed for expansion and reimplantation to confirm the maintenance of the tumorigenic phenotype.

Acknowledgements

Funding for this work was provided, in part, by the University of Alabama at Birmingham Center for Clinical and Translational Science (5UL1RR025777), the Reproductive Scientist Development Program through the Ovarian Cancer Research Fund and the National Institutes of Health (K12 HD00849), and the Department of Defense Ovarian Cancer Research Academy (OC093443).

Literature Cited

Dalerba, P., Cho, R.W., and Clarke, M.F. 2007a. Cancer stem cells: models and concepts. *Annu. Rev. Med.* 58:267-284.

Dalerba, P., Dylla, S.J., Park, I.K., Liu, R., Wang, X., Cho, R.W., Hoey, T., Gurney, A., Huang, E.H., Simeone, D.M., Shelton, A.A., Parmiani, G., Castelli, C., and Clarke, M.F. 2007b. Phenotypic characterization of human colorectal cancer stem cells. *Proc. Natl. Acad. Sci. U.S.A.* 104:10158-10163.

Dontu, G., Al-Hajj, M., Abdallah, W.M., Clarke, M.F., and Wicha, M.S. 2003. Stem cells in normal breast development and breast cancer. *Cell Proliferat.* 36:59-72.

Galli, R., Binda, E., Orfanelli, U., Cipelletti, B., Gritti, A., De Vitis, S., Fiocco, R., Foroni, C., Dimeco, F., and Vescovi, A. 2004. Isolation and characterization of tumorigenic, stem-like neural precursors from human glioblastoma. *Cancer Res.* 64:7011-7021.

Goodell, M.A. 2005. Stem cell identification and sorting using the Hoechst 33342 side population (SP). *Curr. Protoc. Cytom.* 34:9.18.1-9.18.11.

Goodell, M.A., Brose, K., Paradis, G., Conner, A.S., and Mulligan, R.C. 1996. Isolation and functional properties of murine hematopoietic stem cells that are replicating in vivo. *J. Exp. Med.* 183:1797-1806.

Herzenberg, L.A., Tung, J., Moore, W.A., Herzenberg, L.A., and Parks, D.R. 2006. Interpreting flow cytometry data: A guide for the perplexed. *Nat. Immunol.* 7:681-685.

Jordan, C.T., Guzman, M.L., and Noble, M. 2006. Cancer stem cells. *N. Engl. J. Med.* 355:1253-1261.

Lapidot, T., Sirard, C., Vormoor, J., Murdoch, B., Hoang, T., Caceres-Cortes, J., Minden, M., Paterson, B., Caligiuri, M.A., and Dick, J.E. 1994. A cell initiating human acute myeloid leukaemia after transplantation into SCID mice. *Nature* 367:645-648.

O'Brien, C.A., Pollett, A., Gallinger, S., and Dick, J.E. 2007. A human colon cancer cell capable of initiating tumour growth in immunodeficient mice. *Nature* 445:106-110.

Petriz, J. 2013. Flow cytometry of the side population (SP). *Curr. Protoc. Cytom.* 64:9.23.1-9.23.20.

Reynolds, B. and Weiss, S. 1992. Generation of neurons and astrocytes from isolated cells of the adult mammalian central nervous system. *Science* 255:1707-1710.

Reynolds, B.A. and Weiss, S. 1996. Clonal and population analyses demonstrate that an EGF-responsive mammalian embryonic CNS precursor is a stem cell. *Dev. Biol.* 175:1-13.

Robinson, J.P., Darzynkiewicz, Z., Dean, P.N., Orfao, A., Rabinovitch, P.S., Stewart, C.C. Tanke, H.J., and Wheeless, L.L. (eds.) 2013. Current Protocols in Cytometry. John Wiley & Sons, Hoboken, N.J.

Siegel, R., Naishadham, D., and Jemal, A. 2012. Cancer statistics, 2012. *CA Cancer J. Clin.* 62:10-29.

Singh, S.K., Hawkins, C., Clarke, I.D., Squire, J.A., Bayani, J., Hide, T., Henkelman, R.M.,

Cusimano, M.D., and Dirks, P.B. 2004. Identification of human brain tumour initiating cells. *Nature* 432:396-401.

Steg, A.D., Bevis, K.S., Katre, A.A., Ziebarth, A., Dobbin, Z.C., Alvarez, R.D., Zhang, K., Conner, M., and Landen, C.N. 2012. Stem cell pathways contribute to clinical chemoresistance in ovarian cancer. *Clin. Cancer Res.* 18:869-881.

Strober, W. 2001. Trypan blue exclusion test of cell viability. *Curr. Protoc. Immunol.* 21:A.3B.1-A.3B.2.

Zhang, S., Balch, C., Chan, M.W., Lai, H.C., Matei, D., Schilder, J.M., Yan, P.S., Huang, T.H., and Nephew, K.P. 2008. Identification and characterization of ovarian cancer-initiating cells from primary human tumors. *Cancer Res.* 68:4311-4320.

Gynecologic Oncology 132 (2014) 483–489

Contents lists available at ScienceDirect

Gynecologic Oncology

journal homepage: www.elsevier.com/locate/ygyno

Review

Ovarian cancer stem cells: Are they real and why are they important?

Monjri M. Shah, Charles N. Landen *

Division of Gynecologic Oncology, Department of Obstetrics and Gynecology, University of Alabama at Birmingham, Birmingham, AL, USA

HIGHLIGHTS

- Growing evidence supports the presence of a chemoresistant cancer cell population that relies on stem cell pathways for enhanced survival.
- Examination of patient specimens confirms enrichment of stem cell pathways in surviving tumors.
- Targeting ovarian cancer stem cells is a promising approach to overcoming chemotherapy resistance in this subpopulation of heterogeneous tumors.

ARTICLE INFO

Article history:
Received 4 October 2013
Accepted 2 December 2013
Available online 7 December 2013

Keywords:
Ovarian cancer
Cancer stem cells
CD133
ALDH1
CD44
Side population

ABSTRACT

The cancer stem cell hypothesis has been put forward as a paradigm to describe varying levels of aggressiveness in heterogeneous tumors. Specifically, many subpopulations have been clearly demonstrated to possess increased tumorigenicity in mice, broad differentiating capacity, and resistance to therapy. However, the extent to which these experimental findings are potentially clinically significant is still not clear. This review will describe the principles of this emerging hypothesis, ways in which it may be appropriate in ovarian cancer based on the clinical course of the disease, and how we might exploit it to improve outcomes in ovarian cancer patients.

Contents

Introduction — what is the cancer stem cell hypothesis?

Ovarian cancer is the most lethal gynecologic malignancy in the United States. While recent advances in chemotherapy agents, administration, and dosing have yielded modest improvements in overall survival and quality of life, durable cures have not significantly increased [1]. Although deadly, ovarian cancer is actually one of the most chemosensitive solid malignancies. A patient presenting with advanced stage disease will have a 50–70% chance of having a complete clinical response after surgery and chemotherapy, and a 5-year survival rate of 40–50%. By comparison, rarely do patients with advanced stage colorectal or pancreatic cancer have a complete clinical response after surgery and chemotherapy and just 28% and 2% of these patients will survive for 5 years, respectively [2,3]. The clinical course of ovarian cancer and the increasing knowledge about the heterogeneity of malignant cells [4] emphasize that there are distinct cellular populations within a

* Corresponding author at: 176F RM 10250, 619 19th Street South, Birmingham, AL 35249-7333, USA. Fax: +1 205 975 6174.
E-mail address: clanden@uab.edu (C.N. Landen).

0090-8258/$ – see front matter © 2013 Elsevier Inc. All rights reserved.
http://dx.doi.org/10.1016/j.ygyno.2013.12.001

tumor. While most ovarian cancer cells are initially chemosensitive, there is a population of cells that survives initial therapy, only to later grow to a clinical recurrence. Although responses are frequently seen even in the setting of recurrence, virtually all patients will ultimately succumb to disease that has become resistant to all known cytotoxic or biologic therapies. If durable cures are to be achieved in ovarian cancer, there will be a need to determine what allows these small subpopulations to survive.

One model by which to explore ovarian cancer tumor heterogeneity is the cancer stem cell hypothesis. This idea proposes that within a heterogeneous ovarian tumor, there are small populations (generally less than 2% of cells) that have increased tumorigenicity and differentiating capacity than other cells [5]. This subpopulation, like normal stem cells, gives rise to more differentiated progeny that comprise most of the ovarian tumor mass and are more responsive to chemotherapy. Cancer stem cell populations have been shown in some respects to be more tumorigenic in multiple experimental systems, including increased rates of tumorigenicity, metastasis, invasion, angiogenic stimulation, and resistance to therapy [6,7]. While variability of nomenclature within the field has led to some confusion, with cells often (appropriately) described by their function, such as tumor initiating cells (TICs), cancer initiating stem cells (CICs), "stem-cell-like" cells, or therapy-resistant cells (TRCs), this population will be referred to as cancer stem cells (CSCs) for consistency. The latter term has evolved to hold greater meaning than the purely experimentally-derived former terms, specifically that CSCs not only carry increased tumorigenicity, but also may be responsible for tumor initiation, metastatic disease, and resistance to therapy. Although numerous experiments demonstrate that such a privileged population can be isolated, the scope of their importance is sometimes speculated upon. Excitement regarding the cancer stem cell hypothesis lies in its potential: if indeed the population surviving initial therapy (CSCs or other) can be isolated, perhaps the biologic pathways on which they depend for resistance can be identified and targeted, killing all – instead of most – malignant cells with primary therapy. But such excitement may need to be tempered with the current limitations of the hypothesis, including the methods in which they are often studied, and the scope of populations identified.

Why do cancer stem cells in ovarian cancer make sense?

The concept of ovarian cancer as a stem-cell disease is logical for many reasons. The most compelling argument is the most important — the clinical course. Most cells in a presenting advanced tumor are chemosensitive, but almost all patients will recur after growth of a resistant population. The fact that most patients at first recurrence will respond to secondary therapy implies that this recurrent tumor is again composed of a heterogeneous population of chemosensitive and chemoresistant cells, suggesting a differentiating capacity in the initial surviving population. Beyond the clinical course, additional pathologic characteristics support the hypothesis. The ovarian surface epithelium (OSE) is genetically more mesenchymal and less differentiated than other epithelial cells, as evidenced by the preferential expression of N-cadherin over E-cadherin [8,9]. Bowen and colleagues demonstrated through gene expression profiling that human OSE exists in an arrested state, similar to somatic stem cells [10]. This global mesenchymal state may explain how ovarian epithelial stem cells can be present in the normal ovarian surface epithelium despite a lack of convincing evidence that the OSE gives rise to more differentiated structures in the normal ovary (in contrast to normal stem cells of the breast and colonic epithelium). The CSC hypothesis may be even more applicable if the fallopian tube is the origin of many ovarian cancers, since the epithelial lining of the fallopian tube certainly represents tissue in which there is high turnover and normal stem cells giving rise to differentiated (ciliated) cells would be expected. In fact, prominent expression of stem cell genes has been identified in both OSE [11] and fallopian tube epithelium [12]. Additionally, epithelial ovarian cancer encompasses numerous histologic phenotypes, including papillary serous, endometrioid, clear cell, and mucinous subtypes, suggesting a multipotent differentiating capacity. While in many cases these subtypes may have different cells of origin, such as fallopian tube giving rise to papillary serous tumors and endometriotic implants producing endometrioid or clear cell carcinomas, these lineages are not likely absolute. The high rate of multiple "mixed" histologies within the same tumor suggests either a common cell of origin with capacity to differentiate into several phenotypes or multiple CSC phenotypes.

Although we know that tumor heterogeneity is profound, it is still unclear if all of the resistant clones are present within the original tumor and initially identifiable, if they are induced by administration of cytotoxic therapy and change in microenvironment, or a combination of both of these mechanisms. Numerous groups have isolated putative cancer stem cells from primary tumor specimens and demonstrated chemoresistance and self-renewal of this population, suggesting that these cells are present before chemotherapy is given. Lineage tracing experiments done in colonic adenomas support this hypothesis, demonstrating that stem cells exist in a quiescent state but stochastically expand in response to evolution or microenvironment stressors [13]. Although some models have shown that "stemness" can be induced by stressors such as chemotherapy, it seems unlikely that full chemotherapy resistance is induced by administration of primary therapy. In other gynecologic malignancies, such as gestational trophoblastic disease and ovarian germ cell tumors, durable cures are frequently obtained with similarly aggressive and toxic chemotherapeutic regimens. If the population of cells that causes recurrence was induced by chemotherapy, it follows that relapses would be noted at a similar rate in all treated malignancies. While it is possible that cells responsible for recurrence arise from a mutagenic effect of therapy, this does not explain why most recurrent tumors are histologically and genetically very similar to the primary tumor.

Alternatively, there is growing evidence that cell plasticity allows non-CSCs to gain a CSC phenotype. Cobaleda and colleagues found that mature B cells dedifferentiated to an aggressive lymphoma composed of pro-B cells when Pax5, a gene associated with lineage commitment, was deleted in a murine model [14]. Xie et al. described the reprogramming of mature B cells into macrophages by retroviral-forced expression of C/EBPα, a transcription factor involved in lymphoid differentiation [15]. While the majority of work has been done in hematopoietic cells, emerging data suggests that differentiated respiratory epithelial cells exhibit similar plasticity in the presence of injury [16].

Whether cancer stem cells are a very small, but present, population of cells prior to any therapy, develop in response to internal or external stimuli, or are a population comprised of cells derived from both etiologies is unclear. Regardless of origin, the preponderance of evidence suggests that they are associated with recurrence, therefore agents specifically targeting these cells may need to be included in upfront or maintenance therapy or both to minimize the risk of recurrence.

Early evidence and definitions of the cancer stem cell

Lapidot and colleagues first isolated a tumorigenic stem cell population in acute myeloid leukemia in 1994, where a single cell was found to completely reinitiate leukemia in mice [5]. Interest was kindled in solid tumors when populations with increased tumorigenicity were isolated from breast and GBM cancers [17,18]. Multiple experimental models have been used to potentially isolate putative cancer stem cells (Table 1) [19]. Bapat and colleagues were one of the first groups to demonstrate heterogeneous growth properties in ovarian cancer cells in 2005 [20]. They isolated unsorted ascitic cells from a patient and developed 19 spontaneously immortalized clones through low-density culturing. Of these, only two could be passaged sequentially into nude mice. The tumors that formed from these single clones closely resembled the tumor from which they were originally isolated, and had increased expression of stem cell mediators (Nestin, Nanog, and Oct4). Growth

Table 1
Ex vivo characteristics of cancer stem cells.

- Increased tumorigenicity in xenograft models
- Clonogenic
- Unlimited self-renewal
- Pluripotency
- Ability to recapitulate parent tumor
- Chemoresistance
- Radiation resistance
- Form spheroids in suspension

in spheroids, whereby single cells are plated in serum-free media (preventing differentiation) and agar-coated or charged plates (preventing attachment and laying down of an extracellular matrix) creates 3-dimensional balls of cells that have multipotentiality [21]. While these spheroids often are more resistant to cytotoxic therapies, it has been difficult to delineate to what degree this is due to the properties of the cells themselves, or other factors such as decreased penetration of drug or increased production of survival factors mediated by tightly-bound cells. It is now generally agreed upon that a cancer stem cell must have certain characteristics: 1) increased tumorigenicity in xenograft models, whereby isolated CSCs require 100–1000-times fewer cells injected in a mouse to establish a tumor; 2) unlimited self-renewal, generally demonstrated by maintenance of tumorigenicity after multiple passages; and 3) pluripotency, whereby tumors that form after CSC injection are composed of both marker-positive and marker-negative cells [22]. It is preferable that cells initially isolated and sorted by the marker of interest are directly from a patient sample. This has proven challenging, as the process of separating a solid tumor into single cells by mechanical and/or chemical dissociation can be traumatic to the cells if not performed carefully and with well-organized coordination with clinicians, especially when the cells of interest comprise a small percentage of the total tumor.

Which populations represent ovarian cancer stem cells?

Attempts at identification of the CSC population began by isolating cells by markers shown to have CSC properties in other tumors. The evidence behind these markers has been well-described in other review articles [23] and is summarized in Table 2. Some markers are based on functional assays, such as the "side population" (SP), a population of cells expressing ABCG2 (aka breast cancer resistance protein-1); or the ALDEFLUOR assay, which identifies cells with active ALDH1A1 enzyme. This same ALDEFLUOR assay is commonly used to isolate bone marrow stem cells for stem cell transplants [23]. Other isolated populations are based on surface expression of proteins, such as CD133, CD44, and c-kit. CD44 is a receptor for the extracellular matrix component hyaluronic acid, which after binding activates several intracellular survival pathways [24]. C-kit is the receptor for stem cell factor (SCF) that has represented one of the more significant treatment successes in cancers with clonal overexpression of c-kit [25]. Interestingly, the protein most consistently identifying a CSC across different tumor types, CD133, is perhaps the least well understood in its functionality. In some cases, increased expression of these populations is associated with poor survival [26–28], but this has not consistently been the case [29,30]. These studies have been conducted in a variety of cell types including patient tumor samples, patient ascitic samples and cancer cell lines, which may contribute to the heterogeneity of the results. It should be noted that it is unknown if timing of CSC isolation (i.e., before or after surgery or other therapy) affects the ability to isolate, or even the very characteristics of, the population. Indeed, exposure to such stressors of tissue processing or exposure to chemotherapy may induce some stem cell pathways as survival mechanisms. It is for this reason that studies in multiple settings (i.e., use of both in vitro and ex vivo methods) and by several investigators allow the greatest confidence that a putative population does have stem cell properties.

Clinical significance of cancer stem cells

Investigators have successfully identified several cell subpopulations that exhibit aggressive features in experimental ex vivo conditions, but mediators of tumorigenicity in immunocompromised mice are likely different than mediators of chemoresistance in women with ovarian cancer. An important question remains: are these populations also playing a role in outcomes and chemoresistance in patient tumors?

A few studies have examined patient samples to begin to address this question. Correlation between density of CSCs and poor outcome has been observed in the side population [31] and with expression of CD44 [30], CD133[27,29], or ALDH1 [26]. Aktas et al. compared blood samples from healthy patients and patients with metastatic breast cancer, looking for circulating tumor cells (CTCs) positive for markers of epithelial–mesenchymal transition (EMT) and ALDH1 [32]. They theorized that circulating tumor cells are likely responsible for metastasis and that they have characteristics similar to cancer stem cells. They found that healthy women were negative for circulating breast tumor cells with expression of ALDH1, the EMT marker EpCam, MUC-1, and HER2 transcripts. Not all breast cancer samples were positive for CTCs, but in those that were, there was a correlation between expression of EMT markers and ALDH1 with response to treatment. 74% of women who did not respond to treatment were found to have EMT markers, ALDH1 or both, while only 10% of responders had the same profile. This suggests that circulating tumor cells with stem cell markers have prognostic value. Iinuma and colleagues performed a similar analysis on CTCs in patients with colorectal cancer, using the markers CEA, cytokeratin 19, cytokeratin 20, and CD133 [33]. They found that expression of one or several of these markers positively correlated with increasing Dukes' stage as well as colon cancer recurrence after adjuvant chemotherapy. While definitive conclusions regarding the relationship between CTC and cancer stem cells cannot be made from these data, they strongly suggest that a subpopulation of CTCs with stem cell

Table 2
Putative ovarian cancer stem cell markers with enhanced tumorigenicity.

Marker	Endpoint	Reference
CD133+	Increased tumorigenic efficiency (cell lines, primary tumor, ascites, xenograft tumor)	Baba et al. [65] and Curley et al. [66]
	Enhanced vasculogenesis (cell lines, primary tumor, ascites, xenograft tumor)	Kusumbe et al. [67] and Silva et al. [27]
CD44+/MyD88+	Increased tumorigenesis; spheroid formation; chemoresistance (ascites, cell lines)	Alvero et al. [68]
CD44+/CD117+	Increased tumorigenesis; chemoresistance (primary tumor, xenograft tumors)	Zhang et al. [69]
CD44+/CD24−	Spheroid formation; recapitulate parental tumor (cell lines)	Shi et al. [70]
CD44+/CD24+	Increased tumorigenesis (primary tumor, xenograft tumor)	Gao et al. [71]
ALDH1A1+	Increased tumorigenesis; pluripotency (cell lines)	Landen et al. [26]
ALDH1A1+/CD133+	Increased tumorigenesis; chemoresistance (cell lines, primary tumor, xenograft tumor)	Silva et al. [27]
	Increased tumorigenesis; self-renewal (primary tumor)	Kryczek et al. [72]
ABCG2 (Side pop'n)	Increased tumorigenesis (cell lines (murine and human), ascites)	Szotek et al. [36]
	Increased tumorigenesis; chemoresistance (cell lines, ascites, xenograft tumor)	Hu et al. [73]
	Increased tumorigenesis; chemoresistance; self-renewal (cell lines, xenograft tumor)	Dou et al. [74]
	Chemoresistance (cell lines)	Kobayashi et al. [61]

markers exists and elevated levels correlate with poorer clinical outcome.

In ovarian cancer, Rizzo and colleagues examined cells in malignant ascites for the percentage of side-population cells. Ascites from patients who had recurred after first-line platinum therapy was enriched with side-population cells as compared to ascites from chemonaïve patients. Sequential ascitic samples from 3 patients who recurred showed a progressive increase in the percentage of side population cells, implying that cytotoxic agents select for side-population cells [31].

One method to examine a subpopulation for an association with chemoresistance is to compare pre- and post-treatment specimens for changes with the exposure. Kulkarni-Datar showed that CD133/Sca-1 cells persist in tumors treated with carboplatin and paclitaxel treatment, and maintain their tumor-initiating properties [34]. Steg et al. measured expression of stem cell markers in a cohort of matched primary and recurrent tumor patient samples, on the premise that if CSCs are an important population to target, they should represent a denser population within recurrent chemoresistant tumors [35]. Tumors taken at the time of primary cytoreductive surgery showed significant heterogeneity in expression of ALDH1A1, CD44, and CD133, but persistent tumors collected soon after treatment with chemotherapy showed a much higher density of these markers. Other pathways postulated to be important in maintenance of "stemness" such as TGF-beta, Notch, Wnt, and Hedgehog were also upregulated in the recurrent samples as compared to their matched primary samples. While the recurrent patient samples did not show uniform increases in all stem cell markers, all samples showed an increase in at least one marker, once again suggesting that the ovarian CSC population may be quite heterogeneous between patients. Interestingly, in recurrent tumors that were collected at the time of a first clinically apparent recurrence, the density of the CSC populations was similar to the density in the original primary untreated tumor, supporting the hypothesis that these populations can give rise to more differentiated, marker-negative populations that comprise the bulk of the tumor mass. Of note, while the recognized CSC populations were higher in chemoresistant tumors, they still did not make up greater than 75% of the tumor mass, suggesting that we have still not discovered the absolute population that survives traditional treatment.

Targeting cancer stem cells

Given emerging data that cancer stem cells contribute to chemoresistance and clinical outcome, efforts are being made to specifically target this subpopulation. Szotek found that the dye-effluxing side-population isolated from a mouse ovarian cancer cell line was growth-inhibited after treatment with Mullerian-inhibiting substance [36]. Wei and colleagues separated human ovarian cancer cells into unsorted, non-side population, and side-population groups; then treated each with Mullerian-inhibiting substance, doxorubicin and cisplatin. They found that treating unsorted cells with cytotoxic agents enriched the population for side population cells; they also saw that non-side population cells were sensitive to chemotherapy and that side population cells were not. Interestingly, side population cells were inhibited at a much lower dose than non-side population cells when treated with Mullerian-inhibiting substance, giving rationale for exploring a two-pronged treatment strategy in ovarian cancer: one targeted towards the larger, non-CSC population, and the other towards the more quiescent, traditionally chemoresistant CSC population [37].

The hyaluronic acid receptor CD44 has also been explored as a therapeutic target. Bourguignon et al. have demonstrated that the CD44–hyaluronan complex activates Nanog, an embryonic stem cell transcription factor important in maintaining self-renewal and pluripotency [38]. Downstream effects of Nanog include activation of the drug efflux pump MDR1, giving a plausible link between stem-cell marker and chemoresistance. Slomiany and colleagues separated CD44+ cells into CD133-high- and low-expression groups [39]. They found that while the total levels of CD44 were not different between the two groups, the CD133-high cells were associated with high levels of receptor tyrosine kinases, drug and lactate transporters, and emmprin (a matrix metalloproteinase inducer). Interfering with the CD44–hyaluronan complex with small hyaluronan oligosaccharides diminished drug-effluxing capacity and tumorigenicity. Using CD44 to identify cells with high claudin-4 expression, Casagrande et al. exploited claudin-4's high affinity for Clostridium perfringens enterotoxin to selectively kill CD44-positive cells in vitro and in vivo [40]. Impressively, 50% of mice treated with sublethal doses of the enterotoxin had a complete, durable response after 8 treatments. Nanoparticle delivery of siRNA to mediate downregulation of both CD44 and ALDH1A1 expression reduced tumor growth either alone or in combination with chemotherapy [26,41].

If aggressive subpopulations of cells are identified by markers of stemness, it follows that targeting pathways mediating stem cell biology may also be effective, such as Notch, Hedgehog, Wnt, and TGF-beta pathways. The Notch pathway is a highly conserved cell-fate pathway important in embryogenesis and angiogenesis. Park and colleagues found that the Notch pathway, particularly Notch3, was upregulated in approximately 20% of ovarian cancers and may function as an oncogene [42]. They demonstrated increased apoptosis and decreased cellular proliferation by targeting Notch with siRNA and a pan-Notch inhibitor. McAuliffe et al. also found that ovarian CSCs could be specifically targeted with gamma-secretase inhibitors or Notch3-specific siRNA, and when combined with cisplatin the entire pool of CSCs was eliminated [43]. Steg et al. showed that targeting Jagged1, a Notch ligand, restored chemosensitivity in taxane-resistant cells, in part through anti-angiogenic effects [35]. Surprisingly, they also found that the mechanism of chemoresistance through Jagged1 is likely Notch-independent and is mediated at least in part through crosstalk with the Hedgehog transcription factor Gli-2. Similar restoration of chemosensitivity has also been demonstrated by targeting the Hedgehog pathway with clinically available Smoothened inhibitors [44], and is effective in reducing spheroid-forming capacity of cells in differentiating–inhibiting media [45]. The Wnt pathway contributes to platinum resistance and can also be used to sensitize cells to platinum agents, either by downregulation of individual components of the pathway such as Wnt2B [46] or by using the c-kit inhibitor imatinib, which blocks Wnt signaling [47]. Indeed many targeted therapies that failed as single agents may have more efficacy if used in combination with chemotherapy, as chemoresistance pathways are reduced. The complexity of interactions between these developmental pathways remains to be elucidated, but may prove clinically useful.

One of the defining characteristics of cancer stem cells is quiescence, which renders them relatively insensitive to traditional chemotherapy agents that depend on rapid cell cycling to induce cell death. Wnt5A was found to induce senescence in ovarian cancer cells [48]. Bioenergetics, the study of mitochondrial metabolism, is an emerging field of inquiry that looks at an alternate route to apoptosis besides DNA damage, which may allow specific targeting of cancer stem cells. Alvero and colleagues used a novel isoflavone, NV-128, to depress mitochondrial function in CD44+/MyD88+ ovarian cancer stem cells [49]. This led to inhibition of the mTOR pathway and loss of mitochondrial membrane potential that in turn led to caspase-independent cell death. The same group had previously shown decreased tumor growth in a murine model with NV-128, in which apoptosis was induced in both the general cancer population and the cancer stem cell population, without significant murine toxicity [50].

A major control on normal stem cell differentiation lies in epigenetic regulators. Controls on methylation of CpG islands on gene promoters, acetylation of histones to control chromatin unwinding, and gene regulation through microRNA production are important for understanding tumorigenesis and potential targets for therapy. Excellent reviews on this topic as it applies to ovarian cancer are available [51,52], but epigenetics may play a particularly important role in targeting the cancer stem cell population. A comprehensive analysis of methylation profiles

found the sonic hedgehog pathway to be of particular importance [53], and methylation of several genes in the Notch superfamily is prominent and correlates with poor survival in the TCGA dataset [54]. Recent work by Matei et al. showed that hypomethylation via low-dose decitabine can restore chemosensitivity in platinum-resistant ovarian cancer, suggesting reversal of drug evasion characteristic of cancer stem cells [55]. Targeting ovarian cancer epigenetic processes both globally and at the individual gene level has shown promise in numerous preclinical studies [55–57].

Immunotherapy has garnered much attention in the treatment of cancer. Interferon alpha has both anti-viral and anti-tumor effects and has had varying success in the treatment of leukemias and solid tumors, including gynecologic cancers [58,59]. Moserle has demonstrated that interferon-alpha selectively targets side population cells [60]. Kobayashi found that the side population was increased in paclitaxel-resistant ovarian cancer cell lines, and that interferon-alpha strongly induced apoptosis in those cells, but not in cells that were paclitaxel-sensitive [61]. With new insights into the biology of ovarian cancer stem cells, interferon-alpha may be rationally reintroduced as targeted therapy against such side population cells.

Another form of immunotherapy that has gained traction is specific cancer stem cell-targeted dendritic cell vaccination. Pellegatta and colleagues demonstrated that dendritic cells exposed to glioma neurospheres cured up to 80% of mice injected with the same cell line [62]. Xu et al. loaded dendritic cells with glioblastoma cancer stem-like cells and found that cytotoxic T-cell response against the CSCs was increased, prolonging survival in mice [63]. Weng applied similar techniques when looking at immunoresponse to dendritic cells fused with ovarian cancer stem-like cells. Using CD44 and CD24 as sorting antigens, this group isolated CSCs then fused them with dendritic cells. These fusion cells were incubated with T-lymphocytes, which in turn were incubated with unsorted ovarian cancer cells and CD44+ cells from the same line, resulting in preferential large-scale lysis of the CD44+ population [64]. In conjunction with current investigations to develop individualized in vivo ovarian cancer models, inducing a vaccine-generated response against ovarian cancer stem cells is a new treatment prospect in the quest for personalized medicine.

The most effective method of targeting the CSC population still remains to be elucidated. As described above, there are numerous points in CSC biologic pathways that can serve as therapeutic targets. If the CSC population changes in response to treatment, or if there are multiple populations with stem-cell properties, it may be that a multi-agent approach would be required. Some have argued that cells that gain stem cell properties in response to stressors do not truly fit the definition of an inherent "stem cells." Like the epithelial-to-mesenchymal transition postulated to contribute to cancer metastasis, CSC pathways may be inducible, allowing certain cells to survive therapy. Regardless, if these cells are responsible for recurrence, specifically targeting that population (or populations) should be an effective therapeutic strategy. It is yet unknown when is the best timing of administering biologic drugs that specifically treat CSCs. More research is needed to determine if these therapies are most effective when used in combination with traditional cytotoxic chemotherapy, or if they are most effective in a maintenance role. Novel trial designs will be needed to incorporate new therapeutics in the scenario at which targeting these populations is most likely to provide significant clinical benefit —that being at the time of primary therapy, or when these population are at their minimal volume, at the completion of primary therapy.

Conclusion

Evidence is accumulating that stem cell pathways are important drivers of carcinogenesis in ovarian cancer and potential targets for therapy. The natural course of this disease suggests that there is a small subpopulation of cells that is chemotherapy-resistant and is able to repopulate the tumor. As more is discovered regarding ovarian cancer stem cell biology, more can be applied in the clinical setting. However, significant challenges remain. Cancer stem-like cells comprise a very small percentage of the total tumor burden, making them challenging to identify. Most translational studies examine only tissue specimens taken at the time of primary surgery, in which the vast majority of cells are going to be killed by primary chemotherapy, and thus not the population we need to be targeting. Small but important populations can easily be missed. It would be exceedingly valuable to incorporate biopsies of recurrent specimens into clinical trials and studies attempting to develop personalized therapies, since by definition the recurrent tumor is more densely composed of chemoresistant cells. There is no consensus regarding a universal marker (or set of markers) that can identify the treatment-resistant population in ovarian cancer (or any malignancy). Indeed, given the numbers of genes that are dysregulated in ovarian cancer, it is possible that there are numerous combinations of markers that vary not only by histology, but also in individual patients. By their very nature, cancer stem cells evade therapy through mechanisms such as the ABCG2 transporter and ALDH1A1 enzyme, which makes chemical targeting of these cells quite difficult. The importance of pathways stem cells preferentially use, such as Wnt, Notch, and Hedgehog, is under clinical investigation. While the most chemoresistant population may not be absolutely identified with markers currently recognized, it appears clear that stem cell pathways contribute to survival, and that these populations must be targeted in order to achieve durable cures in this deadly disease.

Conflict of interest statement

The authors have no conflicts of interest.

References

[1] Siegel R, Naishadham D, Jemal A. Cancer statistics, 2013. CA Cancer J Clin Jan 2013;63(1):11–30 (PubMed PMID: 23335087).
[2] Society AC. Colorectal cancer statistics: American Cancer Society; 2011 [cited]; 2011 November 1.
[3] Society AC. Pancreatic cancer statistics: American Cancer Society; 2011 [cited]; November 1, 2011.
[4] Yap TA, Gerlinger M, Futreal PA, Pusztai L, Swanton C. Intratumor heterogeneity: seeing the wood for the trees. Sci Transl Med Mar 28, 2012;4(127) (127ps10. PubMed PMID: 22461637).
[5] Lapidot T, Sirard C, Vormoor J, Murdoch B, Hoang T, Caceres-Cortes J, et al. A cell initiating human acute myeloid leukaemia after transplantation into SCID mice. Nature Feb 17, 1994;367(6464):645–8 (PubMed PMID: 7509044. Epub 1994/02/17. eng.).
[6] Foster R, Buckanovich RJ, Rueda BR. Ovarian cancer stem cells: working towards the root of stemness. Cancer Lett Sep 10, 2013;338(1):147–57 (PubMed PMID: 23138176).
[7] Magee JA, Piskounova E, Morrison SJ. Cancer stem cells: impact, heterogeneity, and uncertainty. Cancer Cell Mar 20, 2012;21(3):283–96 (PubMed PMID: 22439924).
[8] Sundfeldt K, Piontkewitz Y, Ivarsson K, Nilsson O, Hellberg P, Brannstrom M, et al. E-cadherin expression in human epithelial ovarian cancer and normal ovary. Int J Cancer Jun 20, 1997;74(3):275–80 (PubMed PMID: 9221804).
[9] Auersperg N, Pan J, Grove BD, Peterson T, Fisher J, Maines-Bandiera S, et al. E-cadherin induces mesenchymal-to-epithelial transition in human ovarian surface epithelium. Proc Natl Acad Sci U S A May 25, 1999;96(11):6249–54 (PubMed PMID: 10339573. Pubmed Central PMCID: 26867. Epub 1999/05/26. eng).
[10] Bowen NJ, Walker LD, Matyunina LV, Logani S, Totten KA, Benigno BB, et al. Gene expression profiling supports the hypothesis that human ovarian surface epithelia are multipotent and capable of serving as ovarian cancer initiating cells. BMC Med Genet 2009;2(71) (PubMed PMID: 20040092. Pubmed Central PMCID: 2806370. Epub 2009/12/31. eng).
[11] Szotek PP, Chang HL, Brennand K, Fujino A, Pieretti-Vanmarcke R, Lo Celso C, et al. Normal ovarian surface epithelial label-retaining cells exhibit stem/progenitor cell characteristics. Proc Natl Acad Sci U S A Aug 26, 2008;105(34):12469–73 (PubMed PMID: 18711140. Pubmed Central PMCID: 2527935).
[12] Auersperg N. The stem-cell profile of ovarian surface epithelium is reproduced in the oviductal fimbriae, with increased stem-cell marker density in distal parts of the fimbriae. Int J Gynecol Pathol Jul 25, 2013;32(5) (PubMed PMID: 23896717).
[13] Humphries A, Cereser B, Gay LJ, Miller DS, Das B, Gutteridge A, et al. Lineage tracing reveals multipotent stem cells maintain human adenomas and the pattern of clonal expansion in tumor evolution. Proc Natl Acad Sci U S A Jul 2, 2013;110(27):E2490–9 (PubMed PMID: 23766371. Pubmed Central PMCID: 3704042).
[14] Cobaleda C, Jochum W, Busslinger M. Conversion of mature B cells into T cells by dedifferentiation to uncommitted progenitors. Nature Sep 27, 2007;449(7161):473–7 (PubMed PMID: 17851532).
[15] Xie H, Ye M, Feng R, Graf T. Stepwise reprogramming of B cells into macrophages. Cell May 28, 2004;117(5):663–76 (PubMed PMID: 15163413).

[16] Tata PR, Mou H, Pardo-Saganta A, Zhao R, Prabhu M, Law BM, et al. Dedifferentiation of committed epithelial cells into stem cells in vivo. Nature Nov 14, 2013;503(7475):218–23 (PubMed PMID: 24196716).
[17] Singh SK, Hawkins C, Clarke ID, Squire JA, Bayani J, Hide T, et al. Identification of human brain tumour initiating cells. Nature Nov 18, 2004;432(7015):396–401 (PubMed PMID: 15549107. eng.).
[18] Al-Hajj M, Wicha MS, Benito-Hernandez A, Morrison SJ, Clarke MF. Prospective identification of tumorigenic breast cancer cells. Proc Natl Acad Sci U S A Apr 1, 2003;100(7):3983–8 (PubMed PMID: 12629218. Pubmed Central PMCID: 153034. Epub 2003/03/12. eng).
[19] Dobbin Z, Landen C. Isolation and characterization of potential cancer stem cells from solid human tumors — potential applications. Curr Protoc Pharmacol 2013;63(14) (in press).
[20] Bapat SA, Mali AM, Koppikar CB, Kurrey NK. Stem and progenitor-like cells contribute to the aggressive behavior of human epithelial ovarian cancer. Cancer Res Apr 15, 2005;65(8):3025–9 (PubMed PMID: 15833827).
[21] Liu T, Cheng W, Lai D, Huang Y, Guo L. Characterization of primary ovarian cancer cells in different culture systems. Oncol Rep May 2010;23(5):1277–84 (PubMed PMID: 20372841).
[22] Reya T, Morrison SJ, Clarke MF, Weissman IL. Stem cells, cancer, and cancer stem cells. Nature Nov 1, 2001;414(6859):105–11 (PubMed PMID: 11689955. Epub 2001/11/02. eng.).
[23] Abitorabi MA, Pachynski RK, Ferrando RE, Tidswell M, Erle DJ. Presentation of integrins on leukocyte microvilli: a role for the extracellular domain in determining membrane localization. J Cell Biol Oct 20, 1997;139(2):563–71 (PubMed PMID: 9334357).
[24] Zoller M. CD44: can a cancer-initiating cell profit from an abundantly expressed molecule? Nat Rev Cancer Apr 2011;11(4):254–67 (PubMed PMID: 21390059).
[25] Lennartsson J, Ronnstrand L. The stem cell factor receptor/c-Kit as a drug target in cancer. Curr Cancer Drug Targets Feb 2006;6(1):65–75 (PubMed PMID: 16475976).
[26] Landen Jr CN, Goodman B, Katre AA, Steg AD, Nick AM, Stone RL, et al. Targeting aldehyde dehydrogenase cancer stem cells in ovarian cancer. Mol Cancer Ther Dec 2010;9(12):3186–99 (PubMed PMID: 20889728. Pubmed Central PMCID: 3005138).
[27] Silva IA, Bai S, McLean K, Yang K, Griffith K, Thomas D, et al. Aldehyde dehydrogenase in combination with CD133 defines angiogenic ovarian cancer stem cells that portend poor patient survival. Cancer Res May 24, 2011;71(11):3991–4001 (PubMed PMID: 21498635. Epub 2011/04/19. Eng).
[28] Deng S, Yang X, Lassus H, Liang S, Kaur S, Ye Q, et al. Distinct expression levels and patterns of stem cell marker, aldehyde dehydrogenase isoform 1 (ALDH1), in human epithelial cancers. PLoS One 2010;5(4):e10277 (PubMed PMID: 20422001. Pubmed Central PMCID: 2858084. Epub 2010/04/28. eng).
[29] Zhang J, Guo X, Chang DY, Rosen DG, Mercado-Uribe I, Liu J. CD133 expression associated with poor prognosis in ovarian cancer. Mod Pathol Nov 11, 2011;25(3):456–64 (PubMed PMID: 22080056. Epub 2011/11/15. Eng).
[30] Steffensen KD, Alvero AB, Yang Y, Waldstrom M, Hui P, Holmberg JC, et al. Prevalence of epithelial ovarian cancer stem cells correlates with recurrence in early-stage ovarian cancer. J Oncol 2011;2011:620523 (PubMed PMID: 21904548. Pubmed Central PMCID: 3166719. Epub 2011/09/10. eng).
[31] Rizzo S, Hersey JM, Mellor P, Dai W, Santos-Silva A, Liber D, et al. Ovarian cancer stem cell-like side populations are enriched following chemotherapy and overexpress EZH2. Mol Cancer Ther Feb 2011;10(2):325–35 (PubMed PMID: 21216927. Pubmed Central PMCID: 3037846. Epub 2011/01/11. eng).
[32] Aktas B, Tewes M, Fehm T, Hauch S, Kimmig R, Kasimir-Bauer S. Stem cell and epithelial-mesenchymal transition markers are frequently overexpressed in circulating tumor cells of metastatic breast cancer patients. Breast Cancer Res 2009;11(4):R46 (PubMed PMID: 19589136. Pubmed Central PMCID: 2750105. Epub 2009/07/11. eng).
[33] Iinuma H, Watanabe T, Mimori K, Adachi M, Hayashi N, Tamura J, et al. Clinical significance of circulating tumor cells, including cancer stem-like cells, in peripheral blood for recurrence and prognosis in patients with Dukes' stage B and C colorectal cancer. J Clin Oncol Apr 20, 2011;29(12):1547–55 (PubMed PMID: 21422427. Epub 2011/03/23. eng).
[34] Kulkarni-Datar K, Orsulic S, Foster R, Rueda BR. Ovarian tumor initiating cell populations persist following paclitaxel and carboplatin chemotherapy treatment in vivo. Cancer Lett Jun 18, 2013;339(2):237–46 (PubMed PMID: 23791886).
[35] Steg AD, Bevis KS, Katre AA, Ziebarth A, Dobbin ZC, Alvarez RD, et al. Stem cell pathways contribute to clinical chemoresistance in ovarian cancer. Clin Cancer Res Feb 1, 2012;18(3):869–81 (PubMed PMID: 22142828. Pubmed Central PMCID: 3271164).
[36] Szotek PP, Pieretti-Vanmarcke R, Masiakos PT, Dinulescu DM, Connolly D, Foster R, et al. Ovarian cancer side population defines cells with stem cell-like characteristics and Mullerian Inhibiting Substance responsiveness. Proc Natl Acad Sci U S A Jul 25, 2006;103(30):11154–9 (PubMed PMID: 16849428. eng).
[37] Wei X, Dombkowski D, Meirelles K, Pieretti-Vanmarcke R, Szotek PP, Chang HL, et al. Mullerian inhibiting substance preferentially inhibits stem/progenitors in human ovarian cancer cell lines compared with chemotherapeutics. Proc Natl Acad Sci U S A Nov 2, 2010;107(44):18874–9 (PubMed PMID: 20952655. Pubmed Central PMCID: 2973919. Epub 2010/10/19. eng).
[38] Bourguignon LY, Peyrollier K, Xia W, Hyaluronan Gilad E. CD44 interaction activates stem cell marker Nanog, Stat-3-mediated MDR1 gene expression, and ankyrin-regulated multidrug efflux in breast and ovarian tumor cells. J Biol Chem Jun 20, 2008;283(25):17635–51 (PubMed PMID: 18441325. Pubmed Central PMCID: 2427357. Epub 2008/04/29. eng).
[39] Slomiany MG, Dai L, Tolliver LB, Grass GD, Zeng Y, Toole BP. Inhibition of functional hyaluronan–CD44 interactions in CD133-positive primary human ovarian carcinoma cells by small hyaluronan oligosaccharides. Clin Cancer Res Dec 15, 2009;15(24):7593–601 (PubMed PMID: 19996211. Pubmed Central PMCID: 2794991. Epub 2009/12/10. Eng).
[40] Casagrande F, Cocco E, Bellone S, Richter CE, Bellone M, Todeschini P, et al. Eradication of chemotherapy-resistant CD44+ human ovarian cancer stem cells in mice by intraperitoneal administration of clostridium perfringens enterotoxin. Cancer Jun 20, 2011;117(24):5519–28 (PubMed PMID: 21692061. Epub 2011/06/22. Eng).
[41] Shah V, Taratula O, Garbuzenko GO, Taratula OR, Rodriguez-Rodriguez L, Minko T. Targeted nanomedicine for suppression of CD44 and simultaneous cell death induction in ovarian cancer: an optimal delivery of siRNA and anticancer drug. Clin Cancer Res Sep 13, 2013;19(22):6193–204 (PubMed PMID: 24036854).
[42] Park JT, Li M, Nakayama K, Mao TL, Davidson B, Zhang Z, et al. Notch3 gene amplification in ovarian cancer. Cancer Res Jun 15, 2006;66(12):6312–8 (PubMed PMID: 16778208. eng).
[43] McAuliffe SM, Morgan SL, Wyant GA, Tran LT, Muto KW, Chen YS, et al. Targeting Notch, a key pathway for ovarian cancer stem cells, sensitizes tumors to platinum therapy. Proc Natl Acad Sci U S A Oct 23, 2012;109(43):E2939–48 (PubMed PMID: 23019585. Pubmed Central PMCID: 3491453).
[44] Steg AD, Katre AA, Bevis KS, Ziebarth A, Dobbin ZC, Shah MM, et al. Smoothened antagonists reverse taxane resistance in ovarian cancer. Mol Cancer Ther Jul 2012;11(7):1587–97 (PubMed PMID: 22553355. Pubmed Central PMCID: 3392529).
[45] Ray A, Meng E, Reed E, Shevde LA, Rocconi RP. Hedgehog signaling pathway regulates the growth of ovarian cancer spheroid forming cells. Int J Oncol Oct 2011;39(4):797–804 (PubMed PMID: 21701772).
[46] Wang H, Fan L, Xia X, Rao Y, Ma Q, Yang J, et al. Silencing Wnt2B by siRNA interference inhibits metastasis and enhances chemotherapy sensitivity in ovarian cancer. Int J Gynecol Cancer Jun 2012;22(5):755–61 (PubMed PMID: 22635028).
[47] Chau WK, Ip CK, Mak AS, Lai HC, Wong AS. c-Kit mediates chemoresistance and tumor-initiating capacity of ovarian cancer cells through activation of Wnt/beta-catenin-ATP-binding cassette G2 signaling. Oncogene May 30, 2013;32(22):2767–81 (PubMed PMID: 22797058).
[48] Bitler BG, Nicodemus JP, Li H, Cai Q, Wu H, Hua X, et al. Wnt5a suppresses epithelial ovarian cancer by promoting cellular senescence. Cancer Res Aug 4, 2011;71(19):6184–94 (PubMed PMID: 21816908. Epub 2011/08/06. Eng).
[49] Alvero AB, Montagna MK, Holmberg JC, Craveiro V, Brown D, Mor G. Targeting the mitochondria activates two independent cell death pathways in ovarian cancer stem cells. Mol Cancer Ther Aug 2011;10(8):1385–93 (PubMed PMID: 21677151. Epub 2011/06/17. eng).
[50] Alvero AB, Montagna MK, Chen R, Kim KH, Kyungjin K, Visintin I, et al. NV-128, a novel isoflavone derivative, induces caspase-independent cell death through the Akt/mammalian target of rapamycin pathway. Cancer Jul 15, 2009;115(14):3204–16 (PubMed PMID: 19472400. Pubmed Central PMCID: 2757274. Epub 2009/05/28. eng).
[51] Chen H, Hardy TM, Tollefsbol TO. Epigenomics of ovarian cancer and its chemoprevention. Front Genet 2011;2(67) (PubMed PMID: 22303362. Pubmed Central PMCID: 3268620).
[52] Balch C, Fang F, Matei DE, Huang TH, Nephew KP. Minireview: epigenetic changes in ovarian cancer. Endocrinology Sep 2009;150(9):4003–11 (PubMed PMID: 19574400. Pubmed Central PMCID: 2736079).
[53] Huang RL, Gu F, Kirma NB, Ruan J, Chen CL, Wang HC, et al. Comprehensive methylome analysis of ovarian tumors reveals hedgehog signaling pathway regulators as prognostic DNA methylation biomarkers. Epigenetics May 10, 2013;8(6) (PubMed PMID: 23774800).
[54] Ivan C, Hu W, Bottsford-Miller J, Zand B, Dalton HJ, Liu T, et al. Epigenetic analysis of the Notch superfamily in high-grade serous ovarian cancer. Gynecol Oncol Mar 2013;128(3):506–11.
[55] Matei D, Fang F, Shen C, Schilder J, Arnold A, Zeng Y, et al. Epigenetic resensitization to platinum in ovarian cancer. Cancer Res May 1, 2012;72(9):2197–205 (PubMed PMID: 22549947. Pubmed Central PMCID: 3700422).
[56] Hu S, Yu L, Li Z, Shen Y, Wang J, Cai J, et al. Overexpression of EZH2 contributes to acquired cisplatin resistance in ovarian cancer cells in vitro and in vivo. Cancer Biol Ther Oct 15, 2010;10(8):788–95 (PubMed PMID: 20686362).
[57] Yang C, Cai J, Wang Q, Tang H, Cao J, Wu L, et al. Epigenetic silencing of miR-130b in ovarian cancer promotes the development of multidrug resistance by targeting colony-stimulating factor 1. Gynecol Oncol Feb 2012;124(2):325–34.
[58] Alberts DS, Hannigan EV, Liu PY, Jiang C, Wilczynski S, Copeland L, et al. Randomized trial of adjuvant intraperitoneal alpha-interferon in stage III ovarian cancer patients who have no evidence of disease after primary surgery and chemotherapy: an intergroup study. Gynecol Oncol Jan 2006;100(1):133–8.
[59] Berek JS, Markman M, Blessing JA, Kucera PR, Nelson BE, Anderson B, et al. Intraperitoneal alpha-interferon alternating with cisplatin in residual ovarian carcinoma: a phase II Gynecologic Oncology Group study. Gynecol Oncol Jul 1999;74(1):48–52.
[60] Moserle L, Indraccolo S, Ghisi M, Frasson C, Fortunato E, Canevari S, et al. The side population of ovarian cancer cells is a primary target of IFN-alpha antitumor effects. Cancer Res Jul 15, 2008;68(14):5658–68 (PubMed PMID: 18632618. Epub 2008/07/18. eng).
[61] Kobayashi Y, Seino K, Hosonuma S, Ohara T, Itamochi H, Isonishi S, et al. Side population is increased in paclitaxel-resistant ovarian cancer cell lines regardless of resistance to cisplatin. Gynecol Oncol May 1, 2011;121(2):390–4.
[62] Pellegatta S, Poliani PL, Corno D, Menghi F, Ghielmetti F, Suarez-Merino B, et al. Neurospheres enriched in cancer stem-like cells are highly effective in eliciting a

dendritic cell-mediated immune response against malignant gliomas. Cancer Res Nov 1, 2006;66(21):10247–52 (PubMed PMID: 17079441. Epub 2006/11/03. eng).
[63] Xu Q, Liu G, Yuan X, Xu M, Wang H, Ji J, et al. Antigen-specific T-cell response from dendritic cell vaccination using cancer stem-like cell-associated antigens. (Dayton, Ohio) Stem Cells Aug 2009;27(8):1734–40 (PubMed PMID: 19536809).
[64] Weng D, Song B, Durfee J, Sugiyama V, Wu Z, Koido S, et al. Induction of cytotoxic T lymphocytes against ovarian cancer-initiating cells. Int J Cancer Oct 15, 2011;129(8):1990–2001 (PubMed PMID: 21154809. Epub 2010/12/15. Eng).
[65] Baba T, Convery PA, Matsumura N, Whitaker RS, Kondoh E, Perry T, et al. Epigenetic regulation of CD133 and tumorigenicity of CD133+ ovarian cancer cells. Oncogene Jan 15, 2009;28(2):209–18 (PubMed PMID: 18836486. Epub 2008/10/07. eng).
[66] Curley MD, Therrien VA, Cummings CL, Sergent PA, Koulouris CR, Friel AM, et al. CD133 expression defines a tumor initiating cell population in primary human ovarian cancer. (Dayton, Ohio) Stem Cells Dec 2009;27(12):2875–83 (PubMed PMID: 19816957. Epub 2009/10/10. eng).
[67] Kusumbe AP, Mali AM, Bapat SA. CD133-expressing stem cells associated with ovarian metastases establish an endothelial hierarchy and contribute to tumor vasculature. (Dayton, Ohio) Stem Cells Mar 2009;27(3):498–508 (PubMed PMID: 19253934).
[68] Alvero AB, Chen R, Fu HH, Montagna M, Schwartz PE, Rutherford T, et al. Molecular phenotyping of human ovarian cancer stem cells unravels the mechanisms for repair and chemoresistance. Cell Cycle Jan 1, 2009;8(1):158–66 (PubMed PMID: 19158483. Pubmed Central PMCID: 3041590).
[69] Zhang S, Balch C, Chan MW, Lai HC, Matei D, Schilder JM, et al. Identification and characterization of ovarian cancer-initiating cells from primary human tumors. Cancer Res Jun 1 2008;68(11):4311–20 (PubMed PMID: 18519691. eng).
[70] Shi MF, Jiao J, Lu WG, Ye F, Ma D, Dong QG, et al. Identification of cancer stem cell-like cells from human epithelial ovarian carcinoma cell line. Cell Mol Life Sci Nov 2010;67(22):3915–25 (PubMed PMID: 20549538. Epub 2010/06/16. eng).
[71] Gao MQ, Choi YP, Kang S, Youn JH, Cho NH. CD24+ cells from hierarchically organized ovarian cancer are enriched in cancer stem cells. Oncogene May 6, 2010;29(18):2672–80 (PubMed PMID: 20190812. Epub 2010/03/02. eng).
[72] Kryczek I, Liu S, Roh M, Vatan L, Szeliga W, Wei S, et al. Expression of aldehyde dehydrogenase and CD133 defines ovarian cancer stem cells. Int J Cancer Jan 1, 2012;130(1):29–39 (PubMed PMID: 21480217. Pubmed Central PMCID: 3164893).
[73] Hu L, McArthur C, Jaffe RB. Ovarian cancer stem-like side-population cells are tumourigenic and chemoresistant. Br J Cancer Apr 13, 2010;102(8):1276–83 (PubMed PMID: 20354527. Pubmed Central PMCID: 2856005. Epub 2010/04/01. eng).
[74] Dou J, Jiang C, Wang J, Zhang X, Zhao F, Hu W, et al. Using ABCG2-molecule-expressing side population cells to identify cancer stem-like cells in a human ovarian cell line. Cell Biol Int Mar 1, 2011;35(3):227–34 (PubMed PMID: 21108606. Epub 2010/11/27. eng).

Gynecologic Oncology xxx (2014) xxx–xxx

Contents lists available at ScienceDirect

Gynecologic Oncology

journal homepage: www.elsevier.com/locate/ygyno

An *ex vivo* assay of XRT-induced Rad51 foci formation predicts response to PARP-inhibition in ovarian cancer

Monjri M. Shah [a], Zachary C. Dobbin [a], Somaira Nowsheen [b], Monica Wielgos [b], Ashwini A. Katre [a], Ronald D. Alvarez [a], Panagiotis A. Konstantinopoulos [c], Eddy S. Yang [b], Charles N. Landen [a,*]

[a] Department of Obstetrics and Gynecology, University of Alabama at Birmingham, Birmingham, AL, USA
[b] Department of Radiation Oncology, University of Alabama at Birmingham, Birmingham, AL, USA
[c] Department of Medicine, Dana Farber Cancer Institute, Harvard Medical School, Boston, MA, USA

HIGHLIGHTS

- Homologous recombination (HR) defects are common in ovarian cancer, suggesting a role for PARP inhibitors.
- No predictive assay for HR defects exists, but Rad51 is a reliable marker for HR.
- An *ex-vivo* IR assay using Rad51 foci formation accurately predicts PARP-inhibitor response.

ARTICLE INFO

Article history:
Received 7 February 2014
Accepted 11 May 2014
Available online xxxx

Keywords:
Ovarian cancer
PARP inhibitor
Homologous recombination deficiency
Rad51

ABSTRACT

Objective. *BRCA*-positive ovarian cancer patients derive benefit PARP inhibitors. Approximately 50% of ovarian cancer tumors have homologous recombination (HR) deficiencies and are therefore "BRCA-like," possibly rendering them sensitive to PARP inhibition. However, no predictive assay exists to identify these patients. We sought to determine if irradiation-induced Rad51 foci formation, a known marker of HR, correlated to PARP inhibitor response in an ovarian cancer model.

Methods. Ovarian cancer cell lines were exposed to PARP-inhibitor ABT-888 to determine effect on growth. Rad51 protein expression prior to irradiation was determined *via* Western blot. Cultured cells and patient-derived xenograft tumors (PDX) were irradiated and probed for Rad51 foci. *In vivo* PDX tumors were treated with ABT-888 and carboplatin; these results were correlated with the *ex vivo* ionizing radiation assay.

Results. Three of seven cell lines were sensitive to ABT-888. Sensitive lines had the lowest Rad51 foci formation rate after irradiation, indicating functional HR deficiency. Approximately 50% of the PDX samples had decreased Rad51 foci formation. Total Rad51 protein levels were consistently low, suggesting that DNA damage induction is required to characterize HR status. The *ex vivo* IR assay accurately predicted which PDX models were sensitive to PARP inhibition *in vitro* and *in vivo*. ABT-888 alone reduced orthotopic tumor growth by 51% in A2780ip2 cell line, predicted to respond by the *ex vivo* assay. Three PDX models' response also correlated with the assay.

Conclusions. The *ex vivo* IR assay correlates with response to PARP inhibition. Analysis of total Rad51 protein is not a reliable substitute.

Introduction

Epithelial ovarian cancer is the most lethal gynecologic malignancy in developed nations, with an estimated 14,270 deaths in the United States alone in 2014 [1]. Even though initial treatment with a standard platinum/taxane regimen is effective in about 80% of women diagnosed with advanced stage disease, median progression-free interval is only approximately 18 months, and median 5-year survival is approximately 40% [2,3].

Over the past decade, great strides have been made in understanding the genetic and molecular basis of cancer. In particular, hereditary cancer syndromes have been very important in informing how specific mutations can give rise to cancer and how those mutations can be selectively therapeutically targeted. Hereditary breast and ovarian cancers caused by mutations in the *BRCA1* and *BRCA2* genes, which are important for homologous recombination (HR)-mediated DNA repair when double-stranded DNA breaks (DSB) are encountered [4,5], are

* Corresponding author at: University of Alabama at Birmingham, Department of Obstetrics and Gynecology, 176F RM 10250, 619 19th Street S, Birmingham, AL 35294, USA.
E-mail address: clanden@uabmc.edu (C.N. Landen).

http://dx.doi.org/10.1016/j.ygyno.2014.05.009
0090-8258/

a prime example of this. BRCA-deficient cells are dependent on single-strand break (SSB) DNA-repair pathways. Poly(ADP-ribose)-polymerase (PARP) inhibitors take advantage of this dependence, causing apoptosis through synthetic lethality in cells defective in HR, either through BRCA deficiency or other genetic abnormalities.

An important protein in DNA repair and HR is Rad51 [6]. When complexed with several other proteins including BRCA1 and BRCA2, Rad51 facilitates DNA exchange between sister chromatids at damaged sites, including those induced by irradiation [6–9]. Embryonic lethality is observed in Rad51 knockout mice after exposure to radiation [10,11], suggesting that it is essential in the repair of DSBs. Rad51 foci formation is therefore diminished in cells that have a defect in HR.

Data recently published by The Cancer Genome Atlas (TCGA) group suggests that as many as 50% of patients with high grade serous ovarian cancer have defects in members of the HR pathway [12]. It is postulated that these patients may benefit from PARP inhibitor therapy, similar to patients with *BRCA* mutations. However, an abnormality discovered by mutation analysis or expression profiling does not always translate to functional compromise. A functional assay identifying defective HR may be more accurate in predicting response to PARP inhibition. Such a functional assay might then be utilized to determine whether a biomarker that is clinically feasible to analyze could be used to predict response in the clinical setting. The goal of this study was to determine whether Rad51 foci formation, a well-known functional marker of HR, could identify ovarian cancers that would respond to PARP inhibitor therapy.

Materials and methods

Established ovarian cancer cell lines and patient-derived xenografts

Established human ovarian carcinoma cell lines A2780ip2, SKOV3ip1, HeyA8, ES2, SKOV3TRip2, A2780cp20, and HeyA8MDR were maintained in RPMI-1640 medium supplemented with 10% fetal bovine serum (Hyclone, Logan, UT). The taxane-resistant lines HeyA8MDR and SKOV3TRip2 were maintained in media with paclitaxel 150 ng/ml. All experiments were conducted with cells that were at 70–80% confluence and less than 20 passages from stock. Stock cell lines were confirmed to be the assumed genotype by microsatellite marker testing.

Patient-derived xenografts (PDX) were established from freshly-collected omental tumor nodules. IRB approval was obtained and patients were consented prior to surgery. Omental tumor nodules from newly diagnosed, untreated patients were excised at the time of primary tumor reductive surgery and processed immediately. Under standard anesthesia and sterile conditions, four separate 2 mm^2 tumor sections were implanted in a subcutaneous manner in severe combined immunodeficiency (SCID) mice (NCI-Frederick). Five mice were used per patient sample. When nodules were 0.75 cm in width, they were randomized to treatment as described below. 5 mm adjacent samples were isolated and snap frozen in liquid nitrogen and stored at −80 °C. The PARP inhibitor ABT-888 was kindly provided by AbbVie Pharmaceuticals.

Proliferation assay

To examine the sensitivity of each of the established ovarian cancer cell lines to ABT-888 alone, cells were plated at a density of 2000 cells/well in a 96-well plate. After allowing for attachment overnight, the cells were exposed to increasing concentrations of ABT-888 in triplicate. Cells were allowed to grow for four days, at which time viability was assessed with 0.15% MTT (Sigma). The IC50 of drug was determined by finding the dose at which 50% of cells were killed, determined by the formula [(OD450MAX − OD450MIN) / 2 + OD450MIN]. In separate experiments, cells were exposed to increasing concentrations of carboplatin in combination with fixed ABT-888 doses (determined *a priori* to be the IC25 and IC50 doses) to determine if sublethal doses of ABT-888 could sensitize cells to platinum agents. Synergy was assessed by the curve shift analysis [13] and calculation of the Combination Index based on the Chou–Talalay modification of Loewe's additivity model [14].

Rad51/IR-induced ex vivo assay

HR competency through Rad51 activation was determined in both established ovarian cancer cell lines and primary ovarian cancer samples after challenging with ionizing radiation (IR). Cells were plated on 6-well plates and exposed to 4 Gy or mock IR. Briefly, PDX tumor samples were mechanically dissociated in 1:5 phosphate buffered saline (PBS) and 0.25% trypsin (Hyclone, Logan, UT) using a sterile scalpel. Dissociated samples were plated on 60 mm tissue culture dishes for 1 h to obtain a purer population of tumor cells. The remaining supernatant was removed, and attached cells were trypsinized. Cancer cell concentration was determined by manual counting of a sample treated with trypan blue. 5×10^4 cells per well were plated on collagen-coated coverslips and allowed to grow for 48 h. Cell lines were trypsinized when 70–80% confluent, replated on collagen-coated coverslips at 5×10^4 cells/well of a 6-well plate, and allowed to grow for 48 h. Plates were then exposed to 4 Gy using an X-ray irradiator (Kimtron Inc., Woodbury, CT). 8 h later (based on optimization in previous studies [15,16]), the cells were rinsed with PBS and fixed with 70% ethanol. Cells were then blocked and incubated with anti-Rad51 antibody (Santa Cruz Biotech, Dallas, TX, dilution 1:500). Anti-rabbit Alexa Fluor 594-conjugated antibody (Invitrogen, Grand Island, NY) at a 1:2000 dilution was used as the secondary antibody. DAPI (4′,6-diamidino-2-phenylindole, dihydrochloride) (Invitrogen) was employed for nuclear staining. Coverslips were then mounted on slides and examined for Rad51 foci with fluorescence microscopy (Carl Zeiss, Thornwood, NY). Total cells were counted, and those with ten or more Rad51 foci were considered positive as previously described [15,16].

Western blot

To determine if Rad51 foci formation after IR induction correlated to baseline Rad51 protein levels, Western blot analysis was performed on both PDX and cell line samples. Primary tumor samples corresponding to each PDX were used. 1 mm sections were shaved from each snap frozen sample, then manually dissociated in modified radioimmunoprecipitation assay (RIPA) lysis buffer with a protease inhibitor cocktail (Roche, Manheim, Germany). Immunoblot analysis was conducted *via* standard technique [17] using anti-Rad51 antibody (Santacruz Biotech, Dallas, TX) at 1:1000 dilution overnight at 4 °C. After washing with PBS/1% Tween-20 (PBS-T), blots were incubated with 0.3 μl IRDye goat anti-rabbit secondary antibody (Li-Cor Biosciences, Lincoln, NE) in 5 ml Odyssey blocking buffer (Li-Cor) at room temperature for 1 h. Blots were washed again in PBS-T, then processed with the Odyssey CLx Infrared Imaging System (Li-Cor). To ensure equal sample loading, blots were incubated with mouse-anti-β-actin antibody at 1:20,000 dilution overnight at 4 °C, washed and exposed to 0.3 μl IRDye goat anti-mouse secondary in 5 ml Odyssey blocking buffer (Li-Cor). The development process was the same as detailed above.

Cell lines at 80% confluence were subjected to the same immunoblot analysis with anti-Rad51 antibody but at a dilution of 1:500 at 4 °C overnight. After washing the blot was then incubated with 1:2000 anti-rabbit secondary antibody (Cell Signaling Technology, Danvers, MA) in PBS-T for 1 h at room temperature. After washing with PBS-T, the immunoblots were processed with a Xerox immunoblot developer (Norwalk, CT). Mouse anti-β-actin antibody was used as a sample loading control. The development process was the same as described above.

Please cite this article as: Shah MM, et al, An ex vivo assay of XRT-induced Rad51 foci formation predicts response to PARP-inhibition in ovarian cancer, Gynecol Oncol (2014), http://dx.doi.org/10.1016/j.ygyno.2014.05.009

PARP inhibitor treatment in vivo

Two *in vivo* models were used to study the effects of the PARP inhibitor ABT-888 on tumor progression. All protocols were approved by the Institution Animal Care and Use Committee at the University of Alabama at Birmingham. Mice were cared for in accordance with the American Association for Accreditation of Laboratory Animal Care guidelines. The first model was a cell-line based orthotopic mouse model. Female athymic nude mice (nu-nu) were obtained from the National Cancer Institute Frederick Cancer Research and Development Center (Frederick, MD). SKOV3ip1 and A2780ip2 intraperitoneal (IP) tumors were established by injection of 1×10^6 cells suspended in 200 μl of serum-free RPMI media. Seven days post-injection, mice in the orthotopic ovarian cancer cell line model were stratified into 4 treatment groups: (1) control, (2) ABT-888 alone, (3) carboplatin alone, and (4) carboplatin plus ABT-888. Each group was comprised of 10 mice for a total of 40 mice per cell line. Carboplatin 90 mg/kg was administered weekly by IP injection. ABT-888 200 mg/kg/day or an equal volume of saline was administered by oral gavage divided in twice daily doses. Mice were treated until animals in the control group showed significant tumor-related morbidity or mortality. Morbidity was defined as ascites limiting movement, limited voluntary enteral intake, or evidence of decreased blood flow. At that time, all mice were sacrificed and tumor was collected from the abdomen. Implants were collected and weighed in aggregate. Samples were stored in formalin, Optimal Cutting Media (Sakura, Leiden, Netherlands), RNAlater (Qiagen, Venlo, Netherlands), and snap frozen in liquid nitrogen.

The second *in vivo* model used was the PDX model. Tumors were isolated and implanted into mice as described above. Once subcutaneous tumors developed to a size of approximately 0.75 cm in maximal diameter, the mice were stratified into two treatment groups: (1) control treatment and (2) ABT-888 alone. ABT-888 200 mg/kg/day was administered by oral gavage divided in twice daily doses. Tumors were measured biweekly, with the primary endpoint being tumor volume, calculated by the formula (length × width^2) / 2. The mice were treated for 60 days and then sacrificed. Tumors were collected and stored in the same fashion as above.

Statistical analysis

Two-way ANOVA analysis was used to compare Rad51 foci after radiation exposure. Pearson's correlation was used to compare Rad51-staining among primary tumor, PDX, and irradiated samples. A two-tailed Student's *T*-test assuming unequal variance was used to compare changes in tumor mass between untreated, ABT-888 alone, chemotherapy alone, and chemotherapy plus ABT-888. All datasets were normally distributed. Differences between samples were considered statistically significant at $p < 0.05$.

Results

Cell viability with PARP inhibition alone and in combination with carboplatin

The sensitivity of each cell line to PARP inhibition was determined using ABT-888 alone and in combination with carboplatin. Of the cell lines tested with single-agent PARP inhibition, A2780ip2 showed the greatest response (IC50 8 μM), while A2780cp20 and ES2 showed an intermediate sensitivity (55 μM and 39 μM, respectively, Fig. 1A, statistically more resistant that A2780ip2, $p < 0.05$). Response to PARP inhibition in A2780ip2 was not unexpected given its known *PTEN* mutation [18]. The SKOV3ip1, SKOV3TR, HeyA8, and HeyA8MDR cell lines were significantly less sensitive to single-agent ABT-888, with IC50s greater than 100 μM ($p < 0.05$, Fig. 1B). Interestingly, previously-published profiles of these cell lines demonstrate that all are *BRCA* wild-type, but only HeyA8 did not contain a mutation in at least one member of the HR family (Table 1). Therefore based on mutation status alone, SKOV3ip1 and SKOV3TRip2 would have been mistakenly assumed to be sensitive to PARP inhibition. Based on the previously reported *BRCA*ness signature [19], A2780ip2, A2780cp20, and ES2 would all have been assessed as fitting a *BRCA*ness profile.

Because the synthetic lethality of PARP inhibition is dependent on some level of DNA damage, possible PARP inhibition-induced sensitization to carboplatin in cells lines was next examined. In the presence of clinically viable doses of ABT-888, the same cell lines that had some level of single-agent PARP inhibitor toxicity were also sensitized to carboplatin. A2780ip2, A2780cp20, and ES2 all had carboplatin IC50 levels reduced (reduced 2.6–7.6-fold) using both IC25 and IC50 levels of ABT-888 for the corresponding cell line (Fig. 1C,D,E). Lowe's additivity model demonstrated a Combination Index less than 1, suggesting synergy (IC = 0.22 in A2780ip2, 0.55 in A2780cp20, and 0.48 in ES2). However, for SKOV3ip1, in which ABT-888 did not have significant single-agent activity, ABT-888 did not sensitize cells to carboplatin (IC = 0.98, Fig. 1F).

Baseline expression of Rad51 protein in unexposed samples

Prior reports have proposed using low Rad51 foci as an assessment tool for HR status [20]. However, because this test uses immunofluorescence, it is not amenable to testing conventionally collected formalin-fixed paraffin-embedded samples. To examine if baseline total Rad51 protein could be used as a surrogate for functional response to PARP inhibition, Western blot analysis for Rad51 was performed. Protein analysis showed that Rad51 expression was prominent in all cell lines (Fig. 2A). Although levels varied, there was no discernible correlation between expression and *in vitro* response to PARP inhibition — the lowest levels of expression were noted in A2780ip2 (the greatest responder *in vitro*) and SKOV3ip1 (a non-responder).

Rad51 foci with radiation exposure

Due to low baseline levels of Rad51, rates of Rad51 foci formation after irradiation were then examined to determine which established ovarian cancer cell lines had defects in HR. Plated cells were exposed to ionizing radiation and subsequently probed for Rad51 foci formation by immunofluorescence (Fig. 2B,C). All cell lines had very few cells (<5%) with Rad51 foci formation without irradiation. However, after irradiation Rad51 foci formation was induced in all cell lines. Interestingly, SKOV3ip1 cells demonstrated the greatest induction of Rad51 foci after radiation (48% of cells, Fig. 2C). ES2 and A2780cp20 cells had an intermediate response at 20–28%, and A2780ip2 cells had the least response, at 11%. These rates of Rad51 foci formation correlated perfectly with the degree of response to single-agent PARP inhibitor therapy and sensitization to carboplatin (demonstrated in Fig. 1). A low induction of Rad51 foci formation functionally demonstrated defective HR and accurately predicted response to PARP inhibition.

Treatment of xenografts with ABT-888 and carboplatin

To determine if the noted *in vitro* response correlated with *in vivo* response, an orthotopic model was utilized examining the "PARP-resistant" SKOV3ip1 and "PARP-sensitive" A2780ip2 cell lines. One week after IP inoculation with cells, treatment was initiated with 1) vehicle, 2) ABT-888 alone, 3) carboplatin alone, or 4) combined ABT-888 and carboplatin. As predicted by the functional HR assay and *in vitro* results, treatment with ABT-888 alone did not have an effect on tumor mass in the SKOV3ip1 orthotopic xenograft (Fig. 3A). However, in A2780ip2, there was a 51% reduction in mean tumor mass, although the difference was not statistically significant due to the variability in tumor size ($p = 0.27$) (Fig. 3B). Carboplatin was effective alone in both cell lines, with a reduction of 92% in SKOV3ip1 and 80% in A2780ip2 ($p = 0.001$ and 0.03, respectively). The addition of ABT-888 to carboplatin did not

Please cite this article as: Shah MM, et al, An ex vivo assay of XRT-induced Rad51 foci formation predicts response to PARP-inhibition in ovarian cancer, Gynecol Oncol (2014), http://dx.doi.org/10.1016/j.ygyno.2014.05.009

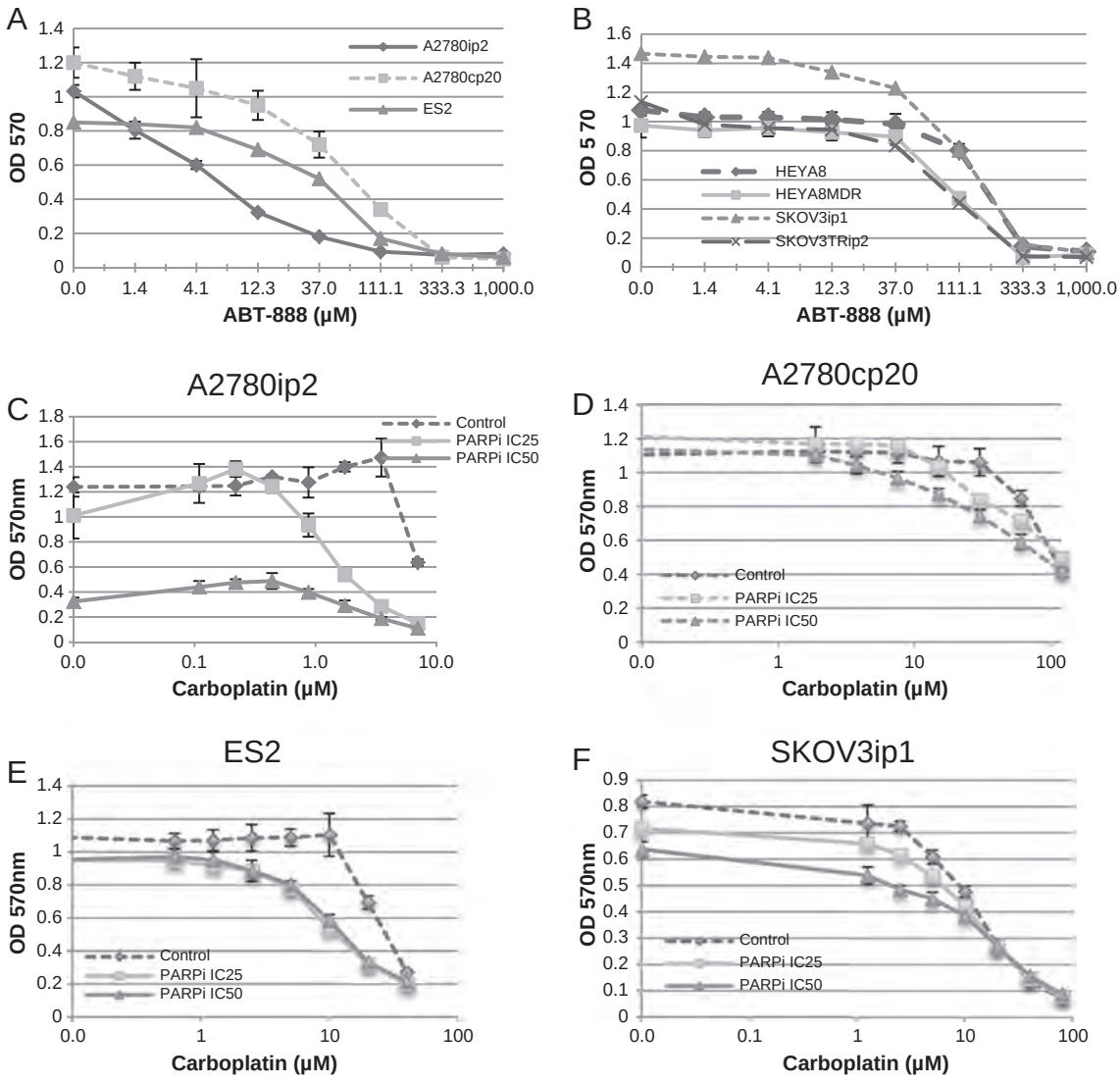

Fig. 1. Single-agent response to ABT-888. (A) IC50 for cell lines that showed single-agent sensitivity; maximum concentration 1000 μM. (B) Nonresponding cell lines, maximum concentration 1000 μM. (C–F) Combination ABT-888 and carboplatin in A2780ip2, A2780cp20, ES2, and SKOV3ip1.

improve on carboplatin alone in SKOV3ip1. In A2780ip2, combination therapy led to an additional 42% reduction in tumor mass over carboplatin alone, though again this was not statistically significant. This is likely due to the high variability in orthotopic growth in these cell lines. Therefore an additional *in vivo* model was examined.

Rad51 foci in first generation PDX tumors

Despite their common use, the SKOV3 and A2780 cell lines from which the above models were derived have recently been shown to poorly reflect expression profiles of papillary serous cancers, as defined by the TCGA dataset [21]. In order to explore the relationship between HR functionality and response in a model that more closely resembles patient tumors, a PDX model was utilized in SCID mice. This model has been demonstrated to have similarity to the patient tumors from which they were derived, at least through the first three generations [22]. Tumors were allowed to grow, and then initially harvested for assessment of Rad51 expression and induction with irradiation ($n = 8$). Among the eight PDX tissue samples, only one had a detectable level of total Rad51 protein (Fig. 4A). This was in stark contrast to

Table 1
Reported mutations and DNA amplifications in common ovarian cancer cell lines.

	SKOV3		A2780		HeyA8		ES2	
	Mutation	CNA	Mutation	CNA	Mutation	CNA	Mutation	CNA
BRCA1	WT [21]	Amplified [31]	WT [21]	None [31]	WT [21]	None [31]	WT [21]	None [31]
BRCA2	WT [21]	None [31]	WT [21]	None [31]	WT [21]	None [31]	WT [21]	None [31]
ATM	Mutated [31,32]	None [31]	Mutated [31]	None [31]	WT [31]	None [31]	Mutated [31]	None [31]
ATR	WT [33]	None [31]	WT [31]	None [31]	WT [31]	Amplified [31]	WT [31]	None [31]
EMSY	Equivocal [21,32]	None [31]	WT [21]	None [31]	WT [21]	None [31]	WT [21]	None [31]
FANCD2	Mutated [32]	Amplified [31]	WT [31]	None [31]	WT [31]	None [31]	WT [31]	None [31]
RAD51c	WT [31]	None [31]	WT [31]	None [31]	WT [31]	None [31]	WT [31]	Amplified [31]
PTEN	WT [21]	None [31]	Mutated [21,31,32]	None [31]	WT [21]	None [31]	WT [21]	None [31]

Please cite this article as: Shah MM, et al, An ex vivo assay of XRT-induced Rad51 foci formation predicts response to PARP-inhibition in ovarian cancer, Gynecol Oncol (2014), http://dx.doi.org/10.1016/j.ygyno.2014.05.009

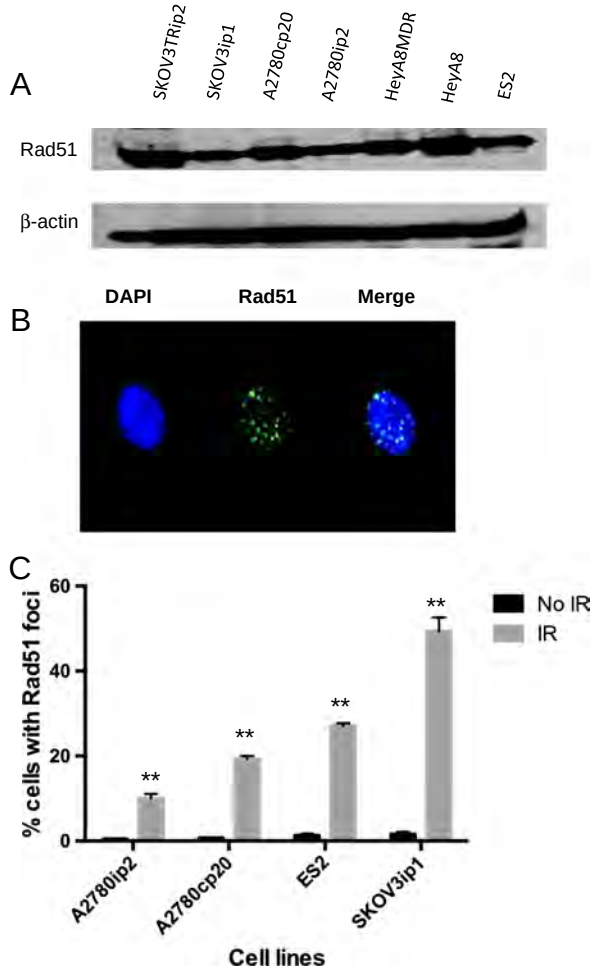

Fig. 2. Rad51 expression (A) Western Blot for Rad51 in established ovarian cancer cell lines. (B) Representative image of immunofluorescence staining of Rad51 foci 8 h after radiation exposure. (C) Comparison of percentage cells positive for Rad51 foci after radiation in cell lines. Note: ** = $p < 0.05$.

what was noted in established ovarian cancer cell lines, in which total Rad51 was prominently expressed in all lines. A query of the TCGA ovarian dataset [12] using cbioportal.org revealed that Rad51 is more than 2-fold downregulated at the mRNA level in just 9 of 316 cases (2.8%), and upregulated in 2 cases (0.6%). Setting a threshold of 1.5-fold increase or decrease, 21/316 cases (6.6%) had downregulation and 12 cases (3.8%) had upregulation. There was no significant trend in survival based on Rad51 over-or under-expression. Therefore total Rad51 expression is likely not a good predictor of HR functionality.

The IR *ex vivo* assay was then performed on PDX tumors to determine if exposure to irradiation produces variable responses in Rad51 foci formation, as they did in cell lines. Two PDX samples (146 and 150) had moderate amounts of Rad51 foci formation at baseline, on the order of 20–30% (Fig. 4B). Exposure to irradiation accentuated the difference, and revealed HR functionality in some samples not notable without irradiation, particularly in PDX 144 and 155. PDX tumors 135, 152 and 157 formed Rad51 foci at the lowest rates (less than 10%), suggesting a defect in HR proficiency. Interestingly, patient 157 had negative *BRCA* testing, suggesting the presence of some other mechanism of defective HR. Two PDX tumors, 136 and 155, had intermediate levels of HR functionality, at 10–25%.

To determine whether response to therapy *in vivo* could be predicted by the IR-induced *ex vivo* assay, three PDX models were examined: PDX 157, predicted to respond due to very low induction of Rad51 foci (2.0% of cells), PDX 136, with an intermediate induction of Rad51 foci (13.1% of cells), and PDX 144 with a predicted resistance profile due to high induction of Rad51 foci (78% of cells). Once implanted tumors had developed to approximately 0.75 cm in maximal diameter, treatment was initiated with either 1) vehicle (n = 3 mice per PDX model) or 2) ABT-888 (n = 2 mice per PDX model). Over the 60-day treatment course, ABT-888 treated PDX 157 had an average tumor volume reduction of 93% compared to a 36% average increase in tumor volume in control mice ($p = 0.003$, Fig. 5A). PDX 136, which was predicted to have a moderate response based on the Rad51 assay, showed stabilization of tumor volume with single-agent ABT-888 while control tumors continued to grow ($p = 0.004$, Fig. 5B). PDX 144 tumors grew at equal rates with control or ABT-888, confirming resistance. Based on these results, the IR-induced *ex vivo* assay accurately predicted response to single-agent ABT-888 therapy.

Discussion

Several trials have demonstrated objective response to PARP inhibitor therapy in ovarian cancer patients with known *BRCA 1/2* mutations [23,24]. However, the clinical impact of PARP inhibition would be significantly limited if only BRCA 1/2 mutation carriers were offered therapy, as only 15–20% of women who develop ovarian cancer have germline mutations [12,25]. It has been recognized that BRCA proteins are only part of a complex mechanism of DNA repair, and that defects in other

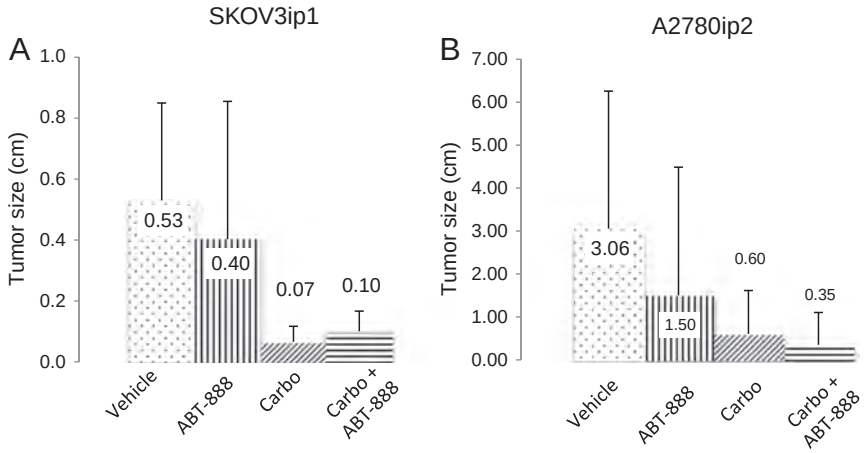

Fig. 3. *In vivo* treatment with ABT-888 alone and with carboplatin in (A) SKOV3ip1 and (B) A2780ip2 cell lines. Treatment groups are vehicle, PARP inhibitor (ABT-888), carboplatin (Carbo), and PARP inhibitor and carboplatin (ABT + Carbo).

Please cite this article as: Shah MM, et al, An ex vivo assay of XRT-induced Rad51 foci formation predicts response to PARP-inhibition in ovarian cancer, Gynecol Oncol (2014), http://dx.doi.org/10.1016/j.ygyno.2014.05.009

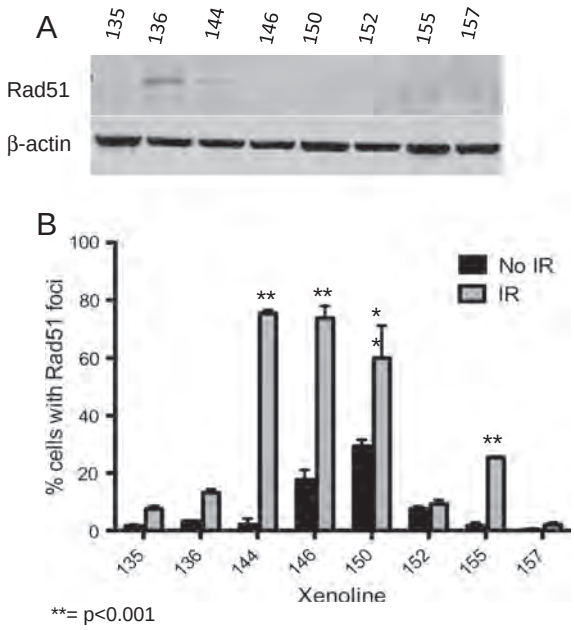

Fig. 4. Patient derived xenografts (A) Western blot for Rad51 in PDX. (B) Comparison of percentage cells positive for Rad51 foci after radiation exposure in xenografts. Note: ** = $p < 0.001$.

proteins involved in homologous repair may lead to the same functional deficiency.

Although PARP inhibitor therapy benefit is still noted for women who are either unselected for the mutation or mutation status is unknown, the effect is less pronounced [26]. Indeed, Gelmon et al. showed that *BRCA* mutation-negative ovarian cancer patients had a response rate of 24% to the PARP inhibitor olaparib, as opposed to a response rate of 41% in BRCA positive patients [27]. Clearly, other pathways may be influenced by PARP inhibition, but the need for a predictive assay is apparent. To that end there have been several approaches. Mukhopadhyay and colleagues isolated and cultured cells from ascitic fluid of ovarian cancer patients [28]. They then exposed these cells to a PARP inhibitor and probed the cultures for γH2AX and Rad51 foci as markers of HR. They found that cells identified as HR deficient by decreased Rad51 foci formation were also sensitive to PARP inhibition. However, it is unknown if ascites-derived cells exhibit the same pathophysiology as cells derived from primary tumor or metastatic implants. Furthermore, they were not able to determine if there was a correlation between response in patients or solid tumors in an *in vivo* model.

Recently Pennington and colleagues examined 390 ovarian, primary peritoneal, and fallopian tube carcinoma samples to determine the rate of mutations in selected HR genes [29]. They found that 31% of unselected patients harbored a somatic or germline HR mutation, which was associated with both platinum sensitivity and improved overall survival. These characteristics are similar to patients with germline *BRCA* mutations, which suggests that these patients may respond similarly to PARP inhibition. As the authors note, PARP inhibition may be useful in a wider range of patients than the traditional cohort of high grade serous cancers, but a predictive assay is necessary to determine who will derive the most benefit.

Our results suggest that it is possible to predict PARP inhibitor response based on *ex vivo* characterization. While we did find some *in vitro* correlation of HR competency and Rad51 formation in established ovarian cancer cell lines, our most intriguing findings involved the association between the heterotopic PDX mouse model and predicted response based on the IR-induced *ex vivo* assay. Clearly this method requires significant refinement to be clinically relevant, but the possibility remains that determining true response is achievable. Correlation between the IR-induced *ex vivo* assay and efficacy of PARP inhibition in the PDX model suggests that with further work, a genetic signature that predicts HR deficiency could be a clinically feasible way to select which patients would respond to PARP inhibitor therapy.

Expanding the concept of synthetic lethality beyond patients with germline *BRCA* mutations is an exciting avenue of inquiry. True advancement in the treatment of ovarian cancer has been slow after the incorporation of platinum agents into first-line therapy, and PARP inhibition may prove to be useful in a variety of settings, from upfront to recurrent to maintenance therapy [30]. However, from the standpoint of both toxicity and health care resources, patients need to be screened for biologic eligibility of these agents. Identifying an effective *ex vivo* assay to help predict the potential utility of PARP inhibitors in epithelial ovarian cancer patients should be a high research priority.

Conflict of interest statement

None of the authors have a conflict of interest.

Acknowledgments

Funding support was provided in part by the Lewis-Moseley Award from the Southeast Cancer Foundation (to ESY and CNL) and the University of Alabama at Birmingham Center for Clinical and Translational Science (5UL1RR025777) to CNL.

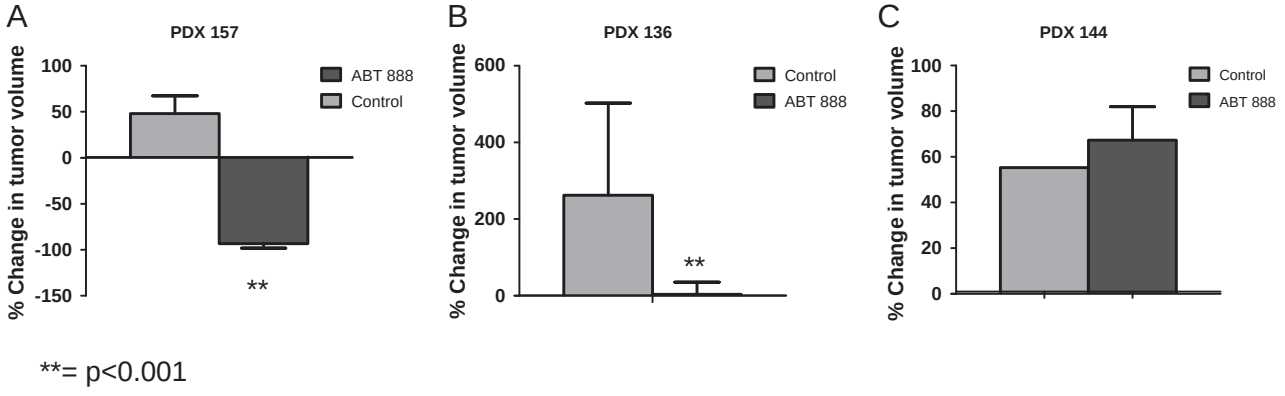

Fig. 5. Patient xenograft (PDX) response to ABT-888 compared to vehicle in three patient-derived xenografts: (A) PDX 157 with defective HR by the *ex vivo* assay, (B) PDX 136 with an intermediate level of Rad51 foci induction, and (C) PDX 144 with intact HR.

References

[1] Siegel R, Ma J, Zou Z, Jemal A. Cancer statistics. CA Cancer J Clin 2014;64:9–29.
[2] Ovarian cancer statistics. American Cancer Society; 2012 [Accessed August 5, 2012, at].
[3] Agarwal R, Kaye SB. Ovarian cancer: strategies for overcoming resistance to chemotherapy. Nat Rev Cancer 2003;3:502–16.
[4] Moynahan ME, Chiu JW, Koller BH, Jasin M. Brca1 controls homology-directed DNA repair. Mol Cell 1999;4:511–8.
[5] Patel KJ, Yu VP, Lee H, et al. Involvement of Brca2 in DNA repair. Mol Cell 1998;1:347–57.
[6] Haaf T, Golub EI, Reddy G, Radding CM, Ward DC. Nuclear foci of mammalian Rad51 recombination protein in somatic cells after DNA damage and its localization in synaptonemal complexes. Proc Natl Acad Sci U S A 1995;92:2298–302.
[7] Scully R, Chen J, Ochs RL, et al. Dynamic changes of BRCA1 subnuclear location and phosphorylation state are initiated by DNA damage. Cell 1997;90:425–35.
[8] Yuan SS, Lee SY, Chen G, Song M, Tomlinson GE, Lee EY. BRCA2 is required for ionizing radiation-induced assembly of Rad51 complex in vivo. Cancer Res 1999;59:3547–51.
[9] Zhou C, Huang P, Liu J. The carboxyl-terminal of BRCA1 is required for subnuclear assembly of RAD51 after treatment with cisplatin but not ionizing radiation in human breast and ovarian cancer cells. Biochem Biophys Res Commun 2005;336:952–60.
[10] Tsuzuki T, Fujii Y, Sakumi K, et al. Targeted disruption of the Rad51 gene leads to lethality in embryonic mice. Proc Natl Acad Sci U S A 1996;93:6236–40.
[11] Lim DS, Hasty P. A mutation in mouse rad51 results in an early embryonic lethal that is suppressed by a mutation in p53. Mol Cell Biol 1996;16:7133–43.
[12] Integrated genomic analyses of ovarian carcinoma. Nature 2011;474:609–15.
[13] Zhao L, Au JL, Wientjes MG. Comparison of methods for evaluating drug–drug interaction. Front Biosci (Elite Ed) 2010;2:241–9.
[14] Chou TC. Drug combination studies and their synergy quantification using the Chou–Talalay method. Cancer Res 2010;70:440–6.
[15] Nowsheen S, Bonner JA, Lobuglio AF, et al. Cetuximab augments cytotoxicity with poly (adp-ribose) polymerase inhibition in head and neck cancer. PLoS One 2011;6:e24148.
[16] Nowsheen S, Bonner JA, Yang ES. The poly(ADP-Ribose) polymerase inhibitor ABT-888 reduces radiation-induced nuclear EGFR and augments head and neck tumor response to radiotherapy. Radiother Oncol 2011;99:331–8.
[17] Landen Jr CN, Goodman B, Katre AA, et al. Targeting aldehyde dehydrogenase cancer stem cells in ovarian cancer. Mol Cancer Ther 2010;9:3186–99.
[18] Sanger Institute Cancer Genome Project. Accessed February 5, 2014, at http://www.sanger.ac.uk/genetics/CGP/CellLines/; 2014.
[19] Konstantinopoulos PA, Spentzos D, Karlan BY, et al. Gene expression profile of BRCAness that correlates with responsiveness to chemotherapy and with outcome in patients with epithelial ovarian cancer. J Clin Oncol 2010;28:3555–61.
[20] Graeser M, McCarthy A, Lord CJ, et al. A marker of homologous recombination predicts pathologic complete response to neoadjuvant chemotherapy in primary breast cancer. Clin Cancer Res 2010;16:6159–68.
[21] Domcke S, Sinha R, Levine DA, Sander C, Schultz N. Evaluating cell lines as tumour models by comparison of genomic profiles. Nat Commun 2013;4:2126.
[22] Weroha SJ, Becker MA, Enderica-Gonzalez S, et al. Tumorgrafts as in vivo surrogates for women with ovarian cancer. Clin Cancer Res 2014;20:1288–97.
[23] Audeh MW, Carmichael J, Penson RT, et al. Oral poly(ADP-ribose) polymerase inhibitor olaparib in patients with BRCA1 or BRCA2 mutations and recurrent ovarian cancer: a proof-of-concept trial. Lancet 2010;376:245–51.
[24] Fong PC, Yap TA, Boss DS, et al. Poly(ADP)-ribose polymerase inhibition: frequent durable responses in BRCA carrier ovarian cancer correlating with platinum-free interval. J Clin Oncol 2010;28:2512–9.
[25] Risch HA, McLaughlin JR, Cole DE, et al. Prevalence and penetrance of germline BRCA1 and BRCA2 mutations in a population series of 649 women with ovarian cancer. Am J Hum Genet 2001;68:700–10.
[26] Ledermann J, Harter P, Gourley C, et al. Olaparib maintenance therapy in platinum-sensitive relapsed ovarian cancer. N Engl J Med 2012;366:1382–92.
[27] Gelmon KA, Tischkowitz M, Mackay H, et al. Olaparib in patients with recurrent high-grade serous or poorly differentiated ovarian carcinoma or triple-negative breast cancer: a phase 2, multicentre, open-label, non-randomised study. Lancet Oncol 2011;12:852–61.
[28] Mukhopadhyay A, Elattar A, Cerbinskaite A, et al. Development of a functional assay for homologous recombination status in primary cultures of epithelial ovarian tumor and correlation with sensitivity to poly(ADP-ribose) polymerase inhibitors. Clin Cancer Res 2010;16:2344–51.
[29] Pennington KP, Walsh T, Harrell MI, et al. Germline and somatic mutations in homologous recombination genes predict platinum response and survival in ovarian, fallopian tube, and peritoneal carcinomas. Clin Cancer Res 2014;20:764–75.
[30] Chan N, Pires IM, Bencokova Z, et al. Contextual synthetic lethality of cancer cell kill based on the tumor microenvironment. Cancer Res 2010;70:8045–54.
[31] Barretina J, Caponigro G, Stransky N, et al. The Cancer Cell Line Encyclopedia enables predictive modelling of anticancer drug sensitivity. Nature 2012;483:603–7.
[32] Forbes SA, Bindal N, Bamford S, et al. COSMIC: mining complete cancer genomes in the Catalogue of Somatic Mutations in Cancer. Nucleic Acids Res 2011;39:D945–50.
[33] Lewis KA, Mullany S, Thomas B, et al. Heterozygous ATR mutations in mismatch repair-deficient cancer cells have functional significance. Cancer Res 2005;65:7091–5.

Please cite this article as: Shah MM, et al, An ex vivo assay of XRT-induced Rad51 foci formation predicts response to PARP-inhibition in ovarian cancer, Gynecol Oncol (2014), http://dx.doi.org/10.1016/j.ygyno.2014.05.009